ON THE SYNTHESIS, MEASUREMENT AND APPLICATIONS OF OCTANUCLEAR HETEROMETALLIC RINGS

A thesis submitted to The University of Manchester for the degree of

Doctor of Philosophy

in the Faculty of Engineering and Physical Sciences

Thomas Benjamin Faust

School of Chemistry

2011

Table of contents

Page count: 202 Word count: 66,378

List of Figures

List of Tables

Abstract

On the Synthesis, Measurement and Applications of Octanuclear Heterometallic Rings: A thesis submitted to The University of Manchester for the degree of Doctor of Philosophy in the Faculty of Engineering and Physical Sciences.

Inorganic macrocycles have stimulated interest in recent years for their magnetic properties, their associated host-guest chemistry and their aesthetically appealing structures. These characteristics have led to suggestions that they could be exploited for the purposes of ion recognition, catalysis, as single molecule magnets, MRI agents, antibacterial agents and as part of larger architectures in a molecular machine.

This thesis explores the properties of a group of chromium(III) macrocycles, with functionality tailored towards different pursuits. Firstly the magnetic properties of a newly synthesised family of ring dimers are investigated. The nature of magnetic exchange within each ring leads to a net electronic spin which, it has been proposed, could represent a quantum binary digit within a quantum information processing system. By linking together pairs of rings, the degree of inter-ring communication can be determined. Such interactions are important for the correlation of spin as initiation of quantum entanglement, a pre-requisite for quantum computing.

The rings can also act as fluoro-metallocrowns, hosting the molecule which templated their formation. A range of rings with different guests are synthesised and their solid and solution state structures are explored. On templating about bulky dialkyl amines hybrid organic-inorganic rotaxanes are formed where the guest is fixed. In contrast when using small amines and alkali metals, exchange of guests is possible. The dynamics of all of these systems are investigated with proton NMR, quite remarkable for such highly paramagnetic complexes.

Thomas Benjamin Faust
December 2011

Declaration

No portion of the work credited to the author in this thesis has been submitted in support of an application for another degree or qualification of this or any other university or institute of learning.

Copyright Statement

I. The author of this thesis (including any appendices and/or schedules to this thesis) owns certain copyright or related rights in it (the "Copyright") and he has given The University of Manchester certain rights to use such Copyright, including for administrative purposes.

II. Copies of this thesis, either in full or in extracts and whether in hard or electronic copy, may be made only in accordance with the Copyright, Designs and Patents Act 1988 (as amended) and regulations issued under it or, where appropriate, in accordance with licensing agreements which the University has from time to time. This page must form part of any such copies made.

III. The ownership of certain Copyright, patents, designs, trademarks and other intellectual property (the "Intellectual Property") and any reproductions of copyright works in the thesis, for example graphs and tables ("Reproductions"), which may be described in this thesis, may not be owned by the author and may be owned by third parties. Such Intellectual Property and Reproductions cannot and must not be made available for use without the prior written permission of the owner(s) of the relevant Intellectual Property and/or Reproductions.

IV. Further information on the conditions under which disclosure, publication and commercialisation of this thesis, the Copyright and any Intellectual Property and/or Reproductions described in it may take place is available in the University IP Policy (see http://www.campus.manchester.ac.uk/medialibrary/policies/intellectualproperty.pdf), in any relevant Thesis restriction declarations deposited in the University Library, The University Library's regulations (see http://www.manchester.ac.uk/library/aboutus/regulations) and in The University's policy on presentation of Theses.

Acknowledgements

Firstly I would like to thank Doctor Ian Tidmarsh and Professor Mike Ward for encouraging me to pursue a PhD and in particular for their recommendation that I consider working at the Molecular Magnetism Group here in Manchester. Without their input I may very well have left academia.

Secondly my gratitude is extended to Professors Richard Winpenny, Eric McInnes and David Collison for their support throughout my time in Manchester; also to Professor José Antonio Real who kindly hosted me for my period at the Institute of Molecular Science at the University of Valencia.

A great number of people have helped contribute to my work and I am indebted to them. Grigore Timco has been a great mentor, lab colleague and friend to me. Floriana Tuna, Rebecca Docherty and John Machin have done the bulk of the EPR measurements, without which my synthesis would be redundant. Pretty much every group member past and present has helped in some way and to them I am grateful.

I had the privilege of supervising two very capable MChem students, Paul and Sarah, and hope that in some small way I convinced them to stay in science at least a little longer.

Finally, thanks to my parents for their never failing support and encouragement.

List of abbreviations

AFM	atomic force microscopy
CW	classical walk
DFT	density functional theory
dmf	dimethyl formamide
Et	ethyl
EPR	electron paramagnetic resonance
GA	Grover's Algorithm
h.s.	high spin
ICP-AES	inductively coupled plasma atomic emission spectroscopy
*i*Pr	iso-propyl
H_5Etglu	*N*-ethyl-D-glucamine
HDVV	Heisenberg-Dirac-Van Vleck
Me	methyl
*n*Pr	n-propyl
NMR	nuclear magnetic resonance
Ph	phenyl
Py	pyridyl

SQUID	super-conducting quantum interference device
thf	tetrahydrofuran
TMS	tetramethylsilane
UQP	universal quantum computer
QIP	quantum information processing
QS	quantum simulator
qubit	quantum binary digit
SMM	single-molecule magnet
*t*Bu	tertiary butyl
ZFS	zero-field splitting

List of symbols and constants

$\subset$	contained inside
B	magnetic field
Δ_{pcs}	pseudocontact shift parameter
δ	chemical shift
D	zero-field splitting parameter
d	distance

$\mathcal{E}$	energy
E	rhombic zero-field splitting parameter
F	structure factor amplitude
FT	Fourier transform
γ	gyromagnetic ratio
g	Landé g-factor
H	magnetic field
h	Planck's constant
I	nuclear angular momentum
I	angular momentum quantum number
J	isotropic exchange parameter
K	pseudocontact shift parameter
k	Boltmann constant
λ	wavelength
λ_r	rhombicity
M	mass
μ	nuclear magnetic moment
μ_B	Bohr magneton
M	magnetisation

m	magnetic quantum number (orbital angular momentum)
m_s	spin projection quantum number
N	population
R	residual factor
S	net spin (resultant spin existing on a defined moiety)
s	spin quantum number (single ion spin)
θ	angle of incidece
T	temperature
T_1	spin-lattice relatation rate
T_2	spin-spin relaxation rate
wR_2	weighted residual factor
χ	magnetic susceptibility
Z	charge

For the purpose of the thesis, many compounds have been given an abbreviated notation. The notation obeys the following rules: They are contained within braces { }, to differentiate them from actual chemical formulae which are generally contained within square brackets [ ]. Usually they take the name of the most significant metal(s) and are followed by its multiplicity in standard script, e.g. $[Cr_8F_8(O_2C\textit{t}Bu)_{16}]$ has the abbreviated notation {Cr8}. Braces may still be used in chemical formulae where nesting is necessary, though of course atom multiplicity will always be subscripted. If required, oxidation states are shown as superscripted Roman numerals, so chromium in the oxidation state plus three is written: Cr^{III}.

Chapter One - Introduction

1.1 Rationale for submitting the thesis in an alternative format

The thesis author has been fortunate in being able to publish his results in peer reviewed journals as results have been gained. Timely publication of results is especially critical in this field for several reasons. Firstly the work is largely interdisciplinary, the research is directed through discussions with other chemists, theorists and physicists around Europe, and so getting up-to-date research into the public domain is of high importance. Secondly the research is equipment intensive. Access to expensive and sought after national facilities (eg. Diamond Light Source) is dependent on quality research, invariably demonstrated by publications in high level journals. The same is true in the pursuit of new funding sources from bodies such as the EPSRC, MolSpinQIP and MagmaNet. It has therefore been necessary, and preferable, to publish during the course of the author's PhD studies. The published papers cover all of the aspects of the author's work and so are deemed suitable for submission as a part of this thesis.

1.2 Organisation of the thesis

Chapter One provides preface to the thesis, and describes the contribution the author has made to the published material. Chapter Two describes the context of the research and reviews the work done up in the field to-date. Chapter Three describes the aims of the project. Chapter Four details the methodology employed during the research, with more in depth discussion of non-standard techniques. Chapters Five to Eleven contain peer-reviewed publications and manuscripts in preparation. Chapter Twelve consists of a summary of the work undertaken and provides an outlook for future study. Chapter Thirteen contains references which are cited outside of Chapters Five to Eleven. The Appendix contains one further peer reviewed paper.

1.3 Contributing authors

Chapter Five, Paper 1, entitled “Linking heterometallic rings for quantum information processing and amusement” is a review paper written principally by Richard Winpenny with contributions from the thesis author, Grigore Timco and Floriana Tuna based on work by the same.

Chapter Six, Paper 2, entitled “Chemical control of spin propagation between heterometallic rings” is a full paper written by the thesis author. Synthesis was performed principally by the thesis author with contributions from Grigore Timco, Laura Carthy and Jasbinder Kenyon. X-ray crystallography was performed principally by the thesis author with contributions from Christopher Muryn, Robin Pritchard, Simon Teat at ALS Berkeley, and George Whitehead. EPR measurements were performed by Rebecca Docherty, John Machin and Floriana Tuna. Micro-SQUID measurements were performed by Wolfgang Wernsdorfer. DFT and theoretical calculations were courtesy of Marco Affronte and his group in Modena and Stefano Carretta in Parma.

Chapter Seven, Paper 3, entitled “Twist and shout” is a draft paper written by the thesis author. Synthesis was principally by the thesis author with contribution from Grigore Timco. X-ray crystallography was entirely by the thesis author. EPR measurement was by Floriana Tuna. Assistance was provided for some of the figures by James Walsh.

Chapter Eight, Paper 4, entitled “Caesium ion sequestration by a fluoro-metallocrown [16]-MC-8” is a communication written by the thesis author. Synthesis was performed principally by the thesis author with contributions from Paul Heath. NMR measurements were performed by the thesis author. X-ray crystallography was performed by the thesis author with contribution from Christopher Muryn.

Chapter Nine, Paper 5, entitled “Alkaline Earth - Transition Metal Octametallic Rings” is a draft paper written by the thesis author. Synthesis was performed by Sarah Varey under the direction of the thesis author. EPR measurements were

performed by Floriana Tuna. X-ray crystallography was performed by the thesis author.

Chapter Ten, Paper 6, entitled “Proton NMR study of Cr-Co heterometallic wheel complexes” is a full paper written by Carolina Sañudo of the University of Barcelona. Synthesis was performed by the thesis author and Grigore Timco. X-ray crystallography was by Christopher Muryn and Robin Pritchard. NMR measurement and interpretation was by Carolina Sañudo and the thesis author.

Chapter Eleven, paper 7, entitled “Synthesis, structure, and dynamic properties of hybrid organic-inorganic rotaxanes” is a full paper written by David Leigh in Edinburgh. Organic synthesis was performed by the group in Edinburgh. Inorganic synthesis was performed by the thesis author and Grigore Timco. NMR measurements of cobalt-containing complexes were performed by the group in Edinburgh. NMR measurements of iron-containing complexes were performed by the thesis author.

The Appendix, Paper 8x, entitled “Propagation of spin information at the supramolecular scale through heteroaromatic linkers” is a communication written by Valero Bellini, and other members of Marco Affronte’s group in Modena, based on measurement and calculations by the same, as well as micro-SQUID analysis by Wolfgang Wernsdorfer in Grenoble on compounds synthesised by the thesis author and Grigore Timco.

Chapter Two - Review of the field

2.1 Metallorings

Reports of the first metallorings were published independently in 1990. In the USA, Taft and Lippard published the synthesis of the {Fe10} 'molecular ferric wheel', a planar decanuclear ring of Fe^{III} where adjacent metal ions are bridged by two methoxides and one monochloroacetate, $[Fe(OMe)_2(O_2CCH_2Cl)]_{10,}$[1] see Figure 1

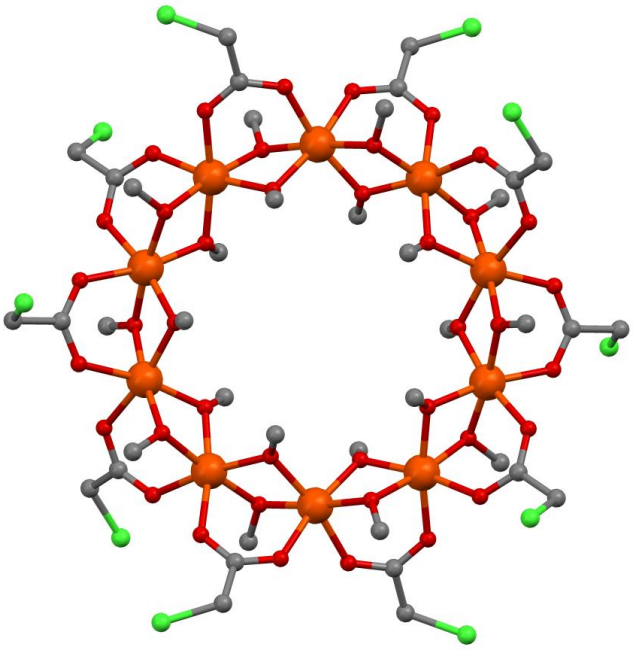

Figure 1 Structure in the crystal of the {Fe10} 'molecular ferric wheel', Colours: Fe, orange; C, grey; O, red; Cl, green. Hydrogen atoms omitted for clarity.[1]

Meanwhile in the USSR, the group of Gerbeleu published the synthesis of {Cr8} (later dubbed the 'green wheel'), a planar octanuclear ring of Cr^{III}, adjacent ions this time being bridged by a single fluoride and two trimethylacetates, $[CrF(O_2C\textit{t}Bu)_2]_8$.[2] (The compound was actually synthesised by G. Timco during his PhD studies. It was patented in the Soviet Union with priority date of 07 August 1985 as an oxidation catalyst, being issued in 1989 (SU 1299116). This delayed the publication until 1990.)

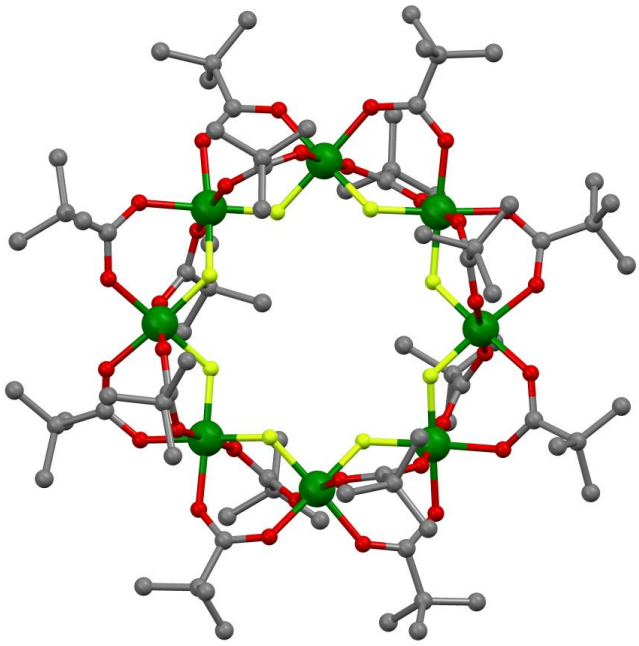

Figure 2 Structure in the crystal of the {Cr8} 'green wheel'. Colours: Cr, green; C, grey; O, red; F, yellow. Hydrogen atoms omitted for clarity.[2]

Since then there has been an explosion in the numbers of metallorings in the literature. The most recent review of the area was performed by Pecoraro in 2007.[3] Table 1 lists the metallorings where the number of metal centres is between eight and twenty four. In fact rings larger than this exclusively consist of multi-threaded 'giant rings', such as Müller's (see later).

Table 1. List of metallorings with between eight and twenty four metals in the ring core. # indicates the number of metals contained within the core. Ref indicates the reference from which the metalloring can be found. See reference for the identity of ligands.

Formula	**#**	**Core metals**	**Ref**
$[AgStBu]_8$	8	Ag	4
$[AgCo(SCH_2CH_2NH_2)_2(NH_2CH_2CH_2NH_2)]$-$(ClO_4)_8$	8	Ag/Co/Pd	5
$[Ag_2\{Pd(Co(aet)_3)_2\}_2]$	8	Ag/Co/Pd	6
$[(AlEt_2)_2(PHSi(i\text{Pr})_2OSi(i\text{Pr})_2PH)]_4$	8	Al	7
$[AlF(O_2Ct\text{Bu})_2]_8$	8	Al	8
$[Au_2\{Pd(Co(aet)_3)_2\}_2]$	8	Au/Co/Pd	6
$[Au_4\{Ni(SCH_2CH_2NC(CH_3))\}_4]$	8	Au/Ni	9
$[Ba_2(C_2H_6O_2)_4]_2[Ge_2(C_2H_4O_2)_6]_2$	8	Ba/Ge	10
$[Bi(OEt)_3]_8$	8	Bi	11

Formula	#	Core metals	Ref
$[Ca_8\{O_3POC_6H_3(NHCOPh)_2\}_8(OCHNMe2)_8$-$(H_2O)_{12}]$	8	Ca	12
$[Co(O_2CMe)(OMe)_2]_8$	8	Co	13
$[Co_8(bpypzbh)_{12}(ClO_4)]^{3+}$	8	Co	14
$[M_7M(O_2CR)_{16}]^-$	8	Co/Cr/Fe/Ga/ Mn/Ni/V	15
$[Cr(OH)(O_2CPh)_2]_8$	8	Cr	16
$[Cr(OH)(O_2CMe)_2]_8$	8	Cr	17
$[Cr_8(OH)_{12}(OAc)_{12}]$	8	Cr	18
$[CrF(O_2C\textit{t}Bu)_2]_8$	8	Cr	19
$[Cr(OH)(O_2C\textit{t}Bu)_2]_8$	8	Cr	2
$[Cr(OH)(O_2CC_6H_4Cl)_2]_8$	8	Cr	20
$[Cr_4Dy_4(OH)_4(N_3)_4(mdea)_4(piv)_4]$	8	Cr/Dy	21
$[Himid]_2[Cr_6Ni_2F_8(O_2C\textit{t}Bu)_{16}]$	8	Cr/Ni	22
$[Cr_7NiF_3(Etglu)(O_2C\textit{t}Bu)_{15}]$	8	Cr/Ni	23
$[Et_2NH_2][Cr_6(VO)_2F_8(O_2C\textit{t}Bu)_{15}]$	8	Cr/V	24
$[Cr_6Y_2F_8(O_2C\textit{t}Bu)_{17}][H_2NEt_2]$	8	Cr/Y	25
$[Cu_8(hpbs)_4(OH)_4]$	8	Cu	26
$[Cu(dmpz)(OH)]_8$	8	Cu	27
$[Cu(OH)(pz)]_8$	8	Cu	28
$[CuSC_6H_2(\textit{i}Pr)_3]_8$	8	Cu	29
$[Cu_8(hpba)_4(OH)_3](ClO_4)$	8	Cu	30
$[Cu_8(NCO)_2(NCO)_4(OH_2)_7(bdmap)_4](ClO_4)_2$	8	Cu	31
$[Cu(SC_6H_2(\textit{i}Pr)_3)]_8$	8	Cu	32
$[CuS_2WS_2CuStBu]_4[NEt_4]_4$	8	Cu/W	33
$[Fe_4Dy_4(teaH)_8(N_3)_8(H_2O)]$	8	Dy/Fe	34
$[Mn_4Dy_4(\textit{n}Budea)_4(HCO_2)_4(OMe)_4(O_2CEt)_8$-$(MeOH)_4]$	8	Dy/Mn	35
$[Fe_8(OH)_4(OPh)_8(O_2C\textit{t}Bu)_{12}]$	8	Fe	36
$[Fe_8(OH)_4(OPh)_8(O_2CPh)_{12}]$	8	Fe	36
$[Fe_{16}S_{16}(PCy_3)_8]$	8	Fe	37
$[Fe_8O_4(bmpd)_4(OH)_4(O_2CMe)_4]$	8	Fe	38
$[Fe_8(PhCOO)_{12}(thme)_4]$	8	Fe	39
$[Fe(O_2C\textit{t}Bu)_2]_8$	8	Fe	40
$[CsFe_8\{N(CH_2CH_2O)_3\}_8]Cl$	8	Fe	41

Formula	**#**	**Core metals**	**Ref**
$[N\textit{n}Pr_2H_2][Fe_8F_8(O_2C\textit{t}Bu)_{16}]$	8	Fe	15
$[CsFe_8\{N(CH_2CH_2O)_3\}_8]Cl$	8	Fe	42
$[Fe_8(C_{11}H_{11}N_2O_3)_8(CH_3OH)_8]$	8	Fe	43
$[Fe_8(OH)_4(OPh)_8(O_2CR)_{12}]$	8	Fe	44
$[(GaEt_2)_2(PHSi(\textit{i}Pr)_2OSi(\textit{i}Pr)_2PH)]_4$	8	Ga	7
$[GaF(O_2C\textit{t}Bu)_2]_8$	8	Ga	8
$[Gd_8(sca)_4(AcO)_8(EtOH)_4(H_2O)_4]$	8	Gd	45
$[Mn_4Gd_4(\textit{n}Budea)_4(HCO_2)_4(OMe)_4(O_2CEt)_8$-$(MeOH)_4]$	8	Gd/Mn	35
$[HgCl_2Ni\{SC(Me)_2CNHC_3H_5\}_2]_4$	8	Hg/Ni	46
$[InF(O_2C\textit{t}Bu)_2]_8$	8	In	8
$[\{Ru(C_5H_3)_2\}Na_4Mg_4\{\textit{i}Pr_2N\}_8]$	8	Mg/Na	47
$[\{Os(C_5H_3)_2\}Na_4Mg_4\{\textit{i}Pr_2N\}_8]$	8	Mg/Na	47
$[\{Fe(C_5H_3)_2\}Na_4Mg_4\{\textit{i}Pr_2N\}_8]$	8	Mg/Na	48
$[CeMn_8O_8(O_2CMe)_{12}(H_2O)_4]$	8	Mn	49
$[Mn_{10}Na(O)_2(O_2CMe)_{13}(pd)_6(py)_2]$	8	Mn	50
$[CeMn_8O_8(O_2CMe)_{12}(py)_3(H_2O)]$	8	Mn	51
$[CeMn_8O_8(O_2CMe)_{12}(bdz)_2(H_2O)_2]$	8	Mn	51
$[Mn_8(O_2CCH_2\textit{t}Bu)_{12}(teaH)_4]$	8	Mn	52
$[Mn_4O\{Mn(aet)_3\}_4]Cl_2$	8	Mn	53
$[Mo_8O_{16}(OCH_3)_8(Me_2Py)_4]$	8	Mo	54
$[MoO_2MoO(OMe)_2]_4[C_2O_4]$	8	Mo	55
$[Mo_8O_{16}(OCH_3)_8\{Me(py)\}_4]$	8	Mo	56
$[Mo_8O_{16}(OCH_3)_8(py)_4]$	8	Mo	57
$[Mo_8S_8O_8(OH)_8\{HWO_5(H_2O)\}]_3$	8	Mo	58
$[Mo_8S_8O_8(OH)_8(C_2O_4)]^{2-}$	8	Mo	58
$[Mo_8S_8O_8(OH)_8\{HMoO_5(H_2O)\}]_3$	8	Mo	58
$[Mo_2O_4(OMe)_2PMe_3]_4$	8	Mo	59
$[Mo_8O_{16}(O_3PPhPO_3H)_4]^{3-}$	8	Mo	60
$[(\textit{n}Bu)_4N]_2[Mo_8O_{16}(OCH_3)_8(C_2O_4)]$	8	Mo	61
$[Na_{12}(PhAsSe_3)_6(15\text{-crown-}5)_6]$	8	Na	62
$[Nd_8(sca)_4(AcO)_8(MeOH)_4(H_2O)_8]$	8	Nd	45
$[Ni_8(abo)_8(Et_2O)_2(MeOH)_2(H_2O)]$	8	Ni	63

Formula	#	Core metals	Ref
$Ni_8(SCH_2COOEt)_{16}$	8	Ni	64
$[\{Pd(SC_6F_5)(dppm)Pd\}(SC_6F_5)]_4$	8	Pd	65
$[Pr_8(sca)_4(AcO)_8(MeOH)_4(H_2O)_8]$	8	Pr	45
$[\{(C_4H_3N)_2C_6H_{10}]Sm\}_8(thf)_4]$	8	Sm	66
$[Sm_8(sca)_4(AcO)_8(EtOH)_4(H_2O)_4]$	8	Sm	45
$[(Me_3Sn)_4(Cp^*W)_4(O)]$	8	Sn/W	67
$[TiO(O_2CNEt_2)_2]_8[NH_3Et][O_2CNEt_2]$	8	Ti	68
$[Ti_9O_8(O\textit{n}Pr)_4(CH_2CMeCOO)_{16}]$	8	Ti	69
$[Ti(O_2CC_6F_5)_2]_8$	8	Ti	70
$[TiO(O_2C\textit{t}Bu)_2]_8$	8	Ti	71
$[TiO(O_2CPh)_2]_8$	8	Ti	72
$[Ti(SO)_4)_2]_8[H_4pip]_8$	8	Ti	73
$[Ti(SO)_4)_2]_8(NH_2(CH_2CH_2NH_3)_2)_5(H_3O)$	8	Ti	73
$(C_4N_2H_{12})_8[TiO(SO_4)_2]_8$	8	Ti	73
$[V_8(OH)_4(OEt)_8(O_2CMe)_{12}]$	8	V	74
$[(\textit{n}Bu)_4N]_2[V_8O_8(OCH_3)_{16}(C_2O_4)]$	8	V	75
$[(VO)_8(OMe)_{16}(C_2O_4)]^{2-}$	8	V	75
$[V_8(OEt)_8(OH)_4(O_2CPh)_{12}]$	8	V	15
$[Zn_4(dmpz)_6(OH)_2]_2$	8	Zn	76
$[H_2N\textit{t}Bu\textit{i}Pr][Cr_8CdF_9(O_2C\textit{t}Bu)_{18}]$	9	Cr/Cd	22
$[H_2\textit{t}BuN\textit{i}Pr][Cr_8NiF_9(O_2C\textit{t}Bu)_{18}]$	9	Cr/Ni	22
$[Himid]_2[Cr_8NiF_{11}(O_2C\textit{t}Bu)_{17}]$	9	Cr/Ni	22
$[(C_6H_{11})_2NH_2][Cr_8NiF_9(O_2CCMe_3)_{18}]$	9	Cr/Ni	77
$[(C_6H_{11})_2NH_2][Cr_7(VO)_2F_9(O_2CCMe_3)_{17}]$	9	Cr/V	77
$[Cu(OH)(pz)]_9$	9	Cu	28
$[Fe_9(OH)_7(O)_2(O_3PC_6H_9)_8(py)_{12}]$	9	Fe	78
$[Fe_6Na_3(bsmp)_3(CH_3COO)_{12}]$	9	Fe/Na	79
$[Ni(SPh)_2]_9$	9	Ni	80
$[Cd(OCH_3)(HOCH_3)(bafca)]_{10}$	10	Cd	81
$[\textit{n}Bu_4N]_2[Co_{10}(OH)_{10}(NO_2pz)_{10}(Me_2pz_{10}](NO_2)_2$	10	Co	82
$[Cr(O_2CMe)(OMe)_2]_{10}$	10	Cr	83
$[Cr(O_2CMe)(OEt)_2]_{10}$	10	Cr	83
$[Cr_nMn_m(OMe)_2(O_2CMe)]_{10}$	10	Cr/Mn	84

Formula	**#**	**Core metals**	**Ref**
$[HNEt(C_6H_{11})_2][Cr_9NiF_{12}(O_2C\textit{t}Bu)_{18}]$	10	Cr/Ni	[22]
$[HNMe(C_6H_{11})_2][Cr_9NiF_{12}(O_2C\textit{t}Bu)_{18}]$	10	Cr/Ni	[22]
$[HNMe(C_6H_{11})_2]_2[Cr_8Ni_2F_{12}(O_2C\textit{t}Bu)_{18}]$	10	Cr/Ni	[22]
$[H_2N\textit{t}Bu\textit{i}Pr][Cr_9NiF_{10}(O_2C\textit{t}Bu)_{20}]$	10	Cr/Ni	[22]
$[HMeimid]_2[Cr_8Ni_2F_{12}(O_2C\textit{t}Bu)_{18}]$	10	Cr/Ni	[22]
$[H\textit{n}Buimid]_2[Cr_8Ni_2F_{12}(O_2C\textit{t}Bu)_{18}]$	10	Cr/Ni	[22]
$[Ni(tacn)_2][Cr_8Ni_2F_{10}(O_2C\textit{t}Bu)_{20}]$	10	Cr/Ni	[85]
$[CuClOC(CF_3)_2CH_2NHCH_2CH_2NMe_2]_{10}$	10	Cu	[86]
$[Dy\ (OC_2H_4OCH_3)_3]_{10}$	10	Dy	[87]
$[Fe(OMe)_2(O_2CMe)]_{10}$	10	Fe	[88]
$[Fe(OMe)_2(O_2C\textit{t}Bu)]_{10}$	10	Fe	[36]
$[Fe(CH_3O)_2(O_2CCH_2OPh)]_{10}$	10	Fe	[89]
$[Fe(OMe)(O_2CCH_2Cl)]_{10}$	10	Fe	[90]
$[Fe(OMe)_2(O_2CCH_2CH_2C(O)C_6H_4Me)]_{10}$	10	Fe	[91]
$[Fe(C_{14}H_9N_2O_3)(CH_3OH)]_{10}$	10	Fe	[92]
$[Ga(OMe)_2\{O_2CC(OH)Ph_2\}]_{10}$	10	Ga	[93]
$[Ga(OMe)_2(O_2CMe)]_{10}$	10	Ga	[94]
$[K_3Mn_{10}(PhCOO)_{10}(PhPO_3)_2(Htea)_6]$	10	Mn	[95]
$[Mn_{10}(C_6H_4\{Me\}\{OH\}CON_2COC_6H_4iPr)_8$-$(C_6H_4\{Me\}\{OH\}CON_2COCtBu)_2(dmf)_{10}]$	10	Mn	[96]
$[Mn(C_{14}H_9N_2O_3)(CH_3OH)]_{10}$	10	Mn	[92]
$[Mo_{10}S_{10}O_{10}(OH)_{10}(H_2O)_5]$	10	Mo	[97]
$(NH_4)_2[Y(H_2O)_5]_2\ [Mo_{10}V_4O_{30}(CH_3COO)_4]$	10	Mo	[98]
$[Na_2(POPh_3)_6][Ni_{20}Se_{12}(SeMe)_{10}]$	10	Ni	[99]
$[Y(OC_2H_4OMe)_3]_{10}$	10	Y	[100]
$[Zn(OCH_3)(HOCH_3)(bafca)]_{10}$	10	Zn	[81]
$[Ni(SPh)_2]_{11}$	11	Ni	[80]
$[Cd_{12}(dpa)_6(pya)_6]$	12	Cd	[101]
$[Co_{12}(chp)_{12}(O_2CMe)_{12}(H_2O)_6(thf)_6]$	12	Co	[102]
$[PPN]_2[Co_{12}(OH)_{12}(NO_2pz)_{12}(Me_2pz)_{12}](NO_2)_2$	12	Co	[82]
$[(\textit{t}Bu_3SiS)CoCl]_{12}$	12	Co	[103]
$[(R_2NH_2)_3\{Cr_6F_{11}(O_2C\textit{t}Bu)_{10}\}(H_2O)]_2$	12	Cr	[104]
$[Cr(O_2C\textit{t}Bu)(OMe)_2]_{12}$	12	Cr	[105]
$[Me_2NH_2]_2[Cr_{10}Cu_2F_{14}(O_2C\textit{t}Bu)_{22}]$	12	Cr/Cu	[24]

Formula	**#**	**Core metals**	**Ref**
$[Cr_xMn_y(OMe)_2(O_2CMe)]_{10}$ (where x + y = 1)	12	Cr/Mn	84
$[Cu(OH)(pz)]_{12}$	12	Cu	28
$Cu_{12}[C_6H_4(CHNC_6H_4S)_2]_6$	12	Cu	106
$[Dy_{10}Co_2(bhmh)_4(OAc)_{16}(SCN)_2(CH_3CN)_2$-$(H_2O)_4(OH)_6]$	12	Dy/Co	107
$[Fe(OMe)_2(dbm)]_{12}$	12	Fe	108
$[Fe(OMe)_2(proline)]_{12}[ClO_4]_{12}$	12	Fe	109
$[\{Fe(OMe)_2[O_2CC(OH)Ph_2]\}_{12}]$	12	Fe	110
$[Fe(SePh)_2]_{12}$	12	Fe	99
$[Fe_6\{Fe(SPhSPhS)_2\}_6]$	12	Fe	111
$[Fe(OCH_3)_2(dbm)]_{12}$	12	Fe	112
$[Fe(Cl)(SSi(t\text{Bu})_3)]_{12}$	12	Fe	103
$[Fe(Br)(SSi(t\text{Bu})_3)]_{12}$	12	Fe	103
$[Fe_{12}(O)_4(O)_4(O_2CCHPh_2)_{14}(t\text{BuPhPO}_3H)_6]$	12	Fe	113
$[Fe_{12}(O)_4(O)_4(O_2CPh)_{14}(C_{10}H_{17}PO_3H)_6]$	12	Fe	113
$[Fe(OCH_3)_2(dbm)]_{12}$	12	Fe	114
$[Ho_{12}(bsca)_6(mal)_4(AcO)_4(H_2O)_{14}]$	12	Ho	115
$[(tmp)_{12}K_6Mg_6(C_6H_5)_6]$	12	K/Mg	116
$[(tmp)_{12}K_6Mg_6(C_6H_4Me)_6]$	12	K/Mg	116
$[EtMgNH\{C_6H_3i\text{Pr}_2\}]_{12}$	12	Mg	117
$[TaMe\{MgC(Ni\text{Pr})_3Cl\}_2Ni\text{Pr}]_6$	12	Mg	118
$[Mn_{12}(bdea)_8(O_2CMe)_{14}]$	12	Mn	119
$[Mn_{12}(mdea)_8(O_2CMe)_{14}]$	12	Mn	119
$[Mn_{12}(edea)_8(O_2CMe)_{14}]$	12	Mn	119
$[\{Mn(salen)\}_6\{Fe(bpmb)(CN)_2\}_6]$	12	Mn/Fe	120
$[\{Mn(salen)\}_6\{Fe(bpClb)(CN)_2\}_6]$	12	Mn/Fe	121
$[\{Mn(salen)\}_6\{Fe(bpdmb)(CN)_2\}_6]$	12	Mn/Fe	121
$[\{Mn(Br(salpn))\}_6\{Fe(bpmb)(CN)_2\}_6]$	12	Mn/Fe	121
$[\{Mn(Cl(salpn))\}_6\{Fe(bpmb)(CN)_2\}_6]$	12	Mn/Fe	121
$[Mo_3O_4(H_2O)_9(OH)_2]_4(CH_3C_6H_4SO_3)_8$	12	Mo	122
$[(MeC_6H_3O_2)_2SbNa(thf)_2]_6$	12	Na/Sb	123
$[Ni_{12}(chp)_{12}(O_2CMe)_{12}(thf)_6(H_2O)_6]$	12	Ni	124
$[Ni_{12}(chp)_{12}(O_2CMe)_{12}(H_2O)_6(thf)_6]$	12	Ni	125
$[Ni_{12}(bhp)_{12}(O_2CMe)_{12}(thf)_6(H_2O)_6]$	12	Ni	126

Formula	**#**	**Core metals**	**Ref**
$[Ni(Br)(t\text{Bu}_3SiS)]_{12}$	12	Ni	[103]
$[Sb_{12}\{(OMe)C_6H_4N\}_{18}]$	12	Sb	[127]
$(NH_4)[(VO)_{12}\{O_3POB(O)_2OPO_3\}_6]^{18-}$	12	V	[128]
$(K)[(VO)_{12}\{O_3POB(O)_2OPO_3\}_6]^{18-}$	12	V	[128]
$[\{ClZnCHMePEt_2NSiMe_3)_{12}]$	12	Zn	[129]
$[(AgStBu)_{14}(Ph_3P)_4]$	14	Ag	[130]
$[Cu(OH)(pz)]_{14}$	14	Cu	[28]
$[FeI(SSi t\text{Bu}_3)]_{14}$	14	Fe	[103]
$[Mn_{32}O_8(OH)_6(Mesao)_{14}(O_2CMe)_{18}Br_8]$	14	Mn	[131]
$[(dppm)_2Au_4(pipzdtc)]_4(PF_6)_8$	16	Au	[132]
$[Fe_{16}(EtO)_4(PhCOO)_{16}(Hthme)_{12}](NO_3)_4$	16	Fe	[39]
$[Mn_{16}O_2(OMe)_{12}(tmp)_8(O_2CMe)_{10}]$	16	Mn	[133]
$[Mn_{22}O_6(OMe)_{14}(O_2CMe)_{16}(tmp)_8(HIm)_2]$	16	Mn	[134]
$[Mn_{16}(O_2CMe)_{16}(teaH)_{12}]$	16	Mn	[52]
$[Pb_{16}(\gamma\text{-CDH})_2]$	16	Pb	[135]
$[Zn_4(dmpz)_6(OH)_2]_4$	16	Zn	[76]
$[(n\text{Pr}_4N)_6Na_4Fe_{18}S_{30}]$	18	Fe	[136]
$[Fe_{18}(pd)_{12}(pdH)_{12}(O2CPh)_6(NO_3)_6](NO_3)_6$	18	Fe	[94]
$[Fe(OH)(xdk)Fe_2(OMe)_4(O_2CMe)_2]_6$	18	Fe	[137]
$[Ga_{18}(pd)_{12}(pdH)_{12}(O_2CMe)_6(NO_3)_6](NO_3)_6$	18	Ga	[94]
$[Mn_{24}(tmp)_{12}(bpy)_{24}(N_3)_6(OAc)_6](ClO_4)_{12}$	18	Mn	[138]
$(n\text{Bu}_4N)_{4.5}Na_{4.5}[Na_9Fe_{20}Se_{38}]$	20	Fe	[136]
$[Fe_{16}Dy_4(tea)_8(teaH)_{12}(OAc)_8](NO_3)_4$	20	Fe/Dy	[139]
$[Fe_{16}Eu_4(tea)_8(teaH)_{12}(OAc)_8](NO_3)_4$	20	Fe/Eu	[139]
$[Fe_{16}Gd_4(tea)_8(teaH)_{12}(OAc)_8](NO_3)_4$	20	Fe/Gd	[139]
$[Fe_{16}Ho_4(tea)_8(teaH)_{12}(OAc)_8](NO_3)_4$	20	Fe/Ho	[139]
$[Fe_{16}Sm_4(tea)_8(teaH)_{12}(OAc)_8](NO_3)_4$	20	Fe/Sm	[139]
$[Fe_{16}Tb_4(tea)_8(teaH)_{12}(OAc)_8](NO_3)_4$	20	Fe/Tb	[139]
$[Ga_4(O_2CMe)_4(OC_3H_6O)_4]_5$	20	Ga	[140]
$[Mn_{22}O_6(OMe)_{14}(O_2CMe)_{16}(tmp)_8(HIm)_2]$	22	Mn	[141]
$[Mn_{22}O_6(OMe)_{14}(O_2CMe)_{16}Br_8(HIm)_2]$	22	Mn	[141]
$[Ni_{24}(OH)_8(mpo)_{16}(O_2CMe)_{24}(Hmpo)_{16}]$	24	Ni	[142]
$[Ni_{24}(O_2CMe)_{42}(mdaH)_6(EtOH)_6]$	24	Ni	[143]

The group of Saalfrank demonstrated elegently how changing the size of an alkali metal templating agent can determine the structure of the synthesised metallocrown host. In his system, using Li^+ or Na^+ leads to a hexaferric ring, $[M\subset Fe_6\{N(CH_2CH_2O)_3\}_6]Cl$, whereas Cs^+ leads to an octaferric ring, $[Cs\subset Fe_8\{N(CH_2CH_2O)_3\}_8]Cl$, and use of K^+ does not lead to any ring formation at all,[42] See Figure 3.

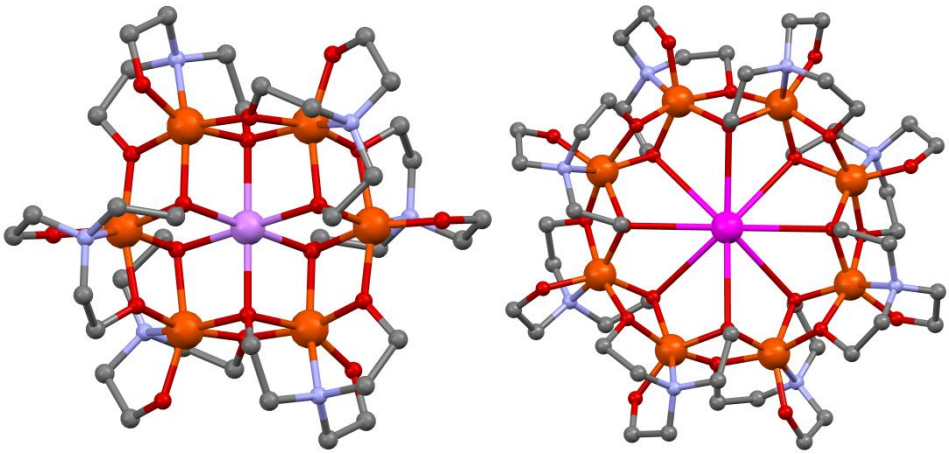

Figure 3 Structure in the crystal of Saalfrank's iron coronates, left, Li/Na centred hexaferric ring and right, Cs centred octaferric ring. Colours: Fe, orange; Li/Na, lilac; Cs, fuscia; C, grey; N, sky blue; O, red. Hydrogen, solvent and counter-ion chloride atoms omitted for clarity.[42]

The potential of any type of host is often determined by its specificity for a particular guest. Rochat and co-workers combined the selectivity of a ruthenium based metallocrown with aromatic fluorophores carefully chosen to promote solubility in aqueous solvent to create a macrocycle which selectively and quantitatively detects Li^+ ions by fluorescence spectroscopy, without interference from Na^+ and K^+.[144]

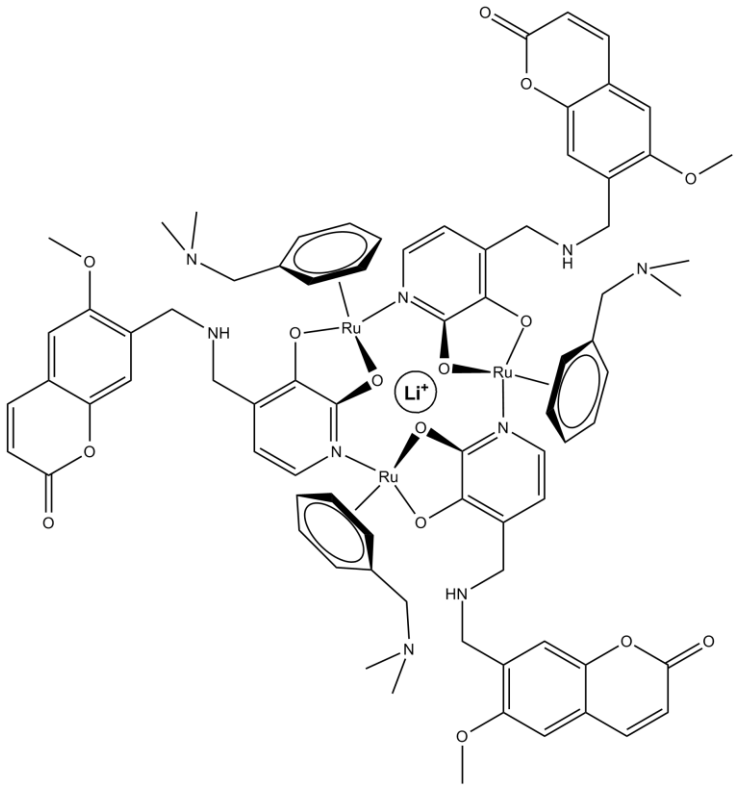

Figure 4 Schematic representation of Rochat's fluorescent lithium detector binding a central Li^+ ion.[144]

Saalfrank's and Rochat's hosts fall into the category of metallocrowns, inorganic analogues of crown ethers, which are μ_2-oxide lined, as is usual for metallocrown cavities. A rare example of a μ_2-fluoride lined metallocrown, or fluoro-metallocrown, is found from the group of Halcrow.[145,146] They present a {Cu6} cavitand, $[(guest)\subset(CuF\{C_5H_4NC_3N_2H\textit{t}Bu\})_6]HF_2$, capable of binding two waters (exogenously), one ammonium (endogenously), two alkyl ammoniums (exogenously) or one alkali metal (endogenously); the preference presumably a result of the complementarity of size, shape, and presence of a charge dipole on the guest, see Figure 5.

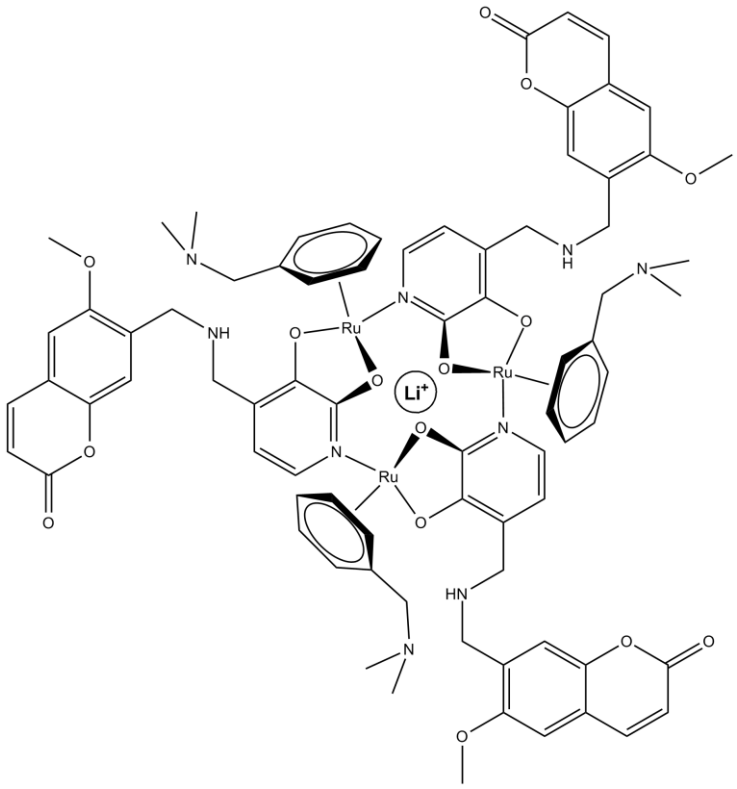

Figure 4 Schematic representation of Rochat's fluorescent lithium detector binding a central Li^+ ion.[144]

Saalfrank's and Rochat's hosts fall into the category of metallocrowns, inorganic analogues of crown ethers, which are μ_2-oxide lined, as is usual for metallocrown cavities. A rare example of a μ_2-fluoride lined metallocrown, or fluoro-metallocrown, is found from the group of Halcrow.[145,146] They present a {Cu6} cavitand, $[(guest)\subset(CuF\{C_5H_4NC_3N_2H\textit{t}Bu\})_6]HF_2$, capable of binding two waters (exogenously), one ammonium (endogenously), two alkyl ammoniums (exogenously) or one alkali metal (endogenously); the preference presumably a result of the complementarity of size, shape, and presence of a charge dipole on the guest, see Figure 5.

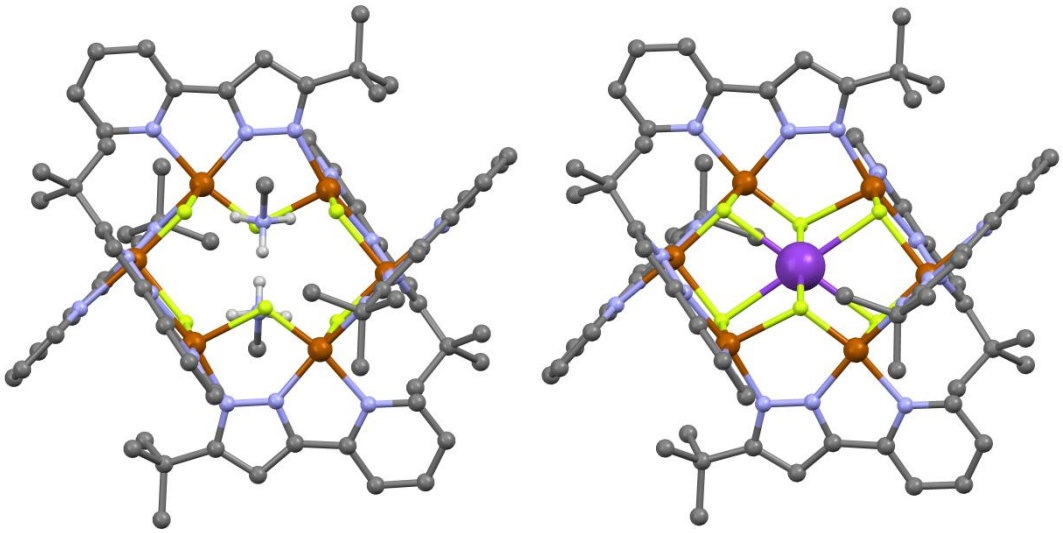

Figure 5 Structure in the crystal of Halcrow's {Cu6} cavitand hosting two $MeNH_3^+$ (left) and a K^+ (right). Colours: Cu, brown; K, purple; C, grey; N, sky blue; O, red. Non-ammonium hydrogen, solvents and counter-ion atoms omitted for clarity.[145,146]

The size of these macrocycles varies greatly. Lei and co-workers recently published a {Mn10}, which consists of a 10-membered ring $[Mn_{10}\{C_6H_4(Me)(OH)CON_2COC_6H_4iPr\}_8\{C_6H_4(Me)(OH)CON_2COCtBu\}_2(dmf)_{10}$,[147] see Figure 6.

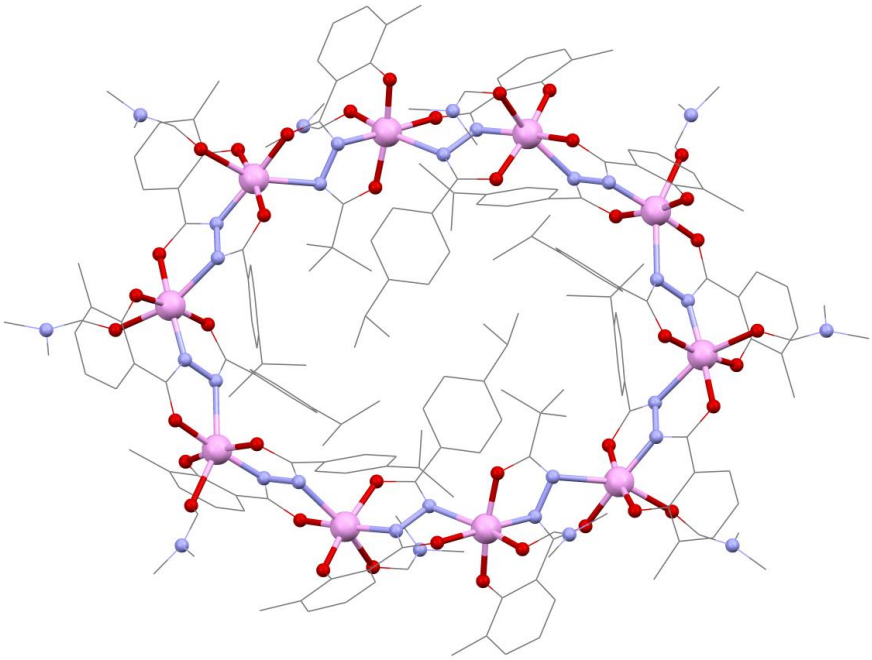

Figure 6 Structure in the crystal of Lei's {Mn10} cycle. Colours: Mn, pink; C, grey (wireframe); N, sky blue; O, red. Hydrogen and solvents atoms omitted for clarity.

Chromium derivatives of the original ferric rings also exist; {Cr10}[83,148] and {Cr12},[105] as seen in Figure 7.

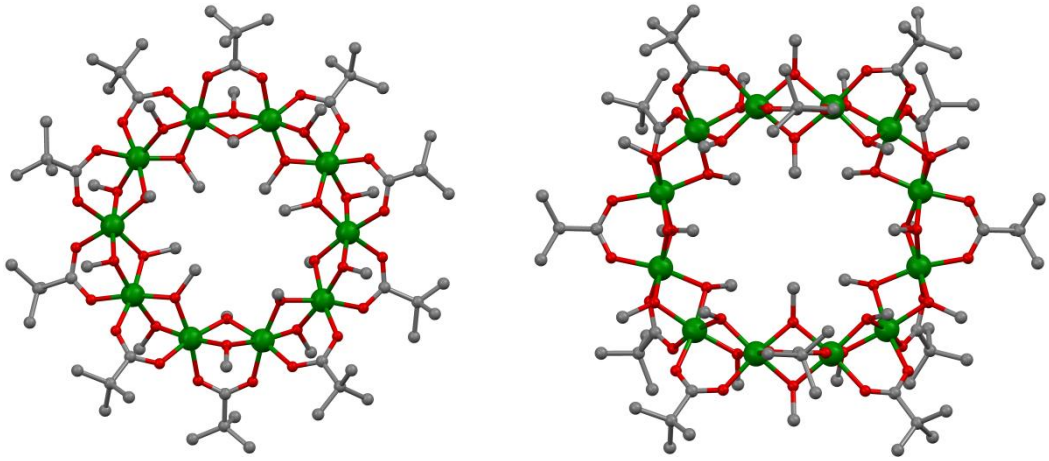

Figure 7 Structure in the crystal of the {Cr10} (left) and {Cr12} (right), methoxy- derivatives of the fluoro-{Cr8} 'green wheel'. Colours: Cr, green; C, grey; O, red; F, yellow. Hydrogen atoms omitted for clarity.[148,105]

The largest known single strand metalloring is a pentagonal {Ga20} ring, $[(Ga_4\{O_2CMe\}_4\{OC_3H_6O)\}_4)_5]$, synthesised by size modification of the {Ga10} 'gallic wheel' (an analogue of Lippard's {Fe10} 'ferric ring'; see Figure 8), both made by Christou.[141]

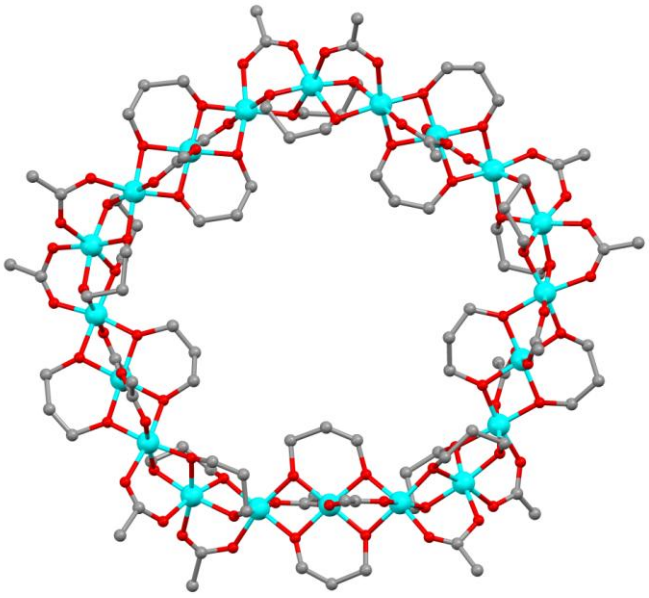

Figure 8 Structure in the crystal of Christou's {Ga20} ring. Colours: Ga, teal; C, grey; O, red. Hydrogen atoms omitted for clarity.[141]

The largest (multithreaded) known metallocycle belongs to the group of Müller; their $[(MoO_3)_{176}(H_2O)_{63}(CH_3OH)_{17}H_n]^{(32-n)-}$, {Mo176}, which is charge balanced by Na^+, represents a truly massive inorganic molecule with a cavity of 2.3 nm. Indeed such is its size that it is capable of hosting two smaller {Mo36} rings to generate the massive {Mo248} cluster.[149,150]

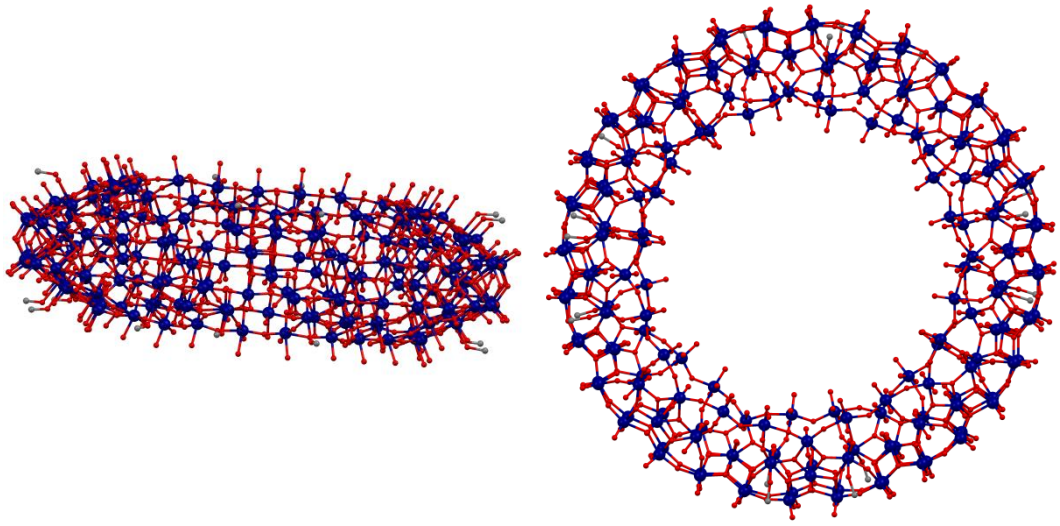

Figure 9 Structure in the crystal of Müller's giant {Mo176}, seen down the a-axis (left) and c-axis (right). Colours: Mo, navy; C, grey; O, red. Hydrogen and sodium ions were not found during the X-ray crystallographic process.[150]

{Mo176} is a mixed valent Mo^V/Mo^{VI}. In fact both mixed valent and mixed metal species are well known. Displaying perhaps the greatest flexibility in metal selection is Timco's 'green ring' system. Under similar conditions to the synthesis of {Cr8} but with the addition of appropriate metal sources, M^{III} in lieu of Cr, a new M^{II}, and suitable cation (alkyl ammoniums are most common), a wide variety of $\{M^{III}7M^{II}\}$ can be generated; M^{III} being Cr, V, Fe or Ga and M^{II} being Mn, Fe, Co, Ni, Zn, Cd, Mg.[15]

The above examples should demonstrate the wide range of compounds within the class, metallocrown. As well as beautiful crystal structures and astounding self-assembled complexity, these compounds have interesting and possibly useful host-guest properties. The scope for inclusion of different metal ions also provides great opportunities to magnetochemists. Cyclic arrays are particularly useful for studying 1-D magnetism since they often possess just one magnetic exchange

interaction (i.e. the pathways between all adjacent ions are identical). Even for mixed metal species e.g. Timco's {Cr7Ni}, just two exchange parameters are required to model the system, $J_{Cr\text{-}Cr}$ and $J_{Cr\text{-}Ni}$ (only nearest neighbour interactions are typically significant).

The vast majority of these rings are homo-metallic, contain even numbers of spin-centres and display antiferromagnetic superexchange between adjacent spin-centres. This inevitably leads to rings with no net spin due to full spin compensation. Of greater interest are molecules with non S = 0 ground states, this is achievable in three ways. Easiest to recognise is synthesis of a ring with ferromagnetic superexchange, for example in {Cr10} where the ten s = 3/2 centres are weakly ferromagnetic leading to an S = 15 ground state.[148] Other examples include the Cu metallorings, $Cu_6[(MeSiO_2)_6]_2 \cdot 6dmf$ whose nearest neighbour ferromagnetic interaction leads to a high spin S = 3 ground state.[151] Secondly, creation of a ring with an odd number of spin-centres (with equal spin amplitude) cannot possibly have full spin compensation. In actual fact there is a paucity of odd-membered metallorings. One is Yao's {Fe9} pseudo-ring (since it has phosphonates capping each side of the cavity) which has the formula $[Fe_9(OH)_7(O)_2(O_3PC_6H_9)_8(NC_5H_5)_{12}]$[78] and is shown in Figure 10.

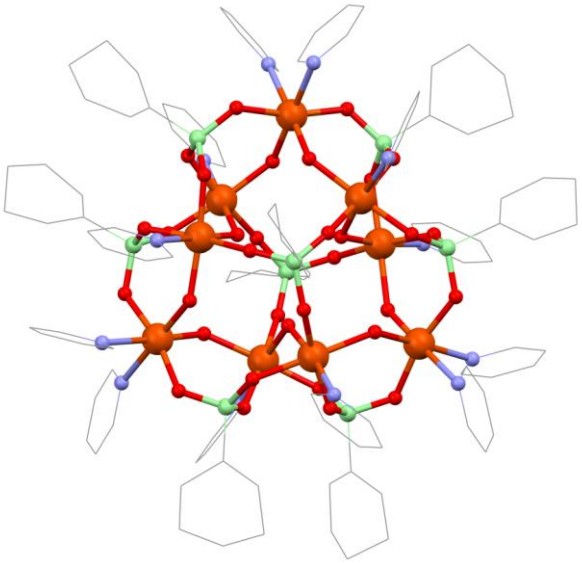

Figure 10 Structure in the crystal of Yao's {Fe9}. Colours: Fe, orange; C, grey (wireframe); N, sky blue; O, red; P, apple green. Hydrogen and solvent atoms omitted for clarity. [78]

Another rare example is Hoshito's *β*-cyclodextrin sandwich, $Na_7[(VO)_7Na_7(H_2O)_7(\beta\text{-CD})_2]$, {V7},[152] which can be seen in Figure 11.

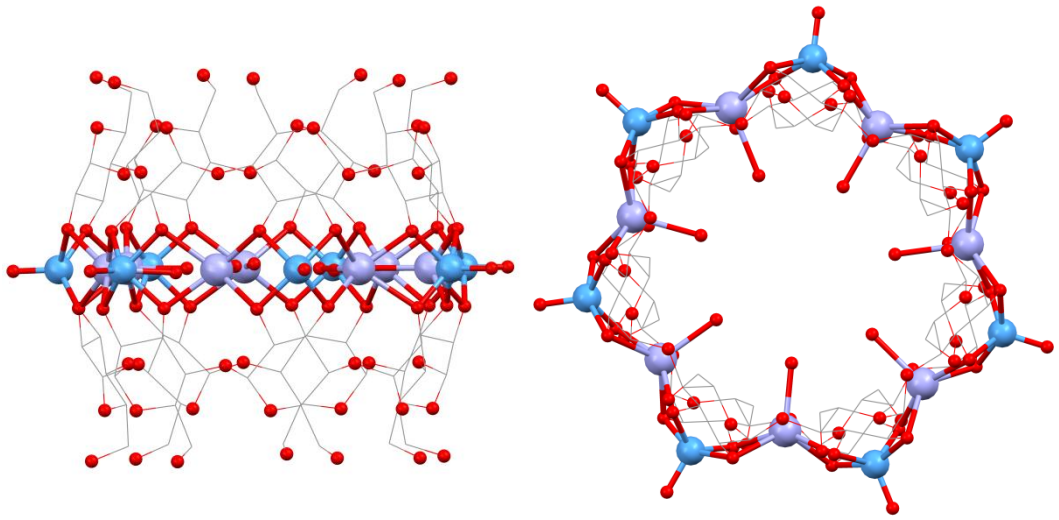

Figure 11 Structure in the crystal of Hoshito's {V7} cyclodextrin sandwich viewed down the a-axis (left) and c-axis (right). Colours: V, pale blue; Na, lilac; C, grey (wireframe); O, red. Hydrogen atoms omitted for clarity.[152]

The inability to satisfy antiferromagnetic exchange between all spin-centres in an odd-membered cyclic array is termed 'spin frustration'. Spin frustration was first properly defined in this context by Kahn.[153] The simplest case to consider is that of a triangle with equal spins at each vertex, (for this example $s_A = s_B = s_C = 1/2$) and equivalent antiferromagnetic (AF) exchange pathways along each edge, which is represented in Figure 12.

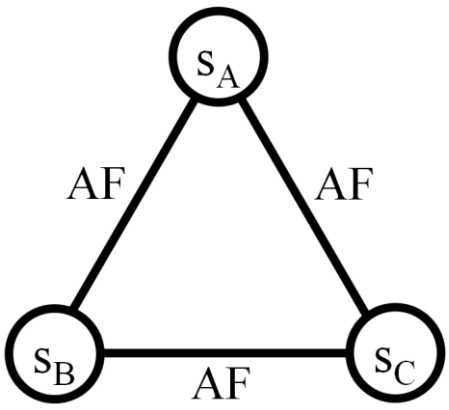

Figure 12 Representation of spin-frustration arising between three spins with antiferromagnetic coupling

In such a case the ground state is S = 1/2, in which one spin (any of s_A, s_B or s_C) is orientated in a different orientation to the other two, generating triple orbital degeneracy. By extension its excited state is a non-degenerate S = 3/2 with all spins in same orientation. Kahn is keen to point out that the term spin frustration should only refer to cases exhibiting orbital degeneracy of the ground state, and not merely to systems exhibiting completing spin interactions.

Odd-membered rings appear intrinsically more difficult to synthesise than their even-membered counterparts. Even when their synthesis is achieved they lack high symmetry and often warrant multiple *J* values. Timco has successfully synthesised a homometallic $[(i\text{Pr})_2\text{NH}_2][\text{Cr}_9\text{F}_{11}(\text{O}_2\text{C}t\text{Bu})_2]$ ring, {Cr9},[154] but not the desirable $[\text{CrF}(\text{O}_2\text{C}t\text{Bu})_2]_9$. He has also developed heterometallic odd-membered rings such as $[(i\text{Pr})_2\text{NH}_2][\text{Cr}_8\text{NiF}_9(\text{O}_2\text{C}t\text{Bu})_{18}]$, {Cr8Ni}, and $[(t\text{Bu})(i\text{Pr})\text{NH}_2][\text{Cr}_8\text{CdF}_9(\text{O}_2\text{C}t\text{Bu})_{18}]$, {Cr8Cd},[155,22] as shown in Figure 13.

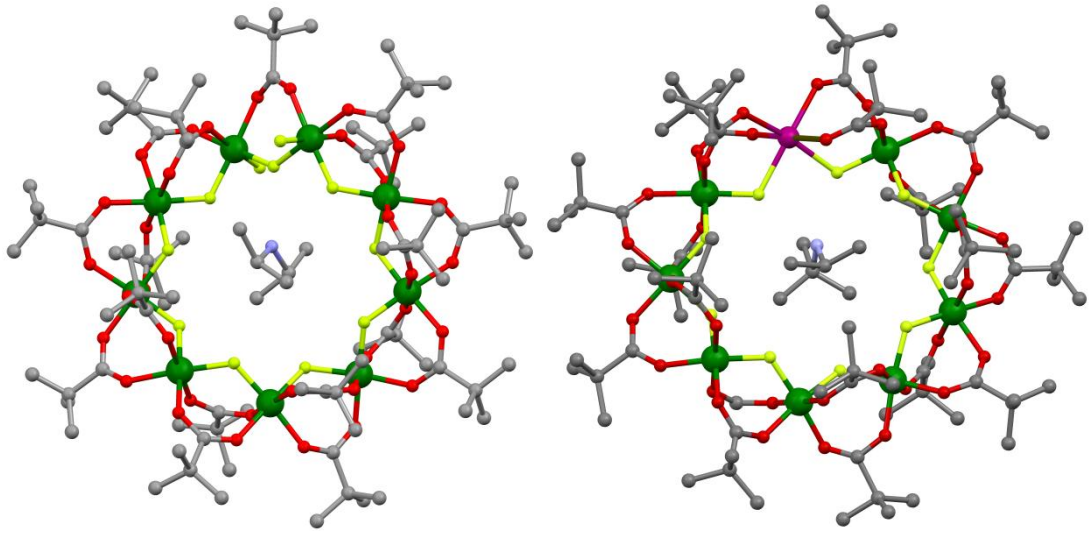

Figure 13 Structure in the crystal of Timco's {Cr9} (left) and {Cr8Cd} (right). Colours: Cr, green; Cd, wine, C, grey; O, red; F, yellow. Hydrogen and solvent atoms omitted for clarity.[154,22]

A final way of generating non S = 0 ground states is to introduce a heterospin-centre to the ring typified by the $\{M^{III}7M^{II}\}$ series.[15] (Of course $\{M^{III}7M^{II}\}$ can result in S = 0 if they still have the same spin, for example {Cr7Co} where all ions possess s = 3/2.) An elegent example is $\{Fe^{III}7Fe^{II}\}$, a homometallic hetero-spin complex.

The most studied of this family is undoubtedly {Cr7Ni} for reasons explained in Section 2.2.

2.2 Linking heterometallic rings

$[R_2NH_2][Cr_7NiF_8(O_2C\textit{t}Bu)]$ or {Cr7Ni} is synthesised in high yield from commercially available starting materials with only limited requirement for purification.[15] Octahedral Cr^{III}, being a relatively chemically inert ion, makes the ring extremely stable once formed. There is a great deal of scope for functionalisation, by varying R or exchanging the carboxylates for ones conveying other functional groups. The antiferromagnetic exchange between adjacent ions means that three pairs of Cr spin compensate leaving Ni^{II}, d^8, s = 1 and the one remaining Cr^{III}, d^3, s = 3/2. The mismatch in spin amplitude leads to a net S = 1/2 for the whole ring in the ground state. At low temperature this doubly degenerate ground state is well separated from the S = 3/2 first excited state.[156] Application of a field induces Zeeman splitting of the $m_s = \pm 1/2$ states leading to a pseudo two-level system. It has been proposed that these levels could represent the states of a quantum binary digit (qubit) within a future quantum information processing (QIP) system.[157]

QIP takes advantage of two phenomena arising from quantum theory. Firstly superposition, which supposes that rather than an object taking one of two definite values, it is possible for it to take both simultaneously. The second phenomenon is entanglement which states that following the weak interaction, or 'correlation' of two objects with quantum states, despite those objects being separated and isolated, one can no longer describe the quantum state of one object without full mention of its counterpart.

For this 'correlation' of spins it is necessary to provide a conduit through which magnetic communication can occur. Various methods have been tried to provide such a pathway. QIP and its requirement are discussed in more detail in Section 2.3.

Common thread

The first attempted method was *via* simultaneous synthesis of two {Cr7Ni} rings about a single C_9 diammonium thread,[158] as in Figure 14.

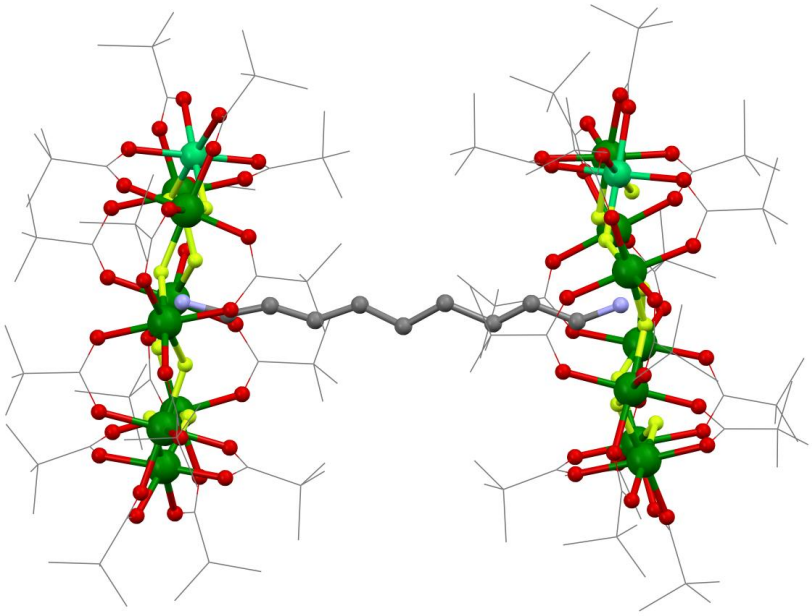

Figure 14 Structure in the crystal of {Cr7Ni}-$H_3NC_9H_{18}NH_3$-{Cr7Ni}. Colours: Cr, green; Ni, apple; C, grey (non-thread in wireframe); O, red; F, yellow. Hydrogen and solvent atoms omitted for clarity.[158]

Susceptibility measurements show the same results as for the single rings and EPR spectroscopy did not reveal the presence of an S = 1 state; both suggesting that there was no sizeable magnetic communication passing along the alkyl bridge. We might suppose this was because the exchange could not traverse the hydrogen bond region and/or because the sigma bonding between the carbons of the thread was not conducive to such a process.

More elegant structures with extended threads and larger rings were explored, largely for their beautiful aesthetics with a long term goal of creating a molecular machine. The result was a range of hybrid organic/inorganic rotaxanes, with a range of architectures, the most impressive being a [4]-rotaxane (shown in Figure 15), consisting of two rings simultaneously around two threads.[159]

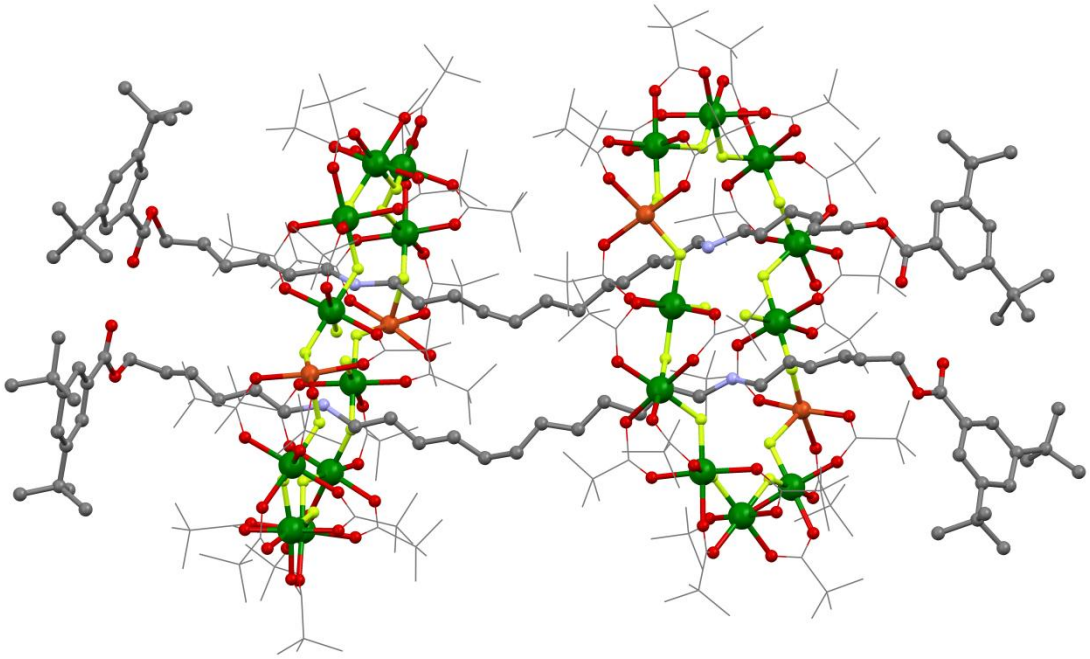

Figure 15 Structure in the crystal of the [4]-rotaxane comprising two {Cr10Cu2} rings about two long diammonium threads with bulky stoppers. Colours: Cr, green; Cu, orange; C, grey (non-thread in wireframe); O, red; F, yellow. Hydrogen atoms omitted for clarity.[159]

The lack of sizeable magnetic interaction in mechanically linked but non-bonded rings in close proximity does also tell us that any weak dipole communication through space does not lead to alteration in the magnetic properties of the rings, which is important if any control over the interaction is to be maintained.

Substituted carboxylate

A second way in which interaction between rings was attempted was by functionalisation of the rings with a 'tethering' moiety which could then be ligated to a new metal centre. This was achieved by substitution of a trimethylacetate for isonicotinate. The reaction in fact produces a statistical range of products with mono- and poly-substitution, which can then be separated by chromatographic techniques. Isolation of {Cr7Ni-isonicotinate} followed by reaction with $[Cu(NO_3)_2]$ or the dimer $[Cu_2(O_2C\textit{t}Bu)_4(HO_2\textit{t}Bu)_4]$ leads to two products consisting of rings with metal containing bridges, $[(NH_2\textit{i}Pr_2)(Cr_7NiF_8\{O_2C\textit{t}Bu\}_{15}\{O_2CC_5H_4N)\})_2][Cu(NO_3)_2(OH_2)]$, {Cr7Ni-Cu-Cr7Ni} and $[(NH_2\textit{i}Pr_2)(Cr_7NiF_8\{O_2C\textit{t}Bu\}_{15}\{O_2CC_5H_4N\})]_2[Cu_2(O_2C\textit{t}Bu)_4]$, {Cr7Ni-Cu2-Cr7Ni} respectively.[160]

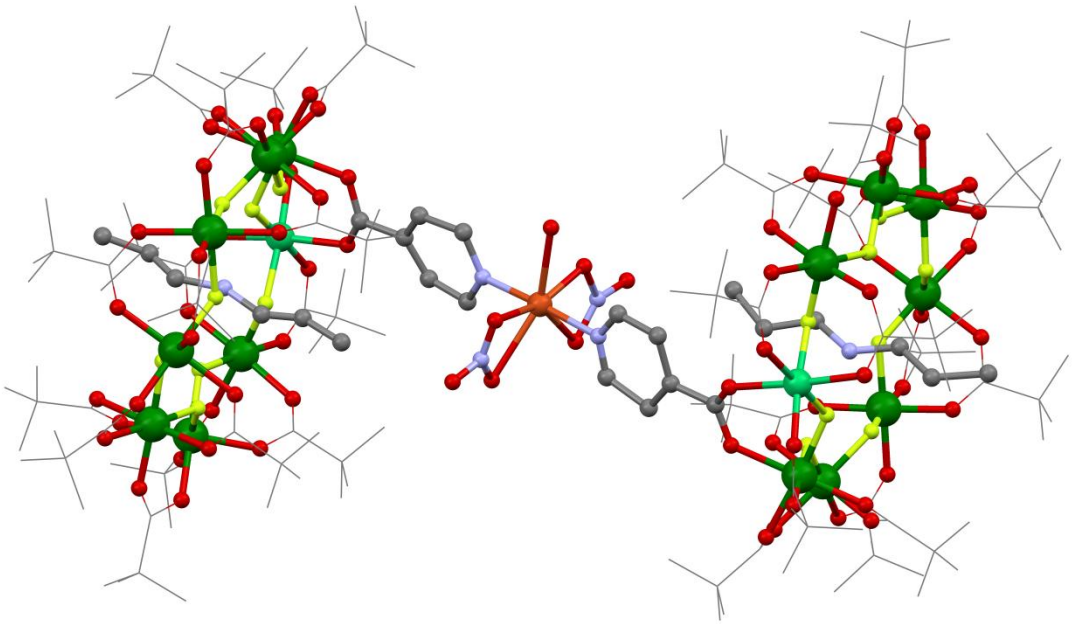

Figure 16 Structure in the crystal of {Cr7Ni-Cu-Cr7Ni}. Colours: Cr, green; Ni, apple; C, grey (non-thread non-bridge in wireframe); O, red; F, yellow. Hydrogen atoms omitted for clarity.[160]

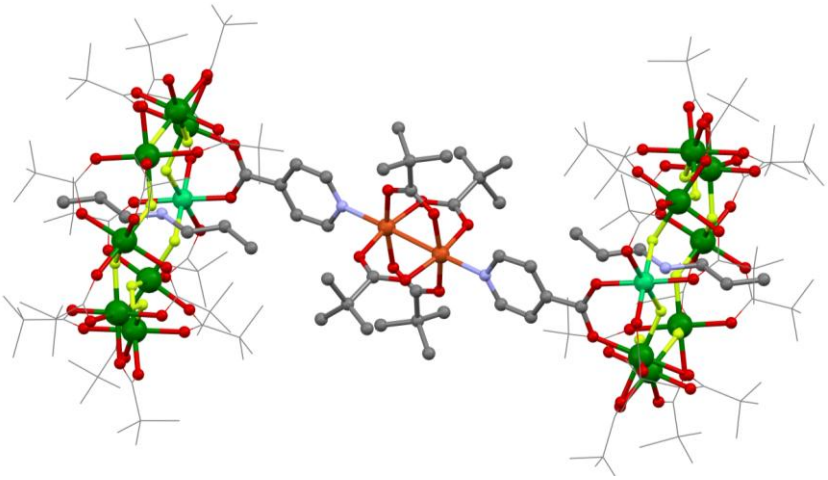

Figure 17 Structure in the crystal of {Cr7Ni-Cu2-Cr7Ni}. Colours: Cr, green; Ni, apple; C, grey (non-thread non-bridge in wireframe); O, red; F, yellow. Hydrogen atoms omitted for clarity.[160]

{Cr7Ni-Cu-Cr7Ni} can be described as a tripartite spin system, the Cu^{II}, d^9, s = 1/2 being a spin centre in its own right. There is magnetic communication between the spins such that there is full mixing of the spin states. In contrast the Cu dimer in {Cr7Ni-Cu2-Cr7Ni} exhibits antiferromagnetic exchange such that its net spin is zero in the ground state (ie. at very low T). The bridge is now magnetically insulating, so the rings are magnetically isolated.[160] Tuning of the dimer interaction such that it could be excited to a ferromagnetic state with a pulse of suitable frequency electromagnetic radiation could prove useful in the creation of a switchable bridge.

Purple rings

More recently a relative of {Cr7Ni} has been synthesised. Rather than templating around an alkyl ammonium, if the sugar *N*-ethyl-D-glucamine, $C_8H_{14}NO_5H_5$ (H_5Etglu) is introduced to the reaction mixture a new eight-membered ring is formed.[161]

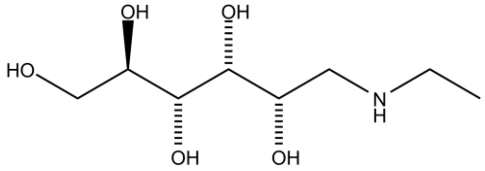

Figure 18 Schematic representation of *N*-ethyl-D-glucamine (H_5Etglu)

The ring consists of a cyclic array of seven Cr and one Ni. Each adjacent pair in Cr1-Cr6 are bridged internally by a μ-2 alkoxide (resulting from the pentadeprotonation of the polyol, H_5Etglu) and externally by two pivalates. Cr6-Cr7 and Cr7-Ni have an internal μ-2 fluoride bridge and again, two pivalates. Ni-Cr1 has an internal μ-2 fluoride bridge but only one pivalate. From the current description the ring is charge neutral but Cr1 and Ni are 5 coordinate. The sixth position on Cr1 is taken by the N of the sugar. The final position on the nickel centre is somewhat labile, and is occupied by coordination of charge neutral solvent in the solid state (labelled L in Figure 19). All metal ions possess a slightly distorted octahedral geometry. The change in crystal field due to bound alkoxide alters the optical properties; the ring now takes on a purple colour in solution and crystal. As a result these rings are commonly referred to as 'purple rings'. Other pseudonyms in circulation include 'sugared rings', 'sugared donuts' and 'glu-ed rings'. For our purposes this new ring shall be termed {Cr7NiEtglu}.

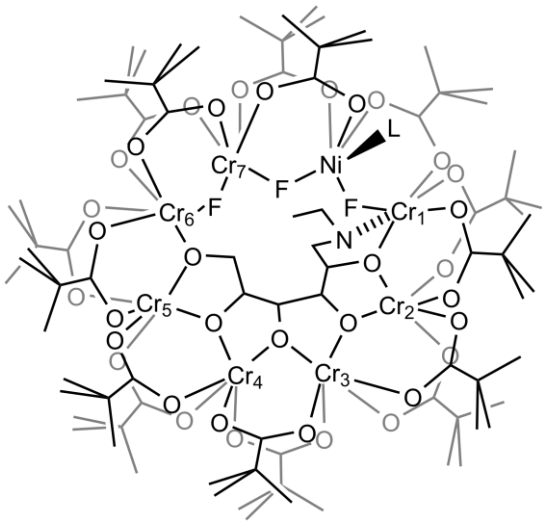

Figure 19 Schematic representation of {Cr7NiEtglu}, L = coordinating solvent

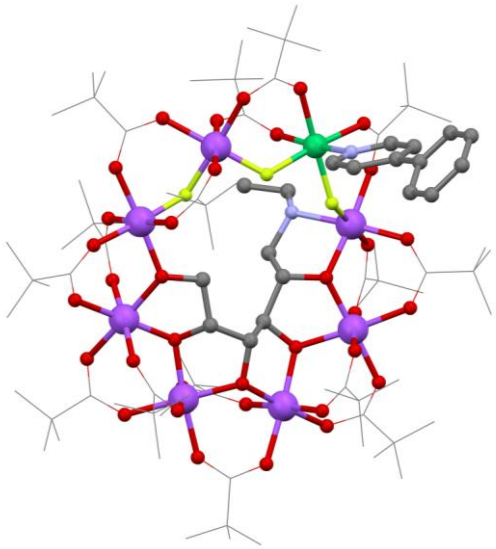

Figure 20 Structure in the crystal of {Cr7NiEtglu}-PyPh. Colours: Cr, purple; Ni, apple; C, grey (non-sugar non-ligand in wireframe); O, red; F, yellow. Hydrogen and solvent atoms omitted for clarity.[161]

The final means of ring-ring dimerisation is using the {Cr7NiEtglu} purple ring. The Ni position, occupied in the solid state by coordinating solvent molecules has a high affinity for sp^2 hybridised N lone pairs such as phenylpyridine (as in Figure 20). Creation of dimers is therefore straightforward, by employing bis-pyridyl type bridging ligands, for example 4,4'-bipyridine.

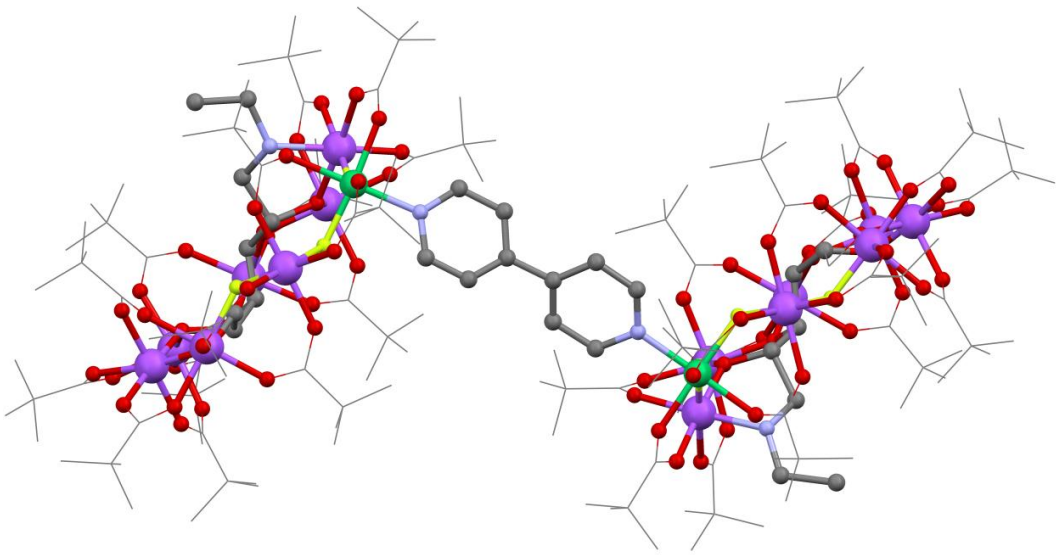

Figure 21 Structure in the crystal of {Cr7NiEtglu}-PyPy-{Cr7NiEtglu}. Colours: Cr, purple; Ni, apple; C, grey (non-sugar non-ligand in wireframe); O, red; F, yellow. Hydrogen and solvent atoms omitted for clarity.

Analysis by EPR for this dimer shows only an S = 1 state was observed below 10 K, demonstrating that the rings are interacting to generate a spin triplet and singlet, which are well separated from the other excited states.

2.3 Quantum information processing

Since the very conception of computing in 1936, with Turing's conceptual Universal Machine,[162] until very recently, all computer systems have operated under the conditions of 'classical physics'. In the macroscale world with which Turing was, and all of us are, immediately familiar these classical approximations hold true (of course Turing would not have considered them to be approximations!). In recent years, with a trend towards the miniaturisation of devices and increase in processing power, it is widely recognised that for further improvements (at least to maintain adherence to Moore's Law),[163] a paradigm shift is necessary since we are reaching an absolute limit in the size of transistors and power of microprocessors. This is because when one gets down to the nanoscopic level, the classical approximations tend to fall down, and we need to take into account quantum effects.

Though miniaturisation might be one factor, it is perhaps not the main driving force behind the quest for the creation of a QIP system. A quantum computer would be capable of calculations which are impossible for classical computers, even in principal (it is worth pointing out that 'classical computers' do of course obey the laws of quantum theory, however we do not consider them as quantum computers as they do not take advantage of quantum phenomena). For example the factorisation of a very large number, say 250 digits or more, into its base primes is extremely computationally intensive for a classical computer to the extent that it is intractable. That is to say that the outcome of such a computation would not be achievable in a reasonable timescale. It is our inability to perform this calculation which enables the data encryption method devised by Rivest, Shamir and Adleman; so called RSA public key encryption.[164] By contrast, a QIP system operating Shor's quantum algorithm could solve the problem in polynomial time,[165] that is to say that it is reasonably achievable on a sensible time-scale, as opposed to exponential algorithms which grow too fast to be computable.

Another commonly cited example is Grover's Algorithm (GA);[166] current computers are adept at searching for a name within a 'phonebook as the entries are listed alphabetically, however searching for a 'phone number within a 'phonebook takes

much longer since each entry must be checked individually, the so-called Classical Walk (CW). GA allows a quadratic speed up of non-ordered database searching by large scale matrix multiplications. So whilst CW on average takes N/2 iterations to reach a target, GA requires only √N. Even before Shor's 1994 suggestion of a quantum algorithm, Feynman had recognised that classical computers were not capable of simulating quantum events.[167] He proposed that the best way to model a quantum system was with another quantum system, he called this a 'quantum simulator', (QS). In 1985 David Deutsch took his ideas a step further, proposing a universal quantum computer (UQP).[168]

2.4 Quantum phenomena

There are two key phenomena arising from quantum theory of which one must be familiar to understand the operation of a QIP system.

Superposition

Classical computing deals in terms of bits, having one of two possible states, arbitrarily termed 0 or 1. Qubits are similar in this respect taking the value $|0\rangle$ or $|1\rangle$. However it is possible for a qubit to take both values at the same time. We may choose to formulate this combination of states into:

$$|\psi\rangle = \alpha|0\rangle + \beta|1\rangle \qquad \text{Eq. 1}$$

Where α and β represent the amplitude of the states and ψ is the quantum state, or wavefunction. Their values must normalised according to:

$$|\alpha|^2 + |\beta|^2 = 1 \qquad \text{Eq. 2}$$

As such one can consider the squared absolute amplitudes as probabilities, but must then bear in mind that α and β are complex, composed of both a real and imaginary part.

Under this approach we can consider a classical bit to possess a certain state with probability of 1.

Following Deutsch's approach, it might be preferable to adopt Hugh Everett's "Many-Universes Interpretation".[169] In doing so it is necessary to consider that the universe with which we are familiar is only a slice of reality as a whole and there exists a number of universes which co-exist with ours. In one universe a qubit might possess the eigenvalue $|0\rangle$, whilst in another $|1\rangle$. In this way the qubit has both values at the same time.

Under this interpretation, classical computations can be considered to be working within a single universe only. Deutsch would see the realisation of quantum computing as affirmation of his 'Multiverse' hypothesis.[170] Regardless of interpretation, described above is the quantum phenomenon known as superposition.

Verschränkung

Suppose two objects exist, each with their own quantum state. If they are 'brought together' (not necessarily spatially) such that they may weakly interact, termed 'correlation', and then isolated, the state of neither object can be described without mention of its counterpart. Schrödinger described this phenomenon as Verschränkung, or 'entanglement'.[171] For example two qubits could be 'anti-correlated' such they take values $|0\rangle$ and $|1\rangle$ and then isolated and spatially separated. Superposition means that each qubit still has an undetermined eigenvalue. Upon measurement of one qubit whose value is $|1\rangle$ the wavefunction of the second qubit simultaneously collapses to $|0\rangle$. Since the phenomenon of entanglement is independent of distance and collapse of the second wavefunction is instantaneous, one must deduce that the information is communicated faster than the speed of light. This appears to contravene Einstein's Theory of Relativity, a cause of concern for both scientists at the time. Entanglement enables quantum processing to become more efficient by allowing multiple states to be acted on simultaneously.

2.5 Qubit construct

A qubit must have a 'Boolean Observable', that is they possess a quantum observable whose spectrum contains exactly two elements, $|0\rangle$ and $|1\rangle$. Quantum computing operating systems should also conform as far as possible to a list of requirements laid out by David DiVicenzo. They are known as "The DiVicenzo Criteria":[172,173]

1) A scalable physical system with well characterized qubits
2) The ability to initialize the state of the qubits to a simple fiducial state, such as $|000\ldots\rangle$
3) Long relevant decoherence times, much longer than the gate operation time
4) A "universal" set of quantum gates
5) A qubit-specific measurement capability

With the immense power that quantum computing has to offer, the race is on to rationalise, design, synthesise and test a working prototype system. Below is a far from exhaustative list of promising leads:

- Nuclear spin[174]
- Trapped ions[175]
- Neutral atoms in an optical lattice[176]
- Cavity QED with atoms[177]
- Linear optics[178]
- Josephson junctions[179]
- Electrons on liquid helium surfaces[180]
- Silicon carbide,[181] diamond[182], fullerene[183] and nanotube[184] based
- Quantum Dots[185]

2.6 Realisation of a molecular spin-based qubit system

In 2001, Leuenberger and Loss published a paper in Nature entitled, 'Quantum computing in molecular magnets'.[186] The article proposed that quantum information processing could be performed using magnetic molecules, citing {Mn12}[187,188] and {Fe8}[189,190] as the most promising candidates of the time. {Mn12} is perhaps the most famous of all magnetic molecules. Its moderate size spin (S = 10) and high negative anisotropy (D value) lead to a large energy barrier between ± m_s states. (It should be noted that whilst the size of this energy barrier is equal to the anisotropy multiplied by the square of the total spin, large spins are invariably accompanied by low anisotropy and as such molecules with moderate spins tend to have higher barriers to the reversal of magnetisation.) A molecule with the ability to retain magnetisation in the absence of an applied field is termed a single-molecule magnet (SMM). Being an SMM is not strictly a requirement of a qubit; the only requisite is that the quantum state is long enough lived that there is time for the calculation/manipulation to be carried out and the output read (*i.e.* they should have a fairly long decoherence time). In fact {Mn12}'s properties as SMMs make them more suitable candidates for data storage than for computation.

A series of {Mn4pyramid} clusters was first synthesised in 1987[191] and investigated as a biomimetic for the study of water oxidation in photosystem II.[192] Its magnetic properties were studied further and its discovery as an SMM[193] attracted much interest from the field. The complex with highest relevance to our study is $[Mn_4O_3Cl_4(O_2CEt)_3(NC_5H_5)_3]_2$ which crystallises as hydrogen bonded dimer.

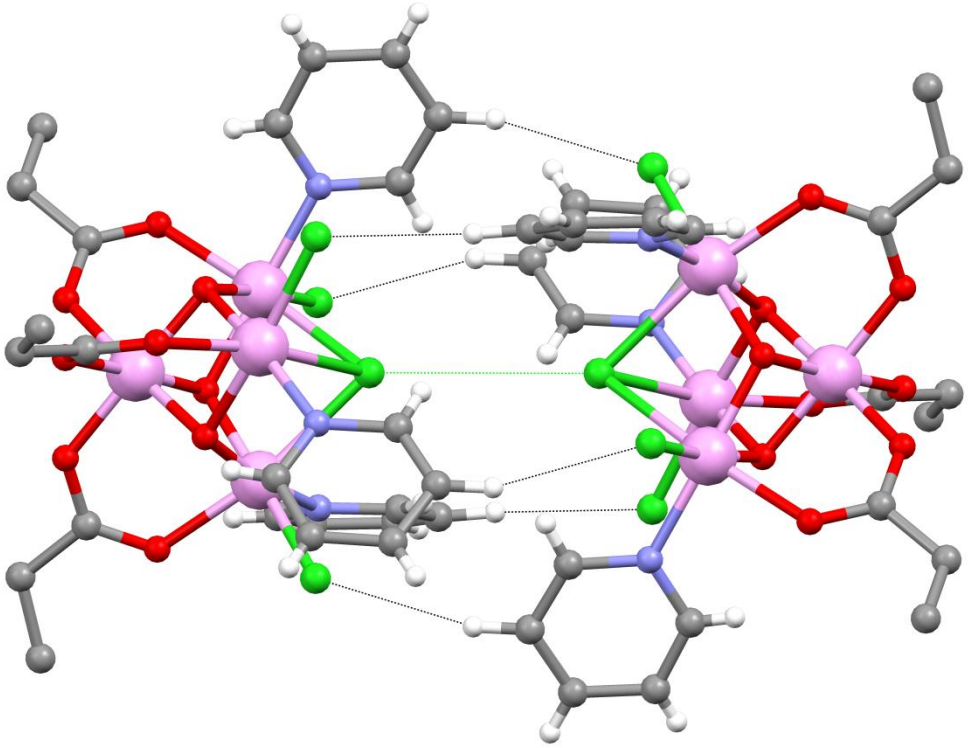

Figure 22 Structure in the crystal of [Mn4pyramid]2. Six Cl-H hydrogen bonds shown as black dotted lines. The long Cl-Cl contact is shown in dotted green. Colours: Mn, pink; C, grey; H, white; O, red; Cl, green. Non-pyridyl hydrogen and solvent atoms omitted for clarity.[193]

Consideration of entanglement of the spin states was reported subsequently.[194,195,196] These studies found that the [Mn4pyramid] clusters consisted of three octahedral Mn^{III}, d^4 l.s., $s = 1$ and one octahedral Mn^{IV}, d^3, $s = 3/2$, which all interact ferromagnetically to generate a well isolated $S = 9/2$ ground state for the species. Seven possible pathways exist for intermolecular exchange between [Mn4pyramid] clusters within the dimer. There is one long contact between μ_3-chlorides (3.86 Å) and six hydrogen bond interactions between the terminal chlorides on one cluster and pyridyl hydrogens (position 3) on the adjoining cluster (each 2.79 Å). The authors concede that each of these exchange pathways is weak, yet the sum effect is significant, in fact leading to an antiferromagnetic exchange and $S = 0$ for the supramolecular entity.

The {Mn4pyramid} does appear to be a useful cluster for studies of low dimensionality magnetism and as an SMM, as with {Mn12}. The magnetic coupling between units does not appear very amenable to tuning, limiting its appeal as a

potential qubit. The large spin values also increase the likelihood of through space dipolar interactions, which could minimise the ability to isolate them.

Other spin based molecular qubits which have been proposed include Aromi's $\{Mn4square\}_2$ system[197] and a set of lanthanide dimers[198]. Indeed the Aromi group has synthesised many interesting magnetic molecules including SMMs.

Takui has taken inspiration for the design of a QIP system from Lloyd's $(ABC)_n$ model.[199] His metal-oligoimidazole helicates[200] offer a somewhat different approach from that offered by Timco and Aromi, in that the electron spin which represents the qubit, is single ion based. The spin-centres are linearly arranged into polymers by oligohelicates. Qubit types (A, B or C) are individually addressable since each exists in a subtly different environment such that the resonant frequencies between their ground and excited states are all distinct. Furthermore the state of the adjacent qubits can alter this frequency. This builds a cellular automaton whereby information can be loaded, computed and read-out. Lloyd's proposal appears compelling, but its physical implementation has not been attempted other than by Takui.

Molecular spin based potential qubits are not limited to those containing metals as exemplified by the fullerene systems proposed by Harneit,[201] Lips,[183] Briggs,[202] amongst others, work and advances in the field being summarised in paper format in 2006,[203] and more recently in the thesis of Polad in 2010[204] with the follow up book in 2011.[205]

Another proposed inorganic spin-based molecular qubit, and subject of this thesis, is {Cr7Ni}/{Cr7NiEtglu}. Like the {Mn4pyramid} it has a well defined, and well isolated ground state and is bigger than a single ion complex; architectures on the nm scale seem to offer greater scope for addressability, for example by application of a local magnetic field from an AFM tip. Unlike {Mn4pyramid}, the Cr-Ni array has a small spin ground state (S = 1/2), and a multitude of routes to functionalisation with different exchange conduits. This allows tuning of the interaction, but also offers the possibility of generating arrays of spin centres in 1-, 2- or 3-D; truly a scalable system.

Intialisation of these spin-based qubits seems achievable by application of uniform field over the entire array.

Stability of the spin-state or maintainance of phase is clearly important for reliable measurement (computation). The phase decoherence of {Cr7Ni} is possible by two well established mechanisms, firstly spin-lattice relaxation (T_1), which studies have found to be long and temperature dependent; 2.9 μs at 4.5 K rising to 5.3 μs at 4.0 K.[206] Secondly spin-spin relaxation (T_2) or phase decoherence, which is the more dominant process. Spin-spin relaxation of the s = 1/2 electron can be effected through spin 1/2 nuclei. It was originally assumed that both fluorides and protons would cause a shortening in T_2, but it appears that the protons are the main channel for such decoherence. Improvement of T_2 was thus predicted, and realised, by perdeuteration of {Cr7Ni} to generate {Cr7Ni-^{2}D144}, T_2 rising from 0.55 μs to 3.8 μs at 1.8 K.[207] These two relaxation pathways, along with some more minor contributors, give rise to empirical 'phase-memory time' T_m, which may be the most convenient parameter when considering total coherence lifetimes,[208] for {Cr7Ni} $T_m \approx 360$ ns.[206] The requirement of decoherence is merely that that the states are long enough lived that they may be manipulated before degradation. The time scale for such manipulations is reckoned to be in the order of 10 ns, which is at least two orders or magnitude less than the proposed phase-memory time.

From the above discussion it can therefore be argued that three of the five DiVicenzo Criteria are fulfilled by {Cr7Ni}. Efforts to create a set a quantum gates are currently underway. The capability of qubit specific measurement appears to require that our rings are fabricated into an addressable array. For these purposes methods are being developed for the deposition of {Cr7Ni} by solution methods on Au (111)[209] and UHV sublimation of rings on Au (111)[210] and graphite[211] surfaces.

Chapter Three - Aims

The aims of this project fall into two broad categories; firstly to investigate the magnetic interaction of {Cr7NiEtglu} rings. This will be achieved by rational design and synthesis of a series of organic bridges with imine functionality, such that they may bind to the labile coordination position on the nickel centre. Upon successful synthesis of ring dimers bridged by these new ligands, they will be structurally characterised by traditional methods, but with a high dependency on single crystal X-ray diffraction. Their interaction will be investigated primarily through in-house multi-frequency EPR spectroscopy, but also in collaboration with other research groups who have expertise in micro-SQUID magnetometry and theoretical calculations including density functional theory (DFT). By comparing the bridge functionality and structural metrics gained from crystallography against the observed magnetic exchange, it is hoped that some hypotheses may be drawn on the requisites for attaining measurable spin-state mixing. These would then be tested empirically by the design and measurement of new dimers in attempt to lend more support to the proposed theories. In doing so it is hoped that a better understanding of how one might tune the interactions such that they may be of use within a quantum information processing system.

The second broad theme is to investigate the scope for inclusion of different cationic guests within $[Cr_7M^{II}F_8(O_2C\textit{t}Bu)_{16}]^-$ rings. Initially the inclusion of small alkyl ammomiums will be investigated and their structure determined both in the solid (by single crystal X-ray diffraction) and solution state (by ^{1}H NMR). The stability of the guests and scope for their substitution will be probed and the possibility of introducing inorganic cations explored. The synthesis of rings about larger dialkyl ammonium guests will also be investigated with a view to investigating the NMR of the resulting rotaxanes, and if possible determining some molecular dynamics in solution.

Chapter Four - Measurement methodologies

4.1 NMR [212] [213] [214] [215] [216]

Nuclei possess nuclear angular momenta, **I**, whose magnitudes are quantised according to $\hbar\sqrt{I(I+1)}$.

Where *I* is the angular momentum quantum number (or nuclear spin) and is specific for each type of nucleus and takes integer or half integer values; and ħ is the Dirac constant or reduced Planck constant. Each nucleus possesses the corresponding *2I+1* magnetic quantum numbers, *m*, in the range *+I* to *–I* according to:

$$m = I, I-1, I-2, \ldots -I+2, -I+1, -I \qquad \text{Eq. 3}$$

These levels are projected onto an arbitrary axis (*z*) according to:

$$I_z = m\hbar \qquad \text{Eq. 4}$$

Where I_z is the *z* component of **I**. This is illustrated in Figure 23:

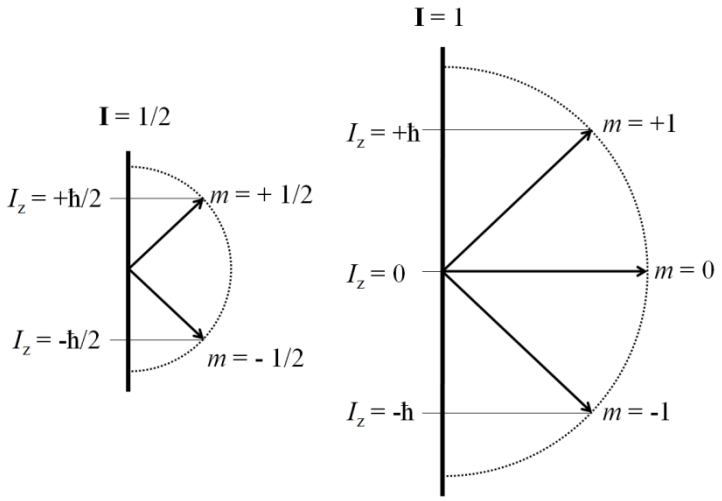

Figure 23 Directional quantisation of angular momentum for a *I* = 1/2 and *I* = 1 nucleus

The magnetic moment of a nucleus, μ, is directly proportional to **I** by the gyromagnetic ratio, γ:

$$\mu = \gamma \mathbf{I} \qquad \text{Eq. 5}$$

In the absence of a field the orientations are degenerate, but on application of a field, $\mathbf{B}_0$, the energy states separate in energy to give multiple nuclear Zeeman levels. The energy of the dipole, Ɛ, is given by the product of the magnetic moment with the applied field:

$$\varepsilon = -\mu_z B \qquad \text{Eq. 6}$$

Where *B* is the magnitude of $\mathbf{B}_0$. Rearranging Eq. 5 to $\mu = \gamma I_z$ and combining with Eq. 4 and Eq. 6, we find:

$$\varepsilon = -m\hbar\gamma B \qquad \text{Eq. 7}$$

Permitted NMR transitions are integer steps between *m* states, ie. between adjacent energy levels:

$$\Delta m = \pm 1 \qquad \text{Eq. 8}$$

Irradiation with light, *h*ν, is capable of stimulating excitation/absorption (a in Figure 24) and relaxation/emission (e in Figure 24) between two states separated by an energy (ΔƐ). The dominant process is dictated by the population distribution between the two levels. If the ground state population (N_α) is greater than that of the excited state (N_β), the absorptive mechanism prevails. If $N_\alpha = N_\beta$ then the processes compensate each other, a situation termed 'saturation'. The actual population need only be very small for NMR to be effective. Typically $N_\alpha / N_\beta \approx 1.000003$, which demonstrates the sensitivity of the technique. The small population variance is a result of ΔƐ being much smaller than $k_B T$.

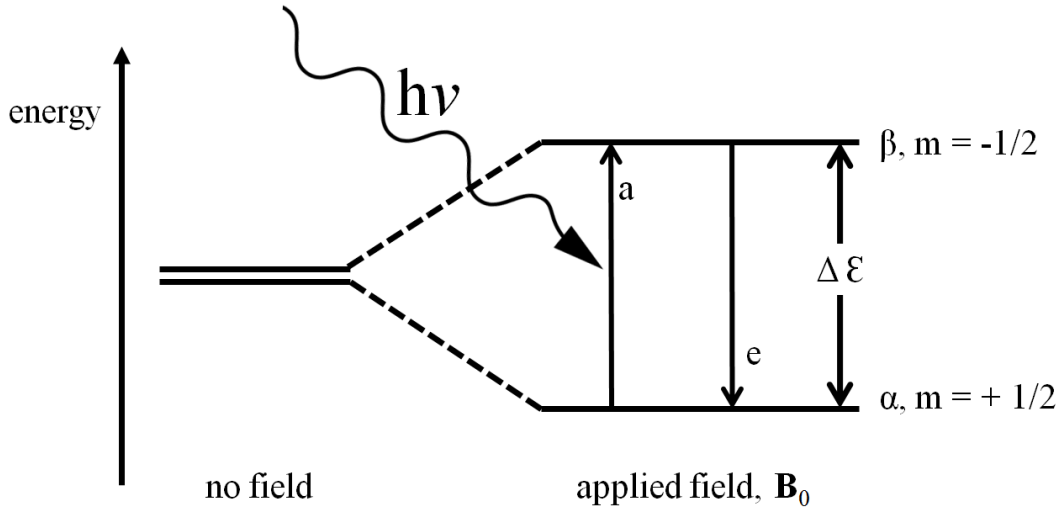

Figure 24 Energy level diagram showing transitions effected by irradiation for nuclei with $I = ½$.

Combining Eq. 7, Eq. 8 and $\Delta\varepsilon = h\nu$ we find:

$$\Delta\varepsilon = h\nu = \hbar\gamma B \qquad \text{Eq. 9}$$

or

$$\nu = \frac{\gamma B}{2\pi} \qquad \text{Eq. 10}$$

Thus by sweeping a sample through a range of frequencies we can find the local field which a certain nucleus is experiencing. Following this one might expect all, say, protons to give a signal at the same frequency, however the field each experiences is not precisely the same as the field applied by the instrument. The effective field a proton experiences (B_{eff}) is dependent on its environment:

$$\boldsymbol{B}_{eff} = \boldsymbol{B}_0 - \sigma\boldsymbol{B}_0 \qquad \text{Eq. 11}$$

Where σ is the shielding constant imposed by the surrounding nuclei and electrons. This results in a new equation:

$$\nu = \frac{\gamma \boldsymbol{B}_0(1-\sigma)}{2\pi} \qquad \text{Eq. 12}$$

The sign of σ is usually positive, though not always. Negative values of σ are frequently experienced due to aromatic ring currents and, significantly for our investigations, paramagnetic effects.

The result is that each unique chemical environment imposes a slightly different field on the target nucleus from that being applied, as such the frequency at which excitation of each nucleus also differs. This variation is termed the 'chemical shift'.

Since the absolute chemical shift varies according to the field being applied, values are quoted as compared with a reference nucleus. The values are made easier to handle by introduction of a scaling factor:

$$\delta = 10^6 \frac{(\nu - \nu_{ref})}{\nu_{ref}} \qquad \text{Eq. 13}$$

The chemical shift (δ) is therefore quoted in parts per million or ppm. The reference nucleus for ^{1}H and ^{13}C NMR is usually that of tetramethylsilane (TMS) which possesses 12 protons in identical chemical environments and just one carbon environment. Nuclei de-shielded more strongly than those in TMS (and most of them are) take positive value and more shielded ones, negative values. Calculating predicted chemical shifts from first principles is extremely complicated for anything other than the very smallest of molecules, but from empirical observation a well established database of typical shifts has been generated for common functional groups.

There are two mechanisms by which unpaired electron can influence the appearance of NMR spectra. Firstly nuclei very close to a paramagnetic centre may experience a Fermi contact interaction causing a 'contact shift'. Such shifts occur because of the magnetic interaction occurring when an unpaired electron resides within the atomic nucleus. Contact shift in non-diamagnetically dilute solutions generally renders proximal nuclei as either grossly broadened and shifted or else totally absent from NMR spectra. The magnitude of contact shift is proportional to r^{-6}, where r is the distance between the paramagnetic centre and the nucleus of interest, the effect therefore falls away very rapidly with increasing separation. This interaction is also observed as hyperfine splitting in EPR spectroscopy.

Secondly, nuclei within a paramagnetic sample experience local fields associated with the unpaired electrons *via* a through space interaction, 'pseudocontact shift'. How the target nucleus is affected by the paramagnetic centre depends on its spatial positioning according to the equation:

$$\Delta_{pcs} = K \frac{3\cos^2\theta - 1}{r^3} \qquad \text{Eq. 14}$$

Where Δ_{pcs} is the pseudocontact shift parameter, K is a constant associated with the identity of the paramagnetic metal ion (found empirically), r is the distance between the paramagnetic centre and the target nucleus and θ is the angle between the effective symmetry axis of the paramagnetic moment and the vector defined by r. From the equation we can pull some key points. Firstly the influence is different for different ions (i.e. K varies for different ions). Secondly the effect of unpaired electrons falls with distance according to a r^{-3} relationship (much less than the r^{-6} relationship for Fermi contact shifts). Also the shift can be positive, negative or zero depending on the angle, θ.

The linewidths of NMR transitions are fairly narrow for most organic compounds thanks to the long lifetime of the excited state β, which is generally in the order of seconds. Linewidths for diamagnetic samples are broadened principally by spin-

lattice and spin-spin relaxation pathways. This is rarely of more than a minor annoyance and can, in fact, be very useful in probing structure (*via* the nuclear Overhauser effect) and molecular dynamics.

This is not the case for complexes containing paramagnetic centres. The unpaired electrons have extremely short relaxation rates (in the range of 10^{-6} to 10^{-13} s) and rapidly flip between orientations, imposing variable magnetic fields upon the target nuclei. This promotes rapid relaxation of the nuclei from their excited state. The line broadening arises as a result of the Heisenberg Uncertainty Principle:

$$\Delta\mathcal{E}\,\Delta t \geq \hbar \qquad \text{Eq. 15}$$

Where $\Delta\mathcal{E}$ is the energy transition between the ground and excited states and Δt is the uncertainty in the lifetime of the excited state. Substituting in $h\nu$ for the transition energy and expanding ħ, we find:

$$h\,\Delta\nu\,\Delta t \geq \frac{h}{2\pi} \qquad \text{Eq. 16}$$

Which reduces to:

$$\Delta\nu \geq \frac{1}{2\pi\Delta t} \qquad \text{Eq. 17}$$

So we see that the (minimum possible) linewidth, $\Delta\nu$, is inversely proportional to the uncertainty in the lifetime of the excited state. Clearly for a particular percentage uncertainty the corresponding absolute uncertainty, Δt, will be much smaller for shorter lifetimes. When this lifetime is reduced to single figure ms timescales, Δt is sufficiently small that it has a noticeable effect on $\Delta\nu$, and the consequently line broadening is observed in the NMR spectrum.

From the above discussion we can see that paramagnetic centres can have significant influences on NMR spectra. Techniques have been developed to exploit the pseudocontact shift for kinetic studies and elucidation of crowded or overlapping spectra by the use of 'lanthanide shift reagents'. Lanthanide complexes, particularly those of Pr^{III}, Eu^{III}, Tb^{III}, Dy^{III}, Tm^{III} and Yb^{III} are frequently used as auxiliaries, which bind weakly to Lewis base functionalities of the target complex. They are ideal since they induce large pseudocontact shifts without significant line broadening. Transition metals are rarely used since their line broadening often renders their spectra incomprehensible.

There is a general misconception that the ^{1}H NMR of highly paramagnetic compounds is of no or very limited value. The work contained in Chapters Nine, Eleven and Twelve serve to dispel this myth further. Indeed we demonstrate that very informative data can be obtained from complexes containing 24 unpaired electrons. That said, there are some caveats which must be considered:

• Any hyperfine splitting by coupling to other nuclei will be lost

• Peaks will be shifted both to higher and lower frequencies and the degree of shifting will be largely unpredictable, definitive assignment of the peaks may not be possible

• Peaks will be significantly broadened and the integral of each peak is not necessarily proportional to the number of protons residing in the corresponding environment

• Some peaks may be lost altogether

4.2 EPR [216 217 218 219]

Electron paramagnetic resonance (EPR) spectroscopy measures the energy difference between electronic states with different spin orientations. The principles are very similar to NMR. A single unpaired electron can take one of two orientations, up or down. In the absence of a magnetic field these two states are degenerate, however upon exposure to an applied field an electron which is aligned parallel to that field (m_s = -1/2) becomes stabilised and its counterparts aligned against the field become destabilised. The separation of states can be calculated according to the equation:

$$\Delta\varepsilon = m_s g \mu_B B \qquad \text{Eq. 18}$$

Where m_s is the magnetic spin quantum number, g is the Landé g-factor, μ_B is a constant relating to the Bohr magneton and B is the applied field.

This 'Zeeman interaction' creates an energy gap which can be probed by EPR spectroscopy. Whilst NMR employs radiofrequency radiation, the energy required for EPR is much greater, in the microwave range. Secondly NMR techniques typically use a static magnetic field and scan a range of frequencies; by contrast EPR generally uses a static microwave frequency and scans a range of fields, known as continuous wave EPR spectroscopy.

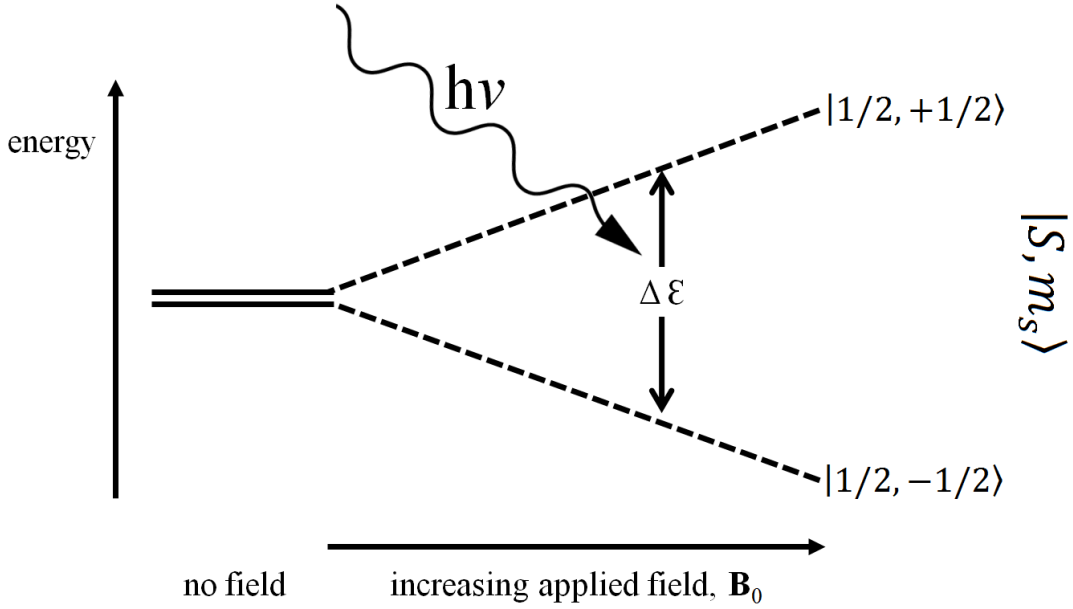

Figure 25 Energy level diagram showing the Zeeman interaction upon an S = 1/2 state

$$\hat{H}_{\mathrm{HDVV}} = -2J\hat{\mathbf{s}}_i\hat{\mathbf{s}}_{i+1} \qquad \text{Eq. 19}$$

The population of the m_s = -1/2 is higher than that of m_s = +1/2 simply because there is a Boltzmann distribution across the energy levels. Irradiation with suitable frequency light causes a net absorption of energy. The signal magnitude is proportional to the population imbalance, as with NMR. The EPR spectrum is the first derivative of this absorption:

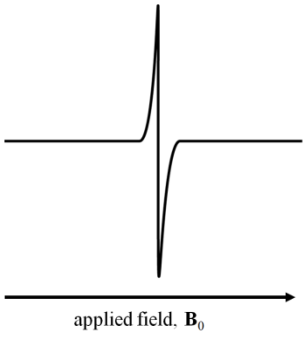

Figure 26 Simulated first derivative EPR spectrum for a single transition.

As so often encountered in coordination chemistry, particularly multimetallic complexes, we consider the case of more than one unpaired electron. The simplest system with two unpaired electrons, the spin-spin interaction generates both $S = 0$ and $S = 1$ states, separated by an energy gap, $2J$. The triplet ($S = 1$) level is composed of $m_s = 0, \pm 1$ states derived from the three possible arrangements of two spins. Intrinsically, these m_s levels are non-degenerate; their energy separation is defined as zero-field splitting (ZFS), indicated by the parameter D. These are similarly split in an applied field where the parallel set ($m_s = -1$) is stabilised relative to the antiparallel pair ($m_s = +1$):

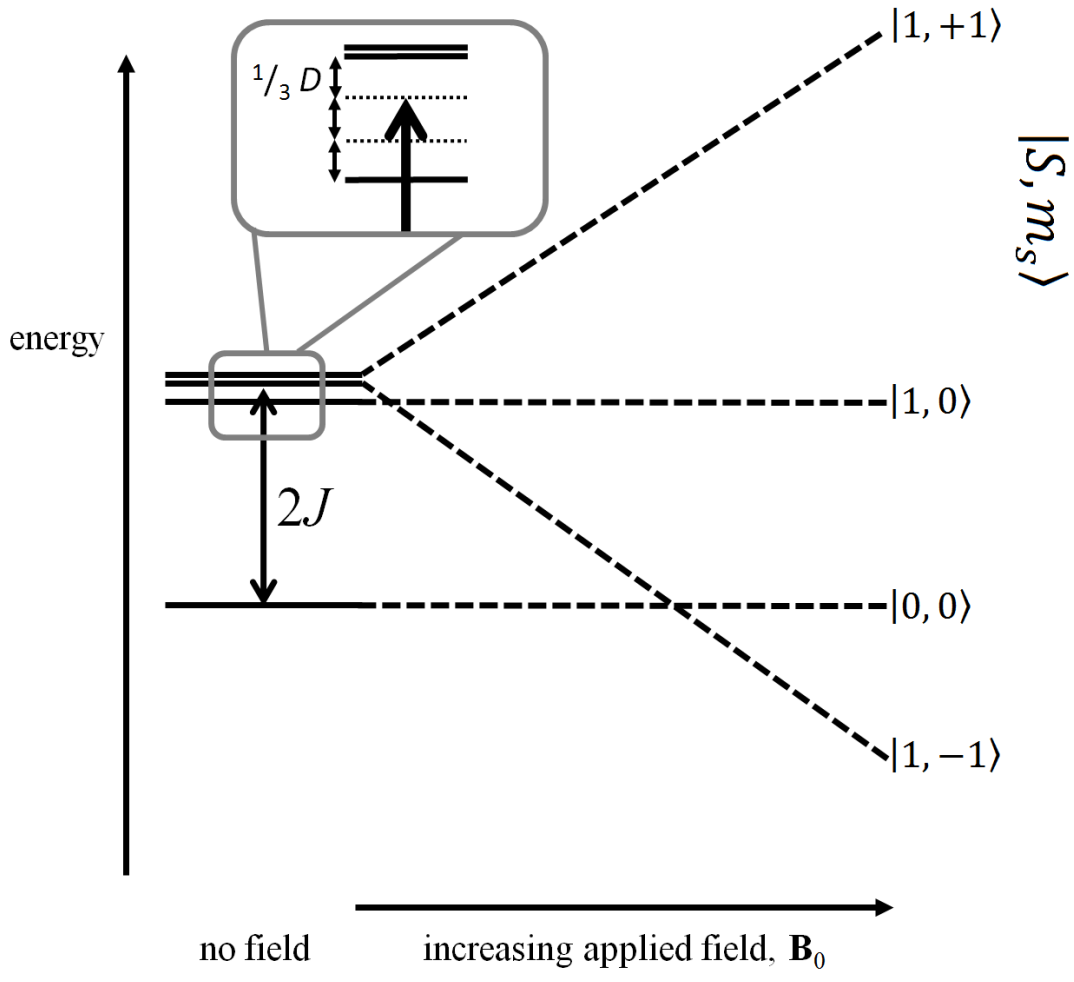

Figure 27 Energy level diagram showing the separation of states and their evolution on application of a field, for a positive D and negative J.

The spin-spin interaction in $S > 1/2$ is attended by the spin-Hamiltonian:

$$\hat{H}_{\mathrm{ss}} = \hat{\mathrm{S}} \cdot \mathbf{D} \cdot \hat{\mathrm{S}} \qquad \text{Eq. 20}$$

Where $\hat{\mathrm{S}}$ is the operator related to the spins concerned and **D** is a traceless tensor (Tr(**D**) = 0) whose diagonal elements, D_{xx}, D_{yy}, and D_{zz}, are defined by the ZFS parameters D and E; this second parameter describes anisotropy in the xy-plane:

$$D = D_{zz} - \frac{D_{xx} + D_{yy}}{2} \qquad \text{Eq. 21}$$

$$E = \frac{D_{yy} - D_{xx}}{2} \qquad \text{Eq. 22}$$

We often define the rhombicity as E/D, whose value can vary from zero (axial) to 1/3 (fully rhombic). D and E present themselves in the anisotropic term of the Hamiltonian as in Eq. 23:

$$\hat{H}_{\mathrm{D}} = D\left(\hat{\mathrm{s}}_{z,i}^2 - \frac{1}{3}\hat{\mathrm{s}}_i(\hat{\mathrm{s}}_i + 1)\right) + E\left(\hat{\mathrm{s}}_{x,i}^2 - \hat{\mathrm{s}}_{y,i}^2\right) \qquad \text{Eq. 23}$$

We can now consider the energy level diagram in Figure 28 (assuming $D < 0$). We can now see that EPR induced transitions m_s = -1 → 0 and 0 → +1 for a set frequency are no longer going to occur at the same field strength which leads to a doublet feature in the EPR spectrum.

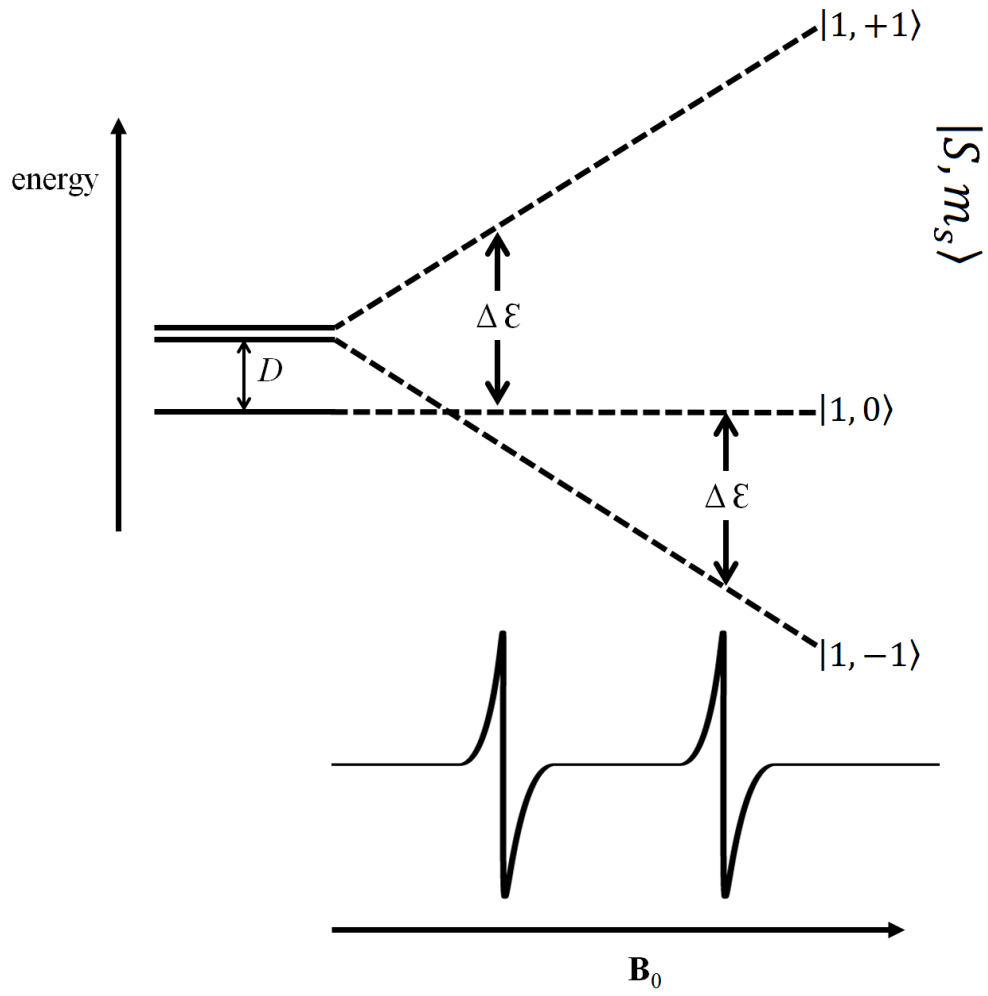

Figure 28 Energy level diagram showing the Zeeman interaction upon an $S = 1$ spin in the presence of any zero field splitting, where D is positive, and the resultant spectrum from the allowed transitions.

The isotropic exchange interaction, J, defining the energy gap between $S = 0$ and $S = 1$, is described by the Heisenberg-Dirac-Van Vleck (HDVV) Hamiltonian:

$$\widehat{H}_{\mathrm{HDVV}} = -2J\hat{\mathbf{s}}_i\hat{\mathbf{s}}_{i+1} \qquad \text{Eq. 24}$$

The HDVV Hamiltonian is a simple method of modelling the coupling of multiple unpaired electrons in an empirical fashion. For the scenario described in Figure 27, $J < 0$, but for a ferromagnetic exchange, $J > 0$. The magnitude of the exchange interaction is traditionally done directly by magnetic susceptibility measurements.

4.3 Magnetic susceptibility [220]

A microSQUID operates under the same principles as SQUID magnetometry, but at much lower temperature (often sub-Kelvin) and on smaller samples (usually very small single crystals).

SQUID magnetometers contain a large superconducting magnet which provides a uniform field in which the sample is magnetised. The sample is then oscillated perpendicular to the field within a superconducting detection coil through which a current is induced. By determination of the voltage of the induced current it is then possible to calculate the susceptibility of the sample. If we consider two interacting spins of equal amplitude and plot χT versus T, where χ is the susceptibility and T is the temperature, we might find one of three possible outcomes (J still being defined as in Section 4.2:

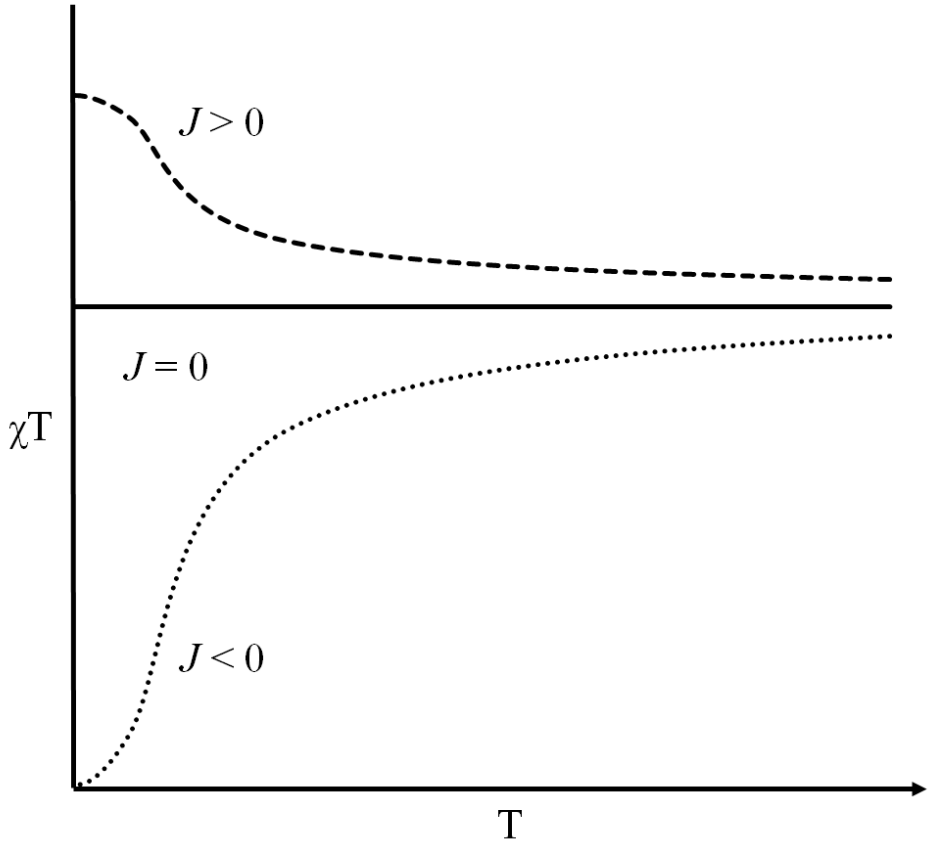

Figure 29 Simulated plot of the product of susceptibility and temperature against temperature for ferromagnetic, antiferromagnetic and non-interacting spins.

At low temperature the product χT minimises to zero for antiferromagnetic dimers (dotted line), saturates to a maximum for ferromagnetic dimers (dashed line) and there is no temperature dependency for non-coupled dimers (solid line).

For the very specific case of two weakly coupled S = 1/2 paramagnets (as arises in Chapters Six and Eight where the experiment is described; and also in Chapter Seven), one can determine the amplitude of *J* by the field dependence of the magnetisation, see Figure 30. The inflection point, best read from a first derivative plot (as inset in Figure 30), indicates the position of maximum rate in increase in magnetisation and correlates with the level crossing of the $|0,0\rangle$ and $|1,-1\rangle$ energy levels (cf. Figure 27).

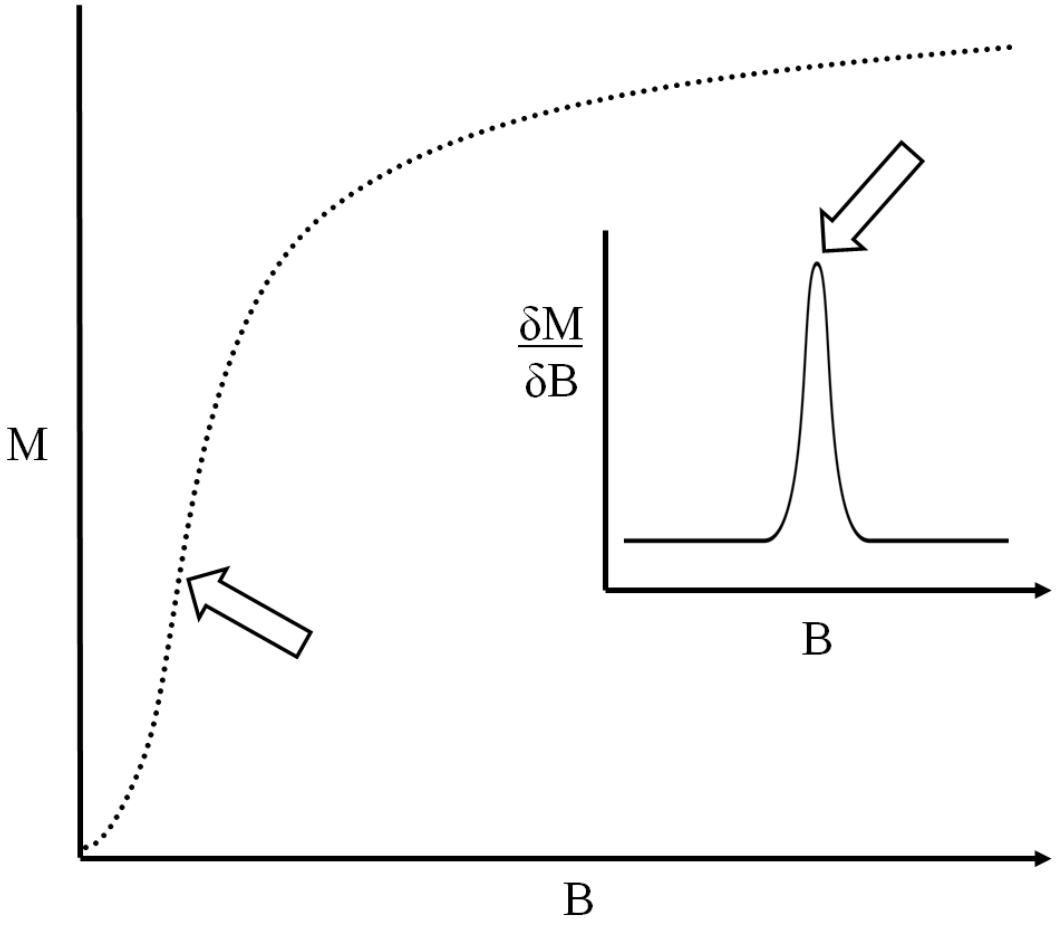

Figure 30 Simulated plot of magnetisation against field for an antiferromagnetic ground state and inset a derivative plot of the same.

Since:

$$\Delta\varepsilon = m_s g\beta B \qquad \text{Eq. 18}$$

And at the level crossing:

$$\varepsilon_{\langle 1|-1\rangle} - \varepsilon_{\langle 0|0\rangle} = 0 \qquad \text{Eq. 25}$$

So:

$$m_s g\beta B_{LC} = 2J \qquad \text{Eq. 26}$$

Where B_{LC} is the field at which the level crossing occurs. It is thus relatively simple to calculate J since m_s is known, g can be read straight from EPR data and β is a constant. (As a quick guide g ≈ 2 and β ≈ 0.5 $cm^{-1}T^{-1}$ so for m_s = -1; $-J$ (cm^{-1}) ≈ B_{LC} (T).)

4.4 X-ray crystallography [221] [222]

X-ray crystallography is perhaps the most powerful tool in solid state structure determination, providing valuable information on bond lengths/angles, symmetry and molecular packing. The caveats are that a good quality single crystal must be grown (not always trivial) and that the structure is only valid in the solid state.

The technique relies upon the diffraction of X-rays through parallel lattice planes running through a single crystal. Reflections off adjacent planes travel different distances between the source and the detector.

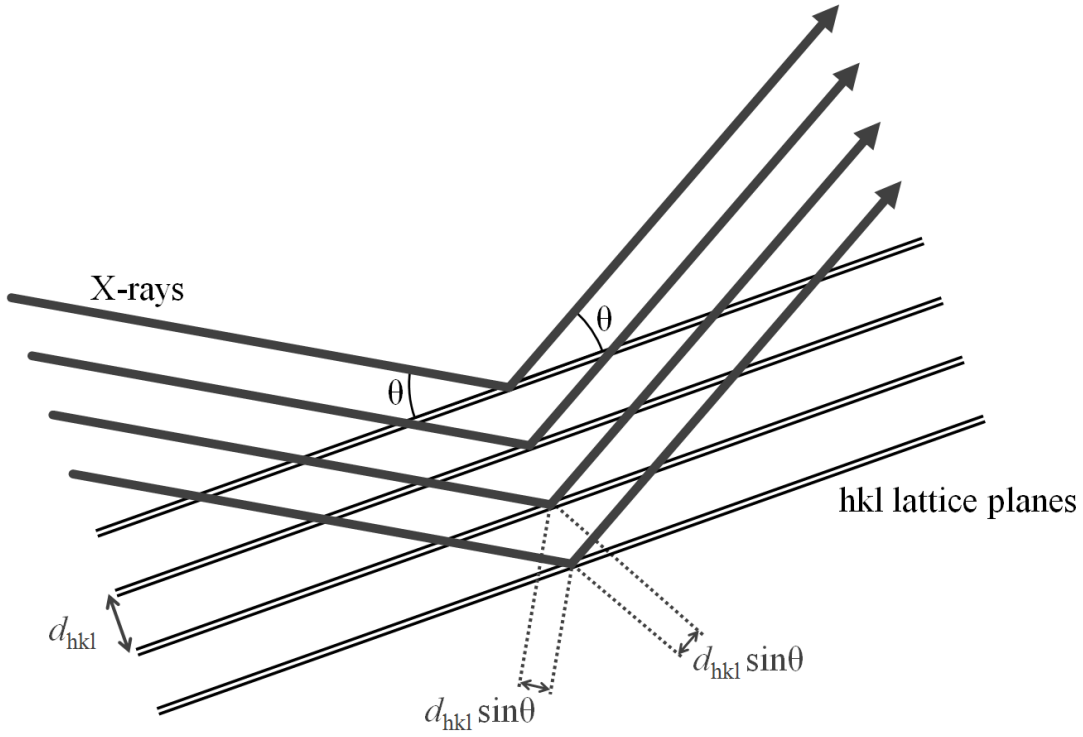

Figure 31 Illustration of Bragg diffraction and increased path length of the bottom beam over its neighbour.

So:

$$path\ length\ difference = 2d_{hkl}sin\theta \qquad \text{Eq. 27}$$

Where d_{hkl} is the separation between lattice planes and θ is the angle of the incident (or indeed reflected) ray from the lattice planes.

Only in-phase X-ray waves (i.e. with constructive interference) will create a pattern at the detector, so it follows that only integer values of the wavelength are important, so we can now consider:

$$2dsin\theta = n\lambda \qquad \text{Eq. 28}$$

Where λ is the wavelength of the X-ray radiation and n is an integer.

The actual diffraction pattern is a result of the summation of the diffracted beams with their associated amplitudes and phases. The pattern is therefore a Fourier transform (**FT**) of the electron density of the sample. To back-calculate the original electron density (and structure) one simply needs to perform an inverse Fourier transform ($\mathbf{FT}^{-1}$). In practice this is not straightforward because a diffraction pattern can tell you the intensity of each spot, but not its phase; this is termed the 'phase problem'. Crystallographers overcome the phase problem by one of three routes. 'Direct methods' work on the basis that all electron density must be positive (there is no such thing as negative electron density). It assumes that the reflections which contribute most to the Fourier transform must be in a positive phase, other phases are calculated by iterative trial-and-error cycles. The 'Patterson function', principally for structures containing heavy atoms, assumes all of the waves are in-phase to create a 'Patterson map' of electron density which indicates the spatial relationship of pairs of atoms. In the third technique, 'charge-flipping', the phases are randomly assigned generating an electron density grid. For any areas where electron density falls below a threshold level, the phase is flipped and the cycle repeats to convergence. Once the structure has been solved by one of these strategies, the structure must be refined manually. During this stage the crystallographer uses knowledge of possible structures and his/her chemical sense, to assign areas of electron density as certain atoms. Performing a (forward) **FT** on the proposed structure, and comparing the

calculated structure factor amplitudes, $|F_c|$, against the observed, $|F_o|$ allows an evaluation of the structure to be carried out:

$$R = \frac{\sum \big| |F_o| - |F_c| \big|}{\sum |F_o|} \qquad \text{Eq. 29}$$

where *R* is the 'residual factor'. The R-factor is thus a number from 0 → 1, zero indicating that the proposed structure would generate the exact pattern observed and numbers >0.5 indicating very little resemblance. Final R-factors are typically 0.04 - 0.08 for small molecules but maybe be higher for structures with large unit cells, those containing significant void space and crystals which diffract very weakly. A second measure of the fit is the 'weighted R-factor' which places greater weighting on the most reliable reflections (based on their standard uncertainty):

$$wR2 = \sqrt{\frac{\sum w(F_o^2 - F_c^2)^2}{\sum w(F_o^2)^2}} \qquad \text{Eq. 30}$$

Both of these values are normally quoted alongside crystallographic data.

The generation of X-rays is normally achieved with an 'X-ray tube'. These offer relatively high X-ray flux, are fairly cheap (circa £5000) and are small such that they may be used in instruments 2 m x 1 m. Weakly diffracting and very small crystals often need very high X-ray flux to achieve diffraction to high enough angles for good resolution. This necessitates the use of high intensity synchrotron light. In contrast to X-ray tubes these are very expensive and massive structures (for example DIAMOND Light Source synchrotron in Didcot, UK; 738 m in circumference, cost £383 million to build but produces X-ray light 100 billion times brighter than a standard laboratory X-ray tube).[223]

4.5 Electrospray time-of-flight mass spectrometry

Mass spectrometry serves to analyse molecular species by their mass. For electrospray, the analytes are dissolved in a solvent carrier, which is dispersed into fine aerosol through a highly charged nozzle. The charged droplets then evaporate to leave charged, solvent-free ions, which are accelerated towards a detector by counter electrodes. The time it takes to reach the detector is a function of its charge, Z, and mass, M. The output is a plot of counts (commonly normalised to a percentage) against (M/Z). Positive ions are generally the result of association with small cations such as H^+, Na^+ or K^+, whilst negative ions can be formed by association with ions like I^- or dissociation of H^+. Ionisation can also occur by partial fragmentation of the analyte. Multiple ionisations to form 2+ (or higher) charges are also possible, leading to peaks around the half mass region (remembering M/Z and Z = 2). Electrospray is a soft ionisation technique which means the integrity of the structure is mostly maintained, unlike hard techniques such as electron bombardment which cause major fragmentation. Other soft ionisation techniques are available, such as matrix assisted laser desorption ionisation (MALDI), but these tend not to work for the complexes reported in this thesis.

4.6 Elemental analysis

Elemental characterisation is achieved for carbon, hydrogen and nitrogen by combustion analysis where samples are burnt in oxygen and the masses of released carbon dioxide, water, and nitric oxide are measured. Metal analysis is achieved by inductively coupled plasma atomic emission spectroscopy (ICP-AES).

Chapter Five - Paper 1

"Linking heterometallic rings for quantum information processing and amusement"

G. A. Timco, T. B. Faust, F. Tuna and Richard E. P. Winpenny, *Chemical Society Reviews*, 2011, **40**, 3067-3075.

Chem Soc Rev

This article was published as part of the

Molecule-based magnets themed issue

Guest editors Joel S. Miller and Dante Gatteschi

Please take a look at the issue 6 2011 table of contents to access other reviews in this themed issue

Chem Soc Rev

Cite this: *Chem. Soc. Rev.*, 2011, **40**, 3067–3075

www.rsc.org/csr

TUTORIAL REVIEW

Linking heterometallic rings for quantum information processing and amusement†‡

Grigore A. Timco,*[a] Thomas B. Faust,[a] Floriana Tuna[a] and Richard E. P. Winpenny*[ab]

Received 20th October 2010
DOI: 10.1039/c0cs00151a

Linking polymetallic cages can be a method for creating new structures and new properties. In this *tutorial review* we use heterometallic anti-ferromagnetically coupled rings (AF-rings) as exemplars for three approaches that can be used to link cage compounds. The first of three routes involves an ion-pair interaction supported by hydrogen-bonding interactions, which allows the synthesis of hybrid rotaxanes among other materials. The second route involves functionalising the exterior of the AF-ring so that it will act as a Lewis base; complexes involving coordination of pyridine to bridging monometallic and dimetallic fragments are discussed. The third route involves creating a vacancy on one site of the AF-ring, and then using the ring as a Lewis acid. Di-imine ligands can then be used to link the AF-rings into dimers. A brief discussion of the physical properties of these systems is also included.

[a] *The Lewis Magnetism Laboratory, School of Chemistry, The University of Manchester, Oxford Road, Manchester M13 9PL, UK. E-mail: grigore.timco@manchester.ac.uk*
[b] *The Photon Science Institute, The University of Manchester, Oxford Road, Manchester M13 9PL, UK. E-mail: richard.winpenny@manchester.ac.uk*

† Dedicated to Prof. David Goodgame in celebration of his seventy-fifth birthday, with gratitude for an education in classical coordination chemistry that has proven remarkably applicable to supramolecular chemistry in the 21st century.

‡ Part of the molecule-based magnets themed issue.

Background

The idea that linking polymetallic cages together to make larger more complex structures is not a new one. For example, very beautiful work in this area was published by the Christou group back in the 1980s,[1] where they showed, for example, that a variety of approaches could be used to link tetrametallic manganese butterflies into octametallic cages.[2] In related recent work Roubeau and Clérac have used such linking to produce single molecule magnets, single chain magnets and molecular magnets that show unusual phase

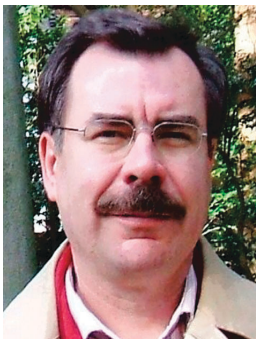

Grigore A. Timco

Grigore Timco completed his PhD research with Prof. Nicolae Gerbeleu at the Institute of Chemistry, Academy of Sciences of Moldova, Chisinau. He was successively Senior Scientific Researcher (1990–) and then Coordinator of Scientific Research (2000–) in the same institute. He obtained fellowships from the Royal Society to work with Prof. Winpenny, and from the Max-Planck Society and DAAD to pursue research with Prof. Karl Wieghardt and Dr Eva Rentschler at the MPI, Mülheim. The Danish Natural Science Research Council funded work with Prof. Finn Larsen (Aarhus). Since May 2003, he has worked in Manchester, as a senior researcher and since April 2008 as an Honorary Lecturer.

Thomas B. Faust

Thomas Faust received a master degree from the University of Sheffield in 2008 where his research, supervised by Prof. Mike Ward, concerned the solvothermal synthesis of octametallic coordination cages. After finishing there he swiftly moved across The Pennines to the University of Manchester where he is working towards a PhD and a European Doctorate in molecular magnetism. His work here, and for a short time at the Institute of Molecular Science, University of Valencia, Spain, involves the design, synthesis, characterisation and measurement of cyclic heterometallic clusters and arrays of clusters with diverse potential applications.

behaviour.[3] Sañudo *et al.* have also shown that {Mn_4} cages can be linked into weakly coupled dimers.[4]

We became interested in linking anti-ferromagnetically coupled rings (AF-rings) due to discussions with Prof. Marco Affronte, who suggested to us that we could use these rings in quantum information processing (QIP).[5] The QIP aspects of this work are reviewed elsewhere in this issue.[6] Here we concentrate on the chemistry that we thought about in designing methods for linking rings. The key consideration was to create methods that could be applied to a range of linkers. If QIP is to be implemented this way it is very likely we will have to meet very strict criteria for the exchange interaction between rings. Therefore the need to be able to tune the communication between rings is imperative. We are highly unlikely to create the correct structure first time, so an ability to modify the structure in a controlled and predictable manner is essential. Nothing we say is strikingly original, however we feel that the remarkable flexibility of these AF-rings is a great tool for teaching how to think about linking polymetallic cages.

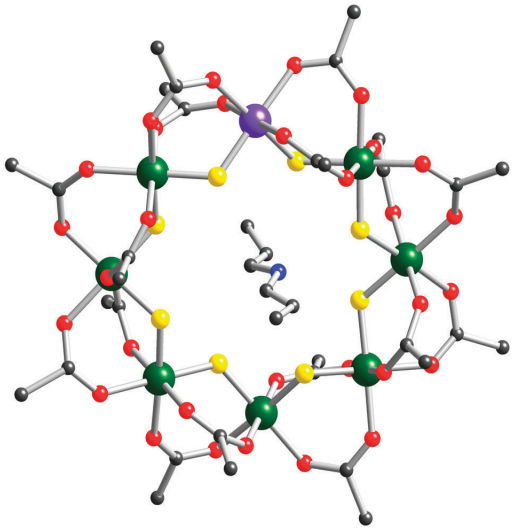

Fig. 1 The structure of $[NH_2Pr_2][Cr_7NiF_8(O_2C^tBu)_{16}]$ in the crystal. Me groups of pivalates excluded for clarity. Colours: Cr, green; Ni, purple; O, red; F, yellow; N, blue; C, black.

Heterometallic anti-ferromagnetic rings

There have been many beautiful reports of homometallic AF-rings, dating back to the seminal work by Gatteschi and Lippard *et al.* on the "ferric wheel".[7] In order to obtain AF rings with non-diamagnetic ground states we realised that targeting heterometallic rings was essential.[8] The method used was adapted from previous work initiated by one of us,[9] where a homometallic $[CrF(O_2C^tBu)_2]_8$ **1** ring can be made from hydrated chromium fluoride reacted with pivalic acid. If a secondary amine and a source of a divalent metal is added to this reaction a heterometallic ring is formed preferentially, with the general formula: $[NH_2R_2][Cr_7MF_8(O_2C^tBu)_{16}]$ (Fig. 1).[8] The structure of these AF-rings consists of an octagon of metal ions, with each edge bridged by a fluoride and two pivalates. The ammonium cation in the heterometallic versions sits at the middle of the ring, forming hydrogen-bonds to the bridging fluoride ligands.

The chemical driving force for forming the heterometallic ring is very simple: the product is an ion-pair and the coulombic attraction between the ammonium cation and the anionic AF-ring favours this product over the neutral molecular cage **1**. During synthesis **1** is formed as a by-product, but it can be separated from the heterometallic AF rings by chromatography. We have previously published some thoughts on how these rings form during synthesis.[10]

This illustrates an advantage of working with chromium(III)—it is an unreactive 3d-ion and hence allows us to use chromatographic separations readily. This isn't the case with many polymetallic cage compounds. The inertness of

Floriana Tuna

Floriana Tuna obtained her PhD in Inorganic Chemistry in 1998 from the Institute of Physical Chemistry of the Romanian Academy. She worked as a senior researcher at the Institute of Physical Chemistry 'Ilie Murgulescu' and teaching associate at the University of Bucharest before moving to the University of Heidelberg as a DAAD fellow in 2000. She did postdoctoral studies in molecular magnetism at ICMCB Bordeaux and held a Marie Curie Individual Fellowship in supramolecular chemistry at the University of Warwick (2001–2003), before moving to Manchester in 2003. Her interests are in molecular magnetism, EPR spectroscopy and quantum computing.

Richard E. P. Winpenny

Richard Winpenny obtained both his degrees from Imperial College, London; his PhD studies with Prof. David Goodgame involved synthesis of coordination polymers. After a period at Texas A&M University, working as a post-doctoral fellow with Prof. John Fackler, Jr., he moved to a lectureship at the University of Edinburgh. In 2000, after ten years in the frozen wastes of Northern Britain, he was appointed to the Chair of Inorganic Chemistry at the University of Manchester. He holds a Royal Society Wolfson Merit Award for his work in molecular magnetism.

chromium(III) also means that the AF-rings maintain their structure in solution, as we have been able to show using NMR spectroscopy[11] for the case where M = Co^{II}. The studies also indicate the enormous advantages pivalate gives as a carboxylate; the *tert*-butyl-groups give solubility in non-polar organic solvents, which removes any solvent interference in chemical reactivity making structures much more predictable than chemistry done in alcohols or even MeCN. The *tert*-butyl groups are also excellent for NMR spectroscopy as we have nine equivalent protons on each ligand.[11] It is worth stressing, the AF-rings and the oligomers of AF-rings we have made are stable in solution, as well as forming beautiful single crystals.

Elsewhere we have reviewed the vast range of carboxylates and templates that can be used in this synthesis.[12] Around forty carboxylates can be introduced in this reaction, creating AF-rings with a wide range of peripheries. We can also use different templates to make nine- and ten-membered rings.

A brief consideration of qubits

By comparison with classical computing, QIP uses "qubits" where classical computing uses "bits". In classical computing, a bit is either on or off, 0 or 1; in QIP a qubit is in a superposition of 0 and 1.[5] For a successful qubit the simplest requirement is that it is a two-level system; in molecular magnetism (or chemistry in general) this would simply mean a paramagnet with $S = 1/2$. The 0 and 1 of the qubit are then $m_S = +1/2$ and $m_S = -1/2$ respectively. For the heterometallic AF-rings, the $S = 1/2$ ground state rings are $\{Cr_7Ni\}$—which conveniently also have the highest chemical stability.[8] As the ground state is $S = 1/2$, the $\{Cr_7Ni\}$ rings give simple EPR spectra, with one resonance. This appears to be isotropic, but is best simulated as an axial spectrum with $g_{xy} = 1.78$, $g_z = 1.74$.[13] These g-values are unusual and this is due to the $S = 1/2$ state arising from anti-ferromagnetic exchange between the Cr^{III} and Ni^{II} sites. The result is that the g-value is given by: $g_{1/2} = 1.666g_{Cr} - 0.666g_{Ni}$;[14] as the g-values for a single nickel(II) ion will be greater than 2.00, and those for a single Cr^{III} will be around 1.98, the result is that the g-value we see for $\{Cr_7Ni\}$ rings is always around 1.80. This is remarkably useful because it allows us to use EPR spectroscopy to study whether the individual rings are speaking to one another; at a trivial level, if we observe a single broad resonance at $g = 1.80$ then we can assume that any ring···ring interaction is very weak.

The next question for a qubit concerns the coherence time, *i.e.* how long information is conserved in the qubit before being lost to the environment. Other spin qubits, such as endohedral fullerenes, exhibit spectacular coherence times, even approaching seconds.[15] There was some concern that in a complex molecular magnet coherence times would be short because of interactions between the electron spin and nuclear spins present in the molecule; such hyperfine interactions could easily lead to rapid relaxation and loss of information.

A method for measuring coherence times is pulsed EPR spectroscopy. By choice of pulse sequence we can measure the spin–spin and spin–lattice relaxation times, T_1 and T_2; T_2 is a reasonable measure of the coherence time. For $[(Et_2NH_2)(Cr_7NiF_8(O_2C^tBu)_{16}]$ we found that the coherence time at 4 K is 0.4 μs;[16] perdeuterating the sample (which we had originally done for inelastic neutron scattering experiments) raises the coherence times by a factor of six—suggesting that electron–proton hyperfine interactions are responsible for decoherence as this ratio is exactly the same as the ratio of the nuclear magnetic moment of the hydrogen and the deuterium nucleus.

This time is sufficient for spin manipulations, albeit it is shorter than we would like. The chemical manipulation of the coherence time, by changing H for D, is intriguing and suggests it could be possible to tune this coherence time further. This is on-going work.

Having established that the coherence times are sufficient for spin manipulation, the next step is to link qubits together to look to establish structures that could carry out computation. This is chemically a very interesting problem.

Analysing the structure of the AF-rings suggested that we had three possible routes to linking these cages. The first route would involve linking through the ammonium cation using H-bonding interactions, the second would require functionalisation of the carboxylate and the third would involve creating an accessible coordination site on the ring for facile monodentate ligand replacement reactions.

Links *via* the ammonium template

Our first attempt used the most trivial idea; we could grow the rings about any ammonium cation, so if we used a diamine we reasoned it should be possible to make a compound with two rings linked by the amine.[17] This works well if the alkyl-chain linked to the NH_2 groups is sufficiently long. The shortest chain that works is C_8, and a di-ring complex $[1,8\text{-daoH}_2]$-$[(Cr_7NiF_8(O_2C^tBu)_{16}]_2$ **2** can be made with 1,8-diaminooctane (1,8-dao) in the middle (Fig. 2). The spectra measured by EPR spectroscopy show a single broad resonance at $g = 1.80$, so there is no evidence for an interaction between the rings by this technique.[17]

We can take the chemistry a step further and use $EtNH_2CH_2py$ as the template. This leads to the AF-ring growing around the amine site, leaving the pyridine free for

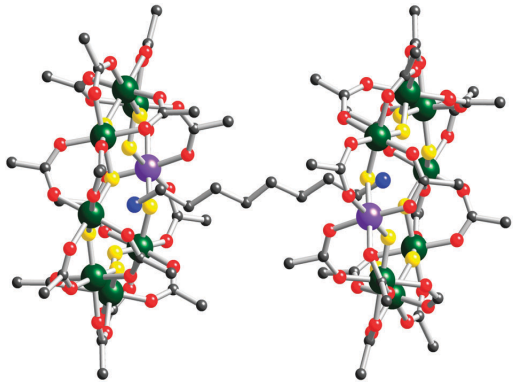

Fig. 2 The structure of **2** in the crystal. Me groups of pivalates excluded for clarity. Colours as in Fig. 1.

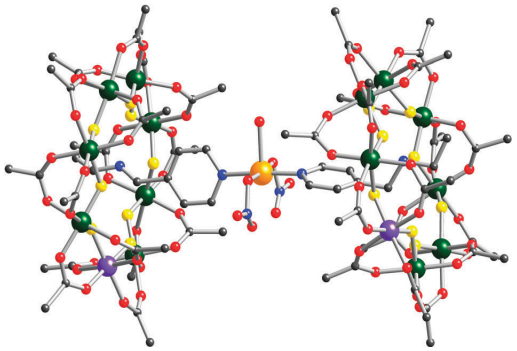

Fig. 3 The structure of $\{[EtNH_2CH_2py][Cr_7NiF_8(O_2C^tBu)_{16}]\}_2[Cu(NO_3)_2(H_2O)]$ in the crystal. Me groups of pivalates excluded for clarity. Colours as in Fig. 1, plus Cu: orange.

coordination. This can then be bound to a monometallic or dimetallic fragment to link the $\{Cr_7Ni\}$ rings. The structure bridged by $[Cu(NO_3)_2]$ is shown in Fig. 3;[17] EPR studies of this linked compound show resonances for an isolated copper ion, and separately the broad resonance at $g = 1.80$ for the $\{Cr_7Ni\}$ ring. We can conclude from the EPR studies that any interaction between spin sites is too small to be measured using this technique.

The structure of **2** led us to work with the Leigh group in Edinburgh, using their expertise in rotaxane chemistry to produce hybrid rotaxanes.[18,19] The Leigh group expertise in design of "threads" gave us a range of organic molecules about which we could grow rings (Scheme 1). This works spectacularly well, giving us hybrid rotaxanes with one ring on one thread, two rings on one thread and a remarkable [4]rotaxane with two rings on two threads (Fig. 4).[18]

NMR studies show that the AF-rings rotate rapidly about the organic thread, and studies of a [2]rotaxane containing two ammonium groups in the thread show that the rings move between the cationic "stations" at a rate of around 1.2 s^{-1}.[18,19]

Extending this work has involved studying the mechanism for formation of rotaxanes.[19] Adding Et_2NH to the reaction, prior to addition of the thread or the divalent metal, increases the yield of rotaxane. This is probably because the presence of Et_2NH in the reaction leads to formation of acyclic chromium fluoride chains—the best characterised examples are $\{Cr_6\}$ horseshoes where each Cr···Cr edge is bridged by a fluoride and two pivalates.[20] In the context of the rotaxane synthesis, these horseshoes clip over the organic thread, and the ring is closed and held in place by the large organic stoppers.

Hybrid rotaxanes can also be made directly from a one-pot "stoppering plus macrocyclisation" reaction.[19] Using bis-(hexamethylene)triamine in the reaction leads to a [2]rotaxane in one step, and in yields of up to 92%. The AF-ring grows about the central secondary amine site, while the primary terminal amines react with the pivalic acid solvent to produce amide groups at the end, with the *tert*-butyl groups acting as stoppers.

The simplicity of this reaction suggests that many further hybrid rotaxanes should be accessible. The relevance to QIP is that we will be able to create model compounds where the rings

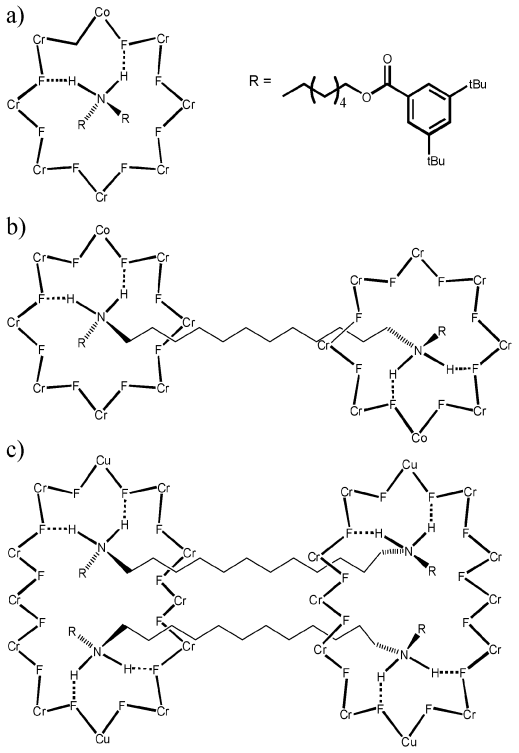

Scheme 1 Representations of the different forms of rotaxane. All μ_2 bridging pivalate groups have been omitted for clarity. (a) Single ring about a single thread; (b) two rings about a single thread; (c) two rings about two threads.

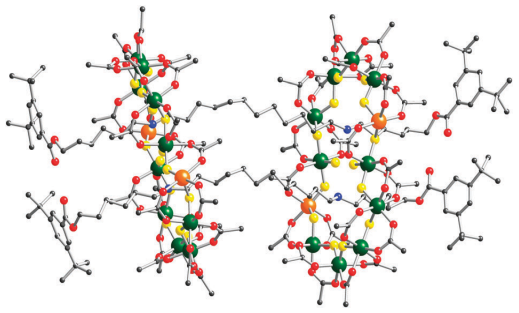

Fig. 4 The structure of a [4]rotaxane involving two organic threads and two $\{Cr_{10}Cu_2\}$ rings. Colours as in Fig. 3.

are held a specific distance apart, without there being a direct interaction between the rings. Coherence time measurements need to be carried out in a dilute matrix—a very dilute frozen solution is ideal—and therefore the interlocked structure of a [3]rotaxane is perfect as no matter how dilute we make the solution, the two AF-rings will not diffuse apart.

Further ideas such as creating different stations on the organic backbone so that we can move AF-rings around the thread in a controlled manner are being pursued.

Links *via* the carboxylate groups

Pivalate is an excellent carboxylate in many ways, creating high solubility in organic solvents. However it is entirely useless for linking rings together as there are no functional groups present. Introducing functional groups to the carboxylates became a significant target for our work.

The heterometallic nature of the $\{Cr_7M\}$ rings is absolutely ideal for this work. It has been known for many years that the rates of reaction of different 3d-metal ions depend on the electronic configuration of those ions. The +3 charge and high crystal field stabilisation energy, due to the d^3 configuration, of Cr^{III} makes it one of the least reactive 3d-metal ions. This can be seen by comparing the rates of water exchange on metal ions: for Cr^{III} the rate of exchange is 2×10^{-6} s^{-1}, for Ni^{II} the rate is 4×10^4 and for Mn^{II} or Zn^{II} the rate is faster still.[21] Reaction on a Cr^{III} site will be 10^{10} slower than reactions on a Ni^{II} site.

In a $\{Cr_7M\}$ ring we have four carboxylates that are bound to the M site. If a carboxylate displacement reaction is carried out we can be sure that it is one of these four carboxylates that will be displaced. Even these carboxylates are bound to chromium ions, so reaction conditions have to be forcing. Therefore if we dissolve a heterometallic ring in an organic solvent (*e.g.* toluene or propanol), and add a second carboxylate we can replace a pivalate with this new carboxylate after several hours refluxing. Chromatography allows us to separate the complex of formula $[NH_2R_2][Cr_7MF_8(O_2C^tBu)_{15}(O_2CR')]$ from the homo-carboxylate ring.

Using iso-nicotinic acid (HNic) leads to a compound where we have a pyridine ligand attached to the backbone of the ring (Fig. 5).[22] This pyridine can be used exactly like any other pyridine, albeit a very bulky pyridine containing fifteen *tert*-butyl groups on its periphery. We can react $[NH_2Pr_2]$-$[Cr_7NiF_8(O_2C^tBu)_{15}(Nic)]$ **3** with a range of monometallic or dimetallic fragments, introducing a wide range of potential bridges.

If reacted with hydrated copper nitrate we produce a compound with a single spin in the bridge (Fig. 6).[22] This

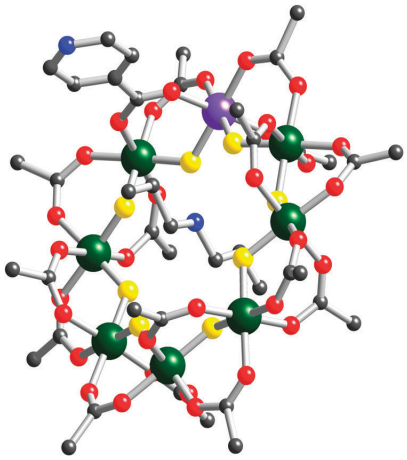

Fig. 5 The structure of **3** in the crystal. Me groups of pivalates excluded for clarity. Colours as in Fig. 1.

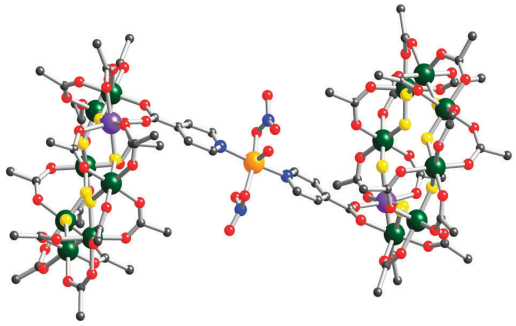

Fig. 6 The structure of $[(\mathbf{3})_2\{Cu(NO_3)_2(H_2O)\}]$ in the crystal. Me groups of pivalates excluded for clarity. Colours as in Fig. 3.

spin now interacts with the $S = 1/2$ ground state of the $\{Cr_7Ni\}$ ring, producing complex EPR spectra at 5 K (Fig. 7). One delightful aspect of these spectra is that they can be analysed using simple equations for trimers of $S = 1/2$ ions. The approach uses the Kambe vector coupling approach,[23] which allows us to move from the Hamiltonian for the spin system to the energy levels.

The spin Hamiltonian for a linear trimer is:

$$\hat{H} = -2J\hat{S}_B(\hat{S}_A + \hat{S}_C) \quad (1)$$

where S_B is the spin on the central ion and S_A and S_C are the spins on the terminal sites. The Kambe approach relies on the relationship:

$$\hat{S}'^2|S\rangle = S'(S' + 1)|S\rangle \quad (2)$$

which means that if we can express the Hamiltonian in terms of the spin operators squared, we can then write out the eigenstates in terms of the allowed spin quantum numbers. Here this requires defining an intermediate spin number S^* which is due to coupling S_A and S_C. The Hamiltonian then becomes:

$$\hat{H} = -2J\hat{S}_B\hat{S}^* \quad (3)$$

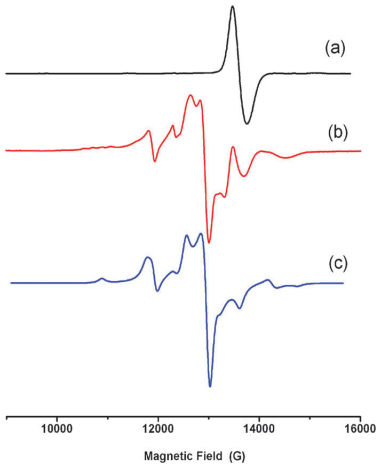

Fig. 7 The Q-band EPR spectra at 5 K of (a) compound **3**; (b) $[(\mathbf{3})_2\{Cu(NO_3)_2(H_2O)\}]$; (c) a simulation of the spectrum of $[(\mathbf{3})_2\{Cu(NO_3)_2(H_2O)\}]$ based on three interacting $S = 1/2$ sites.

The total spin is then given by $\hat{S}_T = \hat{S}_B + \hat{S}^*$. If we square both sides of this equation we get:

$$\hat{S}_T^2 = \hat{S}_B^2 + \hat{S}^{*2} + 2\hat{S}_B\hat{S}^*$$

Rearranging this equation gives:

$$2\hat{S}_B\hat{S}^* = \hat{S}_T^2 - \hat{S}_B^2 - \hat{S}^{*2}.$$

Putting this back into eqn (3) allows us to express the Hamiltonian in terms of squares:

$$\hat{H} = -J(\hat{S}_T^2 - \hat{S}_B^2 - \hat{S}^{*2})$$

The Kambe relationship then allows us to write the eigenstates as:

$$E = -J[S_T(S_T + 1) - S^*(S^* + 1) - S_B(S_B + 1)]$$

as S_B is the same for all eigenstates (*i.e.* the spin on a single centre), this is normally left out when considering the relative energies of the three states. There are three states which we can label using $|S_T, S^*\rangle$ as $|3/2, 1\rangle$, $|1/2, 1\rangle$ and $|1/2, 0\rangle$. The energy gaps between the three states are J and $2J$ respectively.

A longer account of this approach is given in the textbook by Mabbs and Machin,[24] who also show how the g-values for the three spin states can be calculated. This allows us to define the energy levels of each state of the trimer and to predict the g-values for each state. For example, for the $|1/2, 0\rangle$ state the spins on the terminal sites cancel (as $S^* = 0$) and therefore the g-value is defined exclusively by the spin at the central site. As the bridge contains Cu^{II}, we have a signal which appears to be a single copper(II) complex.

If we make the bridge diamagnetic, *e.g.* use $[Cu_2(O_2C^tBu)_4]$ where strong anti-ferromagnetic exchange between the two copper ions in the bridge gives an $S = 0$ ground state, we turn off the communication between $\{Cr_7Ni\}$ rings, at least as measured by EPR spectroscopy.[22]

This approach is general, and we can imagine anything that would bind to pyridine as a potential bridge between $\{Cr_7Ni\}$ rings. It is also an approach that leads to a possibility of a switchable link, because if we can perturb the bridge between states that are diamagnetic and paramagnetic we can switch our interaction on and off. There are several possible bridges that could work, *e.g.* using spin-crossover compounds, or redox-active or photo-active complexes. All these bridges are being explored.

Purple is the new green

The third structural feature that we looked to exploit was to replace some of the bridging fluorides with a group that could link cages together. Among the many experiments we carried out, we used *N*-ethyl-D-glucamine (H_5Etglu, $C_8H_{14}NO_5H_5$), hoping it would act as a templating amine with some of the alcohol oxygens displacing some of the fluorides. The result was unexpected, with the poly-ol being penta-deprotonated, despite the reaction being carried out in boiling pivalic acid.[25] The compound which results has the formula $[Cr_7NiF_3(Etglu)(O_2C^tBu)_{15}(H_2O)]$ **4** (Fig. 8). Unlike the previous rings, which are dark green in colour, compound **4** is purple. The metal centres are again arranged in an octagon, and there are five bridging alkoxide groups within the ring,

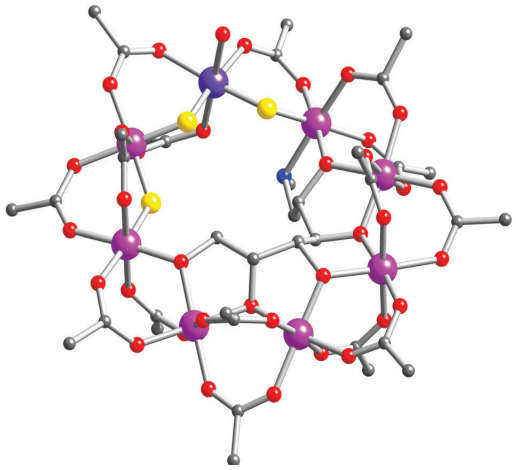

Fig. 8 The structure of **4** in the crystal. Me groups of pivalates excluded for clarity. Colours as in Fig. 1, except Cr, purple; Ni, dark blue.

with only three bridging fluorides. Seven of the eight edges of the octagon have two bridging pivalate ligands attached, however the eighth edge has only a single bridging pivalate and a bridging fluoride. It is also worth noting that as the H_2Etglu unit is chiral, compound **4** is chiral and the linked complexes based on **4** retain this chirality.[25] The purple rings are neutral and the secondary amine from Etglu is involved in coordination to a Cr(III) ion instead of being protonated as in the green $\{Cr_7M\}$ rings.

The formation of **4** is partly serendipitous, but replacing the fluoride ligands in the structure had been a goal of our work. Part of this was associated with an attempt to improve the coherence time of the system. As one path for decoherence is coupling between the electron spin and the nuclear spin, then replacing fluoride, with 100% $I = 1/2$ nuclei with oxygen, which has no naturally abundant nucleus with a significant nuclear spin, should help. Initial studies of the continuous wave EPR spectra suggest this may work, as the line-width of the EPR spectrum of **4** is significantly narrower than for "green" $\{Cr_7Ni\}$ rings such as **3**.[25,26] The g-values are similar.

The most exciting part of the structure of **4** is the presence of a terminal water bound to the nickel site. This is easily displaced by reaction with pyridine or di-imines.[25] By using a simple di-imine such as 4,4′-bipyridyl (bpy) or 1,2-dipyridylethene (dipyet) we create a dimeric cage, $[\{Cr_7NiF_3(Etglu)(O_2C^tBu)_{15}\}_2(L)]$ L = bipy **5** (Fig. 9) or bipyet **6**, and the simplicity of the reaction means we can introduce any other di-imine we can imagine. This means we have enormous control over the degree of interaction between the spin centres on the $\{Cr_7Ni\}$ rings. Our only restriction is one whether we can make the di-imine link.

The two examples we have published in detail show why this could be very powerful as we move towards QIP.[26] For compounds **5** and **6** we can measure EPR spectra that are due to an $S = 1$ state. This is because coupling between the two $S = 1/2$ $\{Cr_7Ni\}$ rings leads to a spin singlet ($S = 0$) and a spin triplet ($S = 1$) state (Fig. 10). As this coupling is very weak, we

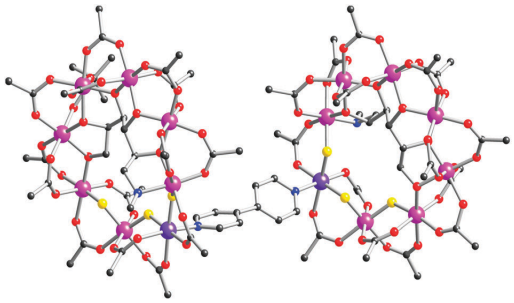

Fig. 9 The structure of **5** in the crystal. Me groups of pivalates excluded for clarity. Colours as in Fig. 8.

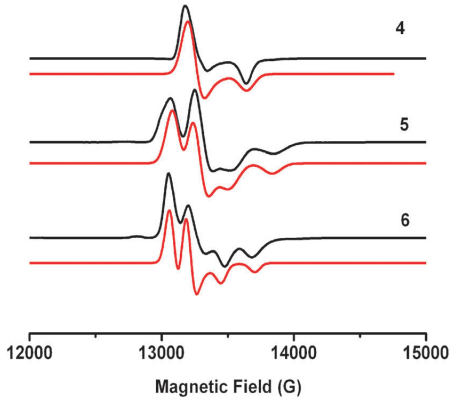

Fig. 10 The Q-band EPR spectra at 5 K of compounds **4**, **5** and **6**. Experimental data are in black, simulations are in red.

see the spectrum from the triplet at 5 K, regardless of whether the single or triplet is the ground state. The triplet has a small zero-field splitting, which in this model arises from anisotropic exchange between the $S = 1/2$ rings.

Very low temperature magnetisation measurements carried out by the Wernsdorfer group demonstrate that the singlet is in fact the ground state, as there is a spin-state crossing as the magnetic field increases.[26] This allows us to calculate the ring···ring interaction as 0.16 K. If we change the bridging group to 1,2-dipyridylethene we can moderate the exchange interaction to a value of 0.13 K. We also see a reduction in the size of the zero-field splitting of the spin triplet as observed by EPR spectroscopy (Fig. 10).[25] The simple-minded idea that making the bridge longer makes the interaction weaker seems to work, but unpublished results suggest there will also be other factors to consider. The key consideration is that this supramolecular approach will allow us to tune the degree of interaction between centres precisely. We can also envisage including switchable units within these bridges—as in the dimers of green rings we discussed above.

As di-imines work, we can also use more complicated groups decorated with pyridine ligands to bridge between purple {Cr_7Ni} rings. The example we have reported is with tetrapyridylporphyrin, where four {Cr_7Ni} rings bind to the periphery of the porphyrin (Fig. 11).[25] The reaction works, despite the tetrapyridylporphyrin (TPP) being insoluble in

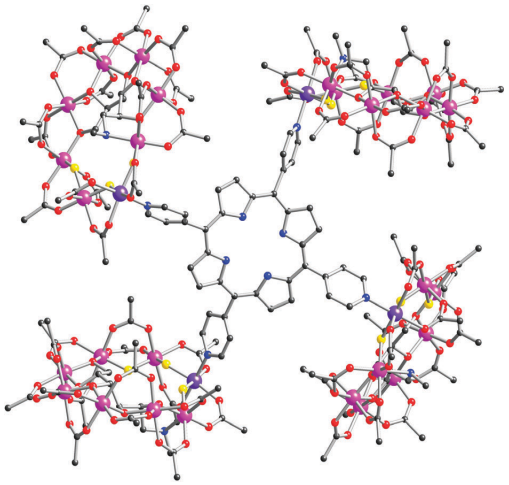

Fig. 11 The structure of TPP(**4**)$_4$ in the crystal. Me groups of pivalates excluded for clarity. Colours as in Fig. 8.

most common solvents—compound **4** is so soluble, it solubilises the porphyrin linker on coordination.

This result suggests that many other poly-pyridines could also be used to link purple wheels. It is very easy to draw schematics for complicated structures involving these chiral polymetallic wheels. Realising these complex structures is a major target. Our belief is that creating such structures will inspire our colleagues in theoretical physics to imagine algorithms that might use such complicated arrays of spin cluster qubits.

Some didactic conclusions

Some ideas in supramolecular chemistry are very new—for example, interlocked structures such as catenanes or rotaxanes have no real analogue in classical chemistry. Many of the other non-covalent interactions used by supramolecular chemists have been used by coordination chemists and others for many years.

In the work described above we have used ideas that any chemistry undergraduate should be able to understand. The H-bonding interaction between an ammonium cation and a fluoride group is a straightforward example of a H-atom bound to an electronegative element interacting with a second electronegative element. We can use it as a structure directing template—for example in making hybrid rotaxanes—and as a means of linking rings together in complex **2**. Previously we have discussed how using other H-bonding templates can be used to control the size of the AF-rings synthesised.[12] So, for example, using bulkier side-chains on the secondary ammonium cation gives a nine-metal ring[27] while using a tertiary ammonium cation gives a ten-metal ring.[28] There is a good deal of physics to study for the nine-metal rings, because the odd-number of metals introduces the possibility of spin frustration.

The second simple idea relates to converting the pivalate coated AF-ring into a complex that can act as a pyridine-ligand. This is related to simple organic chemistry,

where including a functional group into an alkane is vital before organic chemistry can exist. Similarly here we can introduce many other functional groups into our $\{Cr_7M\}$ rings, and we believe an organic chemistry linking such rings into stable arrays should be possible.

The ability to carry out selective substitution reactions is due to simple considerations of rates of reactions at 3d-metal ions. These are well-known, and related to the charge on the ion and the d-electron configuration. This allows us to perform selective substitution reactions on the periphery of the AF-rings, and hence control how many functional groups we introduce into the cages.

A related approach has been used for the well-known single molecule magnet, $\{Mn_{12}\}$. Firstly, the Christou group showed that the carboxylates on the Jahn–Teller axes of the Mn^{III} sites could be selectively displaced by nitrate ligands.[29] Cornia and co-workers have used this insight and ligand design to attach functionalised carboxylates to specific sites of $\{Mn_{12}\}$ and hence bind it to gold surfaces.[30] For the AF-rings we can follow a similar approach to introduce surface-binding functions.[31,32] We have the alternatives of introducing sixteen surface binding ligands, *e.g.* 3-thiophenecarboxylate, by using this carboxylate in the initial synthesis, or a single surface binder by a carboxylate exchange reaction after the initial synthesis. There is also the possibility to using H-bonding to the centre of the ring as a means to introduce surface-binders.

The pyridine functionalised rings act as Lewis bases. Our third simple idea is that if we can create a single "vacancy" on one site, and this happens partly by chance in the purple $\{Cr_7M\}$ rings, we then have a polymetallic cage that can be linked through acting as a Lewis acid.

Thus the AF-rings can act as H-bond acceptors, Lewis bases or Lewis acids. We have very recently shown they can also act as metallocrowns, coordinating to alkali metal cations.[11] This makes them ideal candidates to be used as building blocks for further supramolecular chemistry. The chemistry is, on paper at least, easy to envisage. Whether we can utilise these complex new structures in quantum information processing, or another advanced technology, is far more difficult to predict. It will be amusing to see how far we can get.

Acknowledgements

Our work on AF-rings is a collaborative project between many groups, and would be totally impossible without their contributions. The work discussed above highlights results achieved jointly with several of these collaborators. These include: Prof. Marco Affronte's team in Modena, including Valdis Corradini, Alberto Ghirri, Valerio Bellini, Fillipo Troiani, Andrea Candini, Umberto del Pennino and Umberto Biagi; Prof. Dave Leigh's magic circle in Edinburgh, including Chin-Fa Lee, David Schultz and Beatriz Ballesteros; Prof. Giuseppe Amoretti's team of theoreticians in Parma, especially Stefano Carretta and Paolo Santini; Prof. Wolfgang Wernsdorfer in Grenoble; pulsed EPR measurements by John Morton, Olivier Rival, Chris Wedge, Arzhang Ardavan and Steve Blundell at Oxford; crystallography performed by Prof. Finn Larsen and Dr Jacob Overgaard in Aarhus; further X-ray studies by Dr Simon Teat at the ALS, Berkeley; Prof. Eva Rentschler (Mainz) and Profs Dante Gatteschi and Roberta Sessoli and co-workers (Firenze) did initial magnetic studies on green rings. Our colleagues in Manchester who have contributed include: Eric McInnes, David Collison, Andrew Smith, Ian Casson, Carolina Sañudo, Chris Muryn, Robin G. Pritchard, Lapo Gorini, Rachel Davies, Vicki Milway, Paul Heath, Stergios Piligkos, John Machin, Claire Barker, Becky Doherty and Laura Carthy. The work has been funded by the EPSRC (UK), the European Commission (NoE MAGMANet, MC-ITN QueMolNa, FET-OPEN "MolSpinQip") and the University of Manchester. REPW is grateful to the Royal Society for a Wolfson Merit Award.

Notes and references

1 G. Christou, *Acc. Chem. Res.*, 1989, **22**, 328.
2 S. Wang, H.-L. Tsai, K. Folting, J. D. Martin, D. N. Hendrickson and G. Christou, *J. Chem. Soc., Chem. Commun.*, 1994, 671.
3 O. Roubeau and R. Clérac, *Eur. J. Inorg. Chem.*, 2008, 4325 and references therein.
4 E. C. Sañudo, T. Cauchy, R. H. Laye, O. Roubeau, S. J. Teat and G. Aromí, *Inorg. Chem.*, 2007, **46**, 9045.
5 F. Troiani, A. Ghirri, M. Affronte, S. Carretta, P. Santini, G. Amoretti, S. Piligkos, G. Timco and R. E. P. Winpenny, *Phys. Rev. Lett.*, 2005, **94**, 207208.
6 F. Troiani and M. Affronte, this issue.
7 K. L. Taft, C. D. Delfs, G. C. Papaethymiu, S. Foner, D. Gatteschi and S. J. Lippard, *J. Am. Chem. Soc.*, 1994, **116**, 823.
8 F. K. Larsen, E. J. L. McInnes, H. El Mkami, J. Overgaard, S. Piligkos, G. Rajaraman, E. Rentschler, A. A. Smith, G. M. Smith, V. Boote, M. Jennings, G. A. Timco and R. E. P. Winpenny, *Angew. Chem., Int. Ed.*, 2003, **42**, 101.
9 N. V. Gerbeleu, Yu. T. Struchkov, G. A. Timko, A. S. Batsanov, K. M. Indrichan and G. A. Popovich, *Dokl. Akad. Nauk SSSR*, 1990, **313**(6), 1459.
10 E. J. L. McInnes, S. Piligkos, G. A. Timco and R. E. P. Winpenny, *Coord. Chem. Rev.*, 2005, **249**, 2577.
11 T. B. Faust, P. G. Heath, C. A. Muryn, G. A. Timco and R. E. P. Winpenny, *Chem. Commun.*, 2010, **46**, 6258.
12 M. Affronte, S. Carretta, G. A. Timco and R. E. P. Winpenny, *Chem. Commun.*, 2007, 1789.
13 S. Piligkos, H. Weihe, E. Bill, F. Neese, H. El Mkami, G. M. Smith, D. Collison, G. Rajaraman, G. A. Timco, R. E. P. Winpenny and E. J. L. McInnes, *Chem.–Eur. J.*, 2009, **15**, 3152.
14 A. Bencini and D. Gatteschi, *EPR of Exchange Coupled Systems*, Springer-Verlag, Berlin, 1989.
15 J. J. L. Morton, A. M. Tyryshkin, A. Ardavan, K. Porfyrakis, S. A. Lyon and G. A. D. Briggs, *Phys. Rev. Lett.*, 2005, **95**, 200501.
16 A. Ardavan, O. Rival, J. J. L. Morton, S. J. Blundell, A. M. Tyryshkin, G. A. Timco and R. E. P. Winpenny, *Phys. Rev. Lett.*, 2007, **98**, 057201.
17 M. Affronte, I. Casson, M. Evangelisti, A. Candini, S. Carretta, C. A. Muryn, S. J. Teat, G. A. Timco, W. Wernsdorfer and R. E. P. Winpenny, *Angew. Chem., Int. Ed.*, 2005, **44**, 6496.
18 C.-F. Lee, D. A. Leigh, R. G. Pritchard, D. Schultz, S. J. Teat, G. A. Timco and R. E. P. Winpenny, *Nature*, 2009, **458**, 314.
19 B. Ballesteros, T. B. Faust, C.-F. Lee, D. A. Leigh, C. A. Muryn, R. G. Pritchard, D. Schultz, S. J. Teat, G. A. Timco and R. E. P. Winpenny, *J. Am. Chem. Soc.*, 2010, **132**, 15435.
20 F. K. Larsen, J. Overgaard, S. Parsons, E. Rentschler, G. A. Timco, A. A. Smith and R. E. P. Winpenny, *Angew. Chem., Int. Ed.*, 2003, **42**, 5978.
21 S. F. Lincoln, *Helv. Chim. Acta*, 2005, **88**, 523.
22 G. A. Timco, S. Carretta, F. Troiani, F. Tuna, R. G. Pritchard, E. J. L. McInnes, A. Ghirri, A. Candini, P. Santini, G. Amoretti, M. Affronte and R. E. P. Winpenny, *Nat. Nanotechnol.*, 2009, **4**, 173.
23 K. Kambe, *J. Phys. Soc. Jpn.*, 1950, **5**, 48.
24 F. E. Mabbs and D. J. Machin, *Magnetism and Transition Metal Compounds*, Chapman and Hall, London, 1973.

25 G. A. Timco, E. J. L. McInnes, R. G. Pritchard, F. Tuna and R. E. P. Winpenny, *Angew. Chem., Int. Ed.*, 2008, **47**, 9681.
26 A. Candini, G. Lorusso, F. Troiani, A. Ghirri, S. Carretta, P. Santini, G. Amoretti, C. Muryn, F. Tuna, G. Timco, E. J. L. McInnes, R. E. P. Winpenny, W. Wernsdorfer and M. Affronte, *Phys. Rev. Lett.*, 2010, **104**, 037203.
27 O. Cador, D. Gatteschi, R. Sessoli, F. K. Larsen, J. Overgaard, A.-L. Barra, S. J. Teat, G. A. Timco and R. E. P. Winpenny, *Angew. Chem., Int. Ed.*, 2004, **43**, 5196.
28 G. A. Timco, A. S. Batsanov, F. K. Larsen, C. A. Muryn, J. Overgaard, S. J. Teat and R. E. P. Winpenny, *Chem. Commun.*, 2005, 3649.
29 P. Artus, C. Boskovic, J. Yoo, W. E. Streib, L. C. Brunel, D. N. Hendrickson and G. Christou, *Inorg. Chem.*, 2001, **40**, 4199.
30 M. Pacchioni, A. Cornia, A. C. Fabretti, L. Zobbi, D. Bonacchi, A. Caneschi, G. Chastanet, D. Gatteschi and R. Sessoli, *Chem. Commun.*, 2004, 2604.
31 V. Corradini, R. Biagi, U. del Pennino, V. De Renzi, A. Gambardella, M. Affronte, C. A. Muryn, G. A. Timco and R. E. P. Winpenny, *Inorg. Chem.*, 2007, **46**, 4937.
32 A. Ghirri, V. Corradini, C. Cervetti, A. Candini, U. del Pennino, G. A. Timco, R. G. Pritchard, C. A. Muryn, R. E. P. Winpenny and M. Affronte, *Adv. Funct. Mater.*, 2010, **20**, 1552.

Chapter Six - Paper 2

"Chemical control of spin propagation between heterometallic rings"

T. B. Faust, D. R. Allan, V. Bellini, A. Candini, S. Carretta, L. Carthy, D. Collison, R. J. Docherty, J. Kenyon, G. Lorusso, J. Machin, E. J. L. McInnes, C. A. Muryn, H. Nowell, R. G. Pritchard, S. J. Teat, G. A. Timco, F. Tuna, G. F. S. Whitehead, W. Wernsdorfer, M. Affronte and R. E. P. Winpenny, *Chemistry – a European Journal*, 2011, **17**, 14020-14030.

CHEMISTRY
A EUROPEAN JOURNAL

DOI: 10.1002/chem.201101785

Chemical Control of Spin Propagation between Heterometallic Rings

Thomas B. Faust,[a] Valerio Bellini,[b] Andrea Candini,[b] Stefano Carretta,[c] Giulia Lorusso,[d] David R. Allan,[e] Laura Carthy,[a] David Collison,[a] Rebecca J. Docherty,[a] Jasbinder Kenyon,[a] John Machin,[a] Eric J. L. McInnes,[a] Christopher A. Muryn,[a] Harriott Nowell,[e] Robin G. Pritchard,[a] Simon J. Teat,[f] Grigore A. Timco,[a] Floriana Tuna,[a] George F. S. Whitehead,[a] Wolfgang Wernsdorfer,[g] Marco Affronte,[d] and Richard E. P. Winpenny*[a]

Abstract: We present a synthetic, structural, theoretical, and spectroscopic study of a family of heterometallic ring dimers which have the formula $[\{Cr_7NiF_3(Etglu)(O_2CtBu)_{15}\}_2(NLN)]$, in which Etglu is the pentadeprotonated form of the sugar *N*-ethyl-D-glucamine, and NLN is an aromatic bridging diimine ligand. By varying NLN we are able to adjust the strength of the interaction between rings with the aim of understanding how to tune our system to achieve weak magnetic communication between the spins, a prerequisite for quantum entanglement. Micro-SQUID and EPR data reveal that the magnetic coupling between rings is partly related to the through-bond distance between the spin centers, but also depends on spin-polarization mechanisms and torsion angles between aromatic rings. Density functional theory (DFT) calculations allow us to make predictions of how such chemically variable parameters could be used to tune very precisely the interaction in such systems. For possible applications in quantum information processing and molecular spintronics, such precise control is essential.

Keywords: chromium · EPR spectroscopy · heterometallic dimers · magnetic properties · metallacycles

Introduction

To design devices that operate at a molecular level we need to control and manipulate the interactions between molecules. Such control is of fundamental scientific interest, testing our ideas concerning delocalization of charge and spin. In order to make two magnetic units interact weakly, one of the main issues is to understand and then control the propagation of the spin information at a supramolecular (nanometer) scale. Local through-bond interactions are preferable to dipolar interactions, as the latter have essentially long-range character and it is difficult to tune or switch dipolar interactions without large structural modifications to the systems. Aromatic organic linkers were studied previously, by McCleverty and Ward in collaboration with Gatteschi,[1] to link single paramagnetic ions in the context of targeting molecular ferromagnets. The strength of the interaction between the units linked by an aromatic bridge was found to obey some general empirical rules: 1) the larger the number of bonds in the interaction path, the smaller the interaction; 2) charge and spin polarization induced by bonding to a metal site proceed in an alternating fashion around the

[a] T. B. Faust, Dr. L. Carthy, Prof. D. Collison, R. J. Docherty, J. Kenyon, J. Machin, Prof. E. J. L. McInnes, Dr. C. A. Muryn, Dr. R. G. Pritchard, Dr. G. A. Timco, Dr. F. Tuna, G. F. S. Whitehead, Prof. R. E. P. Winpenny
The Lewis Magnetism Laboratory
School of Chemistry and Photon Science Institute
University of Manchester
Oxford Road, Manchester, M13 9PL (UK)
Fax: (+44) 161-275-4616
E-mail: richard.winpenny@manchester.ac.uk

[b] Dr. V. Bellini, Dr. A. Candini
Institute of NanoSciences S3 CNR
Via Campi 213 A, 41125 Modena (Italy)

[c] Dr. S. Carretta
Dipartimento di Fisica Università di Parma
Unità CNISM di Parma
via G.P. Usberti 7/a, 3100 Parma (Italy)

[d] Dr. G. Lorusso, Prof. M. Affronte
Dipartimento di Fisica
Università di Modena e Reggio Emilia
Via Campi 213/A, 41125 Modena (Italy)

[e] Dr. D. R. Allan, Dr. H. Nowell
DIAMOND Light Source
Harwell Science and Innovation Campus
Didcot, Oxfordshire, OX11 0DE (UK)

[f] Dr. S. J. Teat
Advanced Light Source
Lawrence Berkeley Lab
1 Cyclotron Rd, Berkeley, CA 94720 (USA)

[g] Dr. W. Wernsdorfer
Institut Néel, CNRS & UJF
BP 166, 38042 Grenoble Cedex 9 (France)

Supporting information for this article is available on the WWW under http://dx.doi.org/10.1002/chem.201101785.

atoms in aromatic rings; 3) since a magnetic interaction can proceed via different bond paths in the linker, the strength of any interaction should depend on whether constructive or destructive interferences between paths with different lengths arise.

We have previously shown that we can couple magnetically two (or more) complex molecules without perturbing the properties of the individual units.[2] The motivation for this work has been to examine whether molecular magnets can be used as qubits for quantum information processing (QIP).[3] The ability to entangle the spins of individual molecular units could eventually allow us to encode two-qubits gates or to communicate magnetic information across nanometers. Here we show how to tune this interaction, and that we can derive rules useful to design aromatic linkers with a precise interaction between the heterometallic rings.

Linking metal cluster complexes together to make more complicated polymetallic structures has a considerable history. For example, there is beautiful work by Christou and co-workers dating back to the 1990s, which involves linking $\{Mn_4\}$ cages into dimers through bis-pyridyl ligands.[4] At the same time Toma et. al were employing pyrazine and bis-pyridyl bridging ligands to access dimers, trimers, tetramers, and even a cyclic hexamer of oxocentered ruthenium triangles.[5] More recently there has been remarkable work from Clérac and co-workers in which $\{Mn_4\}$ single molecule magnets are linked into 1D- and 2D-polymers and 3D-networks, where the resulting magnetic properties vary depending on the strength of the inter- against intra-cluster coupling.[6] Sañudo et al. have also shown that $\{Mn_4\}$ cages can be linked into weakly coupled dimers.[7] Both discrete and extended polycluster complexes are thus well known.

Our research group has recently been interested in the properties of pivalate bridged octametallic rings in which the metal ions within the cyclic array couple anti-ferromagnetically (AF) with each of their neighbors. For the first member of this family, $[CrF(O_2CtBu)_2]_8$, the AF exchange between the $S=3/2$ centers leads to an $S=0$ ground state.[8] Generation of a nonzero spin ground state can be achieved in two ways, either by synthesis of a macrocycle with an odd number of metal centers or, more easily, one chromium atom can be replaced by a metal ion with a different spin ($S\neq3/2$). The first family we have investigated has the general formula $[Cation][Cr_7MF_8(O_2CR)_{16}]$ (commonly called 'green rings' on account of their physical appearance; O_2CR indicates a wide range of carboxylates).[9] These rings are made by introduction of a second metal in conjunction with an alkyl amine; the amine is protonated under the reaction conditions and the resulting ammonium provides the cation which templates the ring as it forms.

Herein we discuss a second family of rings trivially called 'purple rings', again owing to the physical appearance of crystals and solutions.[2b] These rings have the general formula $[Cr_7MF_3(Etglu)(O_2CtBu)_{15}L]$, where H_5Etglu = *N*-ethyl-D-glucamine (Scheme 1).

For the homometallic ring in which $M=Cr^{III}$, L is fluoride, but for the heterometallic rings where M is a divalent metal, L is a labile neutral solvent molecule. Herein we discuss the cases in which $M=Ni^{II}$ only, and show that this reactive coordination site can be used to develop the chemistry of these 'purple rings'.

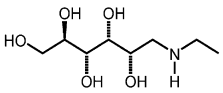

Scheme 1. Chemical structure of *N*-ethyl-D-glucamine (H_5Etglu).

The use of polyols in cluster synthesis is common. For example, they have been used in combination with metallomacrocycles by Saalfrank et al.[10] and with more compact clusters by Brechin[11] and others.[12] Whilst the use of sugars as polyol ligands has also been explored, for example by Klüfers et al.,[13] glucamine does not appear to have been used previously.

Results and Discussion

Structural description: The complexes presented here are based on the structure of $[Cr_7NiF_3(Etglu)(O_2CtBu)_{15}(OEt_2)]$, **1** (Figure 1). This contains an octametallic octagonal array of seven Cr^{III} and one Ni^{II} centers. A central multi-deprotonated sugar provides internal scaffolding in the form of five μ_2-alkoxides, along with three μ_2-fluorides. Seven sides of the octagon are bridged externally by two 2.11-pivalates (Harris notation[14]), the final side incorporating a coordinated N-atom from the Etglu and one 2.11-pivalate, leaving a single free coordination site on the nickel center. The pentaanionic Etglu ligand adopts the 6.222221 mode. This combination of bridging ligands leaves a single free coordination site on the nickel center to make it six coordinate. This

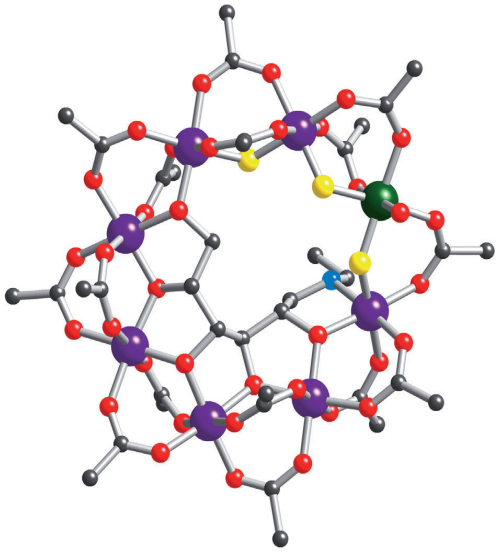

Figure 1. Structure of compound **1** in the crystal. Me groups of pivalate, Et groups of Et_2O, and H atoms have been omitted for clarity. Cr: purple, Ni: green, O: red, N: blue, F: yellow, C: black.

single available coordination position is desirable as it rules out the possibility of forming polymeric networks, making it straightforward to make oligomers of rings.

There are some things of particular note about the structure. The presence of the $Etglu^{5-}$ makes the molecule chiral; four stereogenic centers already existed on the carbon atoms alpha to the nonterminal hydroxyl groups, and an additional one is generated on the nitrogen following its coordination to chromium. The bonding mode of the sugar ligand leads to variation in the coordination environments of the chromium ions: four have four carboxylate and two alkoxide oxygens bound to them; one has four carboxylates, one alkoxide, and one fluoride; a sixth has four carboxylates and two fluorides and the final site has only three carboxylate oxygens, a bridging fluoride, a bridging alkoxide, and the N atom from Etglu. The nickel coordination sphere is composed of three bridging carboxylates, two bridging fluorides, and one labile coordination site, which is occupied by diethyl ether in the case of **1**.

Reaction of **1** with the imine species 4-phenylpyridine (PyPh) results in displacement of the diethyl ether and coordination by the lone pair of the nitrogen to form $[\{Cr_7NiF_3(Etglu)(O_2CtBu)_{15}\}(PyPh)]$ (**2**) in good yield. Similar reactions with diimines give di-ring assemblies. The diimines used are shown in Scheme 2. The general formula for these compounds is: $[\{Cr_7NiF_3(Etglu)(O_2CtBu)_{16}\}_2(NLN)]$ with NLN = 4,4′-bipyridyl, (Py-Py) (**3**), *trans*-1,2-dipyridylethene, (Py-CH=CH-Py) (**4**), 1,2-dipyridylethane, (Py-CH_2-CH_2-Py) (**5**), dipyridylacetylene, (Py-CH≡CH-Py) (**6**), *meso*-alpha,-beta-bispyridylglycol, (Py-CH(OH)-CH_2(OH)-Py) (**7**), 4,4′-azopyridine, (Py-N=N-Py) (**8**), 1,4-dipyridylbenzene, (Py-Bz-Py) (**9**), 3,6-dipyridyl-s-tetrazene, (Py-Tz-Py) (**10**), bis-1,4-(4-pyridylvinyl)benzene, (Py-CH=CH-Bz-CH=CH-Py) (**11**). Ligation is not restricted to simple 4-pyridyl coordination, as exemplified by NLN = 4,4′-bi-3,5-dimethylpyrazole (Me_2Pzl-PzlMe_2) (**12**). We have also been successful in dimerizing a pair of clusters via pyrazine (Pzn; **13**). Representative examples are shown in Figure 2. The structures of the individual rings do not vary between **3** to **13**, and in each case the nitrogen from a diimine is coordinated to nickel, giving the nickel a 2F, 3O, 1N coordination sphere. The Ni···N distance is statistically invariant in the structures **3** to **12**, with an average distance of 2.07 Å. These distances for structure **13** are marginally longer (2.12 Å) probably due to steric limitations imposed by the clashing of bulky *tert*-butyl groups on the rings.

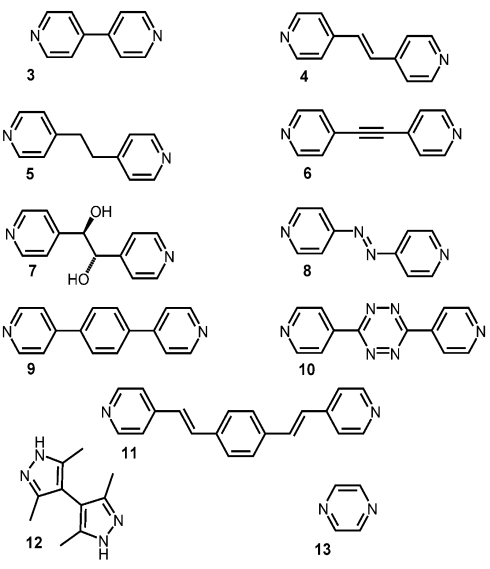

Scheme 2. A guide to the different linkers employed in the dimerization of the $\{Cr_7Ni\}$ rings, the structure to which they belong is noted to their lower left side.

While the internal ring structures are consistent, how the rings are arranged about the linker varies quite considerably. To describe the relative orientation of the rings we define four parameters. First, there is the through-space Ni···Ni distance. This is the closest metal–metal contact in all the structures, except in the contorted structure of **7** (see below). Second, we consider the through-bond Ni···Ni distance. Third, the angle between the mean plane of the metal ions in one ring and the mean plane of the metal ions in the second ring was determined (see Figure 3). Fourth, we define a vector pointing from the Ni center to the distal Cr center (at the five-position of the octagon; see Figure 4). The angle between the vector on one ring and the vector in the second ring shows whether the rings are orientated in the same direction, or opposite. These parameters are listed in Table 1.

Based on these parameters we can group the structures. Compounds **4**, **5**, **6**, and **8** have similar Ni···Ni distances and the angles between the Ni···Cr vector is around 130° in each case. Compounds **4** and **8** differ in the replacement of -CH- with -N- and so the similarity is expected. The same replacement is present between **9** and **10**, which display similar parameters to each other though there is a wide discrepancy in the angle between the Ni···Cr vectors (134.1 and 56.1° respectively). Compound **11** can be grouped with **9** and **10**. Compound **3** is different, with the two rings almost coplanar and with the angle between the vectors 94°. Compound **3** is related to compounds **4**, **5**, **6**, and **8**, but with a shorter Ni···Ni distance forcing the rings to be coplanar.

Compound **7** is unique, with a much shorter Ni···Ni distance through space (10.82 Å) and one ring almost perpendicular to the second (72.5°), both due to significant twisting of the linker (Figure 3a). This compound is the only one where a Cr···Ni through-space contact is shorter than the Ni···Ni contact; the Ni1···Cr8 contact is 10.44 Å.

Compound **12** is interesting in exhibiting two identical moieties with different conformations within the crystallographic asymmetric unit. The five-membered rings in **12** makes the through bond Ni···Ni distance shorter (9.95/9.96 Å) than in **3**, and there is a significant torsion angle (56.59/53.66°) between the planes of the two heterocycles due to the steric clash of the four Me groups (see Figure 2d).

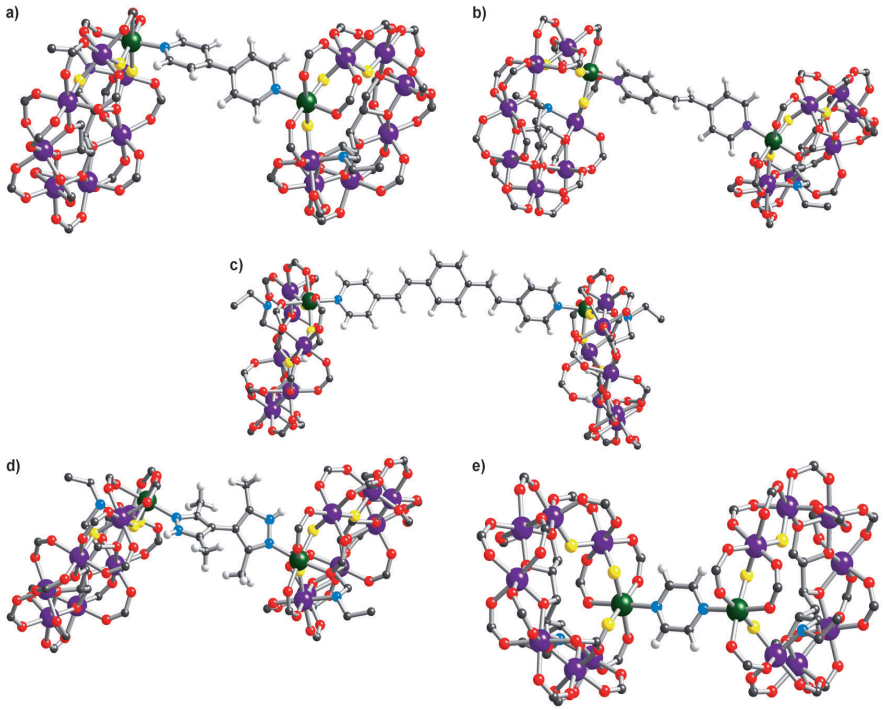

Figure 2. Structures in the crystal of six representative dimers: a) **3**, b) **4**, c) **11**, d) **12**, and e) **13**. *t*Bu groups of carboxylates and nonbridging ligand hydrogens have been omitted for clarity. H: gray, other elements as in Figure 1.

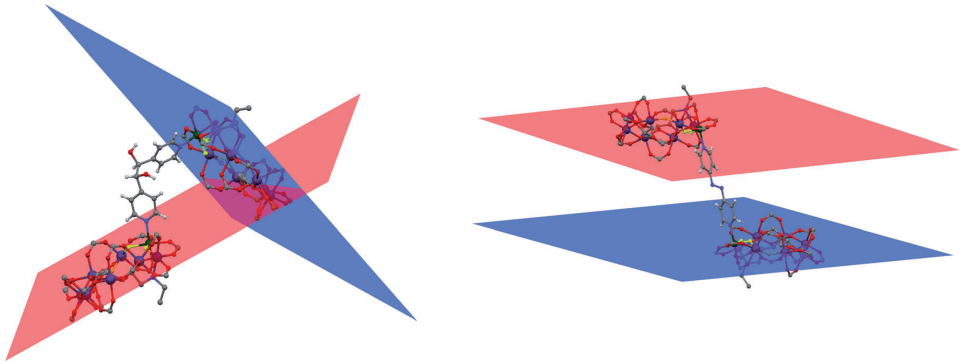

Figure 3. Crystal structures of: a) **7** and b) **8** with the calculated planes of each {Cr_7Ni} ring shown in red and blue for each structure (*tert*-butyl carbons and non-linker hydrogens have been omitted for clarity).

Compound **13** is distinct from the other systems in possessing an exceptionally short Ni···Ni distance (7.03 Å, see Figure 2e). Given the steric bulk of the pivalate groups in the two rings it is perhaps surprising this dimer can form. The ring–ring contacts may be responsible for this dimer possessing the widest vector angle (156.7°) of any of the family members (Table 1 and Table 2).

Physical Studies: Variable temperature magnetic susceptibility behavior of compounds **2** to **13** are very similar (Figure S1 in the Supporting Information). The room temperature value of the product $\chi_m T$ per ring (where χ_m is the molar magnetic susceptibility) is 12.0 emu K mol^{-1}, below that expected for seven Cr^{III} ions and a single Ni^{II} site (calcd value 14.1 emu K mol^{-1} for $g=2.00$). This is consistent with weak anti-ferromagnetic exchange within the rings. With lower temperatures, $\chi_m T$ falls, again consistent with anti-ferromagnetic exchange. The full Hamiltonian for such a ring is given by Equation (1), which is composed of four parts. The first describes the isotropic exchange interaction. The

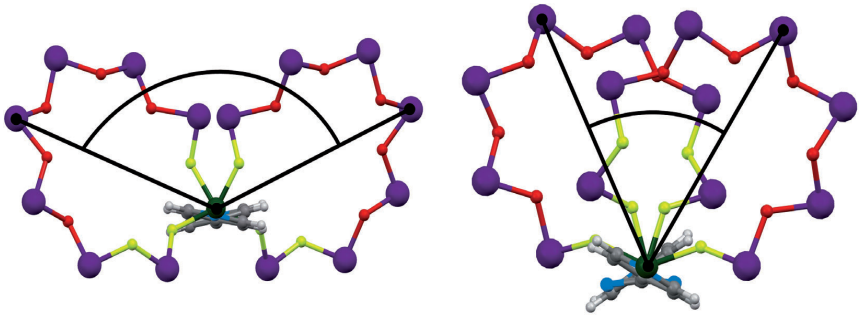

Figure 4. Crystal structures of a) **6** and b) **10**, with black lines overlaid demonstrating the angle between the vectors defined by the Ni site and the distal Cr site (only the bridging ligand and the metallocrown core are shown).

Table 1. Structural metrics for the family of linked ring systems.

Compound	Linker	Ni···Ni distance through space [Å]	Ni···Ni distance through bond [Å] [b]	Angle between mean plane of rings [°]	Angle between Ni···Cr vectors [°]	D [cm^{-1}][c]
3	Py−Py	11.218(3)	13.82(8)	8.4	89.9	+0.013
4	Py-CH=CH-Py	11.430(2)	16.59(6)	33.1	133.6	+0.009
5	Py-CH_2-CH_2-Py	12.898(5)	16.47(6)	31.8	135.3	+0.003
6	Py-CH≡CH-Py	13.680(3)	16.34(9)	33.0	132.3	+0.005
7	Py-CH_2(OH)-CH_2(OH)-Py	10.824(1)	16.78(6)	72.5	(113.4)	+0.003
8	Py-N=N-Py	13.115(2)	16.33(4)	21.4	130.7	+0.012
9	Py-Bz-Py	15.424(1)	19.58(2)	15.1	134.1	
10	Py-Tz-Py	15.171(1)	19.31(3)	23.1	56.1	
11	Py-CH=CH-Bz-CH=CH-Py	19.899(1)	24.95(7)	20.8	80.0	
12[a]	Me_2Pzl-PzlMe_2	9.954(2)/9.957(2)	11.13(5)/11.05(5)	3.4/6.8	100.7/105.0	
13	Pzn	7.027(3)	8.26(4)	24.1	156.7	+0.125

[a] Two dimer pairs exist in the asymmetric unit, both values are listed. [b] The values listed are averaged values of each route around the six-membered aromatic rings, for **12** the shortest (non-averaged) route around the five membered rings were used. [c] The axial zero-field splitting parameter of an $S=1$ state (see below).

second term accounts for the local zero-field splittings. The third term accounts for dipolar and anisotropic spin–spin contributions, and the final term is the Zeeman term.

$$\hat{H} = J\sum_{i=1}^{8} s_i.s_{i+1} + \sum_{i=1}^{8} d_i\left[s_{z,i}^2 - \frac{s_i(s_i+1)}{3}\right] + \sum_{i<j=1}^{8} D_{ij}\left[2s_{z,i}s_{z,j} - s_{x,i}s_{x,j} - s_{y,i}s_{y,j}\right] + \mu_B\sum_{i=1}^{8} B.g_i.s_i \quad (1)$$

We can fit the variable temperature susceptibility behavior in each case to a Hamiltonian only involving intra-ring interactions, which gives us an exchange interaction of $J/k_B = 22.9$ K (a positive sign for J indicates an anti-ferromagnetic exchange). To fit the magnetic susceptibility there is no need to allow for the differing bridging by fluoride and alkoxide groups within the ring and there is no need to include an inter-ring interaction nor a need to allow for anisotropy of individual metal sites (d_i) or anisotropic exchange (D_{ij}).

For five representative compounds, **3**, **4**, **10**, **12**, and **13** micro-SQUID magnetization measurements were performed at 40 mK (Figure 5). Data are normalized to the saturation value M_S. The magnetization loops exhibit a clear hysteresis, which is characteristic of a phonon-bottleneck regime with a

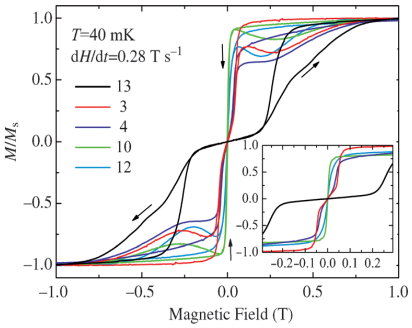

Figure 5. Micro-SQUID magnetization M(H) vs. magnetic field H for: **13**, **3**, **4**, **10**, and **12** The experiments were performed at $T=40$ mK, using sweeping rate $dH/dt = 0.28$ T/s. Data are normalized to the saturation value M_S.The inset focuses on the region where the spin state crossing occurs.

spin-phonon relaxation time to the cryostat of a few seconds.[15] Figure 5 shows clearly a strong adiabatic cooling when sweeping the field down to zero field. Note that this cooling mechanism allows us to assume that the ground state of each ring is uniquely occupied, and therefore for an exchange interaction between the two spin states for the di-ring assembly generates: $S=0$ and $S=1$. If the $S_{tot}=0$ state

Table 2. Structural metrics for the ring monomers **1** and **2** and family of linked ring dimers **3**–**13**.

Compound	**1**	**2**	**3**	**4**	**5**	**6**	**7**
formula	$C_{93}H_{174}Cr_7F_3NNiO_{37.5}$	$C_{100}H_{174}Cr_7F_3N_2NiO_{39}$	$C_{179}H_{314}Cr_{14}F_6N_4Ni_2O_{72}$	$C_{178}H_{308}Cr_{14}F_6N_4Ni_2O_{70}$	$C_{178}H_{310}Cr_{14}F_6N_4Ni_2O_{70}$	$C_{190}H_{358}Cr_{14}F_6N_4Ni_2O_{70}$	$C_{178}H_{308}Cr_{14}F_6N_4Ni_2O_{72}$
M_r	2384.63	2508.12	4633.76	4583.70	4585.72	4778.22	4615.70
Crystal size [mm]	0.30×0.20×0.10	0.30×0.25×0.22	0.30×0.20×0.18	0.30×0.25×0.25	0.13×0.11×0.02	0.3×0.3×0.15	0.20×0.17×0.03
crystal system	orthorhombic	orthorhombic	monoclinic	orthorhombic	orthorhombic	orthorhombic	orthorhombic
space group	$P2_12_12_1$	$P2_12_12_1$	C2	$P2_12_12$	$P2_12_12$	$P2_12_12$	$P2_12_12_1$
a [Å]	16.4250(5)	17.0600(2)	54.7570(6)	23.4760(4)	23.017(11)	23.5407(14)	16.8517(5)
b [Å]	24.9950(5)	26.3540(3)	16.9650(2)	32.8770(7)	32.327(17)	32.4685(17)	38.2743(13)
c [Å]	31.7760(11)	30.4220(4)	35.8310(5)	17.6110(3)	17.180(9)	17.499(3)	39.0045(13)
α [°]	90	90	90	90	90	90	90
β [°]	90	90	125.6330(10)	90	90	90	90
γ [°]	90	90	90	90	90	90	90
V [Å^3]	13045.4(7)	13677.7(3)	27053.1(6)	13592.5(4)	12783(11)	13375(3)	25157.4(14)
Z	4	4	4	2	2	2	4
ρ_{calcd} [mg mm^{-3}]	1.214	1.218	1.138	1.12	1.191	1.186	1.219
T [K]	100(2)	100(2)	100(2)	100(2)	100(2)	100(2)	100(2)
Goof on F^2	1.038	1.040	1.198	1.149	1.039	1.157	1.028
R_1 [$I>2\sigma(I)$]	0.0625	0.0808	0.0871	0.0844	0.1129	0.1096	0.0651
wR_2 [all data]	0.1699	0.2054	0.2363	0.2317	0.327	0.3175	0.1809

Compound	**8**	**9**	**10**	**11**	**12**	**13**
formula	$C_{176}H_{306}Cr_{14}F_6N_6Ni_2O_{70}$	$C_{189}H_{326}Cl_6Cr_{14}F_6N_4Ni_2O_{71}$	$C_{198}H_{344}Cr_{14}F_6N_{10}Ni_2O_{75}$	$C_{186}H_{314}Cr_{14}F_6N_4Ni_2O_{70}$	$C_{182}H_{324}Cr_{14}F_6N_6Ni_2O_{72}$	$C_{175}H_{312}Cl_{10}Cr_{14}F_6N_4Ni_2O_{71.75}$
M_r	4585.69	4962.66	5024.25	4685.85	4707.89	4934.24
crystal size [mm^3]	0.5×0.2×0.2	0.3×0.12×0.04	0.2×0.1×0.08	0.1×0.1×0.1	0.32×0.11×0.02	0.25×0.25×0.1
crystal system	orthorhombic	monoclinic	monoclinic	orthorhombic	monoclinic	orthorhombic
space group	$P2_12_12$	$P2_1$	$P2_1$	$C222_1$	$P2_1$	$P2_12_12_1$
a [Å]	24.173(5)	19.3651(16)	16.7040(10)	16.7843(7)	35.7658(18)	26.7305(5)
b [Å]	32.615(7)	29.609(3)	28.4349(17)	36.8039(14)	22.5863(11)	30.9284(6)
c [Å]	16.996(3)	24.040(2)	28.7413(17)	53.400(2)	37.0900(19)	31.2563(7)
α [°]	90	90	90	90	90	90
β [°]	90	96.012(2)	93.300(2)	90	115.179(3)	90
γ [°]	90	90	90	90	90	90
V [Å^3]	13400(5)	13708(2)	13628.8(14)	32987(2)	27115(2)	25840.6(9)
Z	2	2	2	4	4	4
ρ_{calcd} [mg mm^{-3}]	1.137	1.202	1.224	0.943	1.153	1.268
T [K]	100(2)	100(2)	100(2)	100(2)	100(2)	100(2)
Goof on F^2	0.961	1.040	1.025	1.021	1.132	1.179
R_1 [$I>2\sigma(I)$]	0.0672	0.0756	0.0568	0.0538	0.0702	0.0898
wR_2 [all data]	0.1704	0.2055	0.1654	0.1447	0.1835	0.2241

is the ground state in zero field, we should be able to see a spin-state crossing by increasing the field, with one component of the paramagnetic $S_{tot}=1$ state falling in energy as field increases (visible as an inflection point of the magnetization curve). The crossing point in the magnetization, that is, the gap between inflection points, can then be related to the energy gap between the $S_{tot}=0$ and $S_{tot}=1$ states. The level crossings occur at $B=\pm0.05$ T for **3**; $B\pm0.04$ T for **4** and $B=\pm0.30$ T for **13**. No crossings are observed for **10** or **12**, which suggests the inter-ring interaction is much smaller in these two compounds. The measurement does not rule out the interaction being ferromagnetic in **10** and **12**, but this is unlikely.

Fitting this crossing to a microscopic Hamiltonian (2):

$$\hat{H} = 2J'\vec{S}_{Ni1}\cdot\vec{S}_{Ni2} \quad (2)$$

where J' is the isotropic exchange between the Ni spin moments, and S_{Ni1} and S_{Ni2} are the spin moments of the two Ni ions ($S_{Ni1}=S_{Ni2}=1$), we obtain $J'/k_B=+1.0$ K for **13**, 0.16 K for **3** and 0.14 K for **4**. For compounds **10** and **12** the lack of a crossing allows us to set an upper limit to the J'/k_B value of 100 mK.

We have also examined the EPR spectroscopy of all the compounds discussed here because this is a more convenient technique than micro-SQUID measurements, although it does not give the magnitude of the exchange interaction directly. Multi-frequency studies at Q-band (Figure 6, Figure 7, and Figure 8) and S- and X-band (Figure S2 in the Supporting Information) show that there is an interaction between the individual rings in all cases. The size of the singlet–triplet gap is too small to be determined from the EPR intensity variation at variable temperatures.

The single {Cr_7Ni} ring **2** shows low temperature spectra consistent with an $S=1/2$ ground state with axially symmetric g-values of $g_z=1.78$ and $g_{x,y}=1.84$ in **2**. The ground state g anisotropy is better resolved than that found in previous

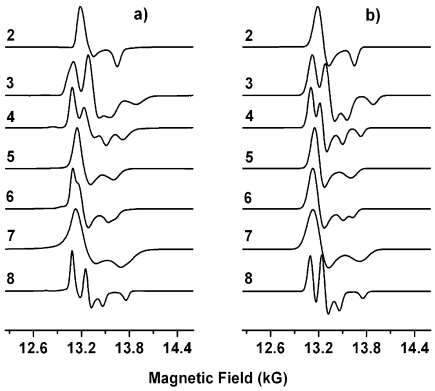

Figure 6. 5 K Q-band EPR spectra of compounds **2**–**8** as polycrystalline powders: a) experimental, b) simulation using the parameters reported in Table 1 and in the text.

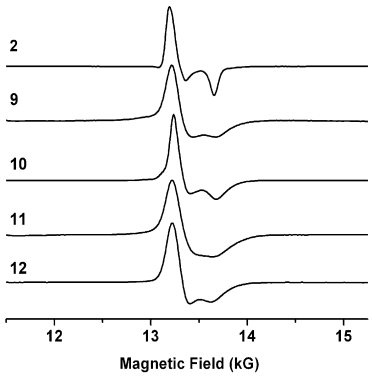

Figure 7. The 5 K Q-band EPR spectra of compounds **2** and **9**–**12**.

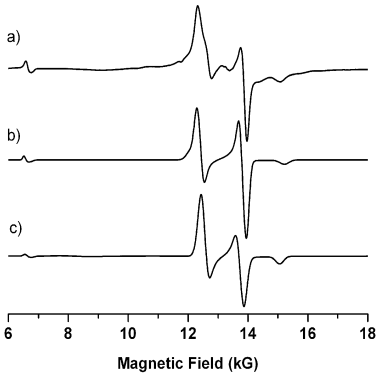

Figure 8. For compound **13**, a) the 5 K Q-band EPR spectrum measured on polycrystalline powers, b) simulated spectrum using Hamiltonian [1], c) simulated spectrum using Hamiltonian [3].

studies of $[NH_2R_2][Cr_7NiF_8(O_2CtBu)_{16}]$ rings (compound **14**);[16] this is partly due to a slightly larger g anisotropy in **2** but mainly due to a reduction in line width. We believe that this reduction in the line width is partially related to unresolved hyperfine interactions to fluoride, and as there are only three fluorides in **2** compared with eight fluorides in **14** this could lead to narrower lines. However it could also be related to crystallographic ordering. In **2** the Ni site is uniquely defined while in **14** the Ni site is disordered over the eight metal sites of the octagon.[16]

As the individual rings are $S=1/2$ centers, communication between the rings in the di-ring complexes will give a spin triplet and singlet well separated from other excited states, but very close in energy because the inter-ring exchange is weak. Therefore, regardless of whether the exchange interaction between rings is ferro- or anti-ferro-magnetic we will see a signal for an $S=1$ triplet if the spin systems are interacting. As the interaction becomes weaker, the zero-field splitting, D, of the triplet will also become smaller and hence the spectrum will begin to resemble that of an isolated $S=1/2$ state. We have used a simple Hamiltonian (3) to model the EPR spectra as a triplet:

$$\hat{H} = \mu_B B.g.\hat{S} + D_{S=1}\left[\hat{S}_z^2 - \frac{S(S+1)}{3}\right] \quad (3)$$

The g values were fixed from the spectra of **2** and D_{xyz} considered to be coincident with g_{xyz}. The spectra show (Figure 8) that the largest $D_{S=1}$ value of $+0.12\ cm^{-1}$ is found in **13**, which contains the shortest bridge, pyrazine. There is also a clear triplet seen for compounds **3**–**8**. Quantifying this interaction by simulating the triplet (Figure 6) gives $D_{S=1}$ (cm^{-1}) = +0.013 in **3**, +0.009 in **4**, +0.005 in **6**, +0.012 in **8**. The calculated spectra are sensitive to the sign of D. The larger D value for **13** (see **3**) and **3** (see **4**) implies stronger exchange where the bridging π system is shorter. If we compare the five compounds, **4**–**8**, that have a two atom link between the pyridines we can see that the -N=N- linker gives a stronger interaction in **8** than the isoelectronic -CH=CH- linker in **4**, presumably due to the nitrogens' greater electronegativity. This has been previously seen in diruthenium complexes.[17] The alkyne link in **6** is slightly weaker than the alkene link in **4**. The weakest interactions are found for the saturated linkers in compounds **5** and **7**, with $D_{S=1} = +0.003\ cm^{-1}$ for both complexes.

For compounds **9**–**12**, the spectra are broadened compared with **2**, but there is no resolved triplet. Unfortunately, the lack of resolved triplet spectra for compounds **9**–**12** makes it difficult to make a quantitative comparison between these compounds (Figure 8). We could model the spectra as unresolved zero-field splitting, that is, use $D_{S=1}$ to broaden the line width, but this does not seem a sensible method for deriving this parameter. The observation that the interaction is weaker for the longer links in **9**, **10**, and **11** appears eminently sensible. The oddity is compound **12**, where both the micro-SQUID and the EPR studies show the interaction is weak, despite the Ni···Ni distance being the second shortest in the entire family studied.

The spectra of **13** are unique in the series in also showing the $\Delta m_s = 2$ transition at low field (Figure 8). We have simulated these spectra using the computationally demanding Hamiltonian [1] using the parameters derived from the micro-SQUID measurement and appropriate single ion anisotropies (Figure 8b);[16] we also used the simple Hamiltonian [3] used for the other dimers, which is much quicker and gives a $D_{S=1}$ value of $+0.125\ cm^{-1}$ (Figure 8c). Where we have performed micro-SQUID and EPR studies on complexes we find that $D_{S=1} = 0.1\ J'$,[18] and the simulation of the spectra of **13** confirms this relationship.

Density functional calculations: We have concentrated on the oddity in the family—the very weak interaction in compound **12**, where there are five-membered N-heterocycles in the bridge rather than six-membered heterocycles in the other compounds. As a comparison we have considered the 4,4′-bipyridyl bridged compound, **3**, where the Ni···Ni distance is longer but the inter-ring exchange greater.

Previous work by Cargill-Thompson et al. nicely demonstrates the principle of spin alternation through different paths around even member rings.[1a] In each case, the spin polarization is complementary since the routes must be odd and odd (as with a *meta*-6-membered ring) or even and even (as with a *para*-6-membered ring). However, for odd membered rings, as in **12**, the paths must be even and odd, thus exchange via five-membered heterocycles should be weaker due to competing spin-polarization paths. This is illustrated in Scheme 3. For a six-membered heterocycle, the spin polarization, represented by up or down arrows on each carbon site, leads to the same spin polarization at the bridge-head carbon regardless of which way you move around the heterocycle. However, for a five-membered ring, depending on whether you move through the two-atom or three-atom part of the heterocycle will induce opposite spin polarization at the bridge-head carbon.

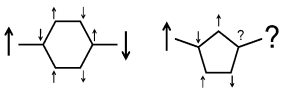

Scheme 3. Representation of constructive interferences around an even membered ring and destructive interferences around an odd membered ring.

We have attempted to quantify this effect through DFT calculations. The full systems (rings and bridge) have been taken into account with some pruning of the organic ligands surrounding the magnetic cores of the rings (see the Supporting Information for further details on the method and on the approximations used). As Ni^{II} ions have a $3d^8$ electronic configurations, in an octahedral environment only d orbitals with e_g symmetry are spin polarized. As the local axis around the Ni atoms are rotated from the plane of the pyridine (or pyrazole) rings in the linkers, and some deviation from a regular geometry is found for the coordination shell of Ni atoms, both σ and π orbitals of the extended molecule can in principle support magnetic interactions between the spin of the two rings. Calculating the spin-polarized electron density isosurfaces for a very low isovalue (= ±0.0003 electrons/a.u.^{3}), and looking specifically at the relevant Ni-linker-Ni coupling region supports the simple picture from spin polarization and also gives further insight (Figure 9). In all the linkers there is an alternation of spin polarization when moving from one atom to the next, and this polarization involves primarily involves orbitals with π character. Polarization of σ orbitals in the linkers, although present on the N atoms bound to Ni, fades away within a few bonds. Because of the spin-alternation rule discussed above, whether ferromagnetic or antiferromagnetic interactions between magnetic centers are seen depends on the number of C/N-atoms in the bonding pathway; if an even number of C/N-atoms is present the exchange is antiferromagnetic, while if an odd number of C/N-atoms is present ferromagnetic coupling should be found. Therefore in **12**, in which two possible paths are found around the five-atom heterocycle, destructive interference between these two paths leads to a very low spin polarization of the orbitals in the inner region of the bipyrazole ligand and hence a

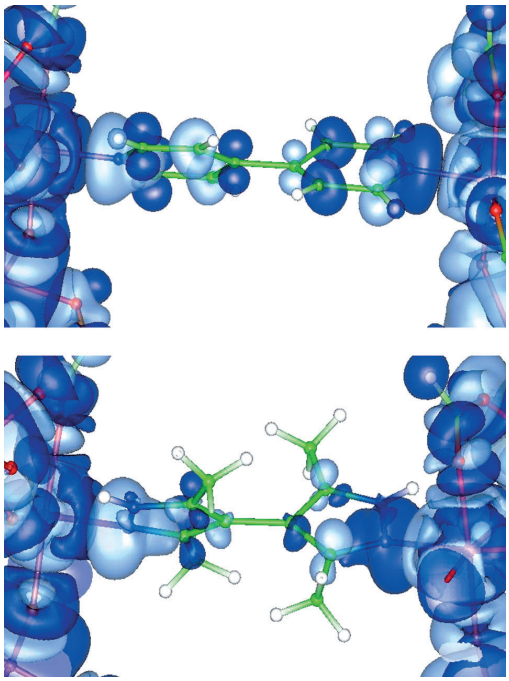

Figure 9. Spin-polarization density in (a) **3** and (b) **13**, zoomed in the region of the bridging ligand for isovalues of + (dark blue) and - (light blue) 0.0003 electrons/a.u.^{3}.

much weaker interaction between the rings than would be predicted on the Ni···Ni distance alone.

The four methyl groups on the bipyrazole ligand force the torsion angle of the five-membered aromatic rings in **12** far from coplanar (53.66/56.59°). This would clearly lead to poor π-orbital overlap and could be an additional key factor in the weakness of the interaction observed. We have recently reported DFT calculations[19] on a the 4,4′-bipyridyl derivatives where we have systematically varied the torsion angle between the pyridyl rings, and found that there is a correlation between the strength of this interaction and the torsion angle between the N heterocycles. Work is underway to obtain experimental data to examine this hypothesis.

Conclusion

Quantum computing, or rather the search for means of its realization has been the sharp focus for both theoreticians and practical researchers in the physical sciences for many years.[3a] The idea to use coordination complexes as qubits for QIP was proposed in 2003[3b–d] and has been examined since then.[20] For incorporation in QIP systems we have looked at {Cr_7Ni} rings with $S = {}^1/_2$ ground states, with the "up"- and "down"-spin states (i.e., $ms = +1/2$ and $-1/2$ respectively) generating the required quantum two-level system. The system satisfies several of the DiVincenzo criteria[21] required for physical implementation of quantum computing, namely: a) The cluster has a well defined ground spin state at low temperature and is well separated from the first excited states. b) Initialization of the system can be achieved by application of a strong magnetic field at low temperature. c) Decoherence times on the order of microseconds should allow gate operation before state degradation can occur. Our metallocycles also have the possible advantages of multiple accessible excited states, a size more amenable to addressability than single ions and, perhaps most importantly, vast chemical versatility.

We have established that the magnetic interaction between these rings is dependent on three factors: through-bond inter-spin distance, spin-polarization mechanisms, and torsion angles. No single parameter can be used to predict the resulting exchange interaction. Certainly length is the principal determinant on whether communication can occur, but even over short distances this can be significantly attenuated by other effects. Good exchange is promoted, as expected, by significant π-orbital conjugation. Studies are underway to probe this effect further by the development of a set of bis-pyridyl ligands with varying torsion angles between the aromatic rings. In addition, there is scope for further study of the destructive interference attributed to spin alternation in the odd membered aromatic rings, investigating both five–five and five–six bi-heterocycles. Development of a read/write mechanism and establishment of a set of universal quantum gates are also upcoming goals. To this end, we are looking at both the potential for surface chemistry and also incorporation of switchable bridging ligands.

Experimental Section

Experimental details: With the exception of 1,4-bis(4-pyridyl)benzene, the organic bridges (NLN) were used as received from commercial suppliers or made in house by literature methods.[22–24]

For 1,4-bis(4-pyridyl)benzene (used in **9**), 1,4-dibromobenzene (0.148 g, 0.63 mmol), pyridyl 4-boronic acid (0.20 g, 1.89 mmol), $Pd(PPh_3)_4$ (0.032 g, 0.046 mmol), $Na_2CO_{3(aq)}$ (1.52 mL, 1 M, 3.04 mmol) and a solvent mixture of DME/H_2O/EtOH = 7:3:2 (14.4 mL) were sealed in a 20 mL microwave vial and heated for 30 min at 160 °C. The mixture was then filtered to remove the catalyst and washed with ethyl acetate. The solvent was removed in vacuo and the residue was purified by column chromatography on silica ($CHCl_3$/hexane 50:50, then $CHCl_3$, and finally $CHCl_3$/MeOH 90:10) with the product coming off with the last eluent. The solvent was removed in vacuo. This gave the final product as a yellow solid (0.137 g, 95.1 %). ^{1}H NMR (400 MHz, $CDCl_3$, 300 K): $\delta = 8.70$ (dd, $J = 1.6$, 4.8 Hz, 4H), 7.77 (s, 4H), 7.56 ppm (dd, $J = 1.8$,4.6 Hz, 4H); ^{13}C NMR (400 MHz, $CDCl_3$, 300 K): $\delta = 150.48$, 147.60, 138.96, 127.90, 121.69 ppm; ESI-MS (+ve): *m/z* calcd: 233.1073; found: 233.1072 $[M+H]^+$; IR: $\tilde{\nu} = 3038$, 1086, 793 (C–H aromatic) 1585, 1479 (C–C aromatic), 1338 cm^{-1} (C–N aromatic stretch); elemental analysis calcd (%) for $C_{16}H_{12}N_2$ with 0.5 H_2O and 0.1 triphenylphosphine oxide: C 79.44, H 5.43, N 10.41, P 1.15; found: C 79.41, H 5.19, N 10.28, P 1.09.

1: Chromium(III) fluoride tetrahydrate (6.00 g, 33.1 mmol), *N*-ethyl-D-glucamine (3.60 g, 17.2 mmol), pivalic acid (30.0 g, 294 mmol), and nickel(II) carbonate hydroxide tetrahydrate (1.20 g, 2.01 mmol) were heated together with constant moderate stirring in a Teflon flask at 160 °C for 34 h. Next, the first 2 h of the reaction the solid which had formed in the flask was broken into small pieces using a spatula. This procedure was repeat-

ed twice during the following 4 h. At the end of the reaction a solid had formed. The reaction was allowed to cool and the solid extracted in diethyl ether (ca. 100 mL). The filtrate was diluted slowly with stirring with acetonitrile (ca. 170 mL) at which time a microcrystalline violet product started to form. The flask was sealed and kept at −10 °C for 2 days. The crystalline product was collected, washed with a mixture of diethyl ether/acetonitrile (1:1), and dried in air. This product was purified from a very fine brown powder by column chromatography on 40–63 μm mesh silica gel (BDH). Compound **1** was eluted with Et_2O as the first main band leaving a brown band on the column. The solvent was then evaporated under reduced pressure and the solid dissolved in diethyl ether (ca. 50 mL) and then diluted with acetonitrile (ca. 50 mL). The crystalline product started to form immediately. The flask was kept at −10 °C for one day, then the crystals were collected by filtration, washed with a mixture of diethyl ether/acetonitrile (1:2), and dried in air. Yield 3.20 g (30 %, based on Cr); ESI-MS (+ve) (sample dissolved in diethyl ether, run in methanol) *m/z*: 2200 (100) $[M]^+$, 2223 $[M+Na]^+$; elemental analysis for calcd (%) for: ($C_{83}H_{151}Cr_7NiF_3N_1O_{36}$): Cr 16.40, Ni 2.65, C 44.93, H 6.86, N 0.63; found: Cr 16.40, Ni 2.54, C 44.42, H 7.11, N 0.55.

2: 4-Phenylpyridine (0.200 g, 1.29 mmol) was added to a warm solution of **1** (0.750 g, 0.338 mmol) in acetone (40 mL) and the solution was refluxed for 10 min and then stirred at RT for 5 h. Dark purple microcrystalline product was collected by filtration, washed with acetone, then extracted in diethyl ether (ca. 10 mL) and the filtrate diluted with acetone (ca. 10 mL), then left for slow evaporation. After two days the crystals that had formed (including suitable for X-ray structure study) were collected by filtration, washed with acetone, and dried in air. Yield: 0.56 g (70 % based on **1**); elemental analysis calcd (%) for ($C_{94}H_{158}Cr_7F_3N_2Ni_1O_{35}$): Cr 15.45, Ni 2.49, C 47.92, H 6.76, N 1.19; found: Cr 15.43, Ni 2.46, C 47.67, H 6.94, N 1.12.

3: 4,4′-Dipyridine (0.035 g, 0.224 mmol) was added to a warm solution of **1** (1.3 g, 0.586 mmol) in acetone (100 mL), and the solution was refluxed while stirring for 1 h and then stirred at RT overnight. The dark purple microcrystalline product was collected by filtration, washed with acetone, then dissolved in diethyl ether (ca. 15 mL), filtered, and the filtrate diluted with acetone (ca. 25 mL), then left for slow evaporation at RT Crystals formed over two days (including suitable for X-ray structure study), and were collected by filtration, washed with acetone, and dried in air. Yield: 0.73 g (71 % based on the ligand); elemental analysis calcd (%) for ($C_{176}H_{306}Cr_{14}F_6N_4Ni_2O_{70}$): Cr 15.97, Ni 2.58, C 46.38, H 6.77, N 1.23; found: Cr 15.06, Ni 2.48, C 45.76, H 6.69, N 1.17.

4: The same procedure as for **3** with the exception that the *trans*-1,2-di(4-pyridyl)ethylene was used instead of the 4,4′-dipyridine and for recrystallization, dichloromethane instead of diethyl ether. Crystals (suitable for X-ray structure study) were grown by slow concentration at RT of a solution of **4** in a mixture of tetrahydrofuran/acetonitrile (2:1). Yield: 91 % (based on the ligand); elemental analysis calcd (%) for ($C_{178}H_{308}Cr_{14}F_6N_4Ni_2O_{70}$): Cr 15.88, Ni 2.56, C 46.64, H 6.77, N 1.22; found: Cr 15.48, Ni 2.60, C 46.11, H 6.87, N 1.14.

5–10 and 12: Compound **1** (650 mg, 0.293 mmol) was refluxed with the appropriate ligand (0.112 mmol) in acetone (50 mL) for 1 h. Upon cooling a crystalline product formed. The solution was left to stand for 12 h after which the product was filtered off and rinsed in cold acetone until the washings ran colorless. The yields are based on **1.** **5**: (490 mg, 0.107 mmol, 95.5 %); elemental analysis calcd (%) for ($C_{178}H_{310}N_4O_{70}F_6Cr_{14}Ni_2$): C 46.62, H 6.81, N 1.22, Cr 15.87, Ni 2.55; found: C 46.43, H 7.05, N 1.08, Cr 15.69, Ni 2.46. **6**: (320 mg, 0.070 mmol, 62.5 %); elemental analysis calcd (%) for ($C_{178}H_{306}N_4O_{70}F_6Cr_{14}Ni_2$): C 46.66, H 6.73, N 1.22, Cr 15.89, Ni 2.56; found: C 46.40, H 7.02, N 1.13, Cr 15.90, Ni 2.47. **7**: (334 mg, 0.072 mmol, 64.6 %); elemental analysis calcd (%) for ($C_{178}H_{310}N_4O_{72}F_6Cr_{14}Ni_2$): C 46.30, H 6.77, N 1.21, Cr 15.76, Ni 2.54; found: C 45.72, H 6.91, N 1.18, Cr 15.83, Ni 2.45. **8**: (460 mg, 0.100 mmol, 89.3 %); elemental analysis calcd (%) for ($C_{176}H_{306}N_6O_{70}F_6Cr_{14}Ni_2$): C 46.09, H 6.73, N 1.83, Cr 15.87, Ni 2.56; found: C 45.74, H 6.47, N 1.78, Cr 15.94, Ni 2.52. **9**: (295 mg, 0.064 mmol, 56.8 %), elemental analysis calcd (%) for ($C_{182}H_{310}N_4O_{70}F_6Cr_{14}Ni_2$): C 47.17, H 6.74, N 1.21, Cr 15.71, Ni 2.53; found: C 46.85, H 6.92, N 0.96, Cr 15.71, Ni 2.69. **10**: (425 mg, 0.092 mmol, 82.1 %), elemental analysis calcd (%) for ($C_{178}H_{306}N_8O_{70}F_6Cr_{14}Ni_2$): C 46.10, H 6.65, N 2.42, Cr 15.70, Ni 2.53; found: C 45.96, H 6.61, N 2.34, Cr 15.51, Ni 2.54. **12**: (495 mg, 0.108 mmol, 96.4 %), elemental analysis calcd (%) for ($C_{178}H_{306}N_8O_{70}F_6Cr_{14}Ni_2$): C 46.10, H 6.65, N 2.42, Cr 15.70, Ni 2.53; found: C 45.96, H 6.61, N 2.34, Cr 15.51, Ni 2.54.

11: **1** (509 mg, 0.230 mmol) and bis-1,4-(4-pyridylvinyl)benzene (34.4 mg, 0.121 mmol) were stirred in dichloromethane (10 mL) at RT for 15 h. The solvent was removed under vacuum and the dry product washed with thoroughly in acetone to yield the final product (208 mg, 0.044 mmol, 36.4 %), elemental analysis calcd (%) for ($C_{186}H_{314}N_4O_{70}F_6Cr_{14}Ni_2$): C 47.68, H 6.75, N 1.20, Cr 15.54, Ni 2.51; found: C 47.15, H 6.71, N 1.15, Cr 15.26, Ni 2.56.

13: was synthesized in two steps. First, **1** (3.50 g, 1.58 mmol) was stirred with pyrazine (0.80 g, 10.0 mmol) in dichloromethane (10 mL) for 12 h after which the solvent was removed and the residue stirred in acetonitrile (30 mL) for 3 h. The fine suspension was filtered off and washed in more acetonitrile to yield $[Cr_7NiF_3(C_8H_{14}NO_5)(t\mathrm{BuCO_2})_{15}(\mathrm{pyrazine})]$, **13i**, (3.55 g, 1.51 mmol, 95.6 %), elemental analysis calcd (%) for ($C_{87}H_{153}N_3O_{35}F_3Cr_7Ni$): C 45.81, H 6.78, N 1.85, Cr 15.96, Ni 2.57; found: C 45.66, H 6.92, N 1.75, Cr 15.99, Ni 2.54. The newly formed pyrazine–ring monomer, **13i** (1.00 g, 0.425 mmol) and **1** (1.00 g, 0.451 mmol) were independently dissolved in dichloromethane (2 × 10 mL). The solutions were then combined and a further portion of dichloromethane added (5 mL, to make a total of 25 mL). The solution was then stirred in a sealed container for 12 h during which time crystals had begun to form. The container was then partially opened and half of the total volume of solvent was allowed to evaporate over a period of 2 days. The solution was filtered and crystals washed in dichloromethane (3 × 5 mL) to yield the final product (1.20 g, 0.254 mmol, 59.8 %); elemental analysis calcd (%) for ($C_{170}H_{302}N_4O_{70}F_6Cr_{14}Ni_2$): C 44.56, H 6.79, N 1.25, Cr 16.24, Ni 2.62; found: C 45.24, H 6.76, N 1.19, Cr 16.01, Ni 2.65.

The combined mass of the linked systems was too high for traditional electrospray mass spectrometry methods and attempts to use matrix-assisted laser desorption ionization mass spectrometry were unsuccessful in producing any high-mass charged species.

Structural analysis: The dimers presented here are not all easy to crystallize, and even when suitable size crystals are obtained, significant X-ray absorption combined with weak diffraction due to large unit cells and abundant void space makes the crystallographic process non-trivial. We optimize our data collections by using synchrotron radiation when available (and for this access we are grateful, see acknowledgements). Nevertheless, even with such equipment diffraction is often only achieved to relatively small angles. We are satisfied that we have undertaken all possible steps to maximize quality and accuracy in our crystallographic process. Data for **1**, **2**, **3**, **4**, and **13** were collected on a Bruker Nonius Kappa CCD diffractometer ($Mo_{K\alpha}$, $\lambda = 0.71073$) at the University of Manchester, UK. Data reduction was performed with Nonius HKL DENZO and SCALEPACK software.[25] Data for **5** were collected on a Rigaku Saturn724+ diffractometer (synchrotron, $\lambda = 0.68890$) at beamline I19 at DIAMOND Light Source, UK. Data reduction was performed with d*TREK software.[26] Data for **6** were collected on an Oxford Diffraction XCalibur 2 diffractometer ($Mo_{K\alpha}$, $\lambda = 0.71073$) at the University of Manchester, UK. Data reduction was performed with CrysAlisPro software.[27] Data for **7**, **9**, **10**, **11** and **12** were collected on a Bruker APEX II diffractometer (synchrotron, $\lambda = 0.77490$) at the Advanced Light Source, Berkeley Lab, USA. Data reduction was performed with Bruker SAINT software.[28] Data for **8** were collected on a Bruker SMART 6000 diffractometer ($Mo_{K\alpha}$, $\lambda = 0.71073$). Data reduction was performed with Bruker SAINT software. In all cases the selected crystals were mounted on a tip using crystallographic oil and placed in a cryostream. Data were collected using ϕ and ω scans chosen to give a complete asymmetric unit. Structure solution and refinement was performed with the Shelx package.[29] The structures were solved by direct methods and completed by iterative cycles of ΔF and full-matrix least-squares refinement against F^2. All non-hydrogen atoms were refined anisotropically. Hydrogen atoms were calculated geometrically and were riding on their respective atoms. CCDC-696012 (**1**), 696014(**2**), 696015 (**3**), 696016 (**4**), 827104 (**5**), 827103 (**6**), 827102 (**7**), 827101 (**8**), 827100 (**9**), 780830 (**10**), 827099 (**11**), 789802 (**12**),

827098 (**13**) contain the supplementary crystallographic data for this paper. These data can be obtained free of charge from The Cambridge Crystallographic Data Centre via www.ccdc.cam.ac.uk/data_request/cif.

Acknowledgements

This work was supported by the EPSRC (UK), by the STREP MolSpinQIP, and partially by the ERC Advanced Grant MolNanoSpin No. 226558. The Advanced Light Source, where some X-ray diffraction measurements were taken, is supported by the Director, Office of Science, Office of Basic Energy Sciences, of the U.S. Department of Energy under Contract No. DE-C02–05CH11231. We also thank DIAMOND Light Source, Oxfordshire, UK, for the provision of additional synchrotron beamtime. R.E.P.W. is supported by a Royal Society Wolfson Merit Award.

[1] a) A. M. W. Cargill Thompson, D. Gatteschi, J.A. McCleverty, J. A. Navas, E. Rentschler M. D. Ward, *Inorg. Chem.* **1996**, *35*, 2701; b) V. A. Ung, A. M. W. Cargill Thompson, D. A. Bardwell, D. Gatteschi, J. C. Jeffery, J. A. McCleverty, F. Totti, M. D. Ward, *Inorg. Chem.* **1997**, *36*, 3447; c) S. R. Bayly, E. R. Humphrey, H. de Chair, C. G. Paredes, Z. R. Bell, J. C. Jeffery, J. A. McCleverty, M. D. Ward, F. Totti, D. Gatteschi, S. Courric, B. R. Steele, C. G. Screttas, *J. Chem. Soc. Dalton Trans.* **2001**, 1401; d) K. M. Stobie, Z. R. Bell, T. W. Munhoven, J. P. Maher, J. A. McCleverty, M. D. Ward, E. J. L. McInnes, F. Totti, D. Gatteschi, *Dalton Trans.* **2003**, 36.

[2] a) G. A. Timco, S. Carretta, F. Troiani, F. Tuna, R. G. Pritchard, E. J. L. McInnes, A. Ghirri, A. Candini, P. Santini, G. Amoretti, M. Affronte, R. E. P. Winpenny, *Nature Nanotech.* **2009**, *4*, 173; b) G. A. Timco, E. J. L. McInnes, R. G. Pritchard, F. Tuna, R. E. P. Winpenny, *Angew. Chem.* **2008**, *120*, 9827; *Angew. Chem. Int. Ed.* **2008**, *47*, 9681.

[3] a) M. N. Leuenberger, D. Loss, *Nature* **2001**, *410*, 789; b) F. Meier, J. Levy, D. Loss, *Phys. Rev. Lett.* **2003**, *90*, 047901; c) F. Meier, J. Levy, D. Loss, *Phys. Rev. B* **2003**, *68*, 134417; d) F. Troiani, M. Affronte, P. Santini, S. Carretta, G. Amoretti, *Phys. Rev. Lett.* **2005**, *94*, 190501.

[4] S. Wang, H.-L. Tsai, K. Folting, J. D. Martin, D. N. Hendrickson and G. Christou, *J. Chem. Soc. Chem. Commun.* **1994**, 671.

[5] H. E. Toma, K. Araki, A. D. P. Alexiou, S. Nikolaou, S. Dovidauskas, *Coord. Chem. Rev.* **2001**, *219*, 187.

[6] a) L. Lecren, O. Roubeau, Y.-G. Li, X. F. Le Goff, H. Miyasaka, F. Richard, W. Wernsdorfer, C. Coulon, R. Clérac, *Dalton Trans.* **2008**, 755; b) H. Miyasaka, K. Nakata, L. Lecren, C. Coulon, Y. Nakazawa, T. Fujisaki, K. Sugiura, M. Yamashita and R. Clérac, *J. Am. Chem. Soc.* **2006**, *128*, 3770; c) H. Miyasaka, K. Nakata, K. Sugiura, M. Yamashita, R. Clérac, *Angew. Chem.* **2004**, *116*, 725.

[7] E. C. Sañudo, T. Cauchy, R. H. Laye, O. Roubeau, S. J. Teat, G. Aromí, *Inorg. Chem.* **2007**, *46*, 9045.

[8] J. van Slageren, R. Sessoli, D. Gatteschi, A. A. Smith, M. Helliwell, R. E. P. Winpenny, A. Cornia, A. L. Barra, A. G. M. Jansen, E. Rentschler, G. A. Timco, *Chem. Eur. J.* **2002**, *8*, 277.

[9] R. H. Laye, F. K. Larsen, J. Overgaard, C. A. Muryn, E. J. L. McInnes, E. Rentschler, V. Sanchez, S. J. Teat, H. U. Güdel, O. Waldmann, G. A. Timco, R. E. P. Winpenny, *Chem. Commun.* **2005**, 1125.

[10] a) R. W. Saalfrank, I. Bernt, E. Uller, F. Hampel, *Angew. Chem.* **1997**, *109*, 2596; b) R. W. Saalfrank, I. Bernt, E. Uller, F. Hampel, *Angew. Chem.* **1997**, *109*, 2596; *Angew. Chem. Int. Ed. Engl. Angew. Chem. Int. Ed.* **1997**, *36*, 2482.

[11] E. K. Brechin, *Chem. Commun.* **2005**, 5141.

[12] For example: a) K. Hegetschweiler, H. Smalle, H. M. Streit, W. Schneider, *Inorg. Chem.* **1990**, *29*, 3625; b) R. Shaw, I. S. Tidmarsh, R. H. Laye, B. Breeze, M. Helliwell, E. K. Brechin, S. L. Heath, M. Murrie, S. Ochsenbein, H.-U. Güdel, E. J. L. McInnes, *Chem. Commun.* **2004**, 1418.

[13] a) P. Klüfers, J. Schumacher, *Angew. Chem.* **1994**, *106*, 1839; *Angew. Chem. Int. Ed. Engl.Angew. Chem. Int. Ed.* **1994**, *33*, 1742; b) P. Klüfers, H. Piotrowski, J. Uhlendorf, *Chem. Eur. J.* **1997**, *3*, 601.

[14] Harris notation describes the binding mode as $[X.Y_1Y_2Y_3...Y_n]$, in which X is the overall number of metals bound by the whole ligand, and each value of Y refers the number of metal atoms attached to the different donor atoms, see: R. A. Coxall, S. G. Harris, D. K. Henderson, S. Parsons, P. A. Tasker, R. E. P. Winpenny, *J. Chem. Soc. Dalton Trans.* **2000**, 2349.

[15] W. Wernsdorfer, D. Mailly, G. A. Timco, R. E. P. Winpenny, *Phys. Rev. B* **2005**, *72*, 060409.

[16] a) F. K. Larsen, E. J. L. McInnes, H. El Mkami, J. Overgaard, S. Piligkos, G. Rajaraman, E. Rentschler, A. A. Smith, G. M. Smith, V. Boote, M. Jennings, G. A. Timco, R. E. P. Winpenny, *Angew. Chem.* **2003**, *115*, 105; b) S. Piligkos, E. Bill, D. Collison, E. J. L. McInnes, G. A. Timco, H. Weihe, R. E. P. Winpenny and F. Neese, *J. Am. Chem. Soc.* **2007**, *129*, 760; c) S. Piligkos, H. Weihe, E. Bill, F. Neese, H. El Mkami, G. M. Smith, D. Collison, G. Rajaraman, G. A. Timco, R. E. P. Winpenny, E. J. L. McInnes, *Chem. Eur. J.* **2009**, *15*, 3152.

[17] J.-P. Launay, M. Tourrel-Pagis, J.-F. Lipskier, V. Marvaud, C. Joachin, *Inorg. Chem. Inorg. Chem.* **1991**, *30*, 1033.

[18] A. Candini, G. Lorusso, F. Troiani, A. Ghirri, S. Carretta, P. Santini, G. Amoretti, C. Muryn, F. Tuna, G. Timco, E. J. L. McInnes, R. E. P. Winpenny, W. Wernsdorfer and M. Affronte, *Phys. Rev. Lett.* **2010**, *104*, 037203.

[19] V. Bellini, G. Lorusso, A. Candini, W. Wernsdorfer, T. B. Faust, G. A. Timco, R. E. P. Winpenny, M. Affronte, *Phys. Rev. Lett.* **2011**, *106*, 227205.

[20] For a brief up-to-date review see: T. D. Ladd, F. Jelezko, R. Laflamme, Y. Nakamura, C. Monroe, J. L. O'Brien, *Nature* **2010**, *464*, 45.

[21] D. P. DiVincenzo, *Fortschr. Phys.* **2000**, *48*, 771.

[22] 3,6-Di(pyridin-4-yl)-1,2,4,5-tetrazine (in **10**): F. Bentiss, M. Lagrenee, M. Traisnel, B. Mernari, *J. Heterocycl. Chem.* **1999**, *36*, 149 was used to generate the intermediate 1,4-dihydro-3,6-di-4-pyridinyl-1,2,4,5-tetrazine, which was oxidized to the final product following the procedure by C.-J. Hsu, S.-W. Tang, J.-S. Wang, W.-J. Wang, *Mol. Cryst. Liq. Cryst.* **2006**, *456*, 201.

[23] Bis-1,4-(4-pyridylvinyl)benzene (in **11**), A. J. Amoroso, A. M. W. Cargill Thompson, J. P. Maher, J. A. McCleverly, M. D. Ward, *Inorg. Chem.* **1995**, *34*, 4828.

[24] 4,4′-Bi-3,5-dimethylpyrazole (in **12**), R. G. Charles, *Org. Synth.* **1959**, *39*, 61; *Org. Synth.* **1961**, *Coll. Vol. 4*, 869. Followed by P. E. Kruger, B. Moubaraki, G. D. Fallon, K. S. Murray, *J. Chem. Soc. Dalton Trans.* **2000**, 713.

[25] a) Z. Otwinowski, W. Minor, *Methods Enzymol.* **1997**, *276*, 307; b) R. H. Blessing, *Acta Crystallogr. Sect. A* **1995**, *51*, 33.

[26] J. W. Pflugrath, *Acta Crystallogr. Sect. A Acta Crystallogr. D* **1999**, *55*, 1718.

[27] Agilent, *CrysAlis PRO* **2010** Agilent Technologies, Yarnton, England.

[28] Bruker, *SAINT Software* **1996**, Bruker AXS, Madison, USA.

[29] G. M. Sheldrick, *Acta Crystallogr. Sect. A* **2008**, *64*, 112.

Received: June 10, 2011
Published online: November 14, 2011

CHEMISTRY
A EUROPEAN JOURNAL

Supporting Information

Chemical Control of Spin Propagation between Heterometallic Rings

Thomas B. Faust,[a] Valerio Bellini,[b] Andrea Candini,[b] Stefano Carretta,[c] Giulia Lorusso,[d] David R. Allan,[e] Laura Carthy,[a] David Collison,[a] Rebecca J. Docherty,[a] Jasbinder Kenyon,[a] John Machin,[a] Eric J. L. McInnes,[a] Christopher A. Muryn,[a] Harriott Nowell,[e] Robin G. Pritchard,[a] Simon J. Teat,[f] Grigore A. Timco,[a] Floriana Tuna,[a] George F. S. Whitehead,[a] Wolfgang Wernsdorfer,[g] Marco Affronte,[d] and Richard E. P. Winpenny*[a]

chem_201101785_sm_miscellaneous_information.pdf

Supplementary Information

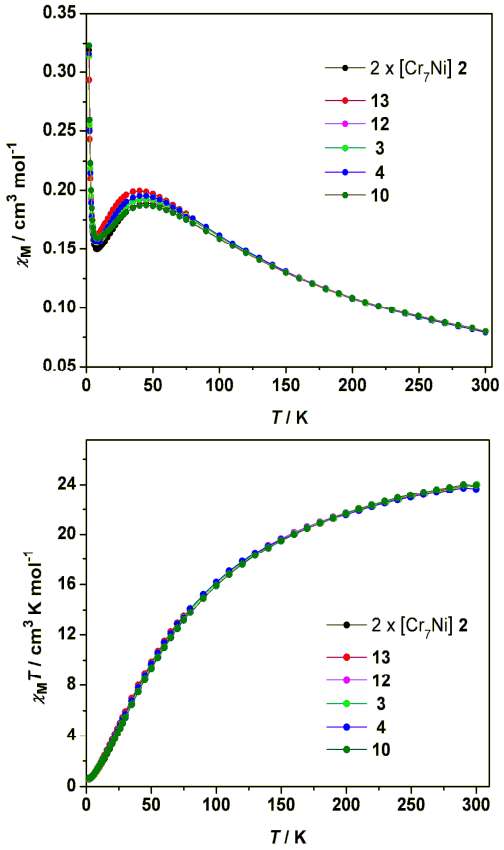

Figure S1: Magnetic susceptibility (χ_M) against T for the dimers of rings (shown left) and $\chi_M T$ against T for the same compounds (shown right). In each case there is no significant difference from the sum of two individual Cr_7Ni rings.

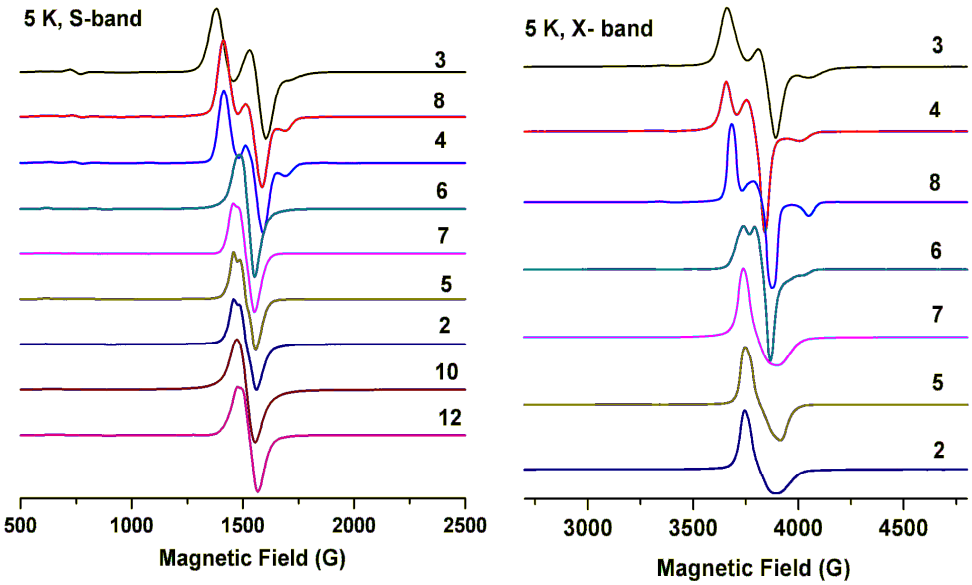

Figure S2: Powder EPR spectra at 5 K for compounds **2 - 12**, recorded at S- (shown left) and X-band (shown right) microwave frequencies.

Chapter Seven - Paper 3

"Twist and shout – magnetic communication through aromatic bridges with different torsion angles"

T. B. Faust, G. A. Timco, F. Tuna and R. E. P. Winpenny, *manuscript in preparation*

Chemical Science

Cite this: DOI: 10.1039/c0xx00000x

www.rsc.org/xxxxxx

EDGE ARTICLE

Twist and shout – magnetic communication through aromatic bridges with different torsion angles

Thomas B. Faust,[a] Floriana Tuna,[b] Grigore A. Timco[a] and Richard E. P. Winpenny*[a,b]

Received (in XXX, XXX) Xth XXXXXXXXX 20XX, Accepted Xth XXXXXXXXX 20XX

DOI: 10.1039/b000000x

A series of heteroaromatic bridging ligands are employed in the synthesis of a family of paramagnetic, hetrometallic ring dimers. The extent of spin propagation between the rings via the organic conduit is investigated through EPR spectroscopy and conclusions over the mechanism of spin-communication are drawn.

Introduction

Intermolecular communication of spin *via* molecular bridges over nanometer distances is of interest to scientists in the fields of molecular magnetism and spintronics. In particular an ability to tailor interactions, and possibly even adjust them *in situ*, would be a significant contribution to the development of a molecular quantum gate. Implementation of such a gate between quantum bits would be recognisable as a significant step in the creation of a quantum information processing system.

We have previously published a study on a family of heterometallic ring dimers whose magnetic communication was studied as a function of the bridging ligand used.[1] From this study we established that exchange was dependant on distance and also had strong reason to suppose that 1) it could only occur along well conjugated π-systems and 2) quantum interference effects arising from spin-alternation rule meant that even-membered heterocycles were superior to odd-membered ones. Theoretical calculations backed up these hypotheses[2] and so we now look to gain further convincing experimental evidence to support them.

The heterometallic rings, $\{Cr_7Ni(N\text{-Et-}D\text{-glu})F_3(O_2CtBu)_{15}\}$, commonly referred to as $\{Cr_7Ni\}$ or 'purple rings' on account of their lustre,[3] have been proposed as possible qubits within a quantum information processing system[4] and so understanding these interactions is of high significance. It also has wider interest as these rings are a convenient way of studying one-dimensional molecular magnetism. The means of inter-ring ligation has traditionally been *via* bis-pyridyl type ligands, of which the simplest member is 4,4'-bipyridine (PyPy). We use PyPy as the basis of this study and investigate how magnetic exchange varies with dihedral angle between the aromatic heterocycles. Firstly we employ 3,3',5,5'-tetramethyl-4,4'-bipyridine ($PyMe_2PyMe_2$) whose four methyl groups induce considerable steric clash, forcing orthogonality between the pyridyl planes. We then consider 3,8-phenanthroline (Phen) whose pyridyl rings are fused such that they are forced to planarity. In order to establish whether quantum interference effects in odd-membered aromatic heterocycles does indeed affect the spin-coupling we investigate the ligand 4-(1*H*-pyrazol-4-yl)pyridine, (PyPz).

Results and discussion

The target compounds were successfully prepared by reaction of a small excess of $\{Cr_7Ni\}$ with the appropriate ligand to give the products $[\{Cr_7Ni(\text{N-ethyl-D-glucamine})F_3(O_2CtBu)_{15}\}_2L]$ where L = PyPy, 1; $PyMe_2PyMe_2$, 2; Phen, 3 and PyPz, 4, all in good yield.

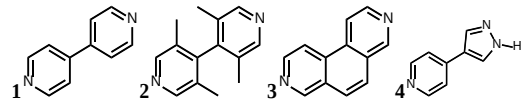

Scheme 1. Structures of the bridging ligands used; the dimer to which they belong is indicated to their lower left hand side.

Our hopes for a range bridging ligands with pyridyl groups at varying twist angles (θ) were pleasingly realised in the series: 2 (81.8) > 1 (40.6) > 3 (1.61°). The other structural metric for these compounds are unremarkable, the Ni•••Ni distances are consistent (through bond circa 11.2 Å, through space circa 13.8 Å). In addition the metallorings within each dimer are all fairly planar (angles between the mean planes all < 10°). The vector angle (defined by taking the angle between lines drawn from the Ni to the distal Cr of each respective metalloring) is different for 1 and 2 (circa 90°) from 3 where the rings are neatly stacked. We do not envisage this parameter to have any influence on the magnetic exchange but it is included for completeness (full details in Table 1).

Table 1. Structural merics and zero-field splitting parameters for compounds 1 – 4.

Compound	Bridging ligand	Ni•••Ni distance through space /Å	Ni•••Ni distance through bond /Å	Angle between mean plane of metallorings /°	Angle between Ni•••Cr vectors /°	Twist angle (θ) /°	$D_{S=1}$ /cm^{-1}
1	PyPy	11.218(3)	13.82(8)	8.37	89.9	40.6	+ 0.013
2	$PyMe_2PyMe_2$	11.204(3)	13.87(6)	5.73	91.6	81.8	<0.001
3	Phen	11.191(4)	13.82(5)	8.51	4.52	1.61	+0.017
4	PyPz	10.400(3)	12.45(5)	34.7	47.9	16.1	<0.001

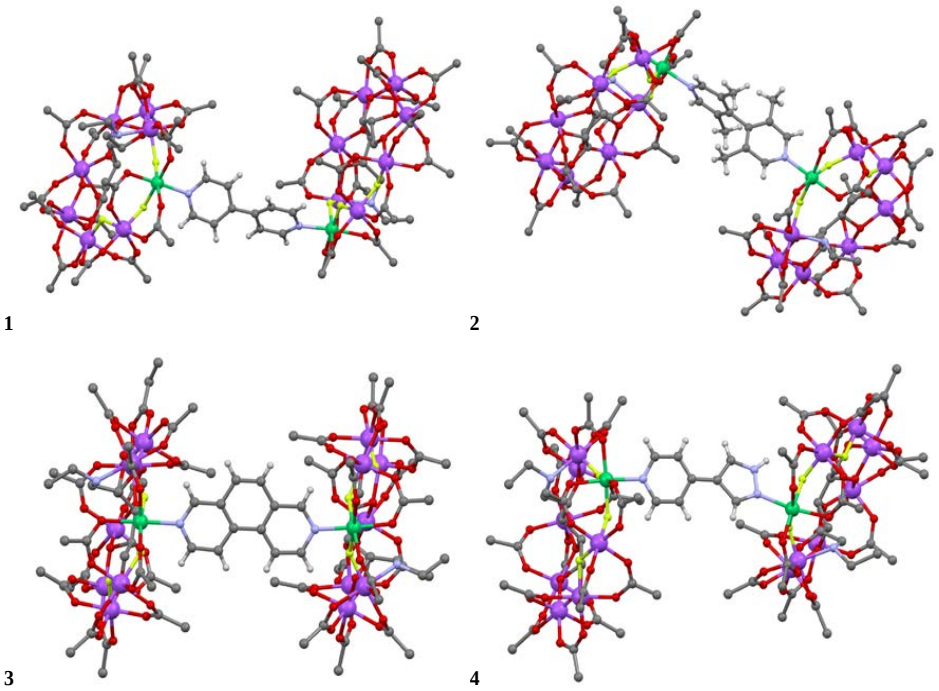

Figure 1. Structure of **1** – **4** in the solid state (methyl group, hydrogens from the metallorings, and solvent are omitted for clarity. Colours: C, grey; H, white; N, blue; O, red; F, yellow; Cr, purple; Ni, green).

Table 2. Crystallographic details for compounds **1** – **4**.

Compound	**1** .MeCOMe .$2H_2O$	**2** .MeCN .$3CHCl_3$	**3**	**4** .5 $CHCl_3$
Empirical formula	$C_{179}H_{314}Cr_{14}F_6N_4Ni_2O_{72}$	$C_{185}H_{320}Cl_9Cr_{14}F_6N_5Ni_2O_{70}$	$C_{178}H_{306}Cr_{14}F_6N_4Ni_2O_{70}$	$C_{179}H_{315}Cl_{10}Cr_{14}F_6N_5Ni_2O_{70}$
M_r	4633.76	5012.93	4581.69	4971.28
Crystal size [mm]	0.30 × 0.20 × 0.18	0.25× 0.10 × 0.10	0.10× 0.10 × 0.07	0.80 × 0.20 × 0.15
Crystal system	Monoclinic	Monoclinic	Monoclinic	Orthorhombic
Space group	C2	C2	$P2_1$	$P2_12_12_1$
a [Å]	54.7570(6)	53.505(4)	18.750(9)	19.751(4)
b [Å]	16.9650(2)	17.0141(5)	29.698(13)	27.554(6)
c [Å]	35.8310(5)	35.9017(19)	24.190(11)	49.470(10)
α [°]	90	90	90	90
β [°]	125.6330(10)	125.176(9)	112.297(5)	90
γ [°]	90	90	90	90
V [Å^3]	27053.1(6)	26714(2)	12462(10)	26923(9)
Z	4	4	2	4
ρ_{calc} [mg mm^{-3}]	1.138	1.246	1.221	1.226
T [K]	100(2)	100(2)	100(2)	100(2)
Goof on F^2	1.198	0.996	1.003	1.337
R_1 [I>2σ (I)]	0.0871	0.0809	0.1059	0.1214
wR_2 [all data]	0.2363	0.1208	0.1464	0.1493

Of course whilst we have tailored the sterics to our requirements, we have made variation in the electronics of our bridges. The four methyl groups of the bridge in 2 are electron donating but so weakly that their influence in this case must surely be eclipsed by the larger effect of diminished π-overlap. Were the methyl groups to make a significant contribution, we might expect greater electron density within the π-system leading to a slightly elevated value of exchange parameter. 3,8-phenanthroline is somewhat more different from 4,4'-bipyridine in that the pyridyl groups are now fused with the formation of an additional aromatic ring. The pi system now runs non-stop from nitrogen to nitrogen as opposed having to span the formally C-C single bond. Whilst not ideal this contribution is unavoidable, and in any case 3,8-phenanthroline seemed preferable to benzo[lmn][3,8]phenanthroline where this enhancing effect might be amplified.

We have found previously that the magnetic exchange within each metalloring is anti-ferromagnetic such that each metal has the opposite spin to each of its neighbours. Full magnetic compensation is not achieved since there is a mismatch in spin amplitude between octahedral Cr(III), d^3, s = $^3/_2$, and octahedral Ni(II), d^8, s = 1; leading to a effective S = $^1/_2$ for the metalloring as a whole.

Communication between metallorings pairs within a dimer generates a spin triplet and singlet which are close in energy (due to the weakness of the exchange) but well-separated from other excited states. Since the triplet-singlet separation is so small we would expect to see the S = 1 triplet even if the inter-metalloring exchange is predominantly anti-ferromagnetic.

Direct measurement of the isotropic exchange parameter, *J*, is not possible by standard magnetometry due to the very weak nature of the interaction being studied. We have, through micro-SQUID measurement in collaboration with Wolfgang Wernsdorfer at the Néel Institute, Grenoble; validated our methodology of using zero-field splitting parameter of the S = 1 state, $D_{S=1}$, derived from low temperature electron paramagnetic resonance (EPR), to derive *J* to a good degree of certainty.[1] We use a simple Hamiltonian [1] to model the triplet generated by the communication between the S = $^1/_2$ metallorings.

$$\hat{H} = \mu_B \mathbf{B}.\mathbf{g}.\hat{S} + D_{S=1}\left[\hat{S}_z^2 - \frac{S(S+1)}{3}\right] \qquad [1]$$

The g-values are fixed from the spectra of a reference monomer compound [{Cr_7Ni}PyPh], 5, (PyPh = 4-phenylpyridine): g_z=1.78 and $g_{x,y}$=1.84 and D_{xyz} is considered to be coincident with g_{xyz}. By comparing *D* with *J* from micro-SQUID measurements of a range of compounds we find the relationship [2], where *J* is the anisotropic exchange between the Ni spin moments and S_{Ni1} and S_{Ni2} are the spin moments of the two Ni ions (S_{Ni1} = S_{Ni2} = 1) according to the spin Hamiltonian [3].

$$D_{|S|=1} = 0.1 \cdot J \qquad [2]$$

$$\hat{H} = -2J'\vec{S}_{Ni1} \cdot \vec{S}_{Ni2} \qquad [3]$$

If D is very small (< 0.001 cm^{-1}) the triplet cannot be resolved by EPR and the spectrum resembles that of an isolate S = $^1/_2$ state.

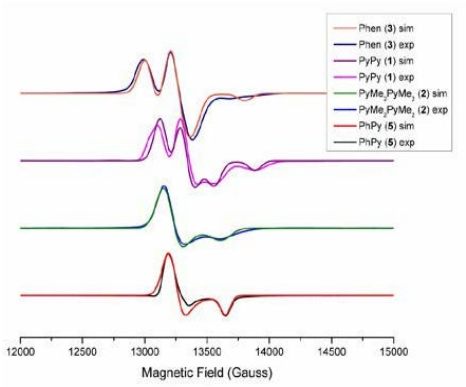

Figure 2. 5 K Q-band EPR experimental (exp) and simulated (sim) spectra of compounds 1-3 and 5 as polycrystalline powders in Eicosane using the parameters reported in Table 1 and in the text.

Q-band experimental and simulated data for 1-3 and 5 are shown in Figure 2. We observe that the spectrum of 2 resembles a slightly broadened version of 5, no well resolved triplet is observed. There seems little value in modeling 2 as S = 1 and modeling the broadening with unresolved ZFS and so the simulation shown is for that of a two S = $^1/_2$ rings. We must therefore conclude that $D_{S=1}$ < 0.001 cm^{-1}. The spectrum of 3 resembles that of 1 though with greater separation of the doublet. This is reflected in the larger $D_{S=1}$ value (3, +0.017 cm^{-1}; 1, +0.013 cm^{-1}).

We have previously suggested a $\cos^2$ relationship between twist angle of the pyridyl rings (θ) and the isotropic exchange interaction parameter, *J*.[2] Plotting $D_{S=1}$ versus the twist angle and overlaying a scaled $\cos^2\theta$ line, as in Figure 3, we can judge the validity of this proposal.

We propose that the apparent enhancement in magnetic exchange in 1 could be due to a change in structural conformation during the EPR measurement. All X-ray crystal data were collected at 100 K and thus the twist angle is valid at this temperature, however EPR measurements were taken on samples at 5 K. We could envisage significant rearrangement in neither 2, for which rotation is extremely sterically hindered, nor in 3, where free rotation is not allowed. In 1 we might expect a small reduction in twist angle, which may explain its deviation from the $\cos^2\theta$ prediction. Of course three points are not sufficient to provide positive confirmation but the data does seem to lend support to the proposal, particularly the case of 2.

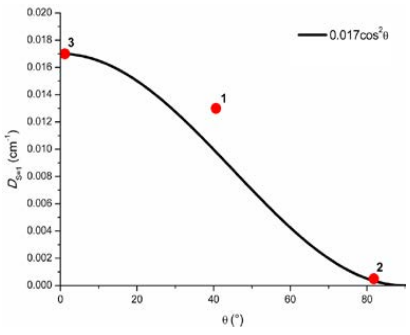

Figure 3. Plot of ZFS parameter $D_{S=1}$ for 1, 2 and 3 against their respective twist angle (red spots) overlaid with a scaled $\cos^2\theta$ (black line).

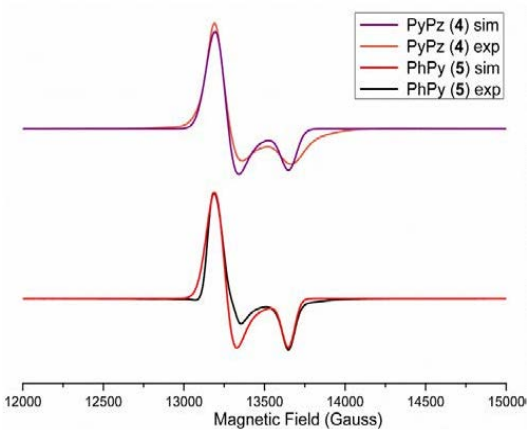

Figure 4. 5 K Q-band EPR experimental (exp) and simulated (sim) spectra of compounds 4 and 5 as polycrystalline powders in Eicosane using the parameters reported in the text.

For 4, the important steric metrics seem to favour stronger magnetic exchange between the metallorings when compared with 1; the Ni•••Ni distance is shorter (10.400 Å through space) and the pyridyl and pyrazolyl rings are closer to being coplanar (θ = 16.1°). The latter is no doubt due to the reduction in imposed H/H steric clash on moving from two six-membered rings to one five- and one six-membered ring. Upon inspection of Figure 4, it is evident that there is no well resolved triplet, indeed there is barely any noticeable line broadening. Once again simulation was performed based on two non-isolated S = $^1/_2$ rings. This must lead us to the conclusion that the severe attenuation in isotropic exchange parameter, noticed by minimisation of ZFS, must be due to an electronic effect, namely quantum interference brought about by the spin alternation rule.

The spin alternation rule, well documented for ligands of this type by McCleverty and Ward,[5] describes the way in which spin polarisation density alternates in sign from one atom to the next. This has the consequence that pathways with even numbers of atoms promote anti-ferromagnetic exchange and pathways with odd numbers of atom promote ferromagnetic exchange. Six-membered rings (such as 4-pyridyl) constitute two pathways consisting of four atoms. As such both pathways promote anti-ferromagnetic exchange. This constructive interference serves to reinforce the interaction as in the case of 1 (See Scheme 2a). Five-membered rings (such as pyrazolyl) offer two pathways of different length (two or three atoms). The difference forces deconstructive interference between the competing anti-ferromagnetic and ferromagnetic pathways (see Scheme 2b).

We have previously used this explanation in the case of [{Cr_7Ni}$_2$(3,3',5,5'-tetramethyl-1H,1'H-4,4'-bipyrazole)] but on that occasion we could not rule out the possibility that the lack of communication was a result of poor π-overlap between the pyrazolyl rings (the angle between them being ~55°).[1] The measurement of 5 seems to confirm the proposal of magnetic exchange attenuation by deconstructive quantum interference.

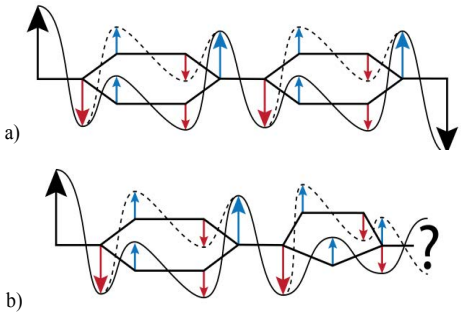

Scheme 2. a) A representation of constructive interference effects on spin polarisation around two six-membered rings leading to anti-ferromagnetic exchange; and b) of the deconstructive interference caused when a five-membered ring is introduced.

Conclusions

Our data serves to support our original hypothesis that, rather than just being determined solely by distance, the magnetic exchange between spin-centres is controlled by the extent of well conjugated π-overlap present in the bridge. Thus, should it be possible to mechanically vary the dihedral angle between aromatic rings in such a system by chemical, electrical or photophysical means; we may be able to control the magnetic communication between spin-centres *via* a 'twist and shout' mechanism. Furthermore we have demonstrated that should well conjugated bridges be employed, communication can still be attenuated by quantum deconstructive interference arising from spin-alternation around odd-membered rings, though practical applications exploiting this phenomenon for switchability seem less realisable.

Experimental

Preparation of complexes

{$Cr_7Ni(Etglu)F_3(O_2CtBu)_{15}$}$H_2O$ and **1** were synthesised according to literature previously published by our group.[4a] 4,4'-bipyridine and 4-(1*H*-pyrazol-4-yl)pyridine were used as supplied from commercial sources.

3,3',5,5'-tetramethyl-4,4'-bipyridine was prepared according to the method published by Rang and co-workers.[6] 3,8-phenanthroline was prepared according to the method published by Botana and co-workers,[7] however it was found more convenient to purify the desired product from the side product (pyrido[3,4-*g*]isoquinoline) by very careful column chromatography (silica gel/ 95% $CHCl_3$, 5% MeOH, 1% NEt_3) rather than the extraction described in their paper.

2 was synthesised by reflux of [Cr_7Ni(N-ethyl-D-glucamine)$F_3(O_2CtBu)_{15}H_2O$] (650 mg, 0.293 mmol) with 3,3',5,5'-tetramethyl-4,4'-bipyridine (23.8 mg, 0.112 mmol) in acetone (50 mL) for 1 h. After cooling, the purple microcrystalline solid was filtered and rinsed in acetone until the washings ran colourless to yield the product (493 mg, 0.107 mmol, 95.5%). $C_{180}H_{314}N_4O_{70}F_6Cr_{14}Ni_2$ Anal. Calcd (Found): C, 46.56 (46.55); H, 6.86 (6.91); N, 1.21 (1.27); Cr, 15.78 (15.98); Ni, 2.54 (2.61).

3 was synthesised by reflux of [Cr_7Ni(N-ethyl-D-glucamine)$F_3(O_2CtBu)_{15}H_2O$] (650 mg, 0.293 mmol) with 3,8-phenanthroline (20.2 mg, 0.112 mmol) in acetone (50 mL) for 1 h. After cooling, the purple microcrystalline solid was filtered and rinsed in acetone until the washings ran colourless to yield the product (440 mg, 0.096 mmol, 85.7%). $C_{178}H_{306}N_4O_{70}F_6Cr_{14}Ni_2$ Anal. Calcd (Found): C, 46.66 (46.42); H, 6.73 (6.61); N, 1.22 (1.21); Cr, 15.89 (16.15); Ni, 2.56 (2.63).

4 was synthesised by mixing [Cr_7Ni(N-ethyl-D-glucamine)$F_3(O_2CtBu)_{15}H_2O$] (650 mg, 0.293 mmol) with the 4-(1*H*-pyrazol-4-yl)pyridine (16.3 mg, 0.112 mmol) in dichloromethane (50 mL) and allowing it to stand. Small crystals grew after a few days which grew larger over a number of weeks. The crystals were filtered and rinsed in dichloromethane until the washings ran colourless to yield the product (370 mg, 0.081 mmol, 72.7%). $C_{174}H_{305}N_5O_{70}F_6Cr_{14}Ni_2$ Anal. Calcd (Found): C, 45.97 (45.76); H, 6.76 (6.70); N, 1.54 (1.46); Cr, 16.01 (15.68); Ni, 2.58 (2.54).

Crystallography

Single crystals of **2** and **3** were grown by slow evaporation of chloroform and dichloromethane respectively from acetonitrile solutions. Suitable crystals of **4** were harvested directly from the reaction vessel (from dichloromethane). X-ray data for **2** and **4** were collected using an Oxford Xcalibur CCD single crystal X-ray diffractometer. X-ray data for **3** were collected at DIAMOND Light Source, Oxfordshire, UK, using a Rigaku Saturn CCD single crystal diffractometer. All data were collected at 100 K. Structures were solved and refined by full-matrix least-squares techniques on F^2 using the SHELX-97 program. The absorption corrections were done by Multiscan methods. Hydrogen atoms were included in the refinement process as per the riding model.

EPR

EPR spectroscopy was carried out on powdered samples in Eicosane at 5 K at Q-band frequency (34 MHz) on a Bruker Elexsys EPR specrometer.

Acknowledgements

This work was supported by the EPSRC (UK) and by the STREP MolSpinQIP, and partially by the ERC Advanced Grant MolNanoSpin No. 226558. We thank DIAMOND Light Source and the staff at beamline I19 for the provision of synchrotron beamtime. R.E.P.W. is supported by a Royal Society Wolfson MeritAward.

Notes and references

[a] The School of Chemistry, [b] The Photon Science Institute, University of Manchester, Oxford Road, Manchester, M13 9PL, UK
E-mail: richard.winpenny@manchester.ac.uk

1 T. B. Faust, V. Bellini, A. Candini, S. Carretta, G. Lorusso, D. R. Allan, L. Carthy, D. Collison, R. J. Docherty, J. Kenyon, J. Machin, E. J. L. McInnes, C. A. Muryn, H. Nowell, R. G. Pritchard, S. J. Teat, G. A. Timco, F. Tuna, G. F. S. Whitehead, W. Wernsdorfer, M. Affronte and R. E. P. Winpenny, *Chem. Eur. J.*, 2011, **17**, 14020.

2 V. Bellini, G. Lorusso, A. Candini, W. Wernsdorfer, T. B. Faust, G. A. Timco, R. E. P. Winpenny and M. Affronte, *Phys. Rev. Lett.*, 2011, **106**, 227205.

3 G. A. Timco, T. B. Faust, F. Tuna and R. E. P. Winpenny, *Chem. Soc. Rev.*, 2011, **40**, 3067.

4 a) G. A. Timco, E. J. L. McInnes, R. G. Pritchard, F. Tuna and R. E. P. Winpenny, *Angew. Chem., Int. Ed.*, 2008, **47**, 9681; b) F. Troiani and M Affronte, *Chem. Soc. Rev.*, 2011, **40**, 3119.

5 J. A. McCleverty and M. D. Ward, *Acc. Chem. Res.*, 1998, **31**, 842.

6 A. Rang, M. Engeser, N. M. Maier, M. Nieger,W. Lindner and C. A. Schalley, *Chem. Eur. J.*, 2008, **14**, 3855.

7 E. Botana, E. Da Silva, J. Benet-Buchholz, P. Ballester, and J. de Mendoza, *Angew. Chem. Int. Ed.*, 2007, **46**, 198.

Chapter Eight - Paper 4

"Caesium ion sequestration by a fluoro-metallocrown [16]-MC-8"

T. B. Faust, P. G. Heath, C. A. Muryn, G. A. Timco and R. E. P. Winpenny, *Chemical Communications*, 2010, **46**, 6258-6260.

Caesium ion sequestration by a fluoro-metallocrown [16]-MC-8†

Thomas B. Faust,[a] Paul G. Heath,[a] Christopher A. Muryn,[a] Grigore A. Timco[a] and Richard E. P. Winpenny*[ab]

Received 29th April 2010, Accepted 14th July 2010
DOI: 10.1039/c0cc01188f

A fluoro-metallocrown selectively binds caesium, extracting it from aqueous solutions into an organic layer; the binding of Cs is monitored by ^{1}H-NMR of the paramagnetic complexes.

The first metallocrown was reported by Lah and Pecoraro in 1989.[1] The mixed valent complex has the formula [Mn(II){Mn(III)(salicylhydroximate)}$_4$(acetate)$_2$(DMF)$_6$] and is classified as a 12-metallocrown-4, ([12]-MC-4), containing the repeating motif –O–Mn(III)–N– four times, binding to a central Mn(II). The range of metallocrowns is expansive,[2] with promising leads in ion recognition,[3] catalysis,[4] as single-molecule magnets,[5] as MRI contrast agents[6] and as anti-bacterial agents.[7] Fluoro-metallocrowns have been reported to bind small cations by Jones *et al.*,[8,9] though they were unable to ascertain the extent to which the guests were bound in solution. The homometallic ring [CrF(tBuCO$_2$)$_2$]$_8$ has also been discussed as a possible fluoro-crown.[10]

Heterometallic [Cr$_7$MF$_8$(tBuCO$_2$)$_{16}$]$^-$ (M = Ni, Co) wheels have been shown to host a wide variety of primary and secondary alkyl ammonium guests in the solid state.[11] ^{1}H-NMR studies show that guest ammonium ions also remain inside the ring cavity in solution.[12] Their cation binding capacity is no doubt due to the charge imbalance created by replacing the trivalent chromium(III) with a divalent metal. The removal of primary and cyclic alkyl ammonium species with concomitant replacement by hydroxonium or sodium ion upon column chromatography has also been demonstrated.[12]

Treatment of [(H$_3$N^{n}Pr)Cr$_7$CoF$_8$(tBuCO$_2$)$_{16}$], **1**,[12] with excess caesium pivalate followed by recrystallisation from diethyl ether/acetonitrile gives [Cs⊂Cr$_7$CoF$_8$(tBuCO$_2$)$_{16}$]·0.5MeCN, **2**. Compound **2** can also be made directly from reaction of hydrated chromium fluoride with pivalic acid in the presence of cobalt pivalate and caesium pivalate.‡ X-Ray crystallographic studies show the caesium ion centrally bound to all eight fluorides and co-planar with the heterometals of the wheel (Fig. 1). The data also clearly show that, in the solid state, four axial pivalate groups on one side of the wheel lean towards the central ion, four on the other side lean away slightly. On this exposed side the caesium is bound to solvate acetonitrile, however, this conformation is not evident in solution.

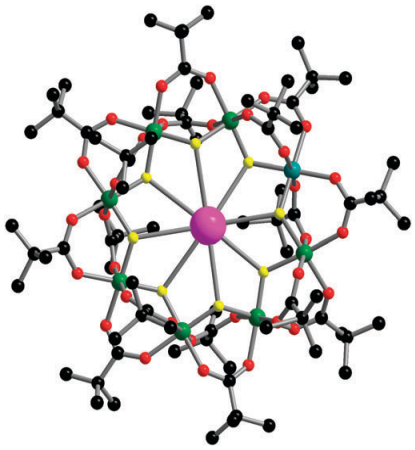

Fig. 1 The structure of **2** (omitting MeCN) in the crystal. Colours: Cs, pink; Cr, green; Co, teal; O, red; F, yellow; C, black; H, omitted.

Most paramagnetic samples suffer from greatly broadened resonances as a consequence of the rapid nuclear relaxation of the metal nuclei. Octahedral high-spin Co(II) is unusual in exhibiting very slow nuclear relaxation[13] and consequently the net effect of the {Cr$_7$Co} system is such that spectral features are sharp enough to impart real chemical insight.[12]

^{1}H-NMR spectroscopy for this new caesium-centred wheel reveals eight proton environments for the sixteen pivalates (Fig. 2b), as a result of the C_2 symmetry axis which extends from the cobalt ion *via* the centre of the caesium and through to the distal chromium. This evidence suggests either a conformation where all eight axial pivalates are perpendicular

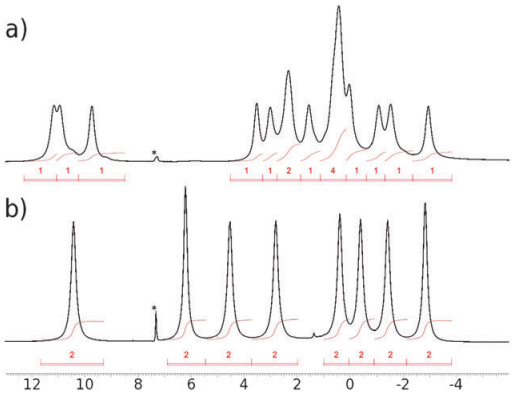

Fig. 2 ^{1}H-NMR of (a) **1** and (b) **2** at 300 MHz in CDCl$_3$. * Indicates protio-solvent impurity.

[a] *School of Chemistry, The University of Manchester, Oxford Road, Manchester, M13 9PL, UK. E-mail: richard.winpenny@manchester.ac.uk; Tel: +44 (0)161 275 4654*
[b] *The Photon Science Institute, The University of Manchester, Oxford Road, Manchester, M13 9PL, UK*

† Electronic supplementary information (ESI) available: ^{1}H-NMR of **1** and **2**. CCDC 784330–784331. For ESI and crystallographic data in CIF or other electronic format see DOI: 10.1039/c0cc01188f.

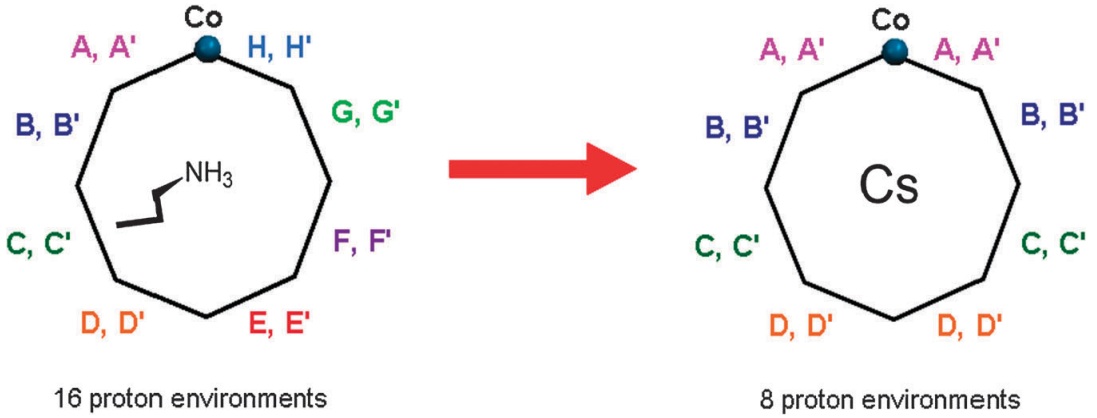

Fig. 3 Schematic showing guest exchange and accompanying increase in symmetry.

to the plane of the wheel or each set of pivalates flips between leaning towards and away from the caesium ion (as in the crystal structure) at a rate that is faster than the NMR timescale (at 300 MHz and RT).

An additional peak at −10 ppm can be attributed to fluxionally coordinating adventitious water, as has been reported previously.[12]

Treatment of $[(H_3N^nPr)Cr_7CoF_8(t BuCO_2)_{16}]$ with rubidium pivalate leads to similar results in both X-ray crystal structure, solution state NMR and electrospray mass spectrometry (ES-MS). The major difference of note is that compound **2** crystallises in the monoclinic space group, $C2/c$; whereas $[Rb\subset Cr_7CoF_8(t BuCO_2)_{16}]$ **3** crystallises in the tetragonal space group $P4$. The latter space group is found for smaller dialkylammonium cation (*e.g.* $Me_2NH_2^+$) centred rings.[11]

Time-resolved ^{1}H-NMR can be used to follow the extent of exchange between the guest species. The primary ammonium template in **1** lowers the symmetry of the ring from that found in **2** (Fig. 3). In principle within $[(H_3N^nPr)Cr_7CoF_8(t BuCO_2)_{16}]$, **1**, there are sixteen proton environments on the pivalate groups; in the measured NMR spectrum some of the resonances coincidentally overlap to give just twelve peaks (Fig. 2a). Further peaks are observed downfield corresponding to the alkyl ammonium. The $-NH_3$ gives a very broad peak and experiences the greatest chemical shift (*circa* −100 ppm). Caesium pivalate was added to **1** (dissolved in deuterated solvent) and spectra recorded every 2.5 min. The symmetry change on replacing the alkyl ammonium guest with caesium changes the number of proton environments from sixteen to eight and at $T > 5$ minutes only peaks of **2** are present. An additional peak is present in the reaction solution due to free pivalate from the caesium source. Peaks due to paramagnetically shifted protons from the ammonium alkyl guest also disappear within 10 min from the start of the reaction (Fig. 4). The result indicates a definite preference for the caesium cation and there is no indication of an intermediate species.

X-Ray crystal structures for $[Cs\subset Cr_7MF_8(t BuCO_2)_{16}]$ (M = Ni, Cu, Fe, Mn, Zn) have also been obtained and are isostructural with that of the cobalt analogue. We can also make analogous metallocrowns with carboxylates other than pivalate (*tert*-butylacetate, methacrylate, *o*-toluate,

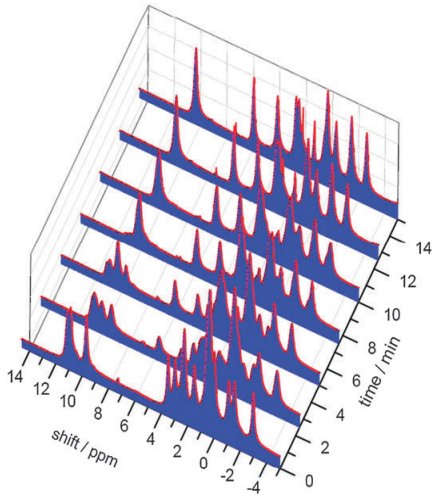

Fig. 4 Pivalate region of the NMR spectra tracing the extent of guest exchange in solution.

diethylacetate and 2,2-dimethylbutyrate). These metallocrowns all show preference for binding to caesium.

Preliminary experiments also suggest that **1** will extract $Cs^+_{(aq)}$ from water into dichloromethane. In a typical experiment, **1** (2.13 mmol) was dissolved in CH_2Cl_2 (25 mL), and CsX (0.44 mmol) (X = Cl^-, NO_3^-) dissolved in H_2O (10 mL) was added as a separate layer. The extraction was monitored by electrospray mass spectrometry (ES-MS); solutions of **2** have the most abundant peak for $[\mathbf{2} + Na]^+$ (Fig. 5). Mass spectral analysis of the organic layer, after extraction was carried out for 18 hours, showed the major peak was again $[\mathbf{2} + Na]^+$ and no peaks that could be assigned to **1**. The precise caesium salt seems unimportant for the phase transfer. Caesium is also extracted preferentially from the water layer in the presence of sodium, potassium and rubidium ions.

Sequestration of long lived radioactive caesium isotopes from high-level radioactive waste following reprocessing of nuclear fuels has long remained an issue for separation scientists. As well as precipitation[14] and ion exchange,[15]

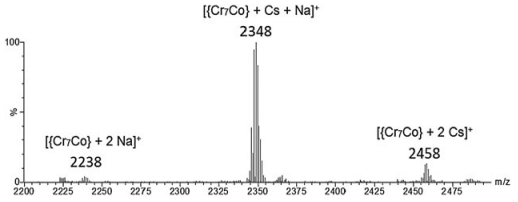

Fig. 5 The ES-MS of **2** run in MeOH.

host-assisted solvent extraction offers viable means of removal. Suitable proposed hosts including complex calixarenes,[16] hydroborate clusters[17] and metallaboranes[18] all have the common drawback of non-trivial fabrication. To this end we suggest that our fluoro-metallocrown represents a novel complexant for such a purpose with the considerable benefit of facile one pot synthesis from commercially available starting materials. As such, future work will quantify our strength of caesium binding, especially from aqueous media.

This work was supported by the EPSRC (UK) and EC Network of Excellence "MAGMANet", and by a Royal Society Wolfson Merit Award (to REPW).

Notes and references

‡ Synthesis of **2**: **1** (564 mg, 250 mmol) and Cs(tBuCO$_2$) (117 mg, 500 mmol) was dissolved in a solution of Et_2O (40 ml), DMSO (350 mg) and tBuCO$_2$H (350 mg). Following stirring for 2 h the solution was filtered and diluted with MeCN (40 ml). Slow evaporation of the Et_2O filtrate yields large green crystals (suitable for X-ray crystallography). These were washed in MeCN and air dried to yield **2** (558 mg, 240 mmol, 96.0%). Microanalysis for **2** ($C_{80}H_{144}CoCr_7CsF_8O_{32}$) calcd: C, 41.31; H, 6.24; N, 0.0; Cr, 15.65; Co, 2.53%. Found: C, 41.03; H, 6.27; N, 0.0; Cr, 15.24; Co 2.52%. ES-MS +ve (m/z): 2348 $[M + Na]^+$. Synthesis of **3** as for **2**, replacing Cs(tBuCO$_2$) with Rb(tBuCO$_2$) gave green crystals of **3** (525 mg, 230 mmol, 92.0%). Microanalysis for **3** ($C_{80}H_{144}Co_1Cr_7F_8O_{32}Rb$) calcd: C, 42.17; H, 6.37; N, 0.0; Cr, 15.98; Co, 2.59%. Found: C, 41.37; H, 6.43; N, 0.0; Cr, 15.63; Co 2.43%. ES-MS +ve (m/z): 2301 $[M + Na]^+$. Crystal data for **2**: $C_{81}H_{145.5}CoCr_7CsF_8N_{0.5}O_{32}$, M = 2346.32, monoclinic, space group $C2/c$, a = 45.069(2), b = 16.3923(3), c = 34.8600(19) Å, β = 114.009(5)°, V = 23526.1(18) Å^3, T = 100(2) K, Z = 8, 45 431 reflections measured, 23 954 independent reflections (R_{int} = 0.0480). The final R-values were: R_1 = 0.0812, wR_2 = 0.2288 ($I > 2\sigma(I)$); R_1 = 0.1401, wR_2 = 0.2559 (all data). Crystal data for **3**: $C_8H_{144}CoCr_7F_8O_{32}Rb$, M = 2278.35, tetragonal, space group $P4$, $a = b$ = 19.8632(3), c = 16.1639(7) Å, V = 6377.4(3) Å^3, T = 100(2) K, Z = 2, 36 433 reflections measured, 11 626 independent reflections (R_{int} = 0.0881). The final R-values were: R_1 = 0.1058, wR_2 = 0.2757 ($I > 2\sigma(I)$); R_1 = 0.1315, wR_2 = 0.2914 (all data).

1 M. S. Lah and V. L. Pecoraro, *J. Am. Chem. Soc*., 1989, **111**, 7258–7259.
2 G. Mezei, C. M. Zaleski and V. L. Pecoraro, *Chem. Rev*., 2007, **107**, 4933–5003.
3 S. Rochat, Z. Grote and K. Severin, *Org. Biomol. Chem*., 2009, **7**, 1147–1153.
4 L. C. Song, J. Gao, H. T. Wang, Y. J. Hua, H. T. Fan, X. G. Zhang and Q. M. Hu, *Organometallics*, 2006, **25**, 5724–5729.
5 Y. Z. Zhang, W. Wernsdorfer, F. Pan, Z. M. Wang and S. Gao, *Chem. Commun*., 2006, 3302–3304.
6 A. J. Stemmler, J. W. Kampf, M. L. Kirk, B. H. Atasi and V. L. Pecoraro, *Inorg. Chem*., 1999, **38**, 2807–2817.
7 M. Alexiou, I. Tsivikas, C. Dendrinou-Samara, A. A. Pantazaki, P. Trikalitis, N. Lalioti, D. A. Kyriakidis and D. P. Kessissoglou, *J. Inorg. Biochem*., 2003, **93**, 256–264.
8 L. F. Jones, C. A. Kilner, M. P. De Miranda, J. Wolowska and M. A. Halcrow, *Angew. Chem., Int. Ed*., 2007, **46**, 4073–4076.
9 L. F. Jones, S. A. Barrett, C. A. Kilner and M. A. Halcrow, *Chem.–Eur. J*., 2008, **14**, 223–233.
10 J. Overgaard, B. B. Iversen, S. P. Palii, G. A. Timco, N. V. Gerbeleu and F. K. Larsen, *Chem.–Eur. J*., 2002, **8**, 2775–2786.
11 M. Affronte, S. Carretta, G. A. Timco and R. E. P. Winpenny, *Chem. Commun*., 2007, 1789–1797.
12 E. C. Sañudo, T. B. Faust, C. A. Muryn, R. G. Pritchard, G. A. Timco and R. E. P. Winpenny, *Inorg. Chem*., 2009, **48**, 9811–9818.
13 For example: E. C. Constable, C. E. Housecroft, T. Kulke and C. Lazzarini, *J. Chem. Soc., Dalton Trans*., 2001, 2864–2871.
14 R. A. Peterson, J. O. Burgess, D. D. Walker, D. T. Hobbs, S. M. Serkiz, M. J. Barnes and A. R. Jensen, *Sep. Sci. Technol*., 2001, **36**, 1307–1321.
15 S. A. Shady, *J. Hazard. Mater*., 2009, **167**, 947–952.
16 A. Casnati, F. Sansone, J.-F. Dozol, H. Rouquette, F. Arnaud-Neu, D. Byrne, S. Fuangswasdi, M.-J. Schwing-Weill and R. Ungaro, *J. Inclusion Phenom. Macrocyclic Chem*., 2001, **41**, 193–200.
17 D. Naoufal, B. Grüner, P. Selucký, B. Bonnetot and H. Mongeot, *J. Radioanal. Nucl. Chem*., 2005, **266**, 145–148.
18 P. Selucký, N. V. Sistkova and J. Rais, *J. Radioanal. Nucl. Chem*., 1997, **224**, 89–94.

Cesium ion sequestration by a fluoro-metallocrown [16]-MC-8

Supporting Information

Figure S1. ^{1}H-NMR spectrum of **1** [$(H_3N^nPr)Cr_7CoF_8(t\text{BuCO}_2)_{16}$] at 300MHz in $CDCl_3$ (Pivalate region)

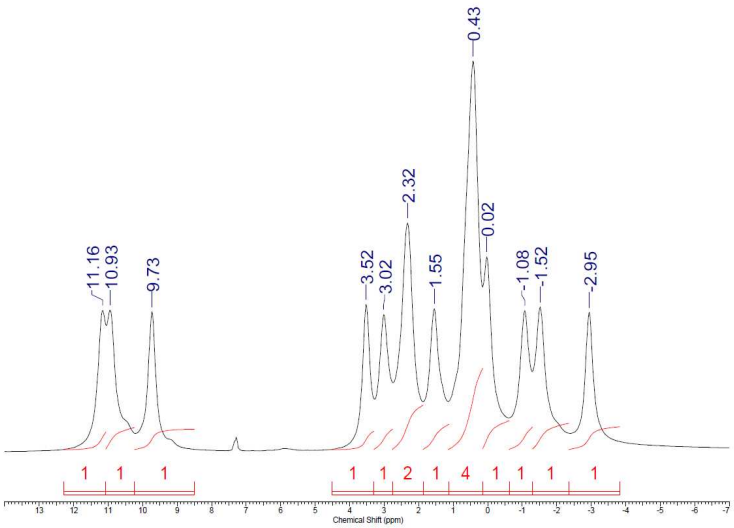

Figure S2. ^{1}H-NMR spectrum of **2** [$Cs \subset Cr_7MF_8(t\text{BuCO}_2)_{16}$] at 300MHz in $CDCl_3$ (Pivalate region)

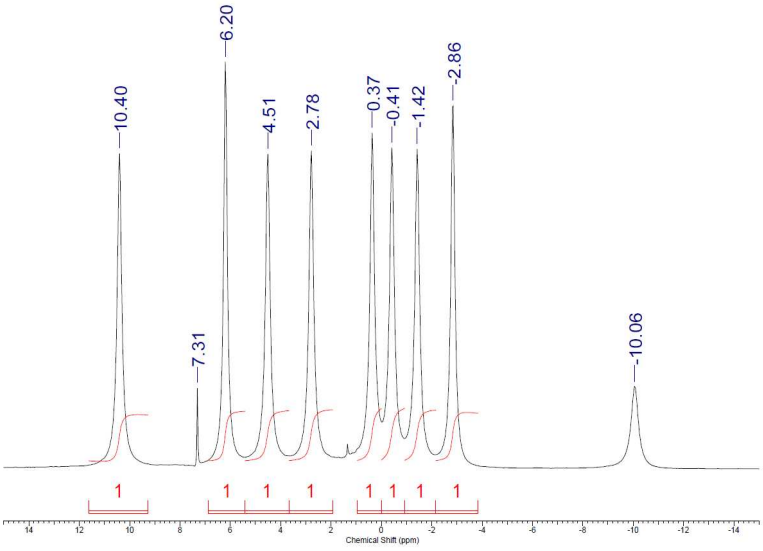

Chapter Nine - Paper 5

"Alkaline Earth - Transition Metal Octametallic Rings"

T. B. Faust, S. A. Varey, F. Tuna, G. A. Timco and R. E. P. Winpenny, *manuscript in preparation*

ChemComm

Cite this: DOI: 10.1039/c0xx00000x

www.rsc.org/xxxxxx

COMMUNICATION

Alkaline Earth - Transition Metal Octametallic Rings

Thomas B. Faust,[a] Sarah A. Varey,[a] Stephen Sproules,[b] Simon J. Teat,[c] Grigore A. Timco,[a] Floriana Tuna,[b] and Richard E. P. Winpenny*[a,b]

Received (in XXX, XXX) Xth XXXXXXXXX 20XX, Accepted Xth XXXXXXXXX 20XX

DOI: 10.1039/b000000x

Through stepwise synthesis *via* a six-membered molecular horseshoe, we demonstrate a route to the inclusion of alkaline earth metals into heterometallic eight-membered rings. The diamagnetic metal leads to a species with a net spin of 3/2 which is conveniently measured by EPR.

Molecular rings have stimulated much interest for two main reasons. Firstly, the discrete array of transition metal ions mean they are ideal candidates for the study of polymetallic one-dimensional magnetism; this is made even more attractive by the high degree of symmetry which often limits the magnetic exchanges to just a few values of J.[1] Secondly, their central cavity offers the promise of host-guest chemistry by complementarity of charge and/or shape leading to applications as molecular containers[2] and in ion sequestration.[3] In addition their complex but symmetric nature leads to aesthetically pleasing crystal structures. The core ring framework itself almost always consists of solely d-block metal ions, thanks to their preference for certain coordination geometries, and μ-2 bridging ligands to bind them together.

The rings presented here are cousins of the 'all transition metal' rings published previously, which conform to the formula $[M(III)_7M(II)_1F_8(O_2CMe_3)_{16}\{R_2NH_2\}]$ where M(III) is usually chromium (but can be aluminium, vanadium, iron, gallium or indium) and M(II) is usually nickel (but can be manganese, iron, cobalt, zinc or cadmium).[4,5] We have previously demonstrated the inclusion into these eight membered rings of the alkali metals; sodium at the edge of the ring,[6] and rubidium and caesium at the centre.[7] In contrast the results here show s-block elements occupying a position as a part of the cycle itself.

Our success in introducing Group one metals into $[Cr_7M(II)F_8Piv_{16}]^-$ rings led us to believe that similar results would be possible with Group two metals. Simple mixing of $[Cr_7M(II)F_8Piv_{16}(H_3N^nPr)]$ with any Group two metal salts does not in fact lead to exchange, as was the case with caesium.[7] We hypothesised that the mono-anionic ring simply had a higher affinity for the mono-cationic ammonium than for the di-cationic metal. As such we synthesised the previously published $[Cr_6Ni_2F_8(O_2C\mathit{t}Bu)_{16}(Himid)_2]$.[8] To our surprise this dianionic host possesses a higher affinity for its two incumbent imidozolium cations than for any Group two metal ion. We now suppose that hosting the imidazolium guests formed a very kinetically stable product, and that their presence in the ring's cavity blocked approach of the metal cation from both sides. We can reconcile this with the fact that we saw substitution for caesium with mono-alkylammoniums which block only one side of the ring whereas no substitution was observed with di-alkylammoniums which block both faces. Nevertheless we felt that having a metal guest would lead to a more thermodynamically stable product, but that we would have to approach its synthesis in a different fashion.

It has long been known that formation of octametallic rings such as ours proceed *via* 6-membered intermediate '$\{Cr_6\}$ horseshoes' which can be isolated if reaction times are shortened.[9] Our initial experiments began with initial formation of $Et_2NH_2^+$ centred horseshoes, which we supposed would host, guest-exchange and ring close in the presence of a Group two metal pivalate and Ni(II). Results from our initial experiments were not consistent with this mechanism and mass spectrometry indicated an abundance of $\{Cr_7M(II)\}$ where M(II) was not nickel but in fact our group two metal.

Optimising the reaction we have successfully demonstrated this reaction in the absence of nickel for M(II) = Mg, **2**; Ca, **3** and Sr, **4**. The magnesium and calcium reactions yield products isostructural with the known $\{Cr_7Ni\}$ variant. Strontium gives a very similar structure though the increased atom size means it favours a seven coordinate geometry, the additional site being occupied by a water molecule (see Figure 1).

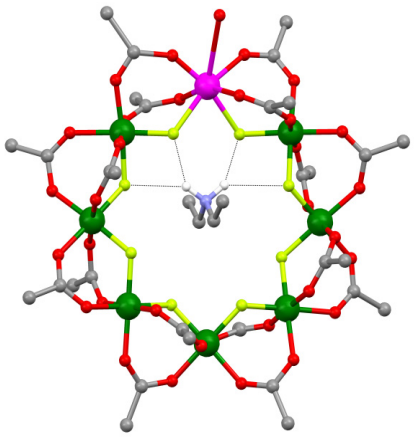

Figure 1. Structure in the crystal of **4** (Colours: C, grey; H, white; N, light blue; O, red; Cr, green; Sr, magenta. Carboxylate methyl groups and non-ammonium H omitted for clarity. Short ammonium-fluoride contacts in black dashed lines.)

This type of ring is axially-chiral owing to the arrangement of carboxylates about the heterometal, though to-date these rings have always crystallised with their chiral twin within the unit cell and no difference is observed here (generally Z = 4, two rings of each handedness).

Reaction with a barium salt appears to generate a range of products which could not be separated but mass spectrometry suggests the formation of both the expected product $[Cr_7BaF_8(O_2C\mathit{t}Bu)_{16}(Et_2NH_2)]$, **5a** and perhaps the precursor $[Cr_7BaF_9(O_2C\mathit{t}Bu)_{15}(Et_2NH_2)]$, **5b**. To demonstrate the generality of the method we repeated the experiment with just a nickel salt and achieved the expected $[Cr_7NiF_8(O_2C\mathit{t}Bu)_{16}(Et_2NH_2)]$, **6**.

It is worth noting that formation of $\{Cr_7M(II)\}$ *via* this method must be concurrent with disintegration of at least some {Cr6} horseshoes, since this is no exogenous source of chromium to facilitate the ring closure.

We also took preliminary steps to investigate the mechanism of the formation of these rings. Initially we repeated the synthesis but added o-toluic acid (o-$TolO_2H$) to the reaction. This resulted in the green powdered product, **7**, which was analysed by mass spectrometry from which we can observe at least 8 different products of the form $[Cr_7CoF_8(O_2C\mathit{t}Bu)_{16-x}(o\text{-}TolO_2)_x(Et_2NH_2)]$ where x = 3-10. It is thus apparent that we have encouraged scrambling of the existing carboxylates of the horseshoe, which was not the aim. We assume the lower pKa of o-$TolO_2H$ promotes substitution and so we chose to introduce the acid instead by using the nickel salt of 1-methylcyclohexane-1-carboxylic acid (HO_2C-1-MeCy). This particular acid was chosen because it should posses a very similar pKa to pivalic acid, hopefully avoiding a scrambling of the existing carboxylates by substitution. Separation of the products of this reaction by column chromatography was non-trivial and it was only possible to collect fractions of mixed products. Nevertheless the products are clearly distinguishable by mass spectrometry and we were able to crystallise the tetraheterocarboxylate product $[Cr_7NiF_8(O_2C\mathit{t}Bu)_{12}(O_2C\text{-}1\text{-}MeCy)_4(Et_2NH_2)]$, **8a**, from the mixture of fraction F1 (See Table 1). The crystal structure contains two rings within the asymmetric unit, which differ only in the orientation of one of the 1-methylcyclohexane-1-carboxylate rings. Both indicate all four new carboxylates are bridging between the new nickel centre and its adjacent chromiums (see Figure 2).

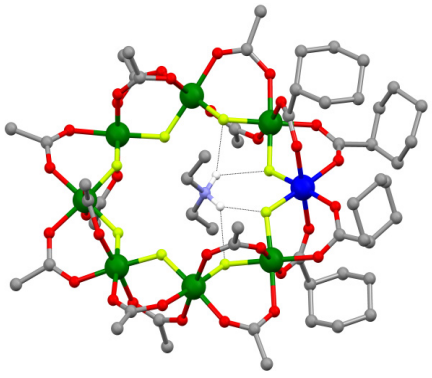

Figure 2. Structure in the crystal of one ring in **8a** (Colours and scheme as for Figure 1 plus: Ni, royal blue.)

Table 1. The ES-MS +ve values for the seven fractions of the column for $[Cr_7NiF_8(O_2CtBu)_{16-y}(O_2C\text{-}1\text{-}MeCy)_y(Et_2NH_2)]$, **8**. The value shown with (*) represents the 100% peak.

Species	F1	F2	F3	F4-6	F7
Unassigned					2225
Unassigned					2254*
$(O_2C\mathit{t}Bu)_{16}$			2294	2294*	2294
$(O_2C\mathit{t}Bu)_{15}(O_2C\text{-}1\text{-}MeCy)_1$		2334	2334	2334	2334
$(O_2C\mathit{t}Bu)_{14}(O_2C\text{-}1\text{-}MeCy)_2$		2368*	2368*	2368	
$(O_2C\mathit{t}Bu)_{13}(O_2C\text{-}1\text{-}MeCy)_3$	2408*	2408	2408	2408	
$(O_2C\mathit{t}Bu)_{12}(O_2C\text{-}1\text{-}MeCy)_4$	2448				

The lack of more than four heterocarboxylates in any species suggests that the pKa of 1-methylcyclohexane-1-carboxylic acid is too high to promote substitution with the existing pivalate bridges. Furthermore the significant amount of products where there are less than four heterocarboxylates indicates that pivalate is being released from somewhere, which lends support to the notion that the 'extra' chromium arises from the breakdown of another horseshoe, which also frees up spare pivalate.

The electronic structure of **2** – **4** was probed by Q-band (34 GHz) EPR spectra of polycrystalline samples recorded at 5 K display an elaborate spectral profile consistent with the $S = {}^3/_2$ ground state seen previously for the horseshoe,[10] indicating the inclusion of a Group 2 dication does not significantly perturb the electronic array of coupled Cr(III) ions. Simulations were conducted on the basis of the spin-Hamiltonian;

$$\hat{H} = -J\sum_{i}^{N-1}\hat{\mathbf{s}}_i\hat{\mathbf{s}}_{i+1} + \mathrm{D}\sum_{i}^{N}\left(\hat{\mathrm{s}}_{z,i}^2 - \frac{1}{3}\hat{\mathrm{s}}_i(\hat{\mathrm{s}}_i+1)\right) + \mathrm{E}\sum_{i}^{N}\left(\hat{\mathrm{s}}_{x,i}^2 - \hat{\mathrm{s}}_{y,i}^2\right) + \sum_{i}^{N}\mu_B\mathbf{B}\cdot\tilde{g}\cdot\hat{\mathbf{s}}_{i+1}$$

where all terms have their usual meaning. The $S = {}^3/_2$ ground state of **2** – **4** was described by g = 1.98 and near-identical zero-field splitting (ZFS) parameters D and E; the latter diagnostic of asymmetry of the D-tensor (Table 2). Satisfactory simulations required inclusion of the first excited state, $S = {}^1/_2$. This was fixed at 11.8 cm^{-1} above the quartet ground state as previously determined by inelastic neutron scattering (INS) measurements of isoelectronic $\{Cr_7Cd\}$.[11]

Table 2. ZFS parameters of the $S = {}^3/_2$ ground state for **2** – **4** and a {Cr7} 'horseshoe' from reference 10.

Compound	M(II)	D (cm^{-1})	E (cm^{-1})
2	Mg	-0.292	-0.042
3	Ca	-0.271	-0.045
4	Sr	-0.271	-0.045
$[(i\mathrm{Pr}_2NH_2)Cr_7F_8(O_2C\mathit{t}Bu)(hfac)_2]$		-0.363	-0.056

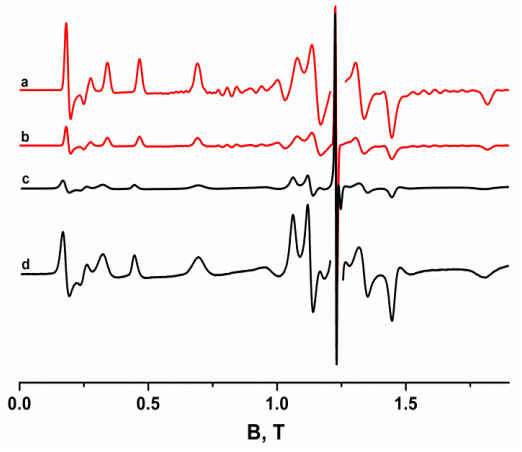

Figure 3. Q-band EPR spectrum of polycrystalline **3** at 5 K (in black) and simulation (red); parameters are discussed in the text. **a** and **d** are expansions of the $S = {}^3/_2$ signal; the sharp resonance at g ≈ 2 in **b** and **c** stem from the $S = {}^1/_2$ excited state.

We have also explored the inclusion of lanthanide ions to chromium horseshoes the results of which can be found in our recently publish sister paper.[12]

This work was supported by the EPSRC (UK) and the EC "Network of Excellence" MAGMANet. The Advanced Light Source, Berkeley, USA, where the X-ray diffraction measurement for **4** was taken, is supported by the Director, Office of Science, Office of Basic Energy Sciences, of the U.S. Department of Energy under Contract No. DE-C02-05CH11231. REPW is grateful to the Royal Society for a Wolfson Merit Award. We also acknowledge Dr. Stefano Carretta (University of Parma) for his EPR simulation softwares.

Notes and references

[a] *School of Chemistry, University of Manchester, Oxford Road, Manchester, M14 6NS, UK*

[b] *The Photon Science Institute, University of Manchester, Oxford Road, Manchester, M14 6NS, UK. Fax: (+44) 161-275-4616; Tel: (+44) 161-275-4654; E-mail: richard.winpenny@manchester.ac.uk*

[c] *Advanced Light Source, Lawrence Berkeley Lab,1 Cyclotron Rd, Berkeley, CA 94720, USA*

†General synthesis for $[Cr_7M(^nPr_2NH_2)(O_2CtBu)_{16}]$: {Cr6} horseshoe, $\{Cr_6F_{11}(O_2CtBu)_{10}(nPr_2NH_2)_3\}_2$ (~0.6 mmol), $M(O_2CtBu)_x(HO_2CtBu)_y(H_2O)_z$ (~1.2 mmol by metal) and pivalic acid (~150 mmol) were heated at 140ºC in a Teflon® flask for 20 hours. Acetonitile (30 mL) was added and the precipitate filtered, extracted in diethyl ether and the solvent removed by vacuum to give a green solid. This was purified *via* a silica column with toluene to remove a $\{Cr_8\}$ fraction and then with diethyl ether to obtain the final product, which was recrystallised from ethyl acetate/acetonitrile, generating yields based on {Cr6} of between 20 and 40%. Synthesis of the heterocarboxylate rings was performed in a simialar fashion but the new carboxylate was introduced as the metal salt, and no additional pivalic acid was used. As such the reaction was carried out in refluxing toluene. A time-exhustative column was performed in toluene, after which the products could not be fully separated so yields are not reported. The crystals which were grown were from toluene/acetonitrile.

‡ Crystal Data for **2**, $C_{86}H_{168}Cr_7F_8MgNO_{33}$, M =2276.46, Monoclinic, a = 24.971(4) Å, b = 16.5415(10) Å, c = 30.845(3) Å, β = 110.059(13)°, U = 11968(2) Å^3, T = 100(2), space group $P2_1/c$ (no. 14), Z = 4, μ(MoKα) = 0.696, 41421 reflections measured, 20380 unique (R_{int} = 0.0542) which were used in all calculations. The final $wR(F_2)$ was 0.2171 (all data).

Crystal Data for **3**, $C_{84}H_{156}CaCr_7F_8No_{32}$, M =2248.18, Monoclinic, a = 25.2470(12) Å, b = 16.5990(7) Å, c = 31.0660(17) Å, β = 111.304(2)°, U = 12129.3(10) Å^3, T = 100(2), space group $P2_1/c$ (no. 14), Z = 4, μ(MoKα) = 0.722, 13206 reflections measured, 13206 unique (R_{int} = 0.0000) which were used in all calculations. The final $wR(F_2)$ was 0.4407 (all data).

Crystal Data for **4**, $C_{84}H_{137}Cr_7F_8NO_{33}Sr$, M =2292.57, Monoclinic, a = 24.5448(8) Å, b = 17.0878(5) Å, c = 30.5956(9) Å, β = 107.950(2)°, U = 12207.7(6) Å^3, T = 100(2), space group $P2_1/c$ (no. 14), Z = 4, μ(synchrotron) = 1.108, 89866 reflections measured, 19451 unique (R_{int} = 0.0416) which were used in all calculations. The final $wR(F_2)$ was 0.4930 (all data).

Crystal Data for **8a**, $C_{220}H_{376}Co_2Cr_{14}F_{16}N_2O_{64}$, M =5223.09, monoclinic, a = 24.727(3) Å, b = 19.4245(11) Å, c = 30.792(6) Å, β = 108.399(16)°, U = 14034(3) Å^3, T = 100(2), space group Pc (no. 7), Z = 2, μ(MoKα) = 0.710, 32180 reflections measured, 19018 unique (R_{int} = 0.0922) which were used in all calculations. The final $wR(F_2)$ was 0.3612 (all data).

1 For example in {Fe8} and {Fe16} wheels: R. Carrasco, J. Cano, T. Mallah, L. F. Jones, D. Collison, and E. K. Brechin, *Inorg. Chem.,* 2004, **43** (17), 5410-5415.

2 For example hosting gadolinium as an MRI contrast agent: T. N. Parac-Vogt, A. Pacco, P. Nockemann, S. Laurent, R. N. Muller, M. Wickleder, G. Meyer, L. V. Elst and K. Binnemans, *Chem. Eur. J.*, 2006, **12**, 204.

3 For example lanthanide extraction: M. Tegoni, M. Furlotti, M. Tropiano, C. S. Lim and V. L. Pecoraro, *Inorg. Chem.*, 2010, **49** (11), 5190.

4 R. H. Laye, F. K. Larsen, J. Overgaard, C. A. Muryn, E. J. L. McInnes, E. Rentschler, V. Sanchez, S. J. Teat, H. U. Güdel, O. Waldmann, G. A. Timco and R. E. P. Winpenny, *Chem. Commun.*, 2005, 1125.

5 E. C. Sañudo, C. A. Muryn, M. A. Helliwell, G. A. Timco, W. Wernsdorfer and R. E. P. Winpenny, *Chem. Commun.*, 2007, 801-803.

6 E. C. Sañudo, T. B. Faust, C. A. Muryn, R. G. Pritchard, G. A. Timco and R. E. P. Winpenny, *Inorg. Chem.*, 2009, **48** (20), 9811.

7 T. B. Faust, P. G. Heath, C. A. Muryn, G. A. Timco and R. E. P. Winpenny, *Chem. Commun.*, 2010, **46**, 6258.

8 A. B. Boeer, D. Collison, C. A. Muryn, G. A. Timco, F. Tuna, R. E. P. Winpenny, *Chem. Eur. J.*, 2009, **15**, 13150–13160.

9 M. Rancan, G. N. Newton, C. A. Muryn, R. G. Pritchard, G. A. Timco, L. Cronin and R. E. P. Winpenny, *Chem. Commun.*, 2008, 1560.

10 M. L. Baker, A. Bianchi, S. Carretta, D. Collison, R. J. Docherty, E. J. L. McInnes, A. McRobbie, C. A. Muryn, H. Mutka, S. Piligkos, M. Rancan, P. Santini, G. A. Timco, P. L. W. Tregenna-Piggott, F. Tuna, H. U. Gudel and R. E. P. Winpenny, *Dalton Trans.*, 2011, **40**, 2725.

11 S. Piligkos, H. Weihe, E. Bill, F. Neese, H. El Mkami, G. M. Smith, D. Collison, G. Rajaraman, G. A. Timco, R. E. P. Winpenny and E. J. L. McInnes, *Chem. Eur. J.*, 2009, **15**, 3152.

12 A. McRobbie, A. R. Sarwar, S. Yeninas, H. Nowell, M. L. Baker, D. Allan, M. Luban, C. A. Muryn, R. G. Pritchard, R. Prozorov, G. A. Timco, F. Tuna, G. F. S. Whitehead and R. E. P. Winpenny, *Chem. Commun.*, 2011, **47**, 6251.

Chapter Ten - Paper 6

"Proton NMR study of Cr-Co heterometallic wheel complexes"

E. C. Sañudo, T. B. Faust, C. A. Muryn, R. G. Pritchard, G. A. Timco and R. E. P. Winpenny, *Inorganic Chemistry*, 2009, **48**, 9811-9818.

Inorganic Chemistry
Article

Inorg. Chem. **2009**, *48*, 9811–9818 **9811**
DOI: 10.1021/ic901418z

Proton NMR Study of Cr−Co Heterometallic Wheel Complexes

E. Carolina Sañudo,*,† Thomas B. Faust,‡ Christopher A. Muryn,‡ Robin G. Pritchard,‡ Grigore A. Timco,‡ and Richard E. P. Winpenny*,‡

†*Institut de Nanociència i Nanotecnologia, Universitat de Barcelona, Diagonal 647, Barcelona 08028, Spain, and* ‡*Department of Chemistry, University of Manchester, Manchester M13 9PL, U.K.*

Received July 20, 2009

^{1}H NMR spectra of the paramagnetic heterometallic complexes of general formula [cation][$Cr_7CoF_8(O_2C^tBu)_{16}$] have been recorded. The NMR spectra have allowed the investigation of the structure of these complexes in solution. These experiments show that the complexes are stable and maintain the solid state structure in solution, retaining the protonated amine in the cavity of the heterometallic ring.

Introduction

High nuclearity transition metal complexes have a wide range of potential applications, from qubits in quantum computers,[1−3] to synthetic models of the active site of enzymes.[4] ^{1}H nuclear magnetic resonance (NMR) is a very useful technique in the characterization of simple coordination and organometallic complexes. However, it is rarely used to characterize paramagnetic, high nuclearity complexes.[5] In most cases this is due mainly to the difficulty in obtaining a resolvable spectrum because of fast nuclear spin relaxation caused by the paramagnetism of the compound, and also because of the complexity of the NMR spectrum of a high-nuclearity complex with a large number of inequivalent organic groups, as is the case in many polynuclear paramagnetic complexes. Paramagnetic NMR is mostly used by bioinorganic chemists[6] or in magnetic resonance imaging (MRI), a technique where paramagnetic metal complexes that are strong NMR relaxers of solvent protons are used clinically as contrast agents.[7] However, proton NMR can be a diagnostic tool to aid in structure elucidation of paramagnetic complexes if used properly, and it can have the bonus of providing information on the structure of these species in solution. One must take into account the main characteristics of paramagnetic NMR: (i) the chemical shifts will not be restricted to the 0−10 ppm scale of common proton NMR, instead, the spectral window will be as wide as 200 ppm; (ii) the proton−proton couplings will not be observed, and (iii) the peaks will be broad compared to the NMR of organic or organometallic complexes.

In 2003 Timco, Winpenny, and co-workers reported the synthesis of the first heterometallic wheel complexes [H_2NR_2][$Cr_7M^{II}F_8(O_2C^tBu)_{16}$],[8] where M^{II} = Ni, Co, Fe, Mn, Cd and R is a linear alkyl-chain. This route has been used to produce an extended family of the heterometallic rings with general formula [H_2NR_2][$M_7M^{II}F_8(O_2CR')_{16}$], where instead of the Cr(III) ion the trivalent metal M^{III} is Fe, V, Ga, In, and Al.[9] The ability to vary both metals present allows us to vary the magnetic properties of the compounds, which in the long term is important in being able to understand the magnetic phenomena seen. In particular, the Cr_7Ni(II) systems have been very carefully considered as models for double-qubit quantum gates. It has been proposed by Troiani et al.[10] that qubit gates could be designed using interactions between excited states of magnetic clusters, and recently it has been shown that two Cr_7Ni rings can be linked and their spins entangled.[11] In related work Cr_7M rings have been used as part of heterorotaxanes.[12] Future applications of these

*To whom correspondence should be addressed. E-mail: carolina.sanudo@qi.ub.es.

(1) Leuenberger, M.; Loss, D. *Nature* **2001**, *410*, 789.
(2) Ardavan, A.; Blundell, S. J. *J. Mater. Chem.* **2009**, *19*, 1754–1760.
(3) Bogani, L.; Wernsdorfer, W. *Nat. Mater.* **2008**, *7*, 179–186.
(4) Lippard, S. J.; Berg, J. M. *Principles of Bioinorganic Chemistry*; University Science Books: Sausalito, CA, 1994.
(5) Some examples: (a) Sañudo, E. C.; Cauchy, T.; Ruiz, E.; Laye, R. H.; Roubeau, O.; Teat, S. J.; Aromí, G. *Inorg. Chem.* **2007**, *46*, 9045. (b) Chakov, N. E.; Lee, S. C.; Harter, A. G.; Kuhns, P. L.; Reyes, A. P.; Hill, S. O.; Dalal, N. S.; Wernsdorfer, W.; Abboud, K. A.; Christou, G. *J. Am. Chem. Soc.* **2006**, *128*, 6975.
(6) Que, L., Jr. *Physical Methods in Bioinorganic Chemistry: Spectroscopy and Magnetism*; University Science Books: Sausalito, CA, 2000.
(7) Thompson, K. H.; Orvig, C. *Chem. Soc. Rev.* **2006**, *35*, 499.
(8) Larsen, F. K.; McInnes, E. J. L.; El Mkami, H.; Overgaard, J.; Piligkos, S.; Rajaraman, G.; Rentschler, E.; Smith, A. A.; Smith, G. M.; Boote, V.; Jennings, M.; Timco, G. A.; Winpenny, R. E. P. *Angew. Chem., Int. Ed.* **2003**, *42*, 101.
(9) Affronte, M.; Carretta, S.; Timco, G. A.; Winpenny, R. E. P. *Chem. Commun.* **2007**, 1789.
(10) Troiani, F.; Affronte, M.; Carretta, S.; Santini, P.; Amoretti, G. *Phys. Rev. Lett.* **2005**, *94*, 190501/1.
(11) Timco, G. A.; Carretta, S.; Troiani, F.; Tuna, F.; Pritchard, R. J.; Muryn, C. A.; McInnes, E. J. L.; Ghirri, A.; Candini, A.; Santini, P.; Amoretti, G.; Affronte, M.; Winpenny, R. E. P. *Nat. Nanotechnol.* **2009**, *4*, 173.
(12) Lee, C.- F.; Leigh, D. A.; Pritchard, R. G.; Schultz, D.; Teat, S. J.; Timco, G. A.; Winpenny, R. E. P. *Nature* **2009**, *458*, 314.

Published on Web 09/22/2009

complexes or their derivatives would require processability, and thus their solution stability must be studied and understood. The Cr_7Co analogues of the well studied Cr_7Ni complexes were chosen for this NMR study because of the fast relaxation of cobalt(II) in an octahedral environment,[13] which would counteract the slow electronic relaxation of Cr(III) ions that usually makes NMR of Cr(III) complexes broadened beyond detection.[14,15] As reported before, the coupling between the metal centers in the wheel complexes is antiferromagnetic, and the ground state for the Cr_7Co complexes appears to be diamagnetic.[8]

In $[H_2NR_2][M_7M^{II}F_8(O_2CR')_{16}]$ complexes the cation is generally a protonated, symmetric secondary amine group, and complexes with dimethyl-, diethyl-, dipropyl-, and dioctyl-protonated amine cations, among other symmetric dialkylamines, have been synthesized and characterized with most of the heterometals.[16,17] Thus, the whole family of heteronuclear wheels comprises hundreds of members, many of these characterized by X-ray crystallography, but this single technique must be supported by other techniques to prove the true heterometallic nature of the complexes, since two different metals cannot be unambiguously distinguished by crystallography. Elemental analyses, including metal analyses, leave no doubt of the composition of the crystals, showing the expected ratio of metals for the heterometallic complexes. Mass spectroscopy confirms the heterometallic nature of the anions and that each anion only contains one divalent metal and seven trivalent metals. The combination of mass spectroscopy and elemental analysis confirm that the complexes are heterometallic, containing only one M(II) and one protonated amine. Finally, to complete the characterization of the heterometallic complexes, a technique was needed to study the structure of these species in solution. We present here a proton NMR study on the solution stability of the heterometallic wheel complexes $[cation][Cr_7Co^{II}F_8(O_2C^tBu)_{16}]$ where the cation is a protonated amine or a Na^+ ion.

Experimental Section

Unless stated otherwise, all reagents and solvents were purchased from Aldrich.

Chemicals were used without further purification. $[Co_2(H_2O)(O_2C^tBu)_4(HO_2C^tBu)_4]$ was prepared as previously reported.[18] The syntheses of the complexes **1**−**8** were carried out in Erlenmeyer Teflon FEP flasks supplied by Fisher. Column chromatography was carried out using Silica 60A (particle size 35−70 μm, Fisher, U.K.) as the stationary phase using a positive pressure of nitrogen, and TLC was performed on precoated silica gel plates (0.25 mm thick, 60 F_{254}, Merck, Germany). The complexes $[Cr_8F_8(O_2C^tBu)_{16}]$ **1**,[19,20] $[Me_2NH_2][Cr_7CoF_8(O_2C^tBu)_{16}]$ **2**, and $[Et_2NH_2][Cr_7CoF_8(O_2C^tBu)_{16}]$ **3** were prepared as previously reported.[21]

$[Pr_2NH_2][Cr_7CoF_8(O_2C^tBu)_{16}]$ 4. The compound **4** was prepared by the method given in ref 21 by using dipropylamine (Pr_2NH) instead of diethylamine (Et_2NH), and the reaction time was for 6 h at 160 °C. Compound **4** was recrystallized from a mixture of pentane/ acetone. X-ray quality crystals were grown also from a mixture of pentane/acetone. Yield (62%, based on Cr). Elemental analysis calcd (%) for $C_{86}H_{160}Co_1Cr_7F_8N_1O_{32}$: Cr 15.86, Co 2.57, C 45.01, H 7.03, N 0.61 ; found: Cr 15.77, Co 2.54, C 45.46, H 7.39, N 0.58.

ES-MS (sample dissolved in Et_2O, run in MeOH): +2294 $[M]^{+\cdot}$; +2317 $[M+Na]^+$ (100%); − 2192 $[M- Pr_2NH_2]^-$.

$[C_4H_8ONH_2][Cr_7CoF_8(O_2C^tBu)_{16}]$ 5. $CrF_3\cdot 4H_2O$ (3.0 g, 16.6 mmol), HO_2C^tBu (20 g, 196 mmol), morpholine (C_4H_8ONH) (0.60 g, 6.73 mmol), and $[Co_2(H_2O)(O_2C^tBu)_4(HO_2C^tBu)_4]$ (1.40 g, 1.48 mmol) were heated together at 160 °C for 43 h. The flask was cooled to room temperature (RT), and acetone (30 mL) was added with stirring. The resulting microcrystalline green precipitate was collected next day by filtration and washed with acetone. Then it was extracted in pentane (∼160 mL), the solution was filtered, and the filtrate was diluted with acetone (∼50 mL). Then the solution was concentrated by distillation while stirring up to ∼1/4 of the initial volume. The product started to crystallize during this time. The flask was cooled to RT, and the product was filtered next day, washed with acetone, and dried in air. Yield 4.4 g (81%, based on Cr). Suitable crystals for X-ray structure characterization were obtained by slow evaporation of a solution of **5** dissolved in pentane and diluted with acetone. Elemental analysis calcd (%) for $C_{84}H_{154}Co_1Cr_7F_8N_1O_{33}$: Cr 15.96, Co 2.58, C 44.23, H 6.81, N 0.61 ; found: Cr 16.41, Co 2.70, C 44.02, H 6.81, N 0.58.

ES-MS (sample dissolved in Et_2O, run in MeOH): +2179 [M − O_2CTBu]+; +2238 [{M − $C_4H_8ONH_2$}+2Na] $^+$; +2280 $[M]^{+\cdot}$; +2303 $[M+Na]^+$ (100%); + 2368 [M+ $C_4H_8ONH_2$]$^+$; −2192 $[M - C_4H_8ONH_2]^-$.

$[C_5H_{10}NH_2][Cr_7CoF_8(O_2C^tBu)_{16}]$ 6. The compound **6** was prepared by an analogous procedure to that for **5** by using piperidine ($C_5H_{10}NH$) instead of morpholine; the reaction time was 24 h, and the extraction was in diethyl ether (Et_2O). Yield 4.2 g (78%, based on Cr). X-ray quality crystals were grown from a mixture of Et_2O/acetone. Yield (62%, based on Cr). Elemental analysis calcd (%) for $C_{85}H_{156}Co_1Cr_7F_8N_1O_{32}$: Cr 15.97, Co 2.59, C 44.80, H 6.90, N 0.61 ; found: Cr 15.77, Co 2.85, C 44.36, H 6.85, N 0.58. ES-MS (sample dissolved in Et_2O, run in MeOH): +2301 $[M+Na]^+$; +2364 $[M+ C_5H_{10}NH_2]^+$ (100%); −2192 $[M - C_5H_{10}NH_2]^-$.

$[PrNH_3][Cr_7CoF_8(O_2C^tBu)_{16}]$ 7. The compound **7** was prepared by an analogous procedure to that for **5** by using 0.35 g (5.92 mmol) of propylamine ($PrNH_2$) instead of morpholine; the reaction time was 26 h at 150 °C. Yield 4.8 g (90%, based on Cr) . X-ray quality crystals were grown from a mixture of Et_2O/ acetone, (62%, based on Cr). Elemental analysis calcd (%) for $C_{83}H_{154}Co_1Cr_7F_8N_1O_{32}$: Cr 16.16, Co 2.62, C 44.25, H 6.89, N 0.62 ; found: Cr 15.74, Co 2.61, C 44.79, H 7.02, N 0.52. ES-MS (sample dissolved in Et_2O, run in MeOH): + 2393 [M+ Na-$(PrNH_2)_2$]+ (100%); −2192 $[M - PrNH_3]^-$.

$[NaCr_7CoF_8(O_2C^tBu)_{16}]$ 8. The compound **8** was initially obtained in an attempt to make compound **5**, via a reaction which had proceeded for 5 h at 140 °C. Purification by

(13) Bertini, I.; Luchinat, C. *NMR of Paramagnetic Molecules in Biological Systems*; Benjamin-Cummings Pub Co.: San Francisco, CA, 1986.
(14) Troiani, F.; Ghirri, A.; Affronte, M.; Carretta, S.; Santini, P.; Amoretti, G.; Piligkos, S.; Timco, G.; Winpenny, R. E. P. *Phys. Rev. Lett.* **2005**, *94*, 207208/1.
(15) Affronte, M.; Troiani, F.; Ghirri, A.; Carretta, S.; Santini, P.; Corradini, V.; Schuecker, R.; Muryn, C.; Timco, G.; Winpenny, R. E. P. *Dalton Trans.* **2006**, 2810.
(16) Laye, R. H.; Larsen, F. K.; Overgaard, J.; Muryn, C. A.; McInnes, E. J. L; Rentschler, E.; Sanchez, V.; Teat, S. J.; Güdel, H. U.; Waldmann, O.; Timco, G. A.; Winpenny, R. E. P. *Chem. Commun.* **2005**, 1125.
(17) Sañudo, E. C.; Muryn, C. A.; Helliwell, M. A.; Timco, G. A.; Wernsdorfer, W.; Winpenny, R. E. P. *Chem. Commun.* **2007**, 801.
(18) Aromi, G.; Batsanov, A. S.; Christian, P.; Helliwell, M.; Parkin, A.; Parsons, S.; Smith, A. A.; Timco, G. A.; Winpenny, R. E. P. *Chem.—Eur. J.* **2003**, *9*, 5142.
(19) Gerbeleu, V.; Struchkov, Yu. T.; Timko, G. A.; Batsanov, A. S.; Indrichan, K. M.; Popovich, G. A. *Dokl. Akad. Nauk SSSR* **1990**, *313*, 1459.
(20) van Slageren, J.; Sessoli, R.; Gatteschi, D.; Smith, A. A.; Helliwell, M.; Winpenny, R. E. P.; Cornia, A.; Barra, A. L.; Jansen, A. G. M.; Rentschler, E.; Timco, G. A. *Chem.—Eur. J.* **2002**, *8*, 277.
(21) Larsen, F. K.; McInnes, E. J. L.; El Mkami, H.; Overgaard, J.; Piligkos, S.; Rajaraman, G.; Rentschler, E.; Smith, A. A.; Smith, G. M.; Boote, V.; Jennings, M.; Timco, G. A.; Winpenny, R. E. P. *Angew. Chem., Int. Ed.* **2003**, *42*, 101.

chromatography on a silica column afforded $[NaCr_7CoF_8(O_2C^tBu)_{16}]$ **8** from the column. Similar results were obtained passing a toluene solution of pure **5** through the silica column. A better procedure was then developed for **8**. Flash chromatography of **5** (1.5 g) on silica gel (~250 mL) using toluene as eluent afforded the product $\mathbf{8\cdot C_6H_5CH_3}$ as the first band (in ~650 mL of eluent). No homometallic complex **1** was observed, which typically is eluted prior to any heterometallic complexes. The solvent was then evaporated under reduced pressure to give 1.35 g (yield 89%) of microcrystalline green product.

Elemental analysis calcd (%) for $C_{87}H_{152}Co_1Cr_7F_8Na_1O_{32}$: Cr 15.77, Co 2.55, Na 1.00, C 45.27, H 6.64, N 0.00 ; found: Cr 15.21, Co 2.56, Na 1.10, C 45.23, H 6.67, N 0.00 ES-MS (sample dissolved in Et_2O, run in MeOH): +2238 $[M+Na]^+$ (100%); −2192 $[M - Na]^-$.

Crystallization of **8** for single crystal structure characterization.

$[Na\{(H_2O)(Me_2CO)\}][Cr_7CoF_8(O_2C^tBu)_{16}]$ 8A. The compound $\mathbf{8\cdot C_6H_5CH_3}$ (1.0 g) obtained by the procedure above was dissolved by refluxing and stirring in acetone (~ 45 mL). The saturated solution obtained was filtered hot and the filtrate kept at RT for 5 days. This produced a crystalline product (including X-ray quality crystals), which was filtered and washed with cold acetone. Elemental analysis calcd (%) for $C_{83}H_{152}Co_1Cr_7F_8Na_1O_{34}$: Cr 15.88, Co 2.57, Na 1.00, C 43.50, H 6.68, N 0.00 ; found: Cr 16.04, Co 2.48, Na 1.12, C 42.73, H 6.74, N 0.00 ES-MS (sample dissolved in Et_2O, run in MeOH): +2238 $[M+Na]^+$ (100%); −2192 $[M - Na]^-$.

$[Na\{(MeCN)(Me_2SO)\}][Cr_7CoF_8(O_2C^tBu)_{16}]$ 8B. The compound **8A** (0.1 g) was dissolved in Et_2O (5 mL) and $HCO_2{}^tBu$ (0.1 g), dimethyl sulfoxide (Me_2SO) (0.1 mL), $NaCO_2{}^tBu$ (0.01 g) dissolved in MeCN (5 mL) was added. The solution was stirred for 3 h, then Et_2O removed by distillation. The precipitate was collected by filtration, washed with acetonitrile, and the crude product redissolved in Et_2O (5 mL), solution filtered, then diluted with acetonitrile (5 mL) to which few drops of dimethyl sulfoxide added. Slow evaporation of the solvents to up to 1/3 of initial volume produced in 2 days a crystalline product in a quantitative yield (including X-ray quality crystals). The product was filtered, washed MeCN, and dried in air. Elemental analysis calcd. (%) $C_{82}H_{150}Co_1Cr_7F_8Na_1O_{33}S$: Cr 15.87, Co 2.57, Na 1.00, C 42.93, H 6.59, N 0.00 ; found: Cr 15.61, Co 2.46, Na 1.11, C 42.71, H 6.62, N 0.00 ES-MS (sample dissolved in Et_2O and run in MeOH): +2238 $[M+Na]^+$ (100%); −2192 $[M - Na]^-$.

Elemental analyses and mass spectroscopy (MS) were performed at the Microanalysis and MS Laboratories at the Department of Chemistry, the University of Manchester. ^1H NMR spectra were recorded in $CDCl_3$, unless said otherwise, on a Varian Gemini 300 Hz spectrometer at the Department of Chemistry, the University of Manchester. The pulse sequence used was the standard for ^1H NMR, with a non standard collection window and reduced acquisition times (ranging from 0.10 to 0.25 s depending on the sample). The spectra were collected at room temperature, each sample was locked and shimmed manually.

Structure Determinations. Data were collected on a Bruker SMART CCD diffractometer (Mo Kα, $\lambda = 0.71069$ Å). In all cases the selected crystals were mounted on the tip of a glass pin using Paratone-N oil and placed in the cold flow (100 K) produced with an Oxford Cryocooling device. Complete hemispheres of data were collected using ω-scans (0.3°, 30 s/frame). Integrated intensities were obtained with SAINT+, and they were corrected for absorption using SADABS.[22] Structure solution and refinement were performed with the SHELX-package.[23] The structures were solved by direct methods and completed by iterative cycles of ΔF syntheses and full-matrix least-squares refinement against F^2. Crystal data are given in Table 1; CCDC 746229−746234.

(22) *Bruker SAINT*; Bruker AXS Inc.: Madison, WI, 2001. Sheldrick, G. M. *SADABS*; University of Göttingen: Göttingen, Germany, 2004.
(23) Sheldrick, G. M. *Acta Crystallogr.* **2008**, *A64*, 112.

Results and Discussion

Syntheses. The reaction of hydrated CrF_3 with $[Co_2(H_2O)(O_2C^tBu)_4(HO_2C^tBu)_4]$ in the presence of a symmetric dialkylamine in molten pivalic acid leads to the isolation of the crude product $[R_2NH_2][Cr_7CoF_8(O_2C^tBu)_{16}]$ (R = Me, **2**; R = Et, **3**; R = Pr, **4**). The crude is then purified by column chromatography and recrystallized. Similarly, to obtain the morpholine $[C_4H_8ONH_2][Cr_7CoF_8(O_2C^tBu)_{16}]$ **5**, piperidine $[C_5H_{10}NH_2][Cr_7CoF_8(O_2C^tBu)_{16}]$ **6**, and propylamine $[PrNH_3][Cr_7CoF_8(O_2C^tBu)_{16}]$ **7** derivatives hydrated CrF_3 is reacted with $[Co_2(H_2O)(O_2C^tBu)_4(O_2C^tBu)_4]$ in molten pivalic acid in the presence of the amine, but the purification process is slightly different. It was observed that upon crystallization of the product obtained after column chromatography of $[C_4H_8ONH_2][Cr_7CoF_8(O_2C^tBu)_{16}]$ **5**, the amine was not present in the crystal structure, and the complex obtained was identified as $[NaCr_7CoF_8(O_2C^tBu)_{16}]$ **8**. The small amounts of Na^+ present in the silica gel (< 0.2%, depending on the brand) can account for the Na^+ in the final product **8A**. To improve the yield of **8**, complex **8A** was recrystallized in the presence of sodium pivalate, the crystal structure of the obtained crystals **8B** showed a localized Na^+ ion in the cavity, along with a MeCN and DMSO molecules. The morpholine derivative **5** was then isolated in pure crystalline form by direct crystallization, avoiding the column chromatography step. Complexes **6** and **7** are obtained in a manner analogous to that for complex **5**, without purification by column chromatography, which also resulted in the exchange of the amine for the Na^+ and the isolation of **8A**. It appears that for these larger amines column chromatography leads to exchange of the amine with sodium.

Description of Crystal Structures. Crystal data and data collection parameters can be found in Table 1. The crystal structure of the anion of all the complexes comprises a cycle of eight metals (Figure 1a), each on a corner of an octagon, bridged by eight μ_2-F^- ions. Sixteen bridging *syn, syn*-pivalate ligands complete the octahedral coordination of all the metal centers. The pivalates can be divided in two groups, eight equatorial pivalate groups lying on the plane of the metallic wheel and eight axial pivalates, alternating their orientation up and down the plane of the wheel. In the crystal structure of complexes **2**, **3**, and **4** the cation can be found lying in the cavity of the wheel, and it is heavily disordered. There is also crystallographic disorder of the position of the Co(II) atom in the wheel. The two alkyl groups of the cation are pointing up and down of the plane defined by the metals, while the nitrogen atom of the amine is roughly in the plane. Figure 1b shows the $[Cr_7CoF_8]$ core with the cation for complexes **4**, **5**, **6**, **7**, and **8B**.

The crystal structure of complexes **5**, **6**, and **7** contain an asymmetric protonated amine cation. Essentially, the structure of the $[Cr_7CoF_8(O_2C^tBu)_{16}]^-$ anion is the same as that of complexes **2**, **3**, and **4**; there are eight equatorial pivalate groups that lie in the plane of the wheel while the eight axial pivalates alternate their orientation up and down the plane defined by the metal centers. However,

Table 1. Crystallographic Data for Complexes **4**, **5**, **6**, **7**, **8A**, and **8B**

	4	**5**	**6**	**7**	**8A**	**8B**
cell setting, space group	monoclinic, *Cc*	monoclinic, *C*2/*c*	monoclinic, *C*2/*c*	monoclinic, *P*2(1)/*C*	monoclinic, *Cc*	monoclinic, $P12_1/n1$
temperature (K)	100 (2)	100 (2)	100 (2)	100 (2)	100 (2)	100 (2)
a (Å)	25.8867 (16)	45.120 (2)	45.1745 (11)	25.1073 (8)	13.5483 (3)	19.6702 (3)
b (Å)	20.2335 (6)	16.3843 (3)	16.3766 (4)	16.6242 (7)	29.7894 (5)	25.7942 (4)
c (Å)	25.9952 (12)	35.0977 (10)	35.1498 (7)	30.8644 (10)	30.3479 (6)	26.3871 (4)
β (deg)	110.045 (6)	114.491 (4)	114.405 (2)	110.275 (3)	100.814 (2)	92.4145 (5)
V (Å^3)	12790.9 (11)	23611.8 (13)	23680.5 (9)	12084.3 (7)	12030.8 (4)	13376.3 (4)
Z	4	8	8	4	4	4
D_x (Mg m^{-3})	1.192	1.283	1.281	1.267	1.259	1.18
radiation type	Mo *K*α	Mo *K*α	Mo *K*α	Mo *K*α	Mo *K*α	Mo *K*α
μ (mm^{-1})	0.77	0.84	0.83	0.82	0.82	0.76
crystal form, color	prismatic, green	block, green	needle, green	block, green	plate, green	prism, green
crystal size (mm)	0.30 × 0.25 × 0.20	0.30 × 0.20 × 0.10	0.50 × 0.20 × 0.10	0.80 × 0.70 × 0.40	0.70 × 0.50 × 0.15	0.3 × 0.2 × 0.15
absorption correction	multiscan	multiscan	multiscan	multiscan	multiscan	multiscan
T_{min}	0.802	0.788	0.681	0.561	0.597	0.952
T_{max}	0.861	0.921	0.921	0.736	0.886	1.061
no. of measured, independent and observed reflections	29667, 17293, 11382	54857, 23656, 15906	115634, 29349, 20883	88706, 24622, 16850	50273, 18275, 16248	144841, 16346, 9057
criterion for observed reflections	$I > 2\sigma(I)$	$I > 2\sigma(I)$	$I > 2\sigma(I)$	$I > 2\sigma(I)$	$I > 2\sigma(I)$	$I > 2\sigma(I)$
R_{int}	0.052	0.042	0.065	0.043	0.030	0.092
θ_{max} (deg)	25.0	26.4	28.3	26.4	25.0	22
refinement	F^2	F^2	F^2	F^2	F^2	F^2
$R[F^2 > 2\sigma(F^2)]$, $wR(F^2)$, S	0.096, 0.295, 1.05	0.060, 0.145, 1.01	0.092, 0.175, 1.17	0.085, 0.220, 1.05	0.058, 0.163, 1.11	0.093, 0.230, 1.15
no. of parameters	1283	1255	1265	1554	1264	1255
H-atom treatment	constrained to parent site	constrained to parent site	constrained to parent site	constrained to parent site	constrained to parent site	constrained to parent site
weighting scheme	calculated $w = 1/[\sigma^2(F_o^2) + (0.2P)^2]$ where $P = (F_o^2 + 2F_c^2)/3$	calculated $w = 1/[\sigma^2(F_o^2) + (0.0612P)^2 + 89.644P]$ where $P = (F_o^2 + 2F_c^2)/3$	calculated $w = 1/[\sigma^2(F_o^2) + (0.0353P)^2 + 225.0936P]$ where $P = (F_o^2 + 2F_c^2)/3$	calculated $w = 1/[\sigma^2(F_o^2) + (0.081P)^2 + 58.8417P]$ where $P = (F_o^2 + 2F_c^2)/3$	calculated $w = 1/[\sigma^2(F_o^2) + (0.0866P)^2 + 48.7616P]$ where $P = (F_o^2 + 2F_c^2)/3$	calculated $w = 1/[\sigma^2(F_o^2) + (0.070P)^2 + 53.P]$ where $P = (F_o^2 + 2F_c^2)/3$
$(\Delta/\sigma)_{max}$	0.014	0.002	0.001	0.001	0.002	0.002
$\Delta\rho_{max}$, $\Delta\rho_{min}$ (e Å^{-3})	1.87, −0.89	1.38, −0.75	1.52, −0.78	1.45, −0.82	1.45, −0.52	1.33, −0.86

there is a marked difference between the two sides of the complex. In one side of the wheel, the cavity formed by the *tert*-butyl groups of the pivalate ligands is occupied by the amine (morpholine **5**, piperidine **6** or propylamine **7**), while the other side is empty. This causes the *tert*-butyl groups of the pivalate ligands to close in on the empty side, and to slightly open-up on the occupied side. Additionally, in the crystal structure of complexes **5** and **6**, the Co(II) site in the heterometallic wheel complex has been localized without ambiguity.

Finally, the crystal structure of complex **8A** and **8B** shows a $[Cr_7CoF_8(O_2C^tBu)_{16}]^-$ anion that is isostructural to that of complexes **2**, **3**, and **4**. In **8A** the anion is bound to a sodium cation that is disordered over three sites, while in **8B** the sodium cation is localized on one edge of the octagon (Figure 1b).

Proton NMR Studies. For a neutral, homometallic wheel of ideal D_{4d} symmetry, in the proton NMR we expect to observe two peaks in a 1:1 ratio. One heterometal in the wheel, with a symmetric protonated dialkylamine in the cavity will break the symmetry among the pivalate groups and split the two expected peaks (one for the equatorial and one for the axial pivalates) into eight, as shown in Scheme 1, making proton NMR a diagnostic tool for this type of complex. New complexes with asymmetric amines have been synthesized and are reported here. In this new case, the axial pivalates oriented up and down are no longer equivalent; thus twelve peaks are expected in the NMR: four peaks integrating two *tert*-butyl groups for the equatorial pivalates, four for the axial pivalates pointing up integrating one *tert*-butyl group each, and four for the axial pivalates pointing down integrating one *tert*-butyl group each. Additionally, proton NMR has the added bonus that the proton on the protonated amine might be observed in an NMR experiment, and its chemical shift will provide us with information on the spin-density distribution in the complexes. As a reference, the ^{1}H NMR of $[Cr_8F_8(O_2C^tBu)_{16}]$ **1** was measured in $CDCl_3$. As expected, the very slow relaxation of Cr(III) made the NMR peaks very broad, and the two different types of carboxylates, axial and equatorial, could not be observed; instead, an extremely broad peak

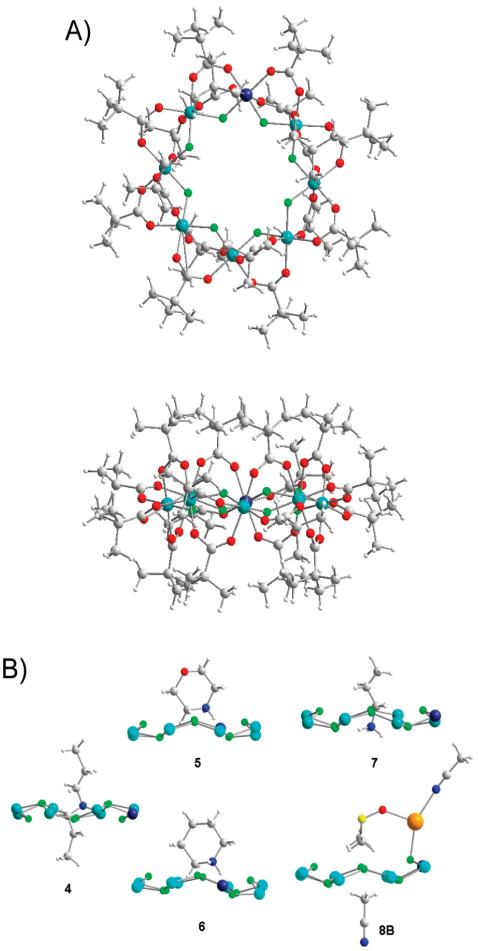

Figure 1. (a) Top view of the crystal structure of the anion $[Cr_7CoF_8(O_2C^tBu)_{16}]^-$, (b) side view of the metal-fluoride core with the cation of complexes **4**, **5**, **6**, **7**, and **8B**. Cr(III) in cyan, Co(II) in dark blue, fluoride in green, oxygen in red, carbon in gray, hydrogen in light gray, nitrogen in blue, sodium in orange, sulfur in yellow. For complexes **4**, **7**, and **8B** the Co(II) ion is not localized in one position in the crystal structure. For complexes **4** and **7** the protonated amine groups are disordered in two positions and only one is depicted for clarity.

between −1 and 4 ppm was seen in the spectrum, comprising the 16 carboxylates. The protons in the pivalate groups are separated from the metal centers by five bonds (see Scheme 2); therefore, their peaks in the NMR spectrum are sharp enough to be observed, even in complex **1**. The attempt to study the proton NMR of Cr_7Ni derivatives was unsuccessful, since the chemical shifts of the inequivalent pivalate groups were too similar and the peaks too broad. The NMR study is restricted to the Cr_7Co derivatives, and the NMR data for complexes **2**−**8** is summarized in Tables 2 and 3.

The proton NMR of complexes **2**, **3**, **4**, and **8** are shown in Figure 2. The NMR spectra show two distinct regions that will be analyzed separately. Between −5 and 15 ppm strong, sharp peaks, common to all the measured samples were observed (Figure 3). These peaks can be assigned to the pivalate groups. This was confirmed by the proton

Table 2. Proton NMR Data for Complexes **2**, **3**, **4**, and **8** in $CDCl_3$

peaks (ppm)								
2	int.	**3**	int.	**4**	int.	**8**	int	group
9.8	2	10.5	2	10.5	2	9.5	2	
2.9	2	4.1	2	4.0	2	5.2	2	
2.5	2	2.6	4	2.9	2	2.3	2	
2.2	2			2.3	2	0.8	2	
1.3	2	1.2	2	1.2	2	0.3	2	pivalates[a]
0.5	2	0.3	2	0.3	2	0.0	4	
−1.7	2	−1.5	2	0.0	2	−1.3	2	
−2.9	2	−2.6	2	−1.5	2			
						−9.5		$[H_2O-H]^+$
				−12.5				γ^b
−22.9		−19 to −22		−21 to −23				α^b
		−29.5		−33.1				β^b
				−37.2				
∼−75		∼−77		∼-80				H^+

[a] Integrals given as number of pivalate groups. [b] Position in the linear alkyl chain: N−Cα−Cβ−Cγ, etc.

Table 3. Proton NMR Data for Complexes **5**, **6**, and **7** in $CDCl_3$

peaks (ppm)						
5	int.	**6**	int.	**7**	int.	group
11.38	2	11.41	2	11.17	1	
6.39	1	11.16		10.84	1	
5.30	1	7.88	1	9.46	1	
4.84	1	5.11	1	3.99	1	
3.26	1	3.47	1	3.01	1	
2.84	2	2.99	2	2.32	1	
2.05	1	1.93	2	1.73	1	
0.33	5	0.68	1	0.82	6	pivalates[a]
0.00		0.01	4	0.48		
−1.71	1	−0.25		0.21		
−2.14	1	−0.42		−1.08	1	
		−0.68		−1.51	1	
		−1.61	1	−2.79	1	
		−1.98	1			
−15.20	CH_2	−9.57	CH_2	−12.57	CH_3	
−17.26		−15.78	CH_2	−20/-25	CH_2	
−27.13	CH_2	−17.83		−39.36	CH_2	protonated amine
−29.23		−21.62	CH_2			
∼−107	NH_2	∼−103	NH_2	∼-94	NH_2	

[a] Integrals given as number of pivalate groups.

NMR spectrum of the deuterated complex $[Me_2NH_2][Cr_7CoF_8(O_2CC(CD_3)_3)_{16}]$, which showed only the peaks further upfield from −5 ppm, which are thus assigned unambiguously to the protonated amine. Because of the lower, ideal C_2 symmetry when there is one heterometal in the wheel, eight peaks are expected, as shown in Scheme 1, four correspond to the four equatorial types of pivalate (A, B, C, and D) and four to the corresponding axial carboxylates (A′, B′, C′, and D′). A close look at the pivalate region shows eight peaks for **2** and **4**, proving the presence of one Co(II) in the wheel. Even though integration is not as reliable in paramagnetic NMR as it is in NMR of diamagnetic samples, the integrals of the peaks are all of the same order, suggesting that they all correspond to the same number of protons, with each peak corresponding to 18 protons from two equivalent pivalate groups. For complexes **3** and **8**, there is some accidental overlap in the congested pivalate region; the NMR spectrum of complex **3** (Figure 2 (b)) shows seven peaks, with

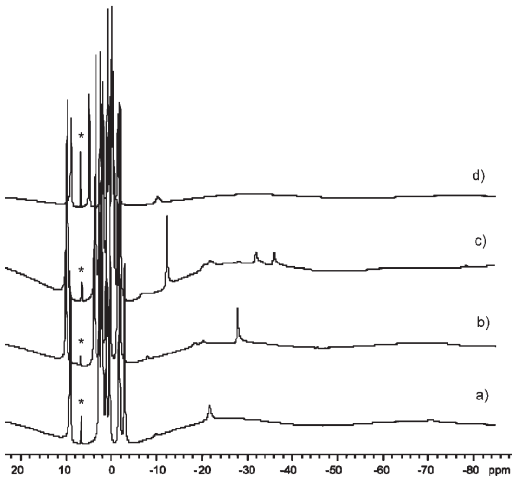

Figure 2. Proton NMR in $CDCl_3$ of: (a) **2**; (b) **3**; (c) **4**; (d) **8**. The protio-impurity of the solvent is marked with an asterisk.

Scheme 1

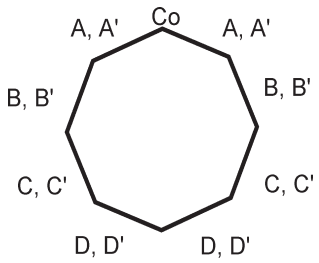

Scheme 2

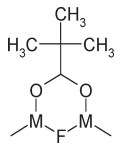

the peak at 2.6 ppm integrating twice as much as the other six, indicating that it corresponds to two groups of pivalate ligands. This is most likely due to accidental overlap. Furthermore, some free amine can be observed in the NMR spectrum of complex **4**, as sharp peaks in the 0 to 4 ppm region.

For the cations, we expect an increasing number of peaks when going from dimethyl to diethyl to dipropyl protonated amine. From −5 to −90 ppm the broad resonances corresponding to the cations can be found. It is known that the protonated amine sits in the cavity in the solid state, but it was not obvious that this would be the case in solution. The peaks are broad and shifted all the way down to −80 ppm; this fact leaves no doubt that the amine is in close proximity to the paramagnetic metal centers in solution. Thus, in solution the protonated amine remains most of the time in the cavity of the wheel as seen in the crystal structure. In all the crystal structures obtained so far of complexes of this type, the two alkyl groups of the symmetric protonated amine seem to be equivalent, one up and one down from the plane of the wheel. This means that in the NMR we expect one peak from the Me groups in complex **2**, three peaks for the ethyl groups of **3**, and five peaks for the propyl chains of **4** (the CH_2 protons in both ethyl and propyl groups are diastereotopic and should be split in two peaks, giving thus the three peaks for an ethyl group and five for a propyl chain). The NMR spectrum of complex **2** shows two peaks in this region: a very broad small peak at ∼−78 ppm and a larger peak at −24 ppm. In some samples, a third peak at −10 ppm is also observed; this peak is very small and if a new, freshly opened $CDCl_3$ bottle is used, it does not appear. The resonance at −24 ppm is assigned to the Me groups of the cation.

The spectrum of **3** shows three peaks, the peak in the −20 ppm region is now split in two and a new peak can be seen at −30 ppm. These peaks are assigned to the CH_2 groups and the Me groups of the ethyl chains, respectively. Additionally, there is a very broad peak around −80 ppm, and as it happened in the NMR spectra of different samples of complex **2**, a resonance is sometimes observed around −10 ppm. The assignment of the peaks corresponding to the protons of the alkyl chains is supported by the T_1 time measurements, which are 0.0026 s for the two peaks between −19 and −21 ppm and 0.0037s for the peak at −29.28, the longer T_1 time indicating a longer distance between the nuclei and the unpaired electrons. Accordingly, the peak in the −30 ppm region should be split in the spectrum of complex **4**. In fact, that is what we observed, along with the appearance of a new sharper peak at −13 ppm, assigned to the Me groups of the propyl chains of the cation. The spectrum of complex **4** also shows the broad resonance around −80 ppm, as well as the appearance of a broad, small peak around −10 ppm. The very broadened peak around −80 ppm, common to the spectra of all the samples, has to be assigned to the protons bound to the neutral amine. Typical N−F distances in these complexes are between 2.7 and 3.1 Å because of N−H--F interactions, which explains the strong influence of the paramagnetic metals in the chemical shift of this proton.

The proton NMR of **8A** was investigated and confirmed the absence of protonated amine as a cation. As shown in Figure 3, the spectrum shows eight peaks between −15 and 15 ppm. Seven of these peaks are exactly in the same region as the pivalate peaks in the NMR of complexes **2**, **3**, and **4**. Furthermore, one of the peaks integrates approximately twice the amount the other six, indicating it corresponds to two peaks accidentally overlapping. These seven peaks correspond to the eight types of carboxylate groups in a heterometallic wheel with one Co(II) and seven Cr(III) ions, establishing the heterometallic nature of complex **8A**. A smaller peak is seen in the spectrum in the −10 ppm region, and it integrates for approximately two or three protons and was assigned to the water bound to the Na^+ cation in the case of **8A**. It has not been possible to clearly observe any resonance around the −80 ppm region for complex **8**. The proton NMR spectrum of complex **8B** is the same as that of **8A**, with the additional peaks of free MeCN and DMSO. As stated above a similar peak is present in the spectra of complexes **2**, **3**, and **4** at around −10 ppm, and depends greatly on the

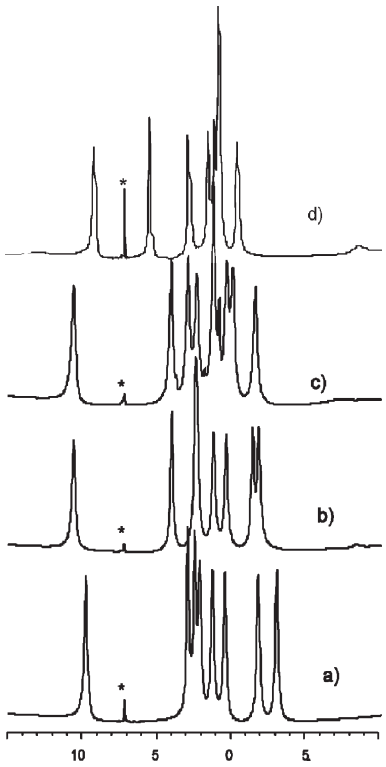

Figure 3. Downfield region of the proton NMR spectrum of complexes **2** (a), **3** (b), **4** (c), and **8** (d) showing the resonances corresponding to the eight different types of pivalate ligands. The protio-impurity of the solvent is marked with an asterisk.

amount of water from the solvent used in the NMR. As an example, in spectra measured in freshly opened CD_2Cl_2 or $CDCl_3$, which contains very little amount of adventitious water, the peak is very small or not observed at all. It is reasonable then to assign this peak to water rapidly exchanging with the neutral amine while the complex is in solution.

Cation Exchange Experiments. Amine exchange experiments with free diethylamine and free dipropylamine were performed within an NMR tube. Also, exchange experiments with D_2O were performed. As the heteronuclear wheel complex is in solution, the ammonium cation could exchange freely with adventitious water from the solvent, generating $(H_3O)[Cr_7CoF_8(^tBuCO_2)_{16}]$ and free amine:

$$[R_2NH_2][Cr_7CoF_8(O_2C^tBu)_{16}]+H_2O \leftrightharpoons (H_3O)[Cr_7CoF_8(O_2C^tBu)_{16}]+R_2NH \quad (1)$$

When a sample of complex **3**, with a protonated diethylamine cation, was treated with free diethylamine the only change observed in the spectrum was the disappearance of the peak at ~−10 ppm. Normally the equilibrium of eq 1 is shifted to the left, as evidenced by the absence of large NMR signals of the free amine. The addition of diethylamine should shift the equilibrium still further to the left, thus the peak at ~−10 ppm, because of the proton

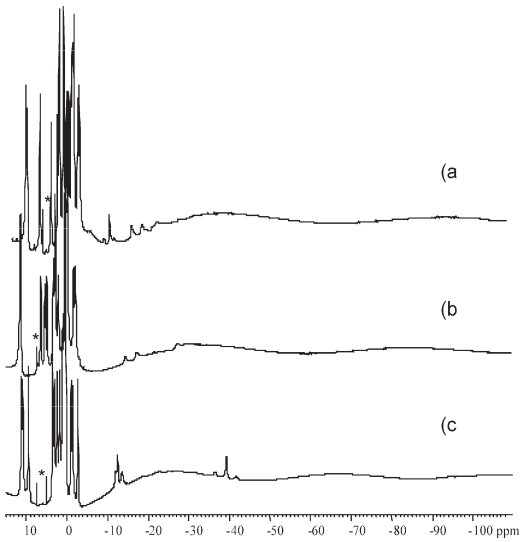

Figure 4. Proton NMR in $CDCl_3$ of (a) **5**; (b) **6**; (c) **7**. The protio-impurity of the solvent is marked with an asterisk.

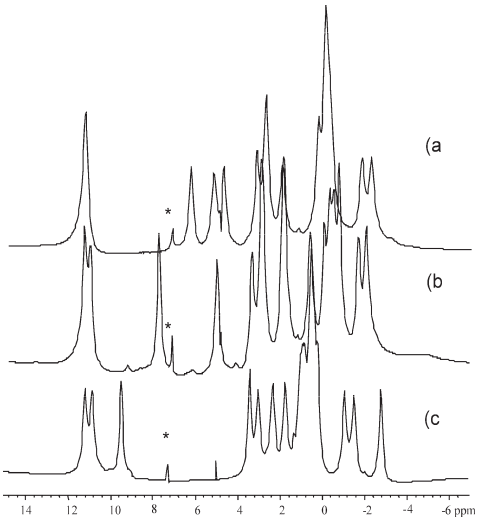

Figure 5. Downfield region of the proton NMR spectrum of (a) **5**; (b) **6**; (c) **7**, which shows the resonances corresponding to the twelve different types of pivalate ligands. The protio-impurity of the solvent is marked with an asterisk.

in the salt $(H_3O)[Cr_7CoF_8(O_2C^tBu)_{16}]$, should disappear entirely, as observed. These observations also indicate that in the apolar solvent the complex is always neutral, the proton remains in the cavity, held in place by short contacts with the fluoride bridges, but the amine is in exchange in solution. To see if the amine could be exchanged for a different one, free diethylamine was added to solutions of complexes **2** and **8**. The results show the conversion of **2** and **8** into **3** because of the excess of diethylamine. Dipropylamine was added to a solution of complex **2**, and the same effect was now observed, the dipropylamine replaced dimethylamine in the cavity.

Scheme 3

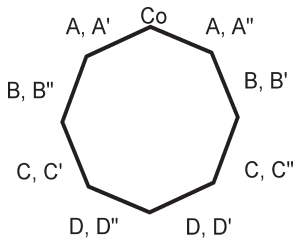

Thus, a general equilibrium can be written for these complexes in solution:

$$[HC][Cr_7CoF_8(O_2C^tBu)_{16}]+C' \leftrightarrows [HC'][Cr_7CoF_8(O_2C^tBu)_{16}]+C$$

where C and C′ are either H_2O or a secondary linear amine. Finally, exchange with D_2O was studied. Exchange experiments of complex **8** with D_2O in $CDCl_3$ showed the broadening of the resonance assigned to the water in the cavity, at ~−10 ppm. The same experiment performed in deuterated acetone, which permitted the use of a higher excess of D_2O, showed the disappearance of the peak at ~−10 ppm before the fast decomposition of the sample.

The NMR spectra of the wheel complexes with nonsymmetric protonated amines as cations were also studied. These spectra are shown in Figures 4 and 5. The complexity of the spectrum is now greater because of the lower ideal symmetry of the complex, which is now C_s. Scheme 3 shows the equivalence of the different pivalate groups, in this scheme the X′ represents the axial pivalate groups pointing up and X″ the axial pivalate groups pointing down. Twelve peaks corresponding to the pivalate groups are thus expected, the four signals corresponding to the equatorial groups should integrate for two pivalate groups, while the eight signals of the axial pivalates should correspond to one pivalate group each. In fact, this is what we observe in the proton NMR spectra of complexes **5**, **6**, and **7**, confirming that the solid state structure is maintained in solution.

Conclusions

A detailed study of the structure in solution of the heterometallic paramagnetic wheel complexes of general formula [cation][$Cr_7CoF_8(O_2C^tBu)_{16}$] has been performed. The proton NMR confirms that the anionic complex is stable in solution. The cation is generally a protonated secondary amine, and in the crystal structure it sits into the cavity within the octanuclear wheel complex. The proton NMR clearly shows that the solid state structure is maintained in solution and that the cation is most of the time in the cavity. This stability makes this type of complexes amenable to nanostructuration and deposition on surfaces.

Acknowledgment. R.E.P.W., T.B.F., and G.T. acknowledge the financial support of EPSRC (U.K.). The work was also supported by the EC Network of Excellence, "MAGMANet". E.C.S. acknowledges the financial support by the Spanish Government (Ramón y Cajal contract) and the Catalan Government (BE-2008 fellowship to E.C.S.). R.E.P.W. thanks the Royal Society for a Wolfson Merit Award.

Supporting Information Available: Crystallographic data in CIF format. This material is available free of charge via the Internet at http://pubs.acs.org.

Chapter Eleven - Paper 7

"Synthesis, structure, and dynamic properties of hybrid organic-inorganic rotaxanes"

B. Ballesteros, T. B. Faust, C.-F. Lee, D. A. Leigh, C. A. Muryn, R. G. Pritchard, D. Schultz, S. J. Teat, G. A. Timco and R. E. P. Winpenny, *Journal of the American Chemical Society*, 2010, **132**, 15435–15444.

J|A|C|S
ARTICLES

Published on Web 10/07/2010

Synthesis, Structure, and Dynamic Properties of Hybrid Organic−Inorganic Rotaxanes

Beatriz Ballesteros,[†] Thomas B. Faust,[‡] Chin-Fa Lee,[†] David A. Leigh,*[,†] Christopher A. Muryn,[‡] Robin G. Pritchard,[‡] David Schultz,[†] Simon J. Teat,[§] Grigore A. Timco,[‡] and Richard E. P. Winpenny*[,‡]

School of Chemistry, University of Edinburgh, The King's Buildings, West Mains Road, Edinburgh EH9 3JJ, United Kingdom, School of Chemistry and Photon Science Institute, University of Manchester, Oxford Road, Manchester M13 9PL, United Kingdom, and Advanced Light Source, Lawrence Berkeley Laboratory, 1 Cyclotron Road, MS2-400, Berkeley, California 94720

Received August 18, 2010; E-mail: david.leigh@ed.ac.uk; richard.winpenny@man.ac.uk

Abstract: The synthesis and characterization of a series of hybrid organic−inorganic [2]rotaxanes is described. The ring components are heterometallic octa- ($[Cr_7MF_8(O_2C^tBu)_{16}]$; M = Co, Ni, Fe, Mn, Cu, Zn, and Cd) nuclear cages in which the metal centers are bridged by fluoride and pivalate ($^tBuCO_2^-$) anions; the thread components feature dialkylammonium units that template the formation of the heterometallic rings about the axle to form the interlocked structures in up to 92% yield in conventional macrocyclization or one-pot 'stoppering-plus-macrocyclization' strategies. The presence in the reaction mixture of additives (secondary or tertiary amines or quaternary ammonium salts), and the nature of the stoppering groups (3,5-$^tBu_2C_6H_3CO_2-$ or $^tBuCONH-$), can have a significant effect on the rotaxane yield. The X-ray crystal structures of 11 different [2]rotaxanes, a pseudorotaxane, and a two-station molecular shuttle show two distinct types of intercomponent hydrogen bond motifs between the ammonium groups of the organic thread and the fluoride groups of the inorganic ring. The different hydrogen bonding motifs account for the very different rates of dynamics observed for the heterometallic ring on the thread (shuttling slow; rotation fast).

Introduction

Although metal ions have been extensively used to template the assembly of catenanes, rotaxanes, knots, and links[1] and form an integral part of the components of some interlocked molecules,[2] there are few examples[3] of the mechanical linking of organic and inorganic components at the molecular level. We recently described the synthesis of rotaxanes in which an essentially inorganic wheel (featuring seven Cr(III) trications and one Co(II) dication or ten Cr(III) trications and two Cu(II) dications) is assembled around a linear organic axle terminated with bulky 3,5-$^tBu_2C_6H_3CO_2-$ 'stoppers'.[4] Here we report on the synthesis and solid state structures of novel hybrid organic−inorganic [2]rotaxanes based on Ni(II), Fe(II), Mn(II), Cu(II), Zn(II), and Cd(II) as the divalent metal ion, together with an investigation of the factors (nature of the stopper groups and the use of amine/ammonium additives in the rotaxane-forming reaction) that can significantly affect the rotaxane yield. The hybrid structures have dynamic properties that hitherto have been the preserve of wholly organic molecules, such as the large amplitude thermal movement of the macrocycle up and down the axle (a molecular shuttle[5]), a motion of interest for synthetic molecular machine systems.[6]

The design of the hybrid organic−inorganic rotaxane system lies in the observation[7] that the formation of heterometallic rings[8] of various shapes and sizes, containing seven or more trivalent Cr(III) ions and one or two divalent metal ions (typically Ni(II), Co(II), Fe(II), Mn(II), or Cu(II)) bridged by multiple fluoride and alkyl or aryl carboxylate anions, is templated by various organic cations,[7d] including imidazolium,[7c] *N*-alkylimidazolium,[7c] and primary[7b] and secondary[7a] ammonium groups. The magnetic characteristics of these heterometallic rings have led to their investigation as potential qubits for quantum information processing.[9] A key question for this proposed application is how to link qubits to entangle spins without causing decoherence; mechanically interlocked structures may allow the manipulation of weak through-space interactions between such components in a manner that is difficult to achieve with conventional molecular architectures. Dialkylammonium salts have previously been used to direct the assembly of rotaxanes based on crown ethers,[10] cucurbituril,[11] and cyclic peptides,[12] and so it seemed plausible that they might also template the formation of rotaxanes featuring heterometallic rings.

[†] University of Edinburgh.
[‡] University of Manchester.
[§] Advanced Light Source.

(1) For reviews on interlocked molecules assembled about transition metal templates, see: (a) Sauvage, J.-P.; Dietrich-Buchecker, C. *Molecular Catenanes, Rotaxanes and Knots*; Wiley-VCH: Weinheim, Germany, 1999. (b) Hubin, T. J.; Busch, D. H. *Coord. Chem. Rev.* **2000**, *200−202*, 5–52. (c) Collin, J.-P.; Dietrich-Buchecker, C.; Gaviña, P.; Jimenez-Molero, M. C.; Sauvage, J.-P. *Acc. Chem. Res.* **2001**, *34*, 477–487. (d) Menon, S. K.; Guha, T. B.; Agrawal, Y. K. *Rev. Inorg. Chem.* **2004**, *24*, 97–133. (e) Cantrill, S. J.; Chichak, K. S.; Peters, A. J.; Stoddart, J. F. *Acc. Chem. Res.* **2005**, *38*, 1–9. (f) Crowley, J. D.; Goldup, S. M.; Lee, A.-L.; Leigh, D. A.; McBurney, R. T. *Chem. Soc. Rev.* **2009**, *38*, 1530–1541.

10.1021/ja1074773

Scheme 1. Synthesis of [2]Rotaxanes with 3,5-^{t}Bu$_2$C$_6$H$_3$CO$_2$− Stoppers, **2a**−**e**[a,b]

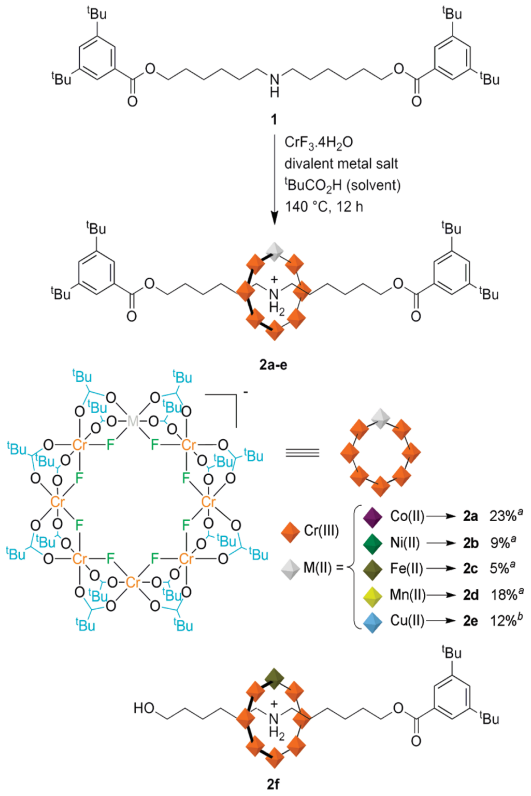

[a] Reaction conditions: Thread **1** (1 equiv), $CrF_3 \cdot 4H_2O$ (5 equiv), divalent metal salt ($[Co(OH_2)(O_2CCMe_3)_4(HO_2CCMe_3)_4]$, $[2NiCO_3 \cdot 3Ni(OH)_2 \cdot 4H_2O]$, $FeCl_2 \cdot 4H_2O$, $MnCl_2 \cdot 4H_2O$ or $CuCO_3 \cdot Cu(OH)_2$) (1 equiv), pivalic acid (50−60 equiv), 140 °C, 12 h. Isolated yields are based on Cr(III) as the limiting reagent. Changing the ester-linked aryl stoppers of the threads to *tert*-butylamide groups increases the isolated [2]rotaxane yields to 42−92% (see Scheme 3); the use of additives and the optimization of the reaction conditions increased the yield of rotaxane **2a** up to 70% (see Scheme 4). [b] 1 equiv of tetraethylammonium chloride was added.

Synthesis and Characterization of 3,5-^{t}Bu$_2$C$_6$H$_3$CO$_2$-Stoppered [2]Rotaxanes. Thread **1** features a secondary amine group separated by a six methylene group spacer from bulky 3,5-^{t}Bu$_2$C$_6$H$_3$CO$_2$− ester groups at each end of the axle to prevent dethreading of the heterometallic ring intended to be assembled around the ammonium template. The thread was reacted[7a] with a 5:1 molar ratio of chromium(III) fluoride ($CrF_3 \cdot 4H_2O$) and a range of different divalent metal salts ($[Co_2(H_2O)(^tBuCO_2)_4(^tBuCO_2H)_4]$, $[2NiCO_3 \cdot 3Ni(OH)_2 \cdot 4H_2O]$, $FeCl_2 \cdot 4H_2O$, $MnCl_2 \cdot 4H_2O$, or $CuCO_3 \cdot Cu(OH)_2$), with pivalic acid as the solvent, at 140 °C for 12 h (Scheme 1). The corresponding [2]rotaxanes **2a**−**d** were produced in 5−23% yield, which is rather efficient for what is essentially a 33 component assembly process (each metal−ligand bond is, in principle, dynamic under the reaction conditions). The Cr_7Fe-rotaxane **2c** proved to be rather unstable in solution and partially decomposed during the purification and crystallization processes. A Cr_7Fe-pseudorotaxane, **2f**, in which one of the stopper groups had been hydrolyzed was also isolated from the rotaxane-forming reaction. Using these conditions with Cu(II) salts produced a complex mixture of products from which no [2]rotaxane could be isolated. However, performing the reaction in the presence of 1 equiv of Et_4NCl (an additive found to increase rotaxane yield, *vide infra*) simplified the product distribution (and probably increased the amount of rotaxane formed) enabling the Cr_7Cu-[2]rotaxane **2e** to be prepared in 12% yield.

In all these rotaxane-forming reactions the octametallic ring is a monoanion (24 monoanionic ligands − 8 fluorides and 16 pivalate groups − bound to seven Cr(III) trications and one dication) whose charge is balanced by the ammonium cation formed by protonation of the thread. Thus the rotaxanes are overall neutral molecules, and as the 'oily' *tert*-butyl groups of the pivalates form the outer-coating of the inorganic ring, they generally exhibit good solubility in nonpolar organic solvents (CH_2Cl_2, $CHCl_3$, toluene, Et_2O, etc.). The synthesis has several possible variables, including the nature of the trivalent metal

(2) For examples of interlocked molecules with transition metals as structural elements, see: (a) Ogino, H. *J. Am. Chem. Soc.* **1981**, *103*, 1303–1304. (b) Fujita, M.; Ibukuro, F.; Hagihara, H.; Ogura, K. *Nature* **1994**, *367*, 720–723. (c) Fujita, M.; Ibukuro, F.; Yamaguchi, K.; Ogura, K. *J. Am. Chem. Soc.* **1995**, *117*, 4175–4176. (d) Piguet, C.; Bernardinelli, G.; Williams, A. F.; Bocquet, B. *Angew. Chem., Int. Ed. Engl.* **1995**, *34*, 582–584. (e) Mingos, D. M. P.; Yau, J.; Menzer, S.; Williams, D. J. *Angew. Chem., Int. Ed. Engl.* **1995**, *34*, 1894–1895. (f) Fujita, M.; Ogura, K. *Coord. Chem. Rev.* **1996**, *148*, 249–264. (g) Fujita, M.; Ibukuro, F.; Seki, H.; Kamo, O.; Imanari, M.; Ogura, K. *J. Am. Chem. Soc.* **1996**, *118*, 899–900. (h) Whang, D.; Park, K.-M.; Heo, J.; Kim, K. *J. Am. Chem. Soc.* **1998**, *120*, 4899–4900. (i) Try, A. C.; Harding, M. M.; Hamilton, D. G.; Sanders, J. K. M. *J. Chem. Soc., Chem. Commun.* **1998**, 723–724. (j) Fujita, M.; Fujita, N.; Ogura, K.; Yamaguchi, K. *Nature* **1999**, *400*, 52–55. (k) Fujita, M. *Acc. Chem. Res.* **1999**, *32*, 53–61. (l) Jeong, K. S.; Choi, J. S.; Chang, S. Y.; Chang, H. Y. *Angew. Chem., Int. Ed.* **2000**, *39*, 1692–1695. (m) Padilla-Tosta, M. E.; Fox, O. D.; Drew, M. G. B.; Beer, P. D. *Angew. Chem., Int. Ed.* **2001**, *40*, 4235–4239. (n) Park, K.-M.; Kim, S.-Y.; Heo, J.; Whang, D.; Sakamoto, S.; Yamaguchi, K.; Kim, K. *J. Am. Chem. Soc.* **2002**, *124*, 2140–2147. (o) Kim, K. *Chem. Soc. Rev.* **2002**, *31*, 96–107. (p) McArdle, C. P.; Irwin, M. J.; Jennings, M. C.; Vittal, J. J.; Puddephatt, R. J. *Chem.−Eur. J.* **2002**, *8*, 723–734. (q) McArdle, C. P.; Van, S.; Jennings, M. C.; Puddephatt, R. J. *J. Am. Chem. Soc.* **2002**, *124*, 3959–3965. (r) Dietrich-Buchecker, C.; Colasson, B.; Fujita, M.; Hori, A.; Geum, N.; Sakamoto, S.; Yamaguchi, K.; Sauvage, J.-P. *J. Am. Chem. Soc.* **2003**, *125*, 5717–5725. (s) Burchell, T. J.; Eisler, D. J.; Puddephatt, R. J. *Dalton Trans.* **2005**, 268–272. (t) Chang, S.-Y.; Jeong, K.-S. *J. Org. Chem.* **2003**, *68*, 4014–4019. (u) Liu, Y.; Song, S.-H.; Chen, Y.; Zhao, Y.-L.; Yang, Y.-W. *Chem. Commun.* **2005**, 1702–1704. (v) Suzaki, Y.; Taira, T.; Osakada, K.; Horie, M. *Dalton Trans.* **2008**, 4823–4833. (w) Wong, W. W. H.; Cookson, J.; Evans, E. A. L.; McInnes, E. J. L.; Wolowska, J.; Maher, J. P.; Bishop, P.; Beer, P. D. *Chem. Commun.* **2005**, 2214–2216. (x) Habermehl, N. C.; Jennings, M. C.; McArdle, C. P.; Mohr, F.; Puddephatt, R. J. *Organometallics* **2005**, *24*, 5004–5014. (y) Fujita, M.; Tominaga, M.; Hori, A.; Therrien, B. *Acc. Chem. Res.* **2005**, *38*, 369–378. (z) Blanco, V.; Chas, M.; Abella, D.; Peinador, C.; Quintela, J. M. *J. Am. Chem. Soc.* **2007**, *129*, 13978–13986. (aa) Yang, H.-B.; Ghosh, K.; Northrop, B. H.; Zheng, Y.-R.; Lyndon, M. M.; Muddiman, D. C.; Stang, P. J. *J. Am. Chem. Soc.* **2007**, *129*, 14187–14189. (bb) Westcott, A.; Fisher, J.; Harding, L. P.; Rizkallah, P.; Hardie, M. J. *J. Am. Chem. Soc.* **2008**, *130*, 2950–2951. (cc) Ghosh, K.; Yang, H.-B.; Northrop, B. H.; Lyndon, M. M.; Zheng, Y.-R.; Muddiman, D. C.; Stang, P. J. *J. Am. Chem. Soc.* **2008**, *130*, 5320–5334. (dd) Ronson, T. K.; Fisher, J.; Harding, L. P.; Rizkallah, P. J.; Warren, J. E.; Hardie, M. J. *Nature Chem.* **2009**, *1*, 212–216.

(3) For metal−organic rotaxane frameworks (MORFs), one-, two-, and three-dimensional arrays of organic rotaxanes linked by metal coordination bonds, see: (a) Loeb, S. J. *Chem. Commun.* **2005**, 1511–1518. (b) For catenanes incorporated into a metal−organic framework (MOF), see: Li, Q.; Zhang, W.; Miljanic, O. Š.; Knobler, C. B.; Stoddart, J. F.; Yaghi, O. M. *Chem. Commun.* **2010**, *46*, 380–382. (c) Li, Q.; Sue, C.-H.; Basu, S.; Shveyd, A. K.; Zhang, W.; Barin, G.; Fang, L.; Sarjeant, A. A.; Stoddart, J. F.; Yaghi, O. M. *Angew. Chem., Int. Ed* **2010**, *49*, 6751–6755. For interpenetrated nets of coordination polymers, see: (d) Batten, S. R.; Robson, R. *Angew. Chem., Int. Ed.* **1998**, *37*, 1460–1494. For polypseudorotaxanes featuring polyoxomolybdate clusters that encircle *p*-phenylenebutadiynylene polymer chains, see: (e) Alam, M. A.; Kim, Y.-S.; Ogawa, S.; Tsuda, A.; Ishii, N.; Aida, T. *Angew. Chem., Int. Ed.* **2008**, *47*, 2070–2073.

ion, the divalent metal ion, the carboxylate, the fluoride, and the amine, leading, in principle, to a wide variety of differently functionalized rotaxanes.[13] In this paper we probe the effect on structure and yield of changing the divalent metal ion, the nature of the rotaxane end-groups, and the addition of amine and ammonium additives to the reaction mixture.

X-ray crystal structures of four of the [2]rotaxanes **2a**, **2b**, **2d**, and **2e**, together with the X-ray structure of the monostoppered Cr_7Fe-pseudorotaxane (**2f**) isolated from the reaction mixture that formed rotaxane **2c**, are shown in Figure 1. The crystal structures of **2a** and **2b** (Figure 1a−c) are almost isostructural, with the divalent metal ion delocalized over the eight metal sites and the ammonium thread cation at the center of the cavity of the macrocycle forming short (2.00−2.03 Å), close-to-linear (167.7°−171.6°) $F^-\cdots HN^+$ hydrogen bonds to two of the bridging fluoride ligands. In the Cr_7Fe-pseudorotaxane **2f** (Figure 1f) the heterometallic ring is slightly rotated with respect to the thread compared to the other solid state structures so that four fluoride anions form the closest contacts with the hydrogen atoms of the ammonium groups. These interactions are longer (2.14−2.23 Å) and rather less linear (131.2°−153.0°) than the $F^-\cdots HN^+$ hydrogen bonds in the Cr_7Co-, Cr_7Ni-, and Cr_7Mn-rotaxanes (Figure 1a−d), illustrating that the interactions of the ammonium group with the various electronegative regions of the heterometallic wheel are a delicate balance of electrostatics (where the close contacts need not be in line with the H−N bonds) as well as conventional hydrogen bonding. In the crystal structure of the Cr_7Mn-[2]rotaxane **2d** (Figure 1d) the manganese ion is localized in the position shown (i.e., the divalent metal ion is not delocalized as it is in the other X-ray structures). The two $F^-\cdots HN^+$ hydrogen bonds of the Cr_7Cu-[2]rotaxane **2e** (Figure 1e) are less similar to each other (1.95 Å, 161.0° cf. 2.18 Å, 165.5°) than in the other rotaxanes, perhaps reflecting that the Cr_7Cu system has slightly different steric and/or electronic characteristics compared to the other heterometallic wheels.

Although the eight metal centers in the heterometallic rings are almost perfectly coplanar in each crystal structure, making the two faces virtually identical in terms of physical shape and geometry, the macrocycles are all chiral. The enantiomers differ in that the one divalent metal ion (Co(II), Ni(II), Fe(II), Mn(II) or Cu(II)) in each ring must have either a (Δ)- or (Λ)-arrangement of the ligands in its octahedral coordination sphere. Only one enantiomer is shown in Figure 1 for each rotaxane, but both enantiomers are present in equal amounts in each crystal.

X-ray crystallography of single crystals grown by a variety of methods (see Supporting Information) was routinely used, together with electrospray ionization mass spectrometry (ESI-MS), to determine the structures of the products of the rotaxane-forming reactions. Nuclear magnetic resonance (NMR) spectroscopy proved useful only for the rotaxanes incorporating Co(II) and Fe(II) as the divalent metals (**2a** and **2c**, respectively).[14] The ^{1}H NMR spectrum of **2a** (Figure 2b) shows the unequal magnetic effect exerted on each geminal proton in the methylene groups of the thread due to the chirality of the ring. Two signals are observed for each pair of methylene protons, due to the two protons of each methylene group (labeled primed and unprimed in Figure 2) being diastereotopic (i.e., magnetically distinct) as a result of the chirality of the heterometallic ring.[15] Comparison of the ^{1}H NMR spectrum of the parent thread, **1** (Figure 2a), with that of the rotaxane, **2a** (Figure 2b), and a partially deuterated analogue, d_{144}-**2a** (Figure 2c), shows the dramatic shifts in the thread protons caused by the paramagnetic Cr(III) and Co(II) ions, the greatest shifts generally occurring for the protons closest to the heterometallic ring.

The presence of one Co(II) ion among seven Cr(III) ions desymmetrizes the ring, resulting in the 16 pivalate groups being in eight magnetically nonequivalent environments (four axial and four equatorial). Slow rotation of the ring about the thread on the NMR time scale (up to eight different C_8-rotational positions of the divalent metal ion around the thread for each of the eight different types of pivalate groups) would result in

(4) (a) Lee, C.-F.; Leigh, D. A.; Pritchard, R. G.; Schultz, D.; Teat, S. J.; Timco, G. A.; Winpenny, R. E. P. *Nature* **2009**, *458*, 314–318. (b) Brechin, E. K.; Cronin, L. *Angew. Chem., Int. Ed.* **2009**, *48*, 6948–6949.

(5) (a) Anelli, P. L.; Spencer, N.; Stoddart, J. F. *J. Am. Chem. Soc.* **1991**, *113*, 5131–5133. (b) Bissell, R. A.; Cordova, E.; Kaifer, A. E.; Stoddart, J. F. *Nature* **1994**, *369*, 133–136. (c) Tian, H.; Wang, Q.-C. *Chem. Soc. Rev.* **2006**, *35*, 361–374.

(6) Kay, E. R.; Leigh, D. A.; Zerbetto, F. *Angew. Chem., Int. Ed.* **2007**, *46*, 72–191.

(7) (a) Larsen, F. K.; McInnes, E. J. L.; El Mkami, H.; Overgaard, J.; Piligkos, S.; Rajaraman, G.; Rentschler, E.; Smith, A. A.; Smith, G. M.; Boote, V.; Jennings, M.; Timco, G. A.; Winpenny, R. E. P. *Angew. Chem., Int. Ed.* **2003**, *42*, 101–105. (b) Cador, O.; Gatteschi, D.; Sessoli, R.; Larsen, F. K.; Overgaard, J.; Barra, A.-L.; Teat, S. J.; Timco, G. A.; Winpenny, R. E. P. *Angew. Chem., Int. Ed.* **2004**, *43*, 5196–5200. (c) Timco, G. A.; Batsanov, A. S.; Larsen, F. K.; Muryn, C. A.; Overgaard, J.; Teat, S. J.; Winpenny, R. E. P. *Chem. Commun.* **2005**, 3649–3651. (d) Affronte, M.; Carretta, S.; Timco, G. A.; Winpenny, R. E. P. *Chem. Commun.* **2007**, 1789–1797.

(8) For some related metallic ring systems, see: (a) Gerbeleu, N. V.; Batsanov, A. S.; Timko, G. A.; Struchkov, Yu. T.; Indrichan, K. M.; Popovich, G. A. Patent SU 1299116, 1985. (b) Taft, K. L.; Lippard, S. J. *J. Am. Chem. Soc.* **1990**, *112*, 9629–9630. (c) Gerbeleu, N. V.; Struchkov, Yu. T.; Timco, G. A.; Batsanov, A. S.; Indrichan, K. M.; Popovich, G. A. *Dokl. Akad. Nauk SSSR* **1990**, *313*, 1459–1462. (d) Stemmler, A. J.; Kampf, J. W.; Pecoraro, V. L. *Inorg. Chem.* **1995**, *34*, 2271–2271. (e) Caneschi, A.; Cornia, A.; Fabretti, A. C.; Gatteschi, D. *Angew. Chem., Int. Ed.* **1999**, *39*, 1295–1297. (f) Waldmann, O.; Koch, R.; Schromm, S.; Schülein, J.; Müller, P.; Bernt, I.; Saalfrank, R. W.; Hampel, F.; Balthes, E. *Inorg. Chem.* **2001**, *40*, 2986–2995. (g) Tasiopoulos, A. J.; Vinslava, A.; Wernsdorfer, W.; Christou, G. *Angew. Chem., Int. Ed.* **2004**, *43*, 2117–2121. (h) King, P.; Stamatos, T. C.; Abboud, K. A.; Christou, G. *Angew. Chem., Int. Ed.* **2006**, *45*, 7379–7383. (i) Low, D. M.; Rajaraman, G.; Helliwell, M.; Timco, G. A.; van Slageren, J.; Sessoli, R.; Ochsenbein, S. T.; Bircher, R.; Dobe, C.; Waldmann, O.; Güdel, H. U.; Adams, M. A.; Ruiz, E.; Alvarez, S.; McInnes, E. J. L. *Chem.−Eur. J.* **2006**, *12*, 1385–1396. (j) Mezei, G.; Zaleski, C. M.; Pecoraro, V. L. *Chem. Rev.* **2007**, *107*, 4933–5003.

(9) (a) Leuenberger, M. N.; Loss, D. *Nature* **2001**, *410*, 789–793. (b) Meier, F.; Levy, J.; Loss, D. *Phys. Rev. Lett.* **2003**, *90*, 047901/1−047901/4. (c) Bertaina, S.; Gambarelli, S.; Mitra, T.; Tsukerblat, B.; Müller, A.; Barbara, B. *Nature* **2008**, *453*, 203–206. (d) Timco, G. A.; Carretta, S.; Troiani, F.; Tuna, F.; Pritchard, R. G.; McInnes, E. J. L.; Ghirri, A.; Candini, A.; Santini, P.; Amoretti, G.; Affronte, M.; Winpenny, R. E. P. *Nat. Nanotechnol.* **2009**, *4*, 173–178.

(10) (a) Kolchinski, A. G.; Busch, D. H.; Alcock, N. W. *J. Chem. Soc., Chem. Commun.* **1995**, 1289–1291. (b) Ashton, P. R.; Glink, P. T.; Stoddart, J. F.; Tasker, P. A.; White, A. J. P.; Williams, D. J. *Chem.−Eur. J.* **1996**, *2*, 729–736.

(11) (a) Mock, W. L.; Irra, T. A.; Wepsiec, J. P.; Adhia, M. *J. Org. Chem.* **1989**, *54*, 5302–5308. (b) Kim, K. *Chem. Soc. Rev.* **2002**, *31*, 96–107.

(12) Aucagne, V.; Leigh, D. A.; Lock, J. S.; Thomson, A. R. *J. Am. Chem. Soc.* **2006**, *128*, 1784–1785.

(13) The use of threads with eight methylene groups between two amine groups can lead to the formation of [3]-and [4]rotaxanes (see ref 4).

(14) The possibility of using ^{1}H NMR analysis is the reason the Cr_7Co-rotaxane forming reaction was studied in the most detail. For the ^{1}H NMR spectrum of the amide-stoppered Cr_7Co-[2]rotaxane **4a** and Cr_7Fe-[2]rotaxane **4c**, see the Supporting Information.

(15) Sanudo, E. C.; Faust, T. B.; Muryn, C. A.; Pritchard, R. G.; Timco, G. A.; Winpenny, R. E. P. *Inorg. Chem.* **2009**, *48*, 9811–9818.

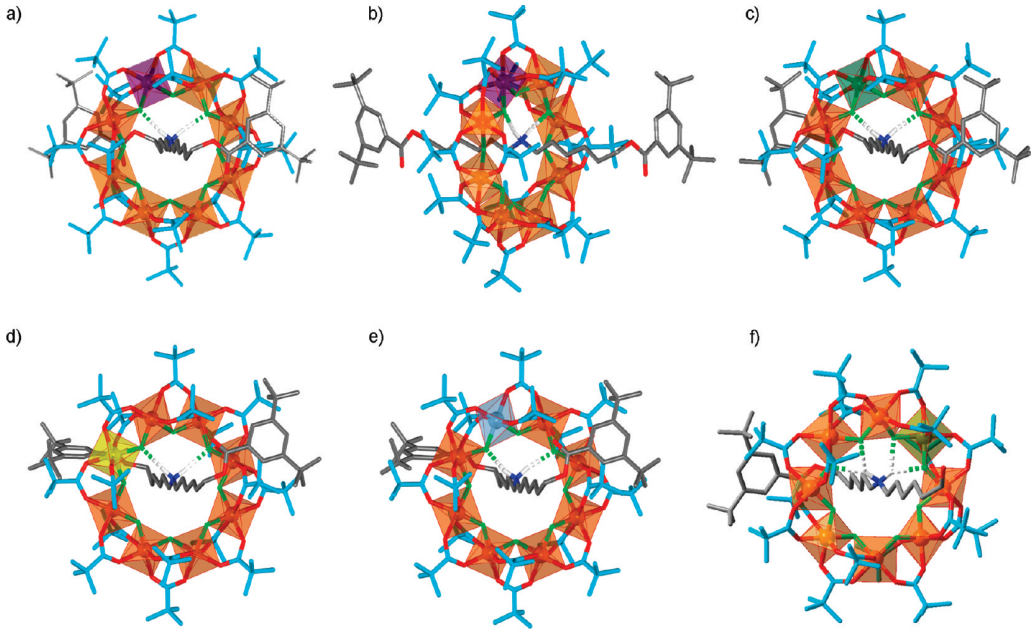

Figure 1. X-ray crystal structures of hybrid organic−inorganic [2]rotaxanes with 3,5-di-*tert*-butylbenzoate stoppers, **2a**, **2b**, **2d**, and **2e**, and Cr_7Fe-pseudorotaxane **2f**. (a) Facial view of Cr_7Co-[2]rotaxane **2a**.[4a] (b) Side view of Cr_7Co-[2]rotaxane **2a**.[4a] (c) Cr_7Ni-[2]rotaxane **2b**. (d) Cr_7Mn-[2]rotaxane **2d**. (e) Cr_7Cu-[2]rotaxane **2e**. (f) Cr_7Fe-pseudo[2]rotaxane **2f** (note only one stopper group is present on the thread). For clarity carbon atoms of the thread are shown in gray, carbon atoms of the pivalate groups in light blue, oxygen atoms in red, nitrogen in dark blue, fluorine in green, cobalt in purple, nickel in dark green, iron in dark yellow, manganese in yellow, copper in pale blue, and chromium in orange. Hydrogen atoms (white) other than those of the ammonium group are omitted for clarity. In (a), (b), (c), (e), and (f), the divalent metal ion (Co(II), Ni(II), Cu(II), Fe(II)) is disordered over the eight metal sites in each heterometallic ring and the structures are shown with the divalent metal ion having a (Λ)-arrangement of the ligands. In (d) the divalent metal ion (Mn(II)) is localized at the position indicated and is shown with a (Δ)-arrangement of the ligands. Hydrogen-bond (shown as dashed cylinders) lengths and N−H−F angles are (a and b) NH1···F1 = 2.03 Å, NH2···F7 = 2.01 Å, N−H1−F1 = 168.9°, N−H2−F7 = 168.2°; (c) NH1···F4 = 2.00 Å, NH2···F2 = 2.02 Å, N−H1−F4 = 167.9°, N−H2−F2 = 167.7°; (d) NH1···F4 = 2.13 Å, NH2···F6 = 2.11 Å, N−H1−F4 = 169.7°, N−H2−F6 = 171.6°; (e) NH1···F7 = 1.95 Å, NH2···F1 = 2.18 Å, N−H1−F7 = 161.0°, N−H2−F1 = 165.5°; (f) NH1···F7 = 2.20 Å, NH1···F8 = 2.14 Å, NH2···F1 = 2.23 Å, NH2···F2 = 2.19 Å, N−H1−F1 = 153.0°, N−H1−F8 = 131.2°, N−H2−F1 = 135.8°, N−H2−F2 = 148.9°. Crystallographic data and experimental details of the structural refinement for **2a**−**f** are provided in the Supporting Information.

many different sets of signals for the pivalate groups. However only eight resonances for pivalate groups (blue signals in Figure 2b) are observed in the spectrum of **2a**, consistent with rapid rotation of the ring on the NMR time scale.

Optimization of Rotaxane Yield. During the course of these studies we found, by accidentally introducing an impurity into a rotaxane-forming reaction,[4] that the presence of ammonium salts could significantly alter the yield in the hybrid organic−inorganic rotaxane-forming reactions. To study the effect of such additives on rotaxane formation, the synthesis of Cr_7Co-rotaxane **2a** was carried out in the presence of differing quantities of (a) diethylamine, (b) triethylamine, (c) (chloromethyl)triethylammonium chloride, and (d) tetraethylammonium chloride (Scheme 2). The results are shown in Figure 3.

Diethylamine is a good template for the formation of the octametallic ring, forming $[H_2NEt_2][Cr_7CoF_8(O_2C^tBu)_{16}]$, **5**, in 68% yield from the cocktail of metal salts and pivalic acid used in the assembly process.[7a] Thus when diethylamine was added to the rotaxane-forming reaction, **5** was isolated from the reaction (several other, unidentified, side products were also formed) as well as rotaxane **2a**, with the ratio of **2a/5** reflecting the competition between the two amines (thread **1** and diethylamine) for the ring (Figure 3, trace (a)). When more than 20 mol % of diethylamine was used the yield of rotaxane **2a** decreased from the 23% yield obtained with no additive (Scheme 1). Interestingly, however, when less than 20 mol % of diethylamine was used, the yield of rotaxane **2a** increased up to 58% (Figure 3, trace (a)). When (chloromethyl)triethylammonium chloride was added to the reaction mixture instead (Figure 3, trace (c)), **5** was also isolated as a side product, the diethylammonium cation apparently being generated under the reaction conditions. The yield of rotaxane **2a** was increased by the use of this salt at any ratio, with the best result (58% rotaxane **2a**) obtained with a loading of 30 mol %. Even higher yields of rotaxane were observed using triethylamine as an additive, with 65−70% of **2a** obtained with 5−100 mol % triethylamine (Figure 3, trace (b)), without the accompanying formation of **5** although other byproducts were formed. Finally, tetraethylammonium chloride improved the yield of **2a** when present in more than 20 mol % (Figure 3, trace (d)). In contrast to the other three additives, the use of Et_4NCl in the rotaxane-forming reaction did not produce **5** or any other side products. This makes purification of the rotaxane easier, and it may be the additive of choice for most rotaxane-forming protocols.

The role of these additives is presumably to template the assembly of the heterometallic ring, or large oligomers[16] that can readily form the ring, and the additives may play this role better than the thread does itself. The additives will form dynamic complexes with such species whereas the thread cannot decomplex from the wheel once the rotaxane has been formed without several metal−ligand bonds being broken concurrently. When not complexed with an ammonium group, the ring will

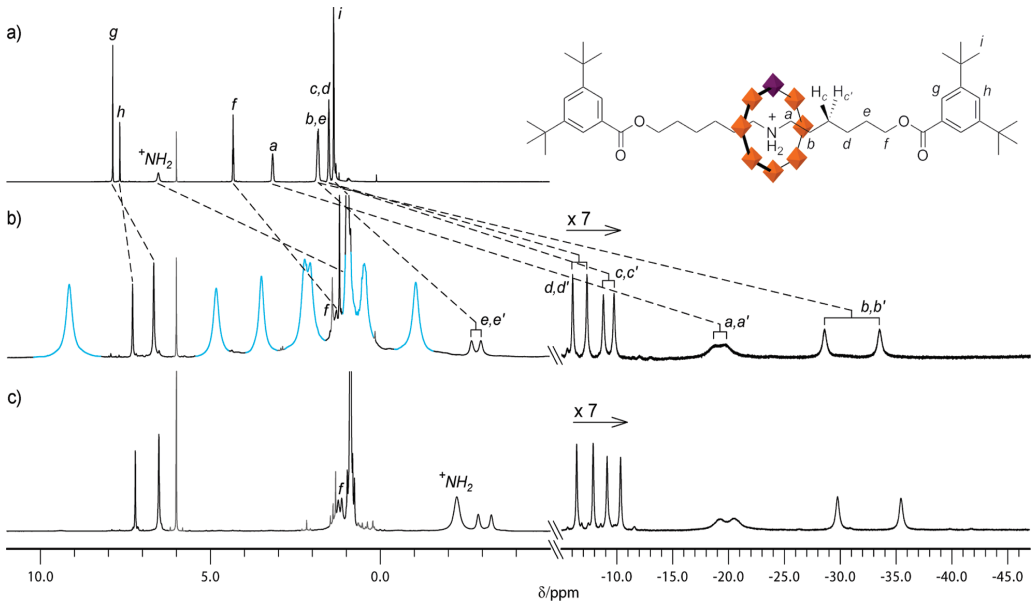

Figure 2. ^{1}H NMR spectra (500 MHz, $C_2D_2Cl_4$, 330 K). (a) Thread **1**·PF_6^-. (b) [2]rotaxane **2a**. (c) d_{144}-**2a**. The eight signals shown in blue in spectrum (b) are due to the 48 pivalate methyl groups of the macrocycle. Per-deuterating the pivalate methyl groups facilitates characterization of the relatively low intensity thread protons in the rotaxane (spectrum (c)). The rotaxane signals below −5 ppm are shown at 7× magnification and on a compacted *X*-axis compared to the signals above −5 ppm. Residual solvent peaks and impurities are shown in gray.

Scheme 2. Synthesis of Cr_7Co-[2]Rotaxane **2a** in the Presence of Additives[a,b]

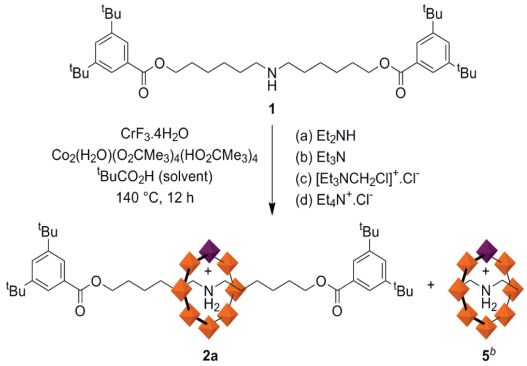

[a] Reaction conditions for the synthesis of [2]rotaxane **2a** in presence of various amounts of additive (a) diethylamine, (b) triethylamine, (c) (chloromethyl)triethylammonium chloride, or (d) tetraethylammonium chloride: **1** (1 equiv), additive (0.05−1 equiv), CrF_3·$4H_2O$ (5 equiv), $[Co(OH_2)(O_2CCMe_3)_4(HO_2CCMe_3)_4]$ (1 equiv), pivalic acid (50−60 equiv), 140 °C, 12 h. Isolated yields (Figure 3) are based on Cr(III) as the limiting reagent. [b] Pseudorotaxane **5** was formed as a side product only when diethylamine (a) or (chloromethyl)triethylammonium chloride (c) was used as the additive.

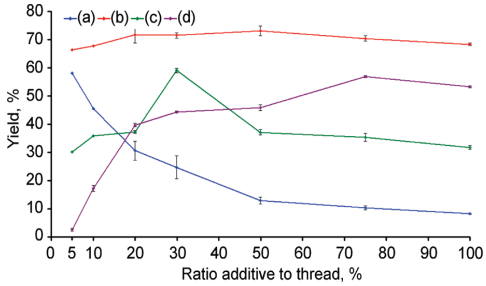

Figure 3. Yield of Cr_7Co-rotaxane **2a** (Scheme 2) as a function of the presence of various amounts of different additives: (a) diethylamine, (b) triethylamine, (c) (chloromethyl)triethylammonium chloride, (d) tetraethylammonium chloride. Each data point is the average of at least two experiments. Vertical error bars show the yields obtained from different runs.

be relatively unstable and more subject to ligand exchange. In other words, the additives probably act as templates that assemble large fragments of the heterometallic wheel that are then kinetically trapped as the rotaxane by the stoppered thread.

Kinetic Stability of Cr_7Co-[2]Rotaxane 2a. Although the metal−ligand bonds must be reversibly formed to some degree under the conditions that the rotaxanes are assembled (pivalic acid as solvent, 140 °C, 12 h), the hybrid organic−inorganic rotaxanes proved to be kinetically stable under less harsh conditions (Scheme 3). Rotaxane **2a** showed no evidence of dethreading or decomposition after 1 week at 60 °C in $C_2D_2Cl_4$. An isotopically labeled analogue in which the pivalate groups were perdeuterated, d_{144}-**2a**, was added, and the mixture was left for a further week at 60 °C (Scheme 3a). No exchange of pivalate ligands (which would indicate disassembly/reassembly of the heterometallic ring was occurring) was observed by mass spectrometry. At 140 °C, the mixture of [2]rotaxane **2a** and its deuterated analogue d_{144}-**2a** in $C_2D_2Cl_4$ did undergo scrambling of the pivalate ligands and about 90% of the rings had exchanged at least 1 of their 16 pivalate groups after 48 h. In order to be certain that the ring does not slip off the thread and reassemble

(16) The most likely candidates for oligomeric precursors to the macrocycles are Cr_6-'horseshoes', which form readily in similar reactions in the presence of dialkylamines when the divalent metal is absent. See: Larsen, F. K.; Overgaard, J.; Parsons, S.; Rentschler, E.; Timco, G. A.; Smith, A. A.; Winpenny, R. E. P. *Angew. Chem., Int. Ed.* **2003**, *42*, 5978–5981.

Scheme 3. Pivalate-Exchange Reactions between (a) [2]Rotaxanes **2a** and d_{144}-**2a** and (b) [2]Rotaxanes d_{144}-**2a** and **4a**

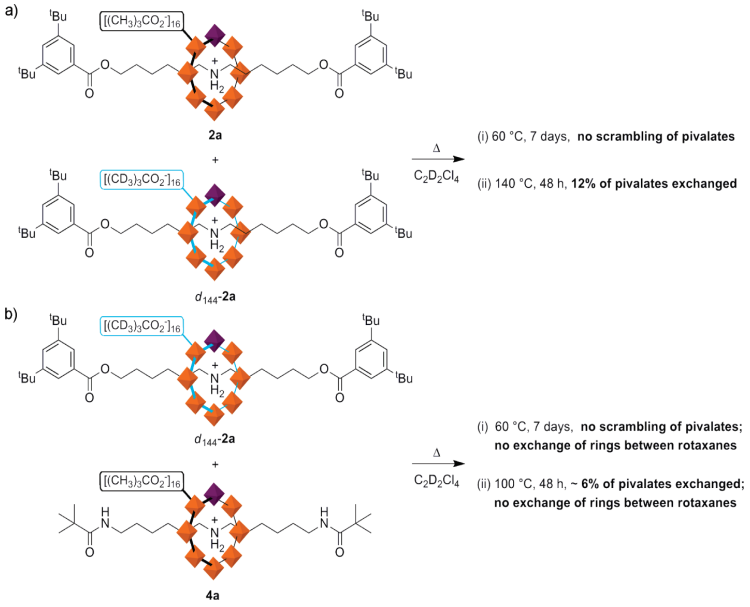

around another one, a second experiment was conducted (Scheme 3b). A mixture of [2]rotaxane with different rings (one isotopically labeled, one not) and stoppers, d_{144}-**2a** and **4a** (for the synthesis of rotaxane **4a**, see Scheme 4), was stirred for 1 week in $C_2D_2Cl_4$ at 60 °C. No exchange of the heterometallic rings between the threads was observed by ESI-MS. At 100 °C the scrambling of individual pivalate groups did occur over 48 h, but still under these conditions there was no whole ring transfer between the two [2]rotaxanes.

Changing the End Groups of the Thread: One Pot 'Stoppering-Plus-Macrocyclization' Assembly of [2]Rotaxanes 4a−g. Although the benzoate esters used to stopper the threads in rotaxanes **2a−e** are reasonably stable to the rather harsh conditions used in the rotaxane-forming reaction (pivalic acid at 140 °C), some cleavage of the ester groups was observed in reaction byproducts (e.g., pseudorotaxanes of the mono-ol or diol derived from the thread; for example, **2f**, Scheme 1 and Figure 1f). The use of simple (nonstoppered) dialkylamines (such as Et_2NH, nPr_2NH, nBu_2NH) as templates[7] generates the heterometallic wheels in good yields (up to 68%[7a]), suggesting that the bulkiness of the stoppers might make the secondary amine in **1** a relatively poor template. Accordingly we investigated the possibility of using a smaller, more stable, stoppering group for the assembly of rotaxanes. CPK models suggested that the heterometallic ring cavities are small enough that even a *tert*-butylamide group should prevent dethreading, and so *bis*(hexamethylene)triamine **3** was used to assemble another series of [2]rotaxanes in a stoppering-plus-macrocyclization reaction that utilizes both pivalic acid and pivalic anhydride[17] (Scheme 4). Under these reaction conditions, in addition to the template macrocyclization of the heterometallic wheel about the thread, the primary amines at either end of **3** react to form amides leading to the one-pot

Scheme 4. One-Pot 'Stoppering-Plus-Macrocyclization' Reaction To Assemble ^{t}BuCONH-Stoppered [2]Rotaxanes **4a−g**[a]

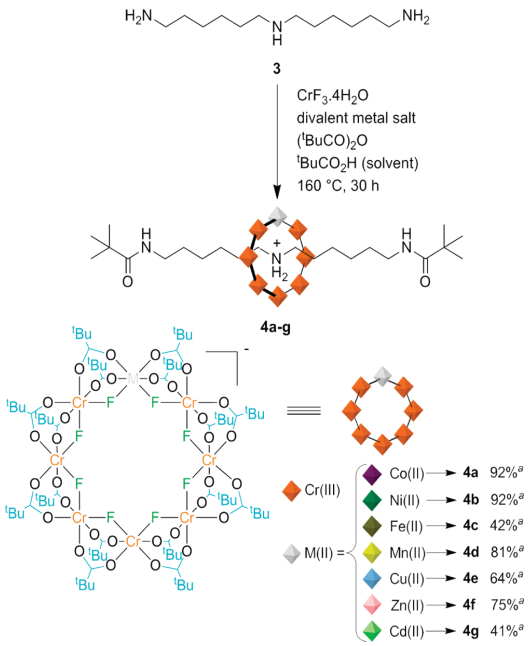

[a] Reaction conditions for the synthesis of [2]rotaxanes with ^{t}BuCONH stoppers, **4a−g**: **3** (1 equiv), $CrF_3 \cdot 4H_2O$ (5 equiv), divalent metal salt ($[Co(O_2CCMe_3)_2]$, $[Ni(OH_2)(O_2CCMe_3)_4(HO_2CCMe_3)_4]$, $Fe(O_2CCH)_2 \cdot 2H_2O$, $MnCO_3 \cdot 2H_2O$, $CuCO_3 \cdot Cu(OH)_2$, $[ZnCO_3]_2 \cdot [Zn(OH)_2]_3$, $CdCO_3$) (1 equiv), pivalic anhydride (6 equiv), pivalic acid (50−60 equiv), 160 °C, 30 h. Isolated yields are based on Cr(III) as the limiting reagent.

formation of amide-stoppered rotaxanes **4a−e** when Co(II), Ni(II), Fe(II), Mn(II), or Cu(II) was used as the divalent metal. The [2]rotaxanes (**4a−e**) assembled by this simultaneous stoppering and macrocyclization protocol were obtained in

(17) The amide-stoppered rotaxanes also form under the original reaction conditions (Scheme 1). However, the addition of pivalic anhydride increases the yield and decreases the reaction time required for efficient rotaxane formation.

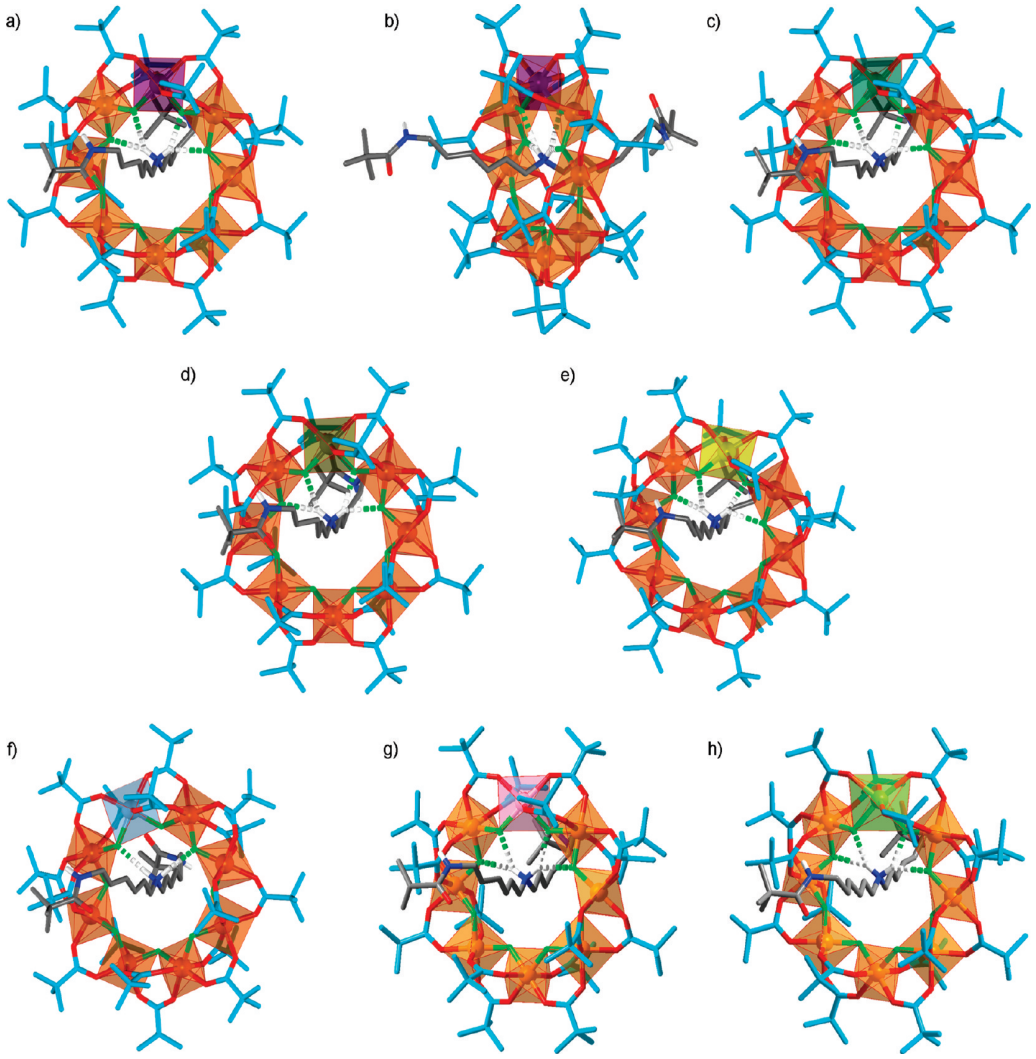

Figure 4. X-ray crystal structures of hybrid organic−inorganic [2]rotaxanes with ^{t}BuCONH stoppers, **4a**−**g**. (a) Facial view of Cr_7Co-[2]rotaxane **4a**. (b) Side view of Cr_7Co-[2]rotaxane **4a**. (c) Cr_7Ni-[2]rotaxane **4b**. (d) Cr_7Fe-[2]rotaxane **4c**. (e) Cr_7Mn-[2]rotaxane **4d**. (f) Cr_7Cu-[2]rotaxane **4e**. (g) Cr_7Zn-[2]rotaxane **4f**. (h) Cr_7Cd-[2]rotaxane **4g**. The atom coloring is as indicated in the Figure 1 caption, plus zinc is pink and cadmium is light green. In (a), (b), (c), (d), (f), and (h), the divalent metal ion (Co(II), Ni(II), Fe(II), Cu(II), Cd(II)) is localized at the position indicated in the heterometallic ring and has a (Λ)-arrangement of the ligands. In (e) and (g) the divalent metal ion (Mn(II) and Zn(II)) is disordered over the eight metal sites in the heterometallic ring and the structure is shown with the divalent metal ion having a (Λ)-arrangement of the ligands. Hydrogen-bond (shown as dashed cylinders) lengths and N−H−F angles are (a and b) NH1···F1 = 2.08 Å, NH1···F2 = 2.45 Å, NH2···F7 = 2.23 Å, NH2···F8 = 2.22 Å, N−H1−F1 = 145.6°, N−H1−F2 = 141.0°, N−H2−F7 = 150.0°, N−H2−F8 = 135.3°; (c) NH1···F7 = 2.32 Å, NH1···F8 = 2.10 Å, NH2···F1 = 2.10 Å, NH2···F2 = 2.32 Å, N−H1−F7 = 141.9°, N−H1−F8 = 142.3°, N−H2−F1 = 135.7°, N−H2−F2 = 148.6°; (d) NH1···F7 = 2.28 Å, NH1···F8 = 2.16 Å, NH2···F1 = 2.12 Å, NH2···F2 = 2.40 Å, N−H1−F7 = 145.5°, N−H1−F8 = 139.6°, N−H2−F1 = 141.1°, N−H2−F2 = 144.9°; (e) NH1···F7 = 2.07 Å, NH1···F8 = 2.21 Å, NH2···F1 = 1.93 Å, NH2···F2 = 2.59 Å, N−H1−F7 = 156.0°, N−H1−F8 = 124.8°, N−H2−F1 = 160.4°, N−H2−F2 = 128.5°; (f) NH1···F2 = 2.13 Å, NH2···F8 = 2.01 Å, N−H1−F2 = 167.2°, N−H2−F8 = 161.5°; (g) NH1···F1 = 2.02 Å, NH1···F2 = 2.43 Å, NH2···F7 = 2.19 Å, NH2···F8 = 2.20 Å, N−H1−F1 = 146.6°, N−H1−F2 = 139.3°, N−H2−F7 = 150.6°, N−H2−F8 = 133.4°; (h) NH1···F1 = 2.05 Å, NH1···F2 = 2.39 Å, NH2···F7 = 2.35 Å, NH2···F8 = 2.08 Å, N−H1−F1 = 144.0°, N−H1−F2 = 142.1°, N−H2−F7 = 143.4°, N−H2−F8 = 141.9°. Crystallographic data and experimental details of the structural refinement for **4a**−**g** are provided in the Supporting Information.

significantly higher yields (up to 92%) than the corresponding benzoate ester rotaxanes (**2a**−**e**). This led us to attempt the rotaxane-forming reaction with Zn(II) and Cd(II) salts, which are generally[7d] poorer divalent metals for the assembly of heterometallic rings but here produced [2]rotaxanes **4f** and **4g** in 75% and 41% yields, respectively (Scheme 4). It is unclear as to whether the 'stoppering-plus-macrocyclization' reaction is so effective only because of the greater stability of the end group in the final rotaxane or whether the amines are playing an additional role in the template assembly of the heterometallic ring prior to the acylation of the primary amines.[17]

The X-ray structures of rotaxanes **4a**−**g** are shown in Figure 4. There are no intramolecular hydrogen bonding interactions between the *tert*-butylamide groups of either stopper and the heterometallic ring, probably as a result of the bulkiness of the *tert*-butyl group adjacent to the amide. The intercomponent

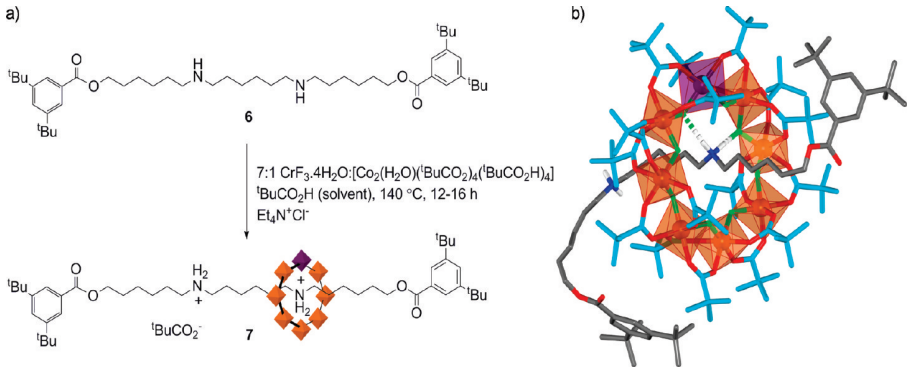

Figure 5. Synthesis (a) and X-ray structure (b) of molecular shuttle **7**. Atom coloring is as indicated in the Figure 1 caption. The divalent metal ion, Co(II), is disordered over the eight metal sites on each heterometallic wheel. Crystallographic data and experimental details of the structural refinement for **7** are provided in the Supporting Information.

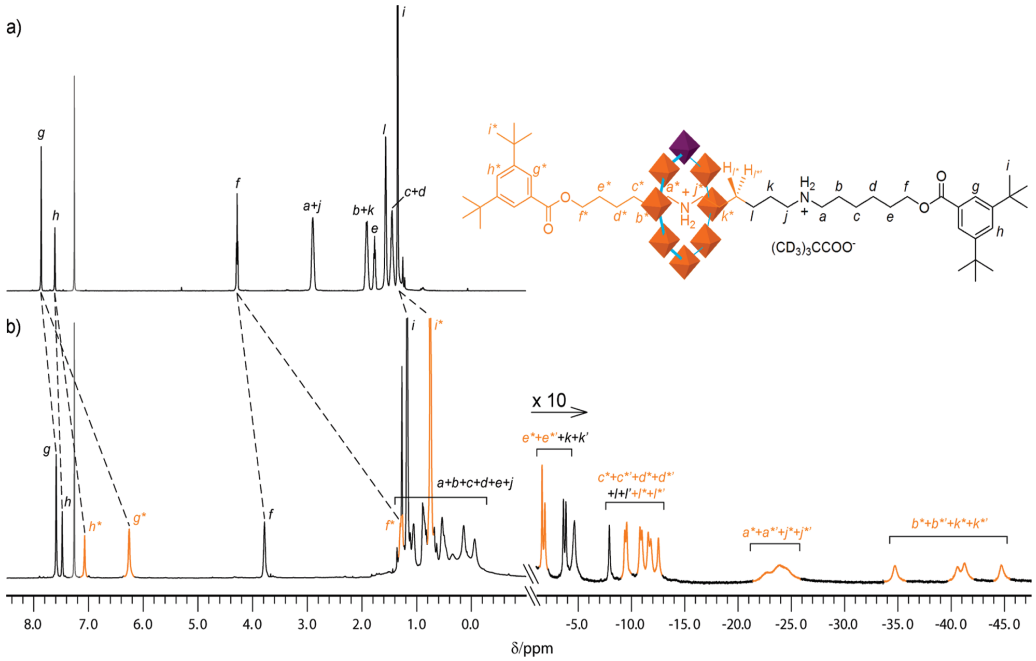

Figure 6. ^{1}H NMR spectra (500 MHz, $CDCl_3$, 298 K): (a) Thread **6**·$2PF_6^-$, (b) [2]rotaxane molecular shuttle d_{144}-**7**. The signals labeled * shown in orange in spectrum (b) belong to the protons of the half thread where the ring is located. Signals labeled ′ are parts of sets of diastereotopic protons. Per-deuterating the pivalate methyl groups facilitates characterization of the relatively low intensity thread protons in the rotaxane (spectrum (b)). The rotaxane signals below −1 ppm are shown at 10× magnification and on a compacted *X*-axis compared to the signals above −1 ppm. Residual solvent peaks and impurities are shown in gray.

hydrogen bonding in the solid state structures of [2]rotaxanes **4a**−**d**, **4f**, and **4g** is reminiscent of the bifurcated $F^-\cdots HN^+$ interactions between four bridging fluoride ligands and the thread ammonium group seen in Cr_7Fe-pseudorotaxane **2f** (Figure 1f). The intercomponent hydrogen bonding in Cr_7Cu-[2]rotaxane **4e** (Figure 4f) is similar to the linear F···HN hydrogen bonds seen in the crystal structures of the other rotaxanes in Figure 1.

Cr_7Co-[2]rotaxane (**4a**) and Cr_7Fe-[2]rotaxane (**4c**) were also characterized in $CDCl_3$ solution by ^{1}H NMR spectroscopy (see Supporting Information). The Fe(II) ions have a relatively slow rate of nuclear relaxation, counterbalancing the fast electronic relaxation of Cr(III)[18] in a similar way to Co(II) (Figure 2), but with greater line broadening and more modest paramagnetic shifts leading to less well-resolved spectra. As with rotaxane **2a**, only eight resonances for the pivalate groups are observed in both **4a** and **4c** indicating rapid rotation of the ring on the NMR time scale.

A Hybrid Organic−Inorganic Molecular Shuttle. The hybrid organic−inorganic rotaxane synthesis was successfully extended to higher architectures (the assembly of [3]- and [4]rotaxanes has been reported elsewhere[4]) including threads containing two

(18) Glass, M. M.; Belmore, K.; Vincent, J. B. *Polyhedron* **1993**, *12*, 133–140.

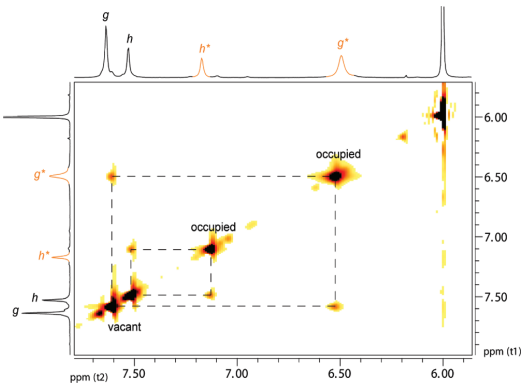

Figure 7. Partial 2D-EXSY spectrum of d_{144}-**7** (500 MHz, $C_2D_2Cl_4$, 330 K, $\tau_m = 50$ ms).

ammonium binding sites. Using the *bis*-amine **6** as a thread, [2]rotaxane **7**, with one Cr_7Co-heterometallic ring on an axle with six methylene groups between the two ammonium groups, was synthesized (Figure 5). The molecular shuttle **7** could not be prepared without the use of an amine/ammonium additive but was isolated in 36% yield from a reaction employing tetraethylammonium chloride and could also be obtained in a more modest yield using diethylamine, (chloromethyl)triethylammonium chloride, or triethylamine. The Cr_7Co-[2]rotaxane **7** was structurally characterized by ESI-MS, X-ray crystallography (Figure 5b), and ^{1}H NMR spectroscopy (Figure 6).

The ^{1}H NMR spectrum of d_{144}-**7** (the deuterated analogue of **7**) in $CDCl_3$ at room temperature shows a well-resolved set of signals for each half of the thread (shown in orange and black in Figure 6); the difference within each set of signals is caused by whether the adjacent ammonium center is vacant or occupied by the heterometallic ring. Remarkably, no line broadening was observed even at 400 K indicating that the shuttling is slow on the NMR time scale even at those elevated temperatures.

The rate of exchange of the ring between the two binding sites on the thread could be measured by polarization transfer between signal pairs using two-dimensional exchange spectroscopy (EXSY[19]) experiments (Figure 7). At 330 K in $C_2D_2Cl_4$, these measurements gave a rate of exchange of 1.2 ± 0.5 s^{-1}, corresponding to a free energy of activation ($\Delta G^{\ddagger}$) of 19.3 ± 0.2 kcal mol^{-1}. This value is at least 10 kcal mol^{-1} larger than the activation barrier for rotation of the ring around the thread. This notable difference in the rates of the intercomponent dynamics can be rationalized by the nature of the intercomponent NH−F hydrogen bonding seen in the various crystal structures. The symmetry of the heterometallic wheels means that a one-eighth turn (45°) is sufficient to transfer of hydrogen bonds of the ammonium group from one bridging fluoride ion to the next one. Furthermore, a one-sixteenth turn (22.5°) maps the $F^-\cdots HN^+$ hydrogen bonding onto the bifurcated hydrogen bond motif seen in several of the crystal structures (Figures 1f, 4a−e, 4g, 4h) meaning that rotation can occur without significant breaking of an existing hydrogen bond before a new one starts to form (Figure 8b). In contrast, the shuttling requires complete breaking of all the intercomponent NH−F hydrogen bonds before translocation can occur, resulting in a much slower process.

Conclusions

Kinetically stable hybrid organic−inorganic rotaxanes and molecular shuttles have been prepared through template syn-

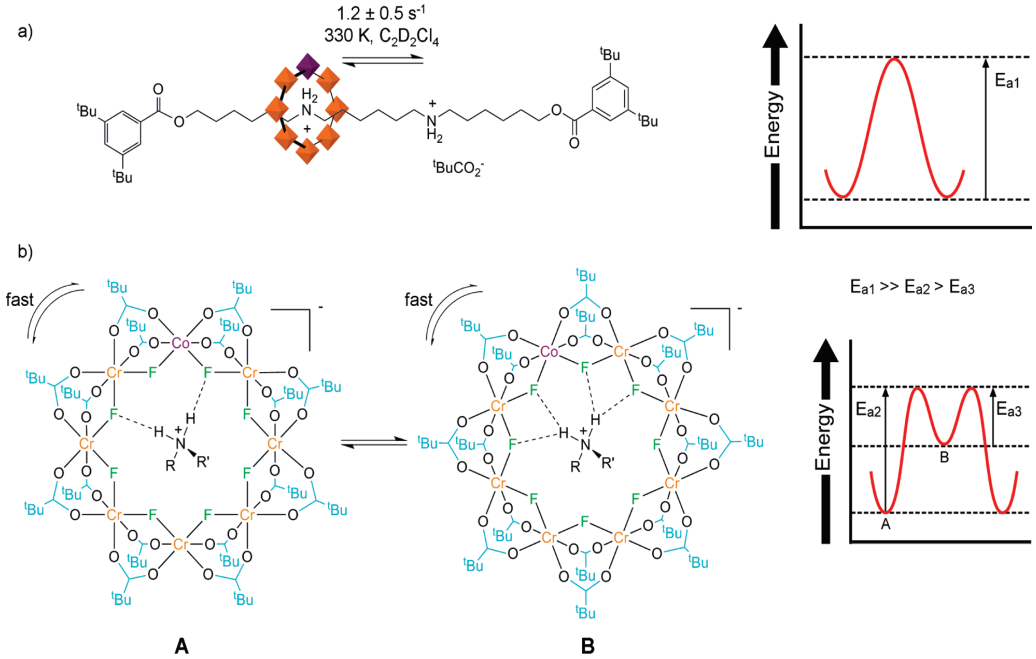

Figure 8. (a) Energy profile for shuttling. (b) Energy profile for rotation. A low energy route for rotation of the heterometallic ring about the ammonium group could involve the system passing through two different types of hydrogen bonded state (A and B). In A, each proton of the ammonium station point is involved in one linear $^+$NH$\cdots$F$^-$ hydrogen bond with one fluoride atom of the ring. In B, each proton of the ammonium station forms bifurcated H-bonds with two fluorides of the ring. Both types of hydrogen bond motif are seen in the X-ray crystal structures of various rotaxanes (Figures 1 and 4).

thesis in yields that range from 5% to 92%. Some of the factors controlling the efficiency of the rotaxane synthesis have been identified, and improved protocols, including the use of additives and a one-pot 'stoppering-plus-macrocyclization' strategy, have been introduced, efficiently generating rotaxanes with a range of different divalent transition metal ions (Co(II), Ni(II), Fe(II), Mn(II), Cu(II), Zn(II), and Cd(II)). In a rotaxane with a free ammonium site on the thread — molecular shuttle **7** — rotational dynamics (of the ring spinning around the thread) are much faster than translational dynamics (the ring moving between ammonium sites on the thread) because of the nature of the intercomponent hydrogen bonding interactions. Hybrid organic—inorganic rotaxanes constitute promising candidates for molecular machines that combine some of the features of the chemistry of inorganic clusters (magnetism, electronic properties) with the dynamic properties typical of organic-based interlocked molecules.[4b] Such systems may prove useful in helping to establish how heterometallic-ring-based qubits can be linked to maximize entanglement of spins without inducing decoherence. Furthermore, the ability to move qubits with respect to one another under the action of an external stimulus could potentially be used to produce arrays where the qubits are close, allowing one type of algorithm to be implemented (an "on" position), or more distant, which could be regarded as a system being on "standby". Much remains to be done before such hypothetical devices can be constructed, in terms of both controlling intercomponent motion and learning how to measure, control, and utilize very weak through-space magnetic interactions.

Acknowledgment. We thank Juraj Bella for the EXSY NMR experiments and the EPSRC National Mass Spectrometry Service Centre (Swansea, U.K.) for high resolution mass spectrometry. This research was funded by the European Commission (through the NoE 'MAGMANet') and the EPSRC. The Advanced Light Source is supported by the Director, Office of Science, Office of Basic Energy Sciences, of the U.S. Department of Energy under Contract No. DE-AC02-05CH11231. We are grateful to the Swiss National Science Foundation for a postdoctoral fellowship to D.S. and the Ministerio de Ciencia e Innovación for a postdoctoral fellowship to B.B. D.A.L. is an EPSRC Senior Research Fellow. R.E.P.W. and D.A.L. hold Royal Society-Wolfson Research Merit Awards.

Supporting Information Available: Experimental procedures and the supplementary crystallographic data. This material is available free of charge via the Internet at http://pubs.acs.org.

JA1074773

(19) Perrin, C. L.; Dwyer, T. J. *Chem. Rev.* **1990**, *90*, 935–967.

Supplementary Information

Synthesis, Structure and Dynamic Properties of Hybrid Organic-Inorganic Rotaxanes

Beatriz Ballesteros, Thomas B. Faust, Chin-Fa Lee, David A. Leigh*, Christopher A. Muryn, Robin G. Pritchard, David Schultz, Simon J. Teat, Grigore A. Timco and Richard E. P. Winpenny*

School of Chemistry, University of Edinburgh, The King's Buildings, West Mains Road, Edinburgh EH9 3JJ, United Kingdom.

School of Chemistry and Photon Science Institute, University of Manchester, Oxford Road, Manchester M13 9PL, United Kingdom.

Advanced Light Source, Lawrence Berkeley Laboratory, 1 Cyclotron Rd, MS2-400, Berkeley, California 94720, USA.

E-mail: david.leigh@ed.ac.uk (D.A.L.); richard.winpenny@man.ac.uk (R.E.P.W.).

1. General Experimental Section

Unless stated otherwise, all reagents and solvents were purchased from Aldrich Chemicals and used without further purification. $[Co_2(H_2O)(O_2CCMe_3)_4(HO_2CCMe_3)_4]$ and $[Co(O_2CCMe_3)_2]$ were prepared according to a procedure reported in G. Aromi, A. S. Batsanov, P. Christian, M. Helliwell, A. Parkin, S. Parsons, A. A. Smith, G. A. Timco, R. E. P. Winpenny, *Chem. Eur. J.* **2003**, *9*, 5142-5161. $[Ni_2(H_2O)(O_2CCMe_3)_4(HO_2CCMe_3)_4]$ was prepared according to a procedure reported in G. Chaboussant, R. Basler, H.-U. Güdel, S. Ochsenbein, A. Parkin, S. Parsons, G. Rajaraman, A. Sieber, A. A. Smith, G. A. Timco, R. E. P. Winpenny, *Dalton Trans.*, **2004**, 2758-2766. The syntheses of the hybrid organic-inorganic rotaxanes were carried out in Erlenmeyer Teflon® FEP flasks supplied by Fisher. Column chromatography was carried out using Silica 60A (particle size 35-70 μm, Fisher, UK) as the stationary phase, and TLC was performed on precoated silica gel plates (0.25 mm thick, 60 F_{254}, Merck, Germany) and observed under UV light. NMR spectra were recorded on Bruker AV 400, and Bruker DMX 500 instruments. Chemical shifts are reported in parts per million (ppm) from low to high frequency and referenced to the residual solvent resonance. Coupling constants (*J*) are reported in hertz (Hz). Standard abbreviations indicating multiplicity were used as follows: s = singlet, d = doublet, t = triplet, dd = double doublet, q = quartet, m = multiplet, b = broad, ddd = doublet of double doublets. Melting points (m.p.) were determined using a Sanyo Gallenkamp apparatus and are reported uncorrected. Low resolution ESI mass spectrometry was performed with a Micromass Platform II mass spectrometer, controlled using Masslynx v2.3 software. High resolution ESI and FAB mass spectrometry were carried out by the mass spectrometry services at the

University of Edinburgh and the EPSRC National Mass Spectrometry Service Centre, Swansea, UK.

2. Synthesis and Experimental Section

2.1 Synthesis of [2]rotaxanes 2a-e

[2]rotaxane 2a

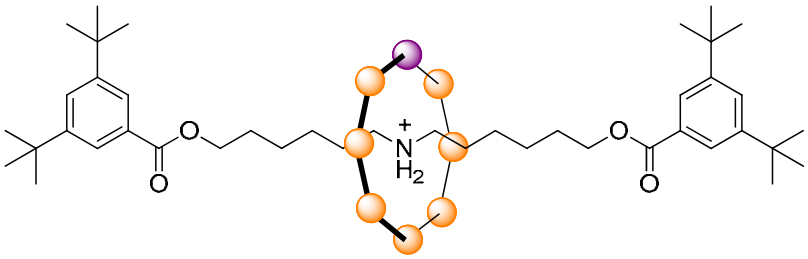

Pivalic acid (7.0 g, 68.54 mmol) and **1** (0.38 g, 0.585 mmol) were heated at 140 °C for 15 min with stirring under nitrogen. Then $CrF_3.4H_2O$ (0.7 g, 3.866 mmol) and $[Co_2(OH_2)(O_2CCMe_3)_4(HO_2CCMe_3)_4]$ (0.32 g, 0.337 mmol) were added to the solution. After 12 h the mixture was cooled to room temperature and CH_3CN (20 mL) was added. The green product was filtered, washed with CH_3CN, dried in air, dissolved in Et_2O (20ml), and concentrated under reduced pressure. Flash chromatography (toluene, then a gradient elution up to 1:1 toluene:EtOAc, then a gradient elution up to 1:1 toluene:CH_3OH) afforded **2a** as a green crystalline solid (0.362 g). Yield: 23% (calculated from $CrF_3.4H_2O$ used). Elemental analysis, calcd (%) for $C_{122}H_{212}Co_1Cr_7F_8N_1O_{36}$: Cr 12.80, Co 2.07, C 51.53, H 7.51, N 0.49; Found: Cr 12.64, Co 2.13, C 50.98, H 7.65, N 0.45. ES-MS (sample dissolved in THF, run in MeOH): *m/z* = 2902 $[M+Na+2H_2O]^+$ (100%); 2866 $[M+Na]^+$; 2843 $[M]^{+\cdot}$. X-Ray quality crystals were obtained from the recrystallization of **2a** from a mixture of Et_2O/CH_3CN. ^1H NMR (500 MHz, 330 K, $C_2D_2Cl_4$): δ = -33.52 (s, 2H, H_b), -28.61 (s, 2H, H_b), -21.00 to -17.80 (br m, 4H, H_a), -9.76 (s, 2H, H_c), -8.79 (s, 2H, H_c), -7.33 (s, 2H, H_d), -6.05 (s, 2H, H_d), -2.96 (s, 2H, H_e), -2.68 (s, 2H, H_e), -1.04 (br s, 18H,

$H_{pivalate}$), 0.48 (br s, 18H, $H_{pivalate}$), 0.97 (br s, 58H, $H_{f+i+pivalate}$), 2.06 (br s, 18H, $H_{pivalate}$), 2.22 (br s, 18H, $H_{pivalate}$), 3.50 (br s, 18H, $H_{pivalate}$), 4.83 (br s, 18H, $H_{pivalate}$), 6.66 (s, 4H, H_g), 7.29 (s, 2H, H_h), 9.15 (br s, 18H, $H_{pivalate}$).

d_{144}-**2a** (deuterated analogue of [2]rotaxane **2a**) was obtained following a similar procedure to that used for the preparation of **2a** but using d_9-pivalic acid and $[Co_2(OH_2)(O_2CC(CD_3)_3)_4(HO_2CC(CD_3)_3)_4]$ in place of pivalic acid and $[Co_2(OH_2)(O_2CCMe_3)_4(HO_2CCMe_3)_4]$ respectively.

[2]rotaxane 2b

Pivalic acid (7.0 g, 68.54 mmol), **1** (0.38 g, 0.585 mmol), $CrF_3.4H_2O$ (0.7 g, 3.866 mmol) and $[2NiCO_3.3Ni(OH)_2.4H_2O]$ (0.08 g, 0.136 mmol) were heated at 140 °C for 10 h with stirring under nitrogen. Then the mixture was cooled to room temperature and CH_3CN (20 mL) was added. The green product was filtered, washed with CH_3CN, dried in air, dissolved in Et_2O (20ml), and concentrated under reduced pressure. Flash chromatography (toluene, then a gradient elution up to 1:1 toluene:EtOAc, then a gradient elution up to 1:1 toluene:CH_3OH) afforded **2b** as a green crystalline solid (0.139 g). Yield: 9% (calculated from $CrF_3.4H_2O$ used). Elemental analysis, calcd (%) for $C_{122}H_{212}Cr_7F_8N_1Ni_1O_{36}$: Cr 12.80, Ni 2.06, C 51.53, H 7.51, N 0.49; Found: Cr 12.64, Ni 2.07, C 51.39, H 7.68, N 0.50. ES-MS (sample dissolved in THF, run in MeOH): *m/z* = 2901 $[M+Na+2H_2O]^+$ (100%); 2865 $[M+Na]^+$; 2842 $[M]^+$. X-Ray quality crystals were obtained from the recrystallization of **2b** from a mixture of Et_2O/CH_3CN.

[2]rotaxane 2c

Pivalic acid (283 mg, 2.762 mmol) and **1** (45 mg, 0.069 mmol) were heated at 140 °C for 15 min with stirring in a glass tube under nitrogen. Then $CrF_3 \cdot 4H_2O$ (63 mg, 0.346 mmol) and $FeCl_2 \cdot 4H_2O$ (14 mg, 0.069 mmol) were added to the solution. After 12 h the mixture was cooled to room temperature and CH_3CN (5 mL) was added. The green product was filtered, washed with CH_3CN, dried in air, dissolved in Et_2O (20ml), and concentrated under reduced pressure. Flash chromatography (petroleum ether:EtOAc, 100:2) afforded **2c** as a green crystalline solid (7 mg). Yield: 5% (calculated from $CrF_3.4H_2O$ used). LRESI-MS (sample dissolved in DCM, run in CH_3CN): *m/z* = 2840 $[M]^+$. X-Ray quality crystals were obtained from the recrystallization of **2c** from a mixture of petroleum ether/CH_3CN. ^{1}H-NMR (500 MHz, 298 K, $CDCl_3$): δ (ppm) = -21.17 (s, 2H, H_b), -17.10 (s, 2H, H_b), -11.57 to -9.93 (br m, 4H, H_a), -5.17 (s, 2H, H_c), -4.07 (s, 2H, H_c), -3.80 (s, 2H, H_d), -2.64 (s, 2H, H_d), -1.09 (s, 2H, H_e), -0.74 (s, 2H, H_e), -0.36 (br s, 18H, $H_{pivalate}$), 1.20 (br s, 76H, $H_{f+i+pivalate}$), 1.81 (br s, 18H, $H_{pivalate}$), 2.54 (br s, 18H, $H_{pivalate}$), 3.13 (br s, 18H, $H_{pivalate}$), 6.49 (br s, 18H, $H_{pivalate}$), 6.85 (br s, 18H, $H_{pivalate}$), 7.12 (s, 4H, H_g), 7.37 (s, 2H, H_h).

[2]rotaxane 2d

Pivalic acid (314 mg, 3.071 mmol) and **1** (50 mg, 0.077 mmol) were heated at 140 °C for 15 min with stirring in a glass tube under nitrogen. Then $CrF_3 \cdot 4H_2O$ (70 mg, 0.384 mmol) and $MnCl_2 \cdot 4H_2O$ (15 mg, 0.077 mmol) were added to the solution. After 12 h the mixture was cooled to room temperature and CH_3CN (5 mL) was added. The green product was filtered, washed with CH_3CN, dried in air, dissolved in Et_2O (20ml), and concentrated under reduced pressure. Flash chromatography (petroleum ether:EtOAc, 100:2) afforded **2d** as a green crystalline solid (28 mg). Yield: 18% (calculated from $CrF_3.4H_2O$ used). LRESI-MS (sample dissolved in DCM, run in

MeOH): *m/z* = 2862 $[M+Na]^+$, 2839 $[M]^+$. X-Ray quality crystals were obtained from the recrystallization of **2d** from a mixture of petroleum ether/CH_3CN.

[2]rotaxane 2e

Pivalic acid (470 mg, 4.610 mmol), **1** (50 mg, 0.077 mmol) and $NEt_4^+Cl^-$ (2 mg, 0.015 mmol) were heated at 140 °C for 15 min with stirring in a glass tube under nitrogen. Then $CrF_3{\cdot}4H_2O$ (70 mg, 0.384 mmol) and $CuCO_3{\cdot}Cu(OH)_2$ (8 mg, 0.039 mmol) were added to the solution. After 12 h the mixture was cooled to room temperature and CH_3CN (5 mL) was added. The green product was filtered, washed with CH_3CN, dried in air, dissolved in Et_2O (20ml), and concentrated under reduced pressure. Flash chromatography (petroleum ether:EtOAc, 100:2) afforded **2e** as a green crystalline solid (19 mg). Yield: 12% (calculated from $CrF_3.4H_2O$ used). LRESI-MS (sample dissolved in DCM, run in MeOH): *m/z* = 2871 $[M+Na]^+$, 2848 $[M]^+$. X-Ray quality crystals were obtained from the recrystallization of **2e** from toluene.

2.2 Synthesis of [2]rotaxanes 4a-g

[2]rotaxane 4a

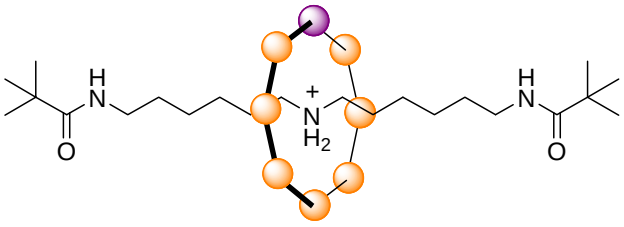

Pivalic acid (15.0 g, 146.87 mmol), $CrF_3{\cdot}4H_2O$ (3.0 g, 16.57 mmol) and bis(hexamethylene)triamine (0.6 g, 2.786 mmol) were heated with stirring at 160 °C for 2 h . $[Co(O_2CCMe_3)_2]$ (0.7 g, 2.68 mmol) and pivalic anhydride (3.0 g, 16.11 mmol) were then added and the mixture was strirred at 160 °C under a slow flow of

nitrogen for 30 h. Then the mixture was allowed to cool to room temperature and CH_3CN (25 mL) was added. The resulting suspension was collected by filtration, washed with CH_3CN, dried in air, dissolved in Et_2O (70 mL), and concentrated under reduced pressure. The green residue was purified by flash column chromatography (toluene:EtOAc, 5:1). An initial faint green band eluted off the column first, followed later by the main second band (intense green) which contained the desired product. The solvents were removed under reduced pressure and the green solid obtained was washed with CH_3CN and then dried under vacuum.

Yield: 5.60 g (91.8%, calculated from $CrF_3.4H_2O$ used). Elemental analysis, calcd. (%) for $C_{102}H_{190}Co_1Cr_7F_8N_3O_{34}$: Cr 14.12, Co 2.29, C 47.53, H 7.43, N 1.63; found (%): Cr 14.11, Co 2.22, C 47.40, H 7.22, N 1.65. ES-MS (sample dissolved in Et_2O, run in MeOH): *m/z* = 2902 $[M+Na]^+$ (100%). X-Ray quality crystals were obtained from crystallization of **4a** from a saturated solution in acetone. ^{1}H NMR (300 MHz, 293 K, $CDCl_3$): δ = -98.1 (s, NH2+), -45.64 (s, 2H, H_b), -41.35 (s, 2H, H_b), -25.64 (br s, 4H, H_a), -12.73 (br s, 4H, H_c), -10.73 (s, 2H, H_d), -8.99 (s, 2H, H_d), -6.15 (s, 2H, H_e), -5.94 (s, 2H, H_e), -1.75 (br s, 18H, $H_{pivalate}$), -1.26 (s, 2H, H_f), -0.99 (s, 2H, H_f), -0.38 (s, 18H, COC(C***H***$_3$)$_3$)), 0.05 (br s, 36H, $H_{pivalate}$), 1.34 (s, 2H, CH_2N***H***CO), 1.65 (br s, 18H, $H_{pivalate}$), 2.62 (br s, 18H, $H_{pivalate}$), 4.50 (br s, 18H, $H_{pivalate}$), 5.53 (br s, 18H, $H_{pivalate}$), 11.25 (br s, 18H, $H_{pivalate}$).

[2]rotaxane 4b

Compound **4b** was prepared by an analogous procedure to **4a** but using $[Ni_2(OH_2)(O_2CCMe_3)_4(HO_2CCMe_3)_4]$ as the source of divalent metal. Yield: 5.62 g (92.1%, calculated from $CrF_3.4H_2O$ used). Elemental analysis, calcd. (%) for $C_{102}Cr_7F_8H_{190}N_3NiO_{34}$: Cr 14.12, Ni 2.28, C 47.53, H 7.43, N 1.63; found (%): Cr

13.71, Ni 2.34, C 47.42, H 7.67, N 1.57. ES-MS (sample dissolved in Et_2O, run in MeOH): *m/z* = 2599 $[M+Na]^+$ (100%). X-Ray quality crystals were obtained from crystallization of **4b** from a saturated solution in acetone.

[2]rotaxane 4c

Compound **4c** was prepared by an analogous procedure to **4a** but using $Fe(O_2CCH)_2{\cdot}2H_2O$ as the source of divalent metal. The reaction was conducted under Argon and the green product was dissolved in pentane instead of diethyl ether.

Yield: 2.36 g (41.6%, calculated from $Fe(O_2CCH)_2{\cdot}2H_2O$ used). Elemental analysis, calcd. (%) for $C_{102}H_{190}Cr_7F_8FeN_3O_{34}$: Cr 14.14, Fe 2.17, C 47.58, H 7.44, N 1.63; found (%): Cr 13.76, Fe 2.05, C 47.71, H 7.42, N 1.48. ES-MS (sample dissolved in Et_2O, run in MeOH): *m/z* = 2597 $[M+Na]^+$ (100%). X-Ray quality crystals were formed by crystallization of **4c** from a saturated solution in acetone under an inert atmosphere. ^{1}H NMR (300 MHz, 293 K, $CDCl_3$): δ = -44.70 (s, NH2+), -21.10 (s, 2H, H_b), -15.95 (s, 2H, H_b), -11.70 (br s, 2H, H_c), -9.63 (br s, 2H, H_c), -8.59 (br s, 4H, H_a), -5.13 (s, 2H, H_d), -3.76 (s, 2H, H_d), -3.14 (s, 2H, H_e), -2.23 (s, 2H, H_e), -1.37 (s, 2H, H_f), -1.17 (s, 2H, H_f), -0.30 (br s, 18H, $H_{pivalate}$), 0.33 (br s, 18H, $COC(C\underline{\boldsymbol{H}}_3)_3$), 0.75 (s, 18H, H_h), 0.87 (br s, 18H, $H_{pivalate}$), 1.18 (s, 2H, $CH_2N\underline{\boldsymbol{H}}CO$), 1.31 (br s, 18H, $H_{pivalate}$), 1.79 (br s, 18H, $H_{pivalate}$), 1.92 (br s, 18H, $H_{pivalate}$), 6.29 (br s, 18H, $H_{pivalate}$), 9.06 (br s, 18H, $H_{pivalate}$).

[2]rotaxane 4d

Compound **4d** was prepared by an analogous procedure to **4a** but by using $MnCO_3{\cdot}2H_2O$ as the source of divalent metal. Yield: 4.96 g (81.4% calculated from $CrF_3.4H_2O$ used). Elemental analysis, calcd. (%) for $C_{102}H_{190}Cr_7F_8Mn_1N_3O_{34}$: Cr

14.14, Mn 2.13, C 47.60, H 7.44, N 1.63; found (%): Cr 14.23, Mn 2.10, C 47.76, H 7.59, N 1.55. ES-MS (sample dissolved in Et_2O, run in MeOH): *m/z* = 2595 $[M+Na]^+$ (100%). X-Ray quality crystals were formed from crystallization of **4d** from a saturated solution in acetone.

[2]rotaxane 4e

Compound **4e** was prepared by an analogous procedure to **4a** but by using $CuCO_3{\cdot}Cu(OH)_2$ as the source of divalent metal. Yield: 3.9 g (63.8% calculated from $CrF_3.4H_2O$ used). Elemental analysis, calcd. (%) for $C_{102}H_{190}Cr_7CuF_8N_3O_{34}$: Cr 14.10, Cu 2.46, C 47.45, H 7.42, N 1.63; found (%): Cr 14.52, Cu 2.41, C 47.33, H 7.89, N 1.59. ES-MS (sample dissolved in Et_2O, run in MeOH): *m/z* = 2604 $[M+Na]^+$ (100%). X-Ray quality crystals were formed from crystallization of **4e** from a saturated solution in acetone.

[2]rotaxane 4f

Compound **4f** was prepared by an analogous procedure to that for **4a** but $[ZnCO_3]_2{\cdot}[Zn(OH)_2]_3$ was used as the source of the divalent metal, and was added at the start of the reaction. The total time of heating was for 64 h. Yield 4.56 g, (74.5% based on available Cr). Elemental analysis calcd (%) for $C_{102}H_{190}Cr_7F_8N_3O_{34}Zn_1$: Cr 14.09, Zn 2.53, C 47.41, H 7.41, N 1.63 ; found (%): Cr 13.65, Zn 2.36, C 47.17, H 7.69, N 1.55. ES-MS (sample dissolved in Et_2O, run in MeOH): + 2605 $[M + Na]^+$ (100%); X-ray quality crystals were formed from crystallization of **3** from a saturated solution in acetone.

[2]rotaxane 4g

Compound **4g** was prepared by an analogous procedure to that for **4** but by using $CdCO_3$ **(**0.5 g, 2.9 mmol and 0.3g, 1.74 mmol). Yield 2.55 g (41% based on available Cr). Elemental analysis calcd (%) for $C_{102}H_{190}Cd_1Cr_7F_8N_3O_{34}$: Cr 13.83, Cd 4.27, C 46.56, H 7.28, N 1.60 ; found (%): Cr 13.82, Cd 4.26, C 46.56, H 7.30, N 1.56. ES-MS (sample dissolved in Et_2O, run in MeOH): + 2654 $[M + Na]^+$ (100%); X-ray quality crystals were formed from crystallization of **5** from a saturated solution in acetone.

2.3 Synthesis of molecular shuttle 7

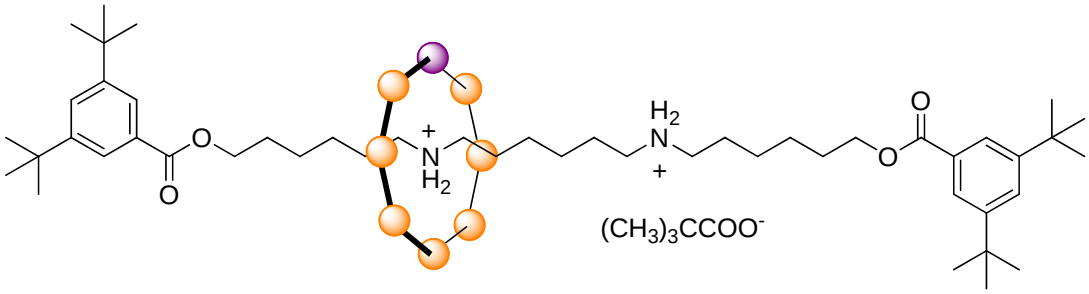

Pivalic acid (280 mg, 2.741 mmol), **6** (50 mg, 0.067 mmol), $CrF_3.4H_2O$ (72 mg, 0.398 mmol), $[Co_2(OH_2)(O_2CCMe_3)_4(HO_2CCMe_3)_4]$ (32 mg, 0.034 mmol), and $NEt_4^+Cl^-$ (8.8 mg, 0.053 mmol) were heated at 140 ºC for 16 h with stirring in a glass tube under nitrogen. Then the mixture was cooled to room temperature and CH_3CN (5 mL) was added while stirring. The product was filtered, washed with CH_3CN, dried in air, and the resulting green solid dissolved in Et_2O (20 mL). Volatile components were removed under reduced pressure. Flash chromatography (hexane:EtOAc 9:1 then 1:1) afforded **7** as a green crystalline solid (61 mg). Yield: 36% (calculated from $CrF_3.4H_2O$ used). LRESI-MS: *m/z* = 2965.1 $[M+Na]^+$ (calcd. for

$C_{128}H_{225}CoCr_7F_8N_2NaO_{36}$, 2964.1). X-Ray quality crystals were obtained from the crystallization of **7** from a mixture of Et_2O/ CH_3CN.

d_{144}-**7** (deuterated analogue of molecular shuttle **7**) was obtained following a similar procedure to that used for the preparation of **7** but using d_9-pivalic acid and $[Co_2(OH_2)(O_2CC(CD_3)_3)_4(HO_2CC(CD_3)_3)_4]$ in place of pivalic acid and $[Co_2(OH_2)(O_2CCMe_3)_4(HO_2CCMe_3)_4]$ respectively.

^{1}H NMR (500 MHz, 300 K, $CDCl_3$): δ = -44.68 to -34.63 (4 br s, 4H, $H_{b+b*'+k*+k*'}$), -26.00 to -21.00 (br m, 4H, $H_{a*+a*'+j*+j*'}$), -12.52 to -7.92 (8 br s, 8H, $H_{c*+c*'+d*+d*'+l+l'+l*+l*'}$), -3.84 to -1.61 (4 br s, 4H, $H_{e+e*'+k+k'}$), -0.05 to 1.28 (m, 50H, $H_{a+b+c+d+e+j+f*+i+i*}$), 3.79 (s, 2H, H_f), 6.27 (s, 2H, H_{g*}), 7.08 (s, 1H, H_{h*}), 7.49 (s, 1H, H_h), 7.60 (s, 2H, H_g).

3. X-Ray Crystallography Data

3.1 X-Ray Crystallographic Data and Intercomponent Binding Motif for [2]Rotaxanes 2a-e

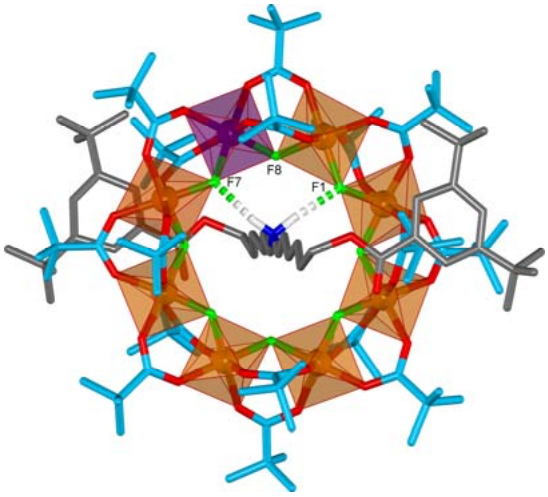

Figure S1: The X-ray crystal structure of [2]rotaxane **2a**[4a]
Carbon atoms of the thread are shown in grey and of the pivalate groups in light blue, oxygen atoms red, nitrogen dark blue, fluorine green, cobalt purple, chromium orange. Hydrogen bond lengths [Å] and N-H-F angles [°]: NH1···F1 = 2.03, NH2···F7 = 2.01 (shown by dashed cylinders in the graphic), NH1···F8 = 2.38, NH2···F8 = 2.56, N-H1-F1 = 168.9, N-H2-F7 = 168.2, N-H1-F8 = 114.2, N-H2-F8 = 101.7.

Chirality of [2]rotaxane 2a

[2]Rotaxane **2a** is intrinsically chiral since the one Co(II) ion must have either a (Δ)- or (Λ)-arrangement of the ligands (nomenclature introduced in S. Herrero, M. A. Usón, *Dalton Trans*. 4993–4998 (2008)) in its octahedral coordination sphere (Figure S2). Both enantiomers are present (in equal amounts) in the crystal.

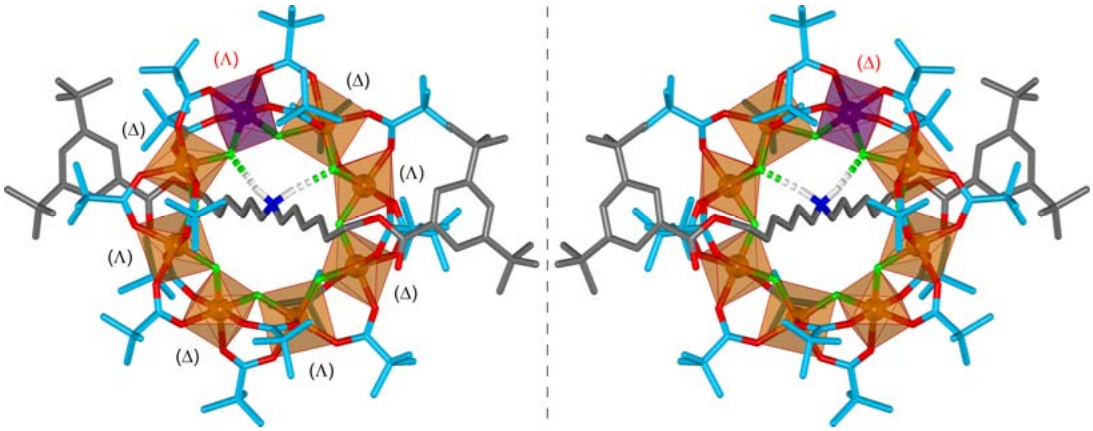

Figure S1bis. The two enantiomers of [2]rotaxane **2a** present in the crystal.

Table S1: Crystal data and structure refinement for [2]rotaxane 2a.[d]

Formula	$C_{122}H_{212}CoCr_7F_8NO_{36}$
M	2843.86
Crystal system	monoclinic
Space group	$P2_1/n$
a/Å	16.8901(2)
b/Å	27.5880(4)
c/Å	36.4428(5)
β/°	102.3930(10)
U/Å^3	16585.3(4)
T /K	150(2)
Z	4
ρ/g cm^{-1}	1.139
Shape and color	Green plate
size (mm)	0.25 x 0.25 x 0.2
λ/ Å	0.71073
μ/mm^{-1}	0.608
Unique data	17704
Absorption correction	multi-scan[a]
transmission max/min	0.8881/0.8629
unique data [$F_o > 4\sigma F_o$)]	8509
parameters/restraints	1469/4171
*R*1, *wR*2[b]	0.1125, 0.3132
weighting scheme[c] [w^{-1}]	$\sigma^2(F_o^2)+(0.1000P)^2+110.0000P]$
goodness of fit	1.058
Largest diff. peak/hole [e Å^{-3}]	0.669/-0.41

[a] R. H. Blessing, *Acta Cryst*. **1995**, *A51*, 33-38.

[b] *R*1 based on observed data, *wR*2 on all unique data.

[c] $P = 1/3[\max(F_o^2,0) + 2F_c]$

[d] CCDC 705132

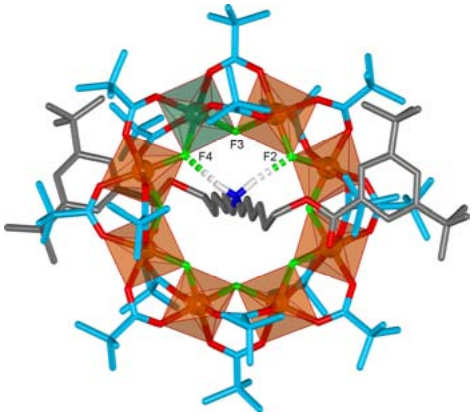

Figure S2: The X-ray crystal structure of [2]rotaxane **2b**
Carbon atoms of the thread are shown in grey and of the pivalate groups in light blue, oxygen atoms red, nitrogen dark blue, fluorine green, nickel sea green, chromium orange. Hydrogen bond lengths [Å] and N-H-F angles [°]: NH1···F4 = 2.00, NH2···F2 = 2.02 (shown by dashed cylinders in the graphic), NH1···F3 = 2.58, NH2···F3 = 2.38, N-H1-F4 = 167.9, N-H2-F2 = 167.7, N-H1-F3 = 100.8, N-H2-F3 = 115.1.

Table S2: Crystal data and structure refinement for [2]rotaxane 2b.[a]

Formula	$C_{122}H_{212}Cr_7F_8NNiO_{36}$
M	2843.63
Crystal system	monoclinic
Space group	$P2_1/n$
a/Å	16.8712(3)
b/Å	27.5463(4)
c/Å	36.4760(7)
β/°	102.2540(10)
U/Å^3	16565.65(5)
T /K	150(2)
Z	4
ρ/g cm^{-1}	1.137
size (mm)	0.25 × 0.14 × 0.08
μ/mm^{-1}	0.574
Unique data	19488
parameters/restraints	1576/112
Final R indexes	R_1 = 0.1074, wR_2 = 0.265
goodness of fit	1.18
Largest diff. peak/hole [e Å^{-3}]	0.738/-0.505

[a] CCDC xxxxxx

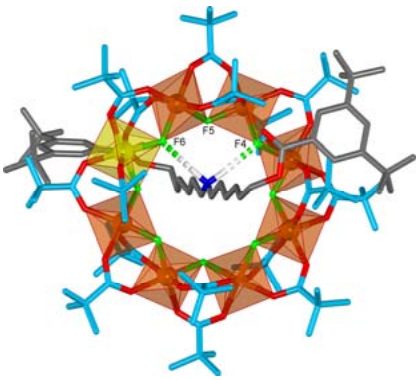

Figure S3: The X-ray crystal structure of [2]rotaxane **2d**
Carbon atoms of the thread are shown in grey and of the pivalate groups in light blue, oxygen atoms red, nitrogen dark blue, fluorine green, manganese yellow, chromium orange. Hydrogen bond lengths [Å] and N-H-F angles [°]: NH1···F4 = 2.13, NH2···F6 = 2.11 (shown by dashed cylinders in the graphic), NH1···F5 = 2.56, NH2···F5 = 2.53, N-H1-F4 = 169.7, N-H2-F6 = 171.6, N-H1-F5 = 108.0, N-H2-F5 = 110.5.

Table S3: Crystal data and structure refinement for [2]rotaxane 2d.[a]

Formula	$C_{122}H_{212}Cr_7F_8MnNO_{36}$
M	2839.87
Crystal system	monoclinic
Space group	$P2_1/n$
a/Å	18.7556(7)
b/Å	29.0775(11)
c/Å	28.6023(14)
β/°	100.790(2)
U/Å^3	15322.9(11)
T /K	100(2)
Z	4
ρ/g cm^{-1}	1.231
size (mm)	0.25 × 0.18 × 0.07
μ/mm^{-1}	0.632
Unique data	14235
parameters/restraints	1576/2670
Final R indexes	R_1 = 0.1071, wR_2 = 0.2691
goodness of fit	1.107
Largest diff. peak/hole [e Å^{-3}]	0.58/-0.358

[a] CCDC xxxxxx

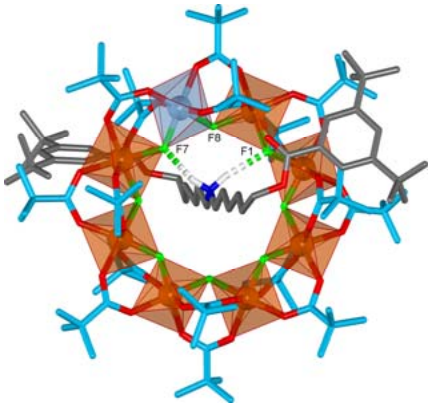

Figure S4: The X-ray crystal structure of [2]rotaxane **2e**
Carbon atoms of the thread are shown in grey and of the pivalate groups in light blue, oxygen atoms red, nitrogen dark blue, fluorine green, copper pale blue, chromium orange. Hydrogen bond lengths [Å] and N-H-F angles [°]: NH1···F7 = 1.95, NH2···F1 = 2.18 (shown by dashed cylinders in the graphic), NH1···F8 = 2.64, NH2···F8 = 2.33, N-H1-F7 = 161.0, N-H2-F1 = 165.5, N-H1-F8 = 97.0, N-H2-F8 = 119.6.

Table S4: Crystal data and structure refinement for [2]rotaxane 2e.[a]

Formula	$C_{122}H_{212}Cr_7CuF_8NO_{36}$
M	2848.47
Crystal system	monoclinic
Space group	$P2_1/n$
a/Å	18.7450(11)
b/Å	29.0923(13)
c/Å	28.5250(12)
β/°	100.458(5)
U/Å^3	15297.3(13)
T /K	100(2)
Z	4
ρ/g cm^{-1}	1.237
size (mm)	0.30 × 0.25 × 0.10
μ/mm^{-1}	0.690
Unique data	15983
parameters/restraints	1636/931
Final R indexes	R_1 = 0.0778, wR_2 = 0.2358
goodness of fit	0.978
Largest diff. peak/hole [e Å^{-3}]	1.1270/-0.963

[a] CCDC xxxxxx

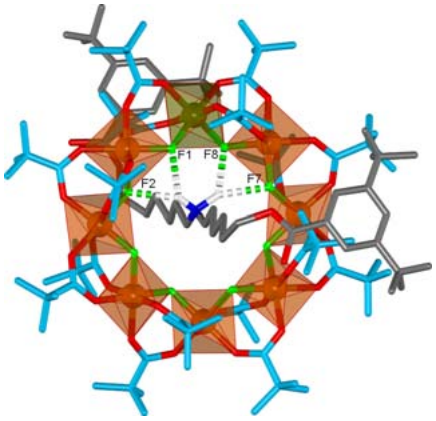

Figure S5: The X-ray crystal structure of pseudo[2]rotaxane **2f**
Carbon atoms of the thread are shown in grey and of the pivalate groups in light blue, oxygen atoms red, nitrogen dark blue, fluorine green, iron dark yellow, chromium orange. Hydrogen bond lengths [Å] and N-H-F angles [°]: NH1···F7 = 2.20, NH1···F8 = 2.14, NH2···F1 = 2.23, NH2···F2 = 2.19, N-H1-F1 = 153.0, N-H1-F8 = 131.2, N-H2-F1 = 135.8, N-H2-F2 = 148.9.

Table S5: Crystal data and structure refinement for pseudo[2]rotaxane 2f.[a]

Formula	$C_{122}H_{212}Cr_7F_8FeNO_{36}$
M	2840.78
Crystal system	Orthorhombic
Space group	Pbca
a/Å	29.8280(9)
b/Å	27.8513(6)
c/Å	32.3305(10)
β/°	90
U/Å^3	26858.5(13)
T /K	150(2)
Z	8
ρ/g cm^{-1}	1.298
size (mm)	0.3 × 0.25 × 0.12
μ/mm^{-1}	0.729
Unique data	12453
parameters/restraints	1422/973
Final R indexes	R_1 = 0.1114, wR_2 = 0.244
goodness of fit	1.228
Largest diff. peak/hole [e Å^{-3}]	0.472/-0.675

[a] CCDC xxxxxx

3.2 X-Ray Crystallographic Data and Intercomponent Binding Motif for [2]Rotaxanes 4a-g

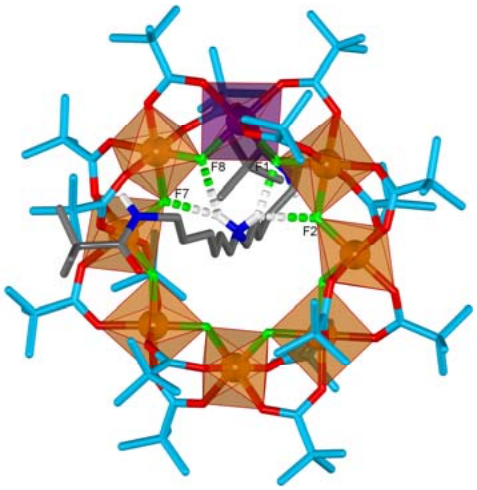

Figure S6: The X-ray crystal structure of [2]rotaxane **4a**
Carbon atoms of the thread are shown in grey and of the pivalate groups in light blue, oxygen atoms red, nitrogen dark blue, fluorine green, cobalt purple, chromium orange. Hydrogen bond lengths [Å] and N-H-F angles [°]: NH1···F1 = 2.08, NH1···F2 = 2.45, NH2···F7 = 2.23, NH2···F8 = 2.22, N-H1-F1 = 145.6, N-H1-F2 = 141.0, N-H2-F7 = 150.0, N-H2-F8 = 135.3.

Table S6: Crystal data and structure refinement for [2]rotaxane 4a.[a]

Formula	$C_{108}H_{202}CoCr_7F_8N_3O_{36.5}$
M	2701.66
Crystal system	monoclinic
Space group	$P2_1/n$
a/Å	16.5136(5)
b/Å	31.3861(7)
c/Å	28.4164(9)
β/°	94.6221(10)
U/Å^3	14680.3(7)
T /K	100(2)
Z	4
ρ/g cm^{-1}	1.222
size (mm)	0.25 × 0.18 × 0.08
μ/mm^{-1}	0.684
Unique data	13440
parameters/restraints	1476/2518
Final R indexes	R_1 = 0.1071, wR_2 = 0.2772
goodness of fit	1.133
Largest diff. peak/hole [e Å^{-3}]	0.836/-0.45

[a] CCDC xxxxxx

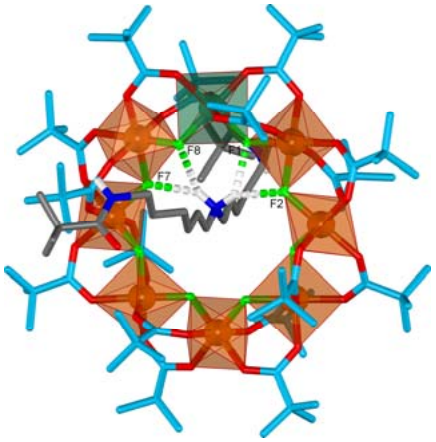

Figure S7: The X-ray crystal structure of [2]rotaxane **4b**
Carbon atoms of the thread are shown in grey and of the pivalate groups in light blue, oxygen atoms red, nitrogen dark blue, fluorine green, nickel sea green, chromium orange. Hydrogen bond lengths [Å] and N-H-F angles [°]: NH1···F7 = 2.32, NH1···F8 = 2.10, NH2···F1 = 2.10, NH2···F2 = 2.32, N-H1-F7 = 141.9, N-H1-F8 = 142.3, N-H2-F1 = 135.7, N-H2-F2 = 148.6.

Table S7: Crystal data and structure refinement for [2]rotaxane 4b.[a]

Formula	$C_{107}H_{203.25}Cr_7F_8N_3NiO_{37.25}$
M	2702.69
Crystal system	monoclinic
Space group	$P2_1/n$
a/Å	16.4959(8)
b/Å	31.4557(15)
c/Å	28.2556(13)
β/°	94.122(3)
U/Å^3	14623.6(12)
T /K	90(2)
Z	4
ρ/g cm^{-1}	1.228
size (mm)	0.4 × 0.22 × 0.1
μ/mm^{-1}	0.702
Unique data	12047
parameters/restraints	1512/2854
Final R indexes	R_1 = 0.0843, wR_2 = 0.2089
goodness of fit	1.127
Largest diff. peak/hole [e Å^{-3}]	1.075/-0.488

[a] CCDC xxxxxx

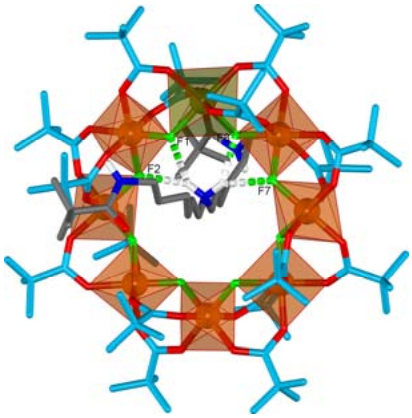

Figure S8: The X-ray crystal structure of [2]rotaxane **4c**
Carbon atoms of the thread are shown in grey and of the pivalate groups in light blue, oxygen atoms red, nitrogen dark blue, fluorine green, iron dark yellow, chromium orange. Hydrogen bond lengths [Å] and N-H-F angles [°]: NH1···F7 = 2.28, NH1···F8 = 2.16, NH2···F1 = 2.12, NH2···F2 = 2.40, N-H1-F7 = 145.5, N-H1-F8 = 139.6, N-H2-F1 = 141.1, N-H2-F2 = 144.9.

Table S8: Crystal data and structure refinement for [2]rotaxane 4c.[a]

Formula	$C_{105}H_{196}Cr_7F_8FeN_3O_{38}$
M	2680.51
Crystal system	monoclinic
Space group	$P2_1/n$
a/Å	16.5354(4)
b/Å	31.3895(6)
c/Å	28.3451(7)
β/°	94.2540(10)
U/Å^3	14671.6(6)
T /K	100(2)
Z	4
ρ/g cm^{-1}	1.213
size (mm)	0.22 × 0.22 × 0.07
μ/mm^{-1}	0.67
Unique data	13278
parameters/restraints	1481/2528
Final R indexes	R_1 = 0.1107, wR_2 = 0.2862
goodness of fit	1.244
Largest diff. peak/hole [e Å^{-3}]	0.77/-0.426

[a] CCDC xxxxxx

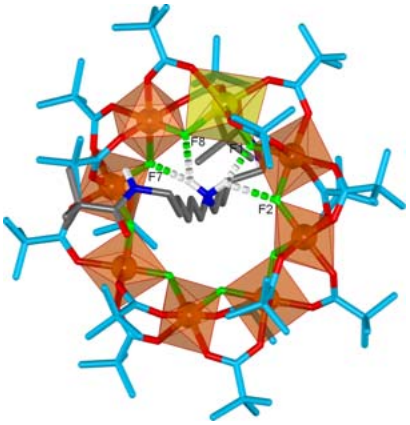

Figure S9: The X-ray crystal structure of [2]rotaxane **4d**
Carbon atoms of the thread are shown in grey and of the pivalate groups in light blue, oxygen atoms red, nitrogen dark blue, fluorine green, manganese yellow, chromium orange. Hydrogen bond lengths [Å] and N-H-F angles [°]: NH1···F7 = 2.07, NH1···F8 = 2.21, NH2···F1 = 1.93, NH2···F2 = 2.59, N-H1-F7 = 156.0, N-H1-F8 = 124.8, N-H2-F1 = 160.4, N-H2-F2 = 128.5.

Table S9: Crystal data and structure refinement for [2]rotaxane 4d.[a]

Formula	$C_{110.5}H_{207.5}Cr_7F_8MnN_3O_{37}$
M	2741.23
Crystal system	monoclinic
Space group	$P2_1/n$
a/Å	16.4713(2)
b/Å	31.6375(4)
c/Å	28.1919(5)
β/°	94.5400(10)
U/Å^3	14645.0(4)
T /K	100(2)
Z	4
ρ/g cm^{-1}	1.243
size (mm)	0.4 × 0.22 × 0.1
μ/mm^{-1}	0.66
Unique data	17559
parameters/restraints	1466/2553
Final R indexes	R_1 = 0.0854, wR_2 = 0.2346
goodness of fit	1.007
Largest diff. peak/hole [e Å^{-3}]	0.792/-0.462

[a] CCDC xxxxxx

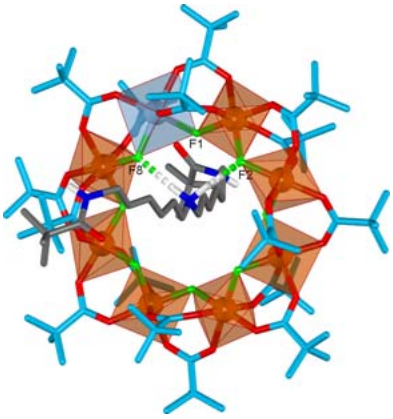

Figure S10: The X-ray crystal structure of [2]rotaxane **4e**
Carbon atoms of the thread are shown in grey and of the pivalate groups in light blue, oxygen atoms red, nitrogen dark blue, fluorine green, copper pale blue, chromium orange. Hydrogen bond lengths [Å] and N-H-F angles [°]: NH1···F2 = 2.13, NH2···F8 = 2.01 (shown by dashed cylinders in the graphic), NH1···F1 = 2.40, NH2···F1 = 2.56, N-H1-F2 = 167.2, N-H2-F8 = 161.5, N-H1-F1 = 114.9, N-H2-F1 = 103.0.

Table S10: Crystal data and structure refinement for [2]rotaxane 4e.[a]

Formula	$C_{106.5}H_{200.5}Cr_7CuF_8N_3O_{36.5}$
M	2686.74
Crystal system	monoclinic
Space group	$P2_1/n$
a/Å	16.8601(2)
b/Å	32.0521(4)
c/Å	28.4030(5)
β/°	94.2490(10)
U/Å^3	15306.7(4)
T /K	100(2)
Z	4
ρ/g cm^{-1}	1.166
size (mm)	0.25 × 0.20 × 0.10
μ/mm^{-1}	0.686
Unique data	13942
parameters/restraints	1450/2487
Final R indexes	R_1 = 0.091, wR_2 = 0.2423
goodness of fit	1.062
Largest diff. peak/hole [e Å^{-3}]	0.603/-0.528

[a] CCDC xxxxxx

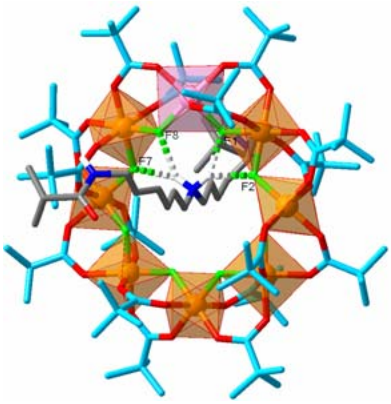

Figure S11: The X-ray crystal structure of [2]rotaxane **4f**
Carbon atoms of the thread are shown in grey and of the pivalate groups in light blue, oxygen atoms red, nitrogen dark blue, fluorine green, zinc pink, chromium orange. Hydrogen bond lengths [Å] and N-H-F angles [°]:NH1···F1 = 2.02Å, NH1···F2 = 2.43Å, NH2···F7 = 2.19Å, NH2···F8 = 2.20Å, N-H1-F1 = 146.6°, N-H1-F2 = 139.3°, N-H2-F7 = 150.6°, N-H2-F8 = 133.4°.

Table S11: Crystal data and structure refinement for [2]rotaxane 4f.[a]

Formula	$C_{107.25}H_{200.5}Cr_7F_8N_3O_{36.5}Zn$
M	2697.58
Crystal system	monoclinic
Space group	$P2_1/n$
a/Å	16.5125(2)
b/Å	31.3755(4)
c/Å	28.3801(4)
β/°	94.6440(10)
U/Å^3	14655.1(3)
T /K	100(2)
Z	4
ρ/g cm^{-1}	1.223
size (mm)	0.40 × 0.22 × 0.10
μ/mm^{-1}	0.735
Unique data	15600
parameters/restraints	1453/2535
Final R indexes	R_1 = 0.0926, wR_2 = 0.2306
goodness of fit	1.096
Largest diff. peak/hole [e Å^{-3}]	0.828/-0.637

[a] CCDC xxxxxx

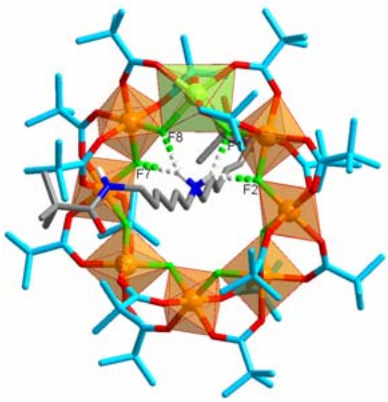

Figure S12: The X-ray crystal structure of [2]rotaxane **4g**
Carbon atoms of the thread are shown in grey and of the pivalate groups in light blue, oxygen atoms red, nitrogen dark blue, fluorine green, cadmium pale green, chromium orange. Hydrogen bond lengths [Å] and N-H-F angles [°]:NH1···F1 = 2.05Å, NH1···F2 = 2.39Å, NH2···F7 = 2.35Å, NH2···F8 = 2.08Å, N-H1-F1 = 144.0°, N-H1-F2 = 142.1°, N-H2-F7 = 143.4°, N-H2-F8 = 141.9°.

Table S12: Crystal data and structure refinement for [2]rotaxane 4g.[a]

Formula	$C_{106.5}H_{199}CdCr_7F_8N_3O_{36}$
M	2726.09
Crystal system	monoclinic
Space group	$P2_1/n$
a/Å	16.8642(2)
b/Å	32.2599(4)
c/Å	28.2099(5)
β/°	93.7900(10)
U/Å^3	15313.7(4)
T /K	100(2)
Z	4
ρ/g cm^{-1}	1.182
size (mm)	0.25 × 0.18 × 0.10
μ/mm^{-1}	0.685
Unique data	14203
parameters/restraints	1441/ 2481
Final R indexes	R_1 = 0.0877, wR_2 = 0.2391
goodness of fit	1.081
Largest diff. peak/hole [e Å^{-3}]	0.748/-0.804

[a] CCDC xxxxxx

3.3 X-Ray Crystallographic Data for molecular shuttle 7

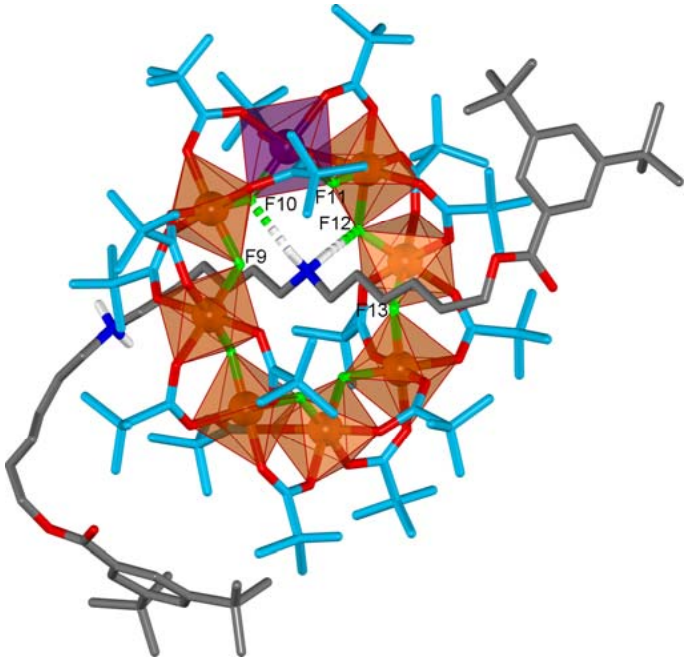

Figure S13: The X-ray crystal structure of molecular shuttle **7**
Carbon atoms of the thread are shown in grey and of the pivalate groups in light blue, oxygen atoms red, nitrogen dark blue, fluorine green, cobalt purple, chromium orange. Hydrogen bond lengths [Å] and N-H-F angles [°]: NH1···F12 = 2.05, NH2···F10 = 2.12 (shown by dashed cylinders in the graphic), NH1···F11 = 2.26, NH1···F13 = 2.93, NH2···F9 = 2.54, NH2···F11 = 2.58, N-H1-F12 = 156.3, N-H2-F10 = 156.3, N-H1-F11 = 120.3, N-H1-F13 = 110.5, N-H2-F9 = 133.0, N-H2-F11 = 96.5.

Table S13: Crystal data and structure refinement for molecular shuttle 7.[a]

Formula	$C_{133}H_{235}CoCr_7F_8N_2O_{38}$
M	3045.16
Crystal system	Orthorhombic
Space group	Pbca
a/Å	70.178(4)
b/Å	31.5931(18)
c/Å	31.206(2)
U/Å^3	69189(8)
T /K	100(2)
Z	16
ρ/g cm^{-1}	1.169
size (mm)	0.20 × 0.20 × 0.10
μ/mm^{-1}	0.588
Unique data	13034
parameters/restraints	1643/10806
Final R indexes	R_1 = 0.1447, wR_2 = 0.4002
goodness of fit	1.261
Largest diff. peak/hole [e Å^{-3}]	1.098/-0.580

[a] CCDC xxxxxx

4. Kinetic Studies

First experiment (Scheme 2a).

A mixture of **2a** (7.6 mg, 2.7 mmol) and its deuterated analogue d_{144}-**2a** (8 mg, 2.7 mmol) was stirred in $C_2D_2Cl_4$ (2 mL) at 60 °C. After one week a sample of the mixture was diluted in CH_3OH and analyzed by mass spectroscopy. Only **2a** and d_{144}-**2a** could be detected by ESI-MS indicating that no exchanges occurred. The mixture was then heated to 140 °C and after 2 days ESI-MS analysis showed that exchanges of pivalate ligands occurred. The 15 mixed species with intermediate masses and having the chemical formula [**1**][$Cr_7CoF_8(O_2C^tBu)_n(d_9$-$O_2C^tBu)_{16-n}$] (with $1 \leq x \leq 15$) were present in the mixture in addition to **2a** (n = 16) and d_{144}-**2a** (n = 0). The analysis also revealed the presence of some products of decomposition.

Second experiment (Scheme 2b).

A mixture of d_{144}-**2a** (6.0 mg, 2.0 mmol) and **4a** (5.1 mg, 2.0 mmol) was stirred in $C_2D_2Cl_4$ (2 mL) at 60 °C. After one week a sample of the mixture was diluted in CH_3OH and analyzed by mass spectroscopy. Only **4a** and d_{144}-**2a** could be detected by ESI-MS indicating that no exchanges (neither pivalate ligands nor whole ring) occurred. The mixture was then heated to 100 °C. After 2 days ESI-MS analysis revealed that pivalate exchanges occurred (more slowly than in the first experiment) as a few mixed species were detected. However neither **2a** nor d_{144}-**4a**, products which would result from entire ring exchange, were observed.

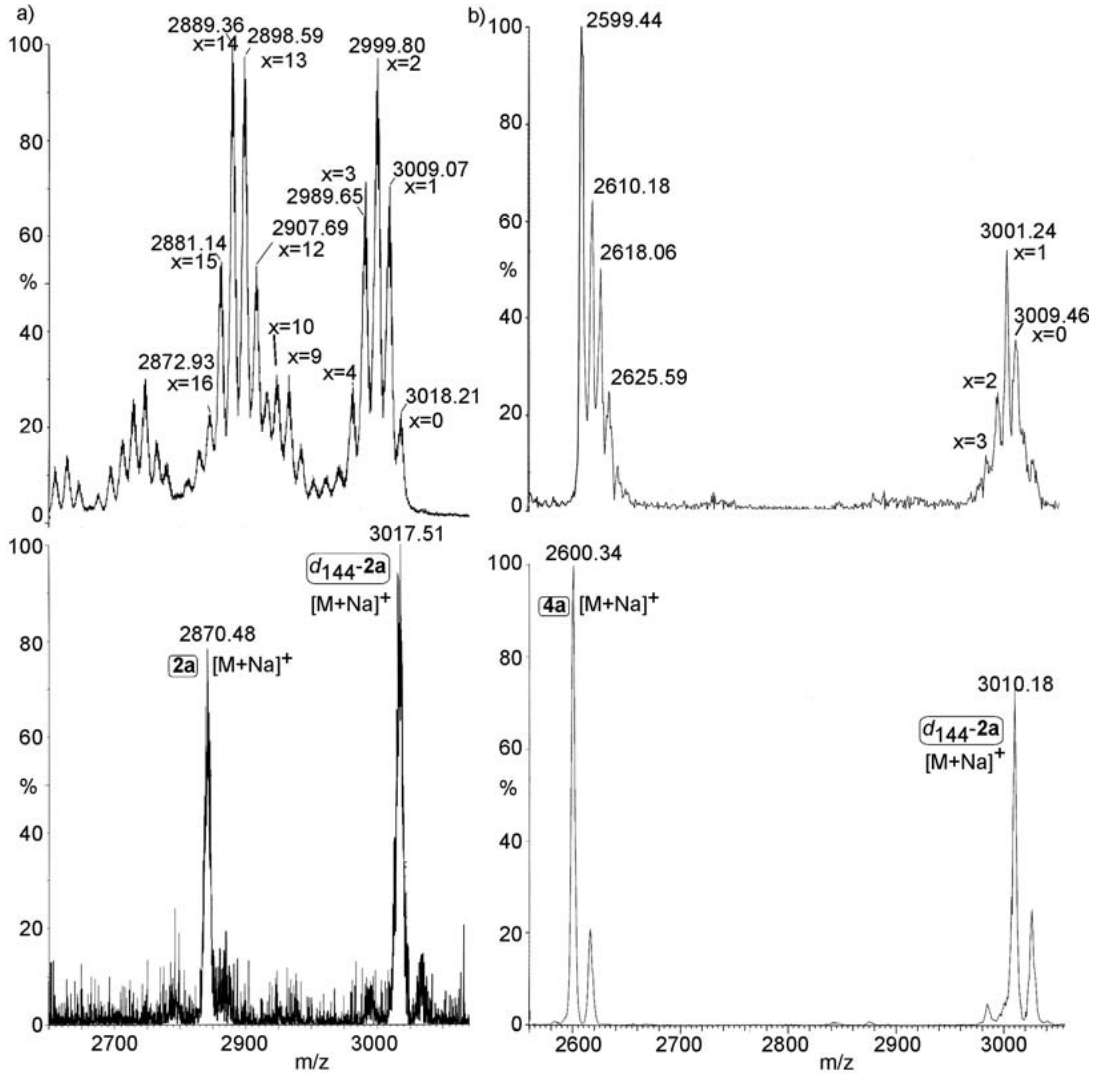

Figure S15: Partial ESI mass spectra obtained in the pivalate-exchange experiments. (a) [2]rotaxanes **2a** and d_{144}-**2a**. Bottom: after 7 days at 60 ºC. Top: after 2 days at 140 ºC, showing the number of deuterated pivalate anions (x) exchanged in the process by the deuterated derivative d_{144}-**2a**. (b) [2]rotaxanes d_{144}-**2a** and **4a**. Bottom: after 7 days at 60 ºC. Top: after 2 days at 100 ºC, showing the number of deuterated pivalate anions (x) exchanged in the process by the deuterated derivative d_{144}-**2a**.

5. Yield Optimization

All experiments were conducted following the general procedure described below. Four series of experiments were realized using four different additives (diethylamine, triethylamine, chloromethyl triethylammonium chloride, and tetraethylammonium chloride). For each series, eight experiments were conducted using successively: 0.05, 0.1, 0.2, 0.3, 0.5, 0.75, and 1 equiv of the corresponding additive.

General procedure.

Thread **1** (1 equiv) and the additive were mixed in pivalic acid and heated at 140°C for 15 min under nitrogen. Then $CrF_3.4H_2O$ and $[Co_2(OH_2)(O_2CCMe_3)_4(HO_2CCMe_3)_4]$ were added to the mixture. After 12 h the flask was cooled to room temperature and CH_3CN was added. The green product was filtered, washed with CH_3CN, dried in air, dissolved in Et_2O, and concentrated under reduced pressure. Flash chromatography (100:2 petroleum ether:EtOAc, then a gradient elution up to 100:6 petroleum ether:EtOAc) afforded **2a** as a green crystalline solid. The various yields obtained were calculated based on $CrF_3.4H_2O$ used. Each experiment was repeated at least twice.

6. ^{1}H NMR spectra

6.1 ^{1}H NMR spectrum of **4a** (300 MHz, $CDCl_3$, 293 K)

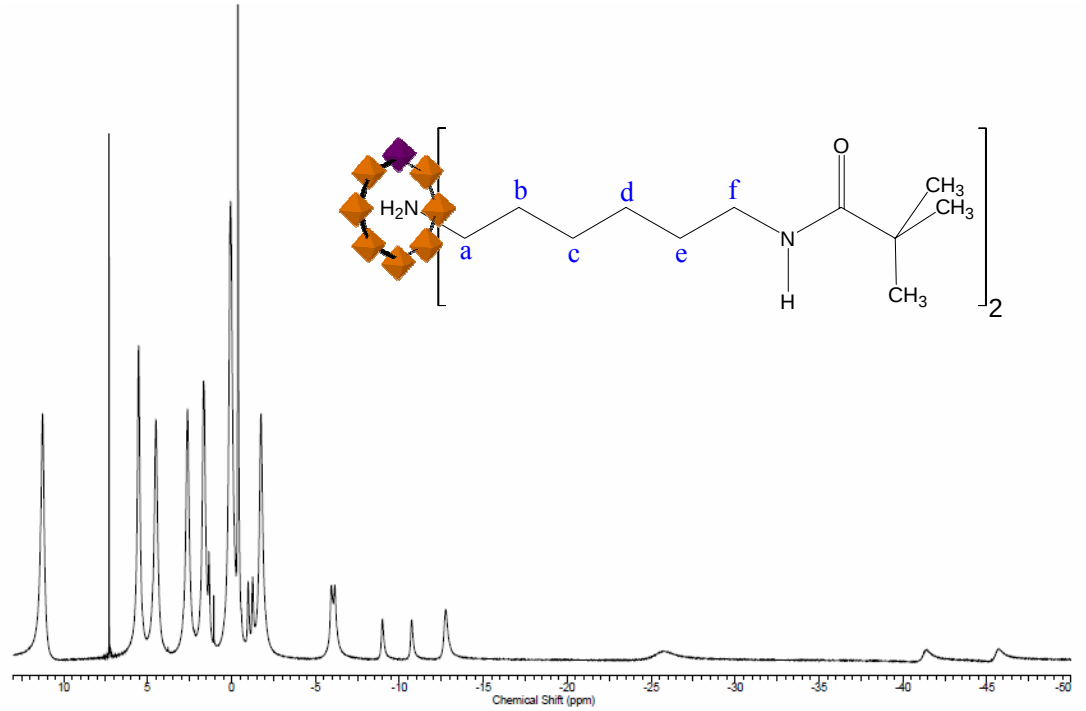

(ppm)	proton
-98.10	$N\underline{\boldsymbol{H}}_2^+$
-45.64	b
-41.35	b'
-25.64	a
-12.73	c
-10.73	d
-8.99	d'
-6.15	e
-5.94	e'
-1.75	pivalate
-1.26	f
-0.99	f'
-0.38	$COC(C\underline{\boldsymbol{H}}_3)_3$
0.05	pivalate x 2
1.34	$CH_2N\underline{\boldsymbol{H}}CO$
1.65	pivalate
2.62	pivalate
4.50	pivalate
5.53	pivalate
11.25	pivalate

6.2 ^{1}H NMR spectrum of **4c** (300 MHz, $CDCl_3$, 293 K)

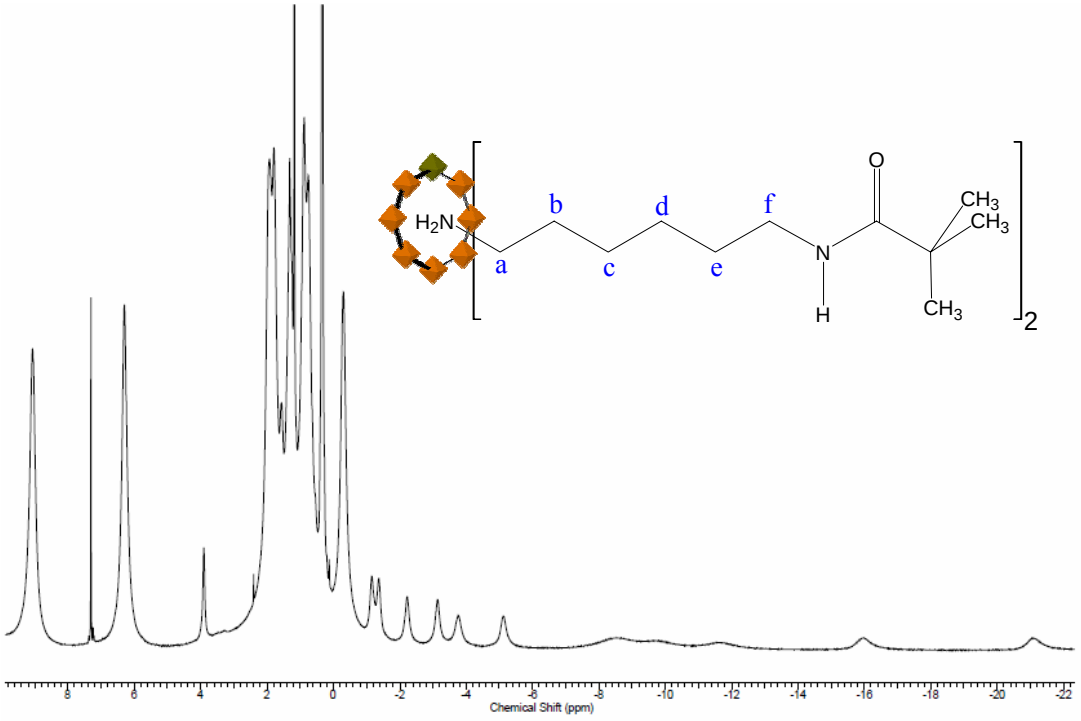

(ppm)	proton
-44.70	$N\underline{\boldsymbol{H}}_2^+$
-21.10	b
-15.95	b'
-11.70	c
-9.63	c'
-8.59	a
-5.13	d
-3.76	d'
-3.14	e
-2.23	e'
-1.37	f
-1.17	f'
-0.30	pivalate
0.33	$COC(C\underline{\boldsymbol{H}}_3)_3$
0.75	pivalate
0.87	pivalate
1.18	$CH_2N\underline{\boldsymbol{H}}CO$
1.31	pivalate
1.79	pivalate
1.92	pivalate
6.29	pivalate
9.06	pivalate

Chapter Twelve - Summary of conclusions and outlook

Following on from foundation work on the synthesis of purple {Cr7NiEtglu} heterometallic rings published in Reference 161 in 2008, Chapters Six, Seven and Eight show the attempts to develop our understand and control the spin propagation between the effective spin 1/2 systems by systematic variation of the intermolecular bridge. Reference 161 investigated two bridges, namely 4,4'-bipyridine and *trans*-1,2-dipyridylethene, both demonstrating magnetic communication by the generation of spin triplet and singlet, the former observable as a doublet in the EPR Q-band (34 GHz) spectrum at 5 K. Since *J* was small both singlet and triplet would be thermally populated and so the triplet-singlet order was unknown at this point. The Bleaney-Bowers equation[224] predicted ferromagnetic exchange though with a very low degree of certainty whilst a simple spin polarisation model[225] predicted an antiferromagnetic exchange. The true nature of the interaction would be elucidated with later experiments. The authors confirm calculations for bipyridine and dipyridyl ethane of $D = +0.013$ and $+0.009$ cm^{-1} respectively, though relationship between *D* and *J* was still only tentative.

The Appendix, Paper 8x considers an additional three bridging ligands, 4,4'-bi-3,5-dimethylpyrazole, the longer 3,6-dipyridyl-s-tetrazene and the exceptionally short pyrazine. From the results it was immediately apparent that the coupling was not merely a function of the ligand length. Pyrazine did generate a relatively massive *D*, $+0.125$ cm^{-1}, ten times that of bipyridine and the EPR spectrum for dipyridyltetrazine did not reveal an S = 1 state. However bi(dimethylpyrazole), which is a comparable length to bipyridine, also lacked a low lying S = 1 state. The reasoning behind this was probed theoretically. Firstly the effects of spin polarisation in all of the compounds were explored by density functional theory (DFT). These revealed that 1) spin polarisation alternates between adjacent atoms, 2) spin polarisation density falls off fairly rapidly with increasing distance and 3) competing exchange mechanisms around the odd-membered pyrazole rings was causing a

minimisation of spin density at the centre of the ligand. Secondly the degree of pi-orbital overlap between aromatic rings in the bridge was considered. The bipyridine dimer exhibited a small twist angle of 40.6° when compared with bi(dimethylpyrazole), 81.1°. Whilst magnetic communication can in principle be conveyed through sigma bonds it is only appreciable over any distance through conjugated pi-systems. As such this difference in torsion angle could be the cause of the attenuation of exchange in latter's case. Indeed computational experiments performed backed up this theory and suggested a $\cos^2$ relationship between the twist angle and the magnitude of exchange. Which, if either, of these was the principal factor would be investigated in Chapter Seven. As well as EPR, micro-SQUID magnetometry is used to probe the nature of the magnetic exchange. From these results it was possible to determine that there was indeed a good relationship between the ZFS parameter, D, and the isotropic exchange parameter, J namely that $D_{S=1} = 0.1\ J$ (with the convention of a $-2J$ Hamiltonian).

Chapter Six investigates a further six bridges. 1,4-dipyridylbenzene and bis-1,4-(4-pyridylvinyl)benzene were, as expected, too long for spin state mixing and show only broadening of their EPR spectra, no well resolved spin triplet. Four relatives of trans-1,2-dipyridylethane were investigated in 1,2-dipyridylethane, dipyridylacetylene, meso-alpha,beta-bispyridylglycol and 4,4'-azopyridine. The alkane and glycol derivatives, lacking in any conjugation, did not display a spin triplet, as expected. The added electronegativity of the nitrogens in the azo group over the carbons in the ethene promoted exchange slightly ($D = +0.012\ cm^{-1}$) whilst that of the alkyne was slightly diminished ($D = +0.005\ cm^{-1}$).

Chapter Seven seeks to answers the questions raised by exchange attenuation discovered in the measurement of the bi(dimethylpyrazole) linked dimer. Is the lack of interaction observable by EPR a product of lack of pi-orbital overlap between the aromatic rings caused by a severe torsion angle? Or is it a result of deconstructive interference leading to minimisation in spin density bought about the spin alternation rule? In order to answer the first question two new dimers were designed containing the ligands 3,8-phenanthroline, with a twist angle close to zero, and

3,3',5,5'-tetramethyl-4,4'-bipyridine whose steric bulk imposes a twist angle of nearly 90°. The results from EPR tend to support the $\cos^2$ relationship which had been suggested previously, the phenanthroline dimer showing an enhancement to $D = +0.017$ cm^{-1} whilst tetramethylbipyridine showed an attenuation such that no spin triplet could be resolved. A third bridge, 4-(1*H*-pyrazol-4-yl)pyridine, containing a pair of co-planar five- and six-membered rings was used to promote good pi-conjugation so that the effect of deconstructive interference of spin polarisation in odd-membered heterocycles could be studied in isolation. EPR could not distinguish any difference in the magnetic nature of this dimer from that of an isolated {Cr7NiEtglu} ring. Thus both rationales for the attenuation observed in bi(dimethylpyrazole) appear to be corroborated. These results were especially pleasing since they represented significant examples of rational prediction being borne out in empirical observation. We thus have a better understanding of the mechanism of magnetic exchange and more importantly we have shown that we have the knowledge required to tune the interaction towards a magnitude of our liking.

Going forward, these findings should be considered in the design of new bridges with switchable functionality. The ability to change the interaction between adjacent qubits is a key requisite for a QIP system. Prime candidates are molecules whose structural or electronic properties can be altered by the application of an external influence. Global environmental changes such as those of temperature, pH, electrical potential and magnetic field all offer solutions. Perhaps more promising are perturbations which can be applied locally, for example a field or potential applied *via* an AFM tip (giving molecular resolution); or laser pulse for region specific optical or thermal excitation (giving μm scale resolution).

There are other key issues surrounding the implementation of these qubits which have not been mentioned in this thesis. For example, neither manipulation of the magnetic communication nor read-out of the resulting states could be achieved in solution or in a bulk crystal. The best approach under consideration for the creation of a structured array is by the tethering of the molecular rings to a suitable surface.

The aurophilicity of sulfur makes thiol and methyl thiolate functionalisation of the rings one possible route to gold surface binding. The incorporation of polyaromatic appendages such as pyrenyl or fluorenylmethyloxycarbonyl is another interesting proposal, which may promote pi-stacking on surfaces such as graphite, graphene, and carbon nanotubes. It is the wide scope for functionality of the {Cr7NiEtglu} rings without disruption of their magnetic properties which makes these challenges seem surmountable.

In Chapter Ten the synthesis of a range of compounds with the formula [{cation}$Cr_7CoF_8(O_2C\mathit{t}Bu)_{16}$] where {cation} is either an alkyl ammonium or sodium, are described. ^{1}H NMR spectroscopy was used to determine their structure in solution and it was possible to determine the persistence of the guest. During the purification process it was determined that monoalkyl and cyclic ammonium species were labile from their {Cr7Co} host during column chromatography leading [Na{Cr7Co}] species, the sequestered sodium being an impurity in the silica gel. The system seemed somewhat reminiscent of Saalfrank's iron coronates.[42] This led to the investigation of sequestering other alkali metals from solution and also templating rings about them in Chapter Eight. As Saalfrank found, there was a nice complementarity fit between the octametallic 'metallocrown' and the alkali metal ion, Cs^+. Indeed it was found that there was very strong sequestration mechanism for this ion in particular and also that rings could be templated about it. Ions of rubidium showed similar properties but no similar effects could be reproduced with the smaller potassium ions nor the tiny lithium ions. ^{1}H NMR was of great value in probing the stability of the compounds in solution. Perhaps the most impressive use of NMR was in the 'reaction in a test tube' which traced the progress of guest exchange, n-propylammonium for Cs^+, over time. The time scales of such reactions are often conjecture or at best trial-and-error, but by this approach it was found that with a 10× excess of Cs^+, with the NMR tube rotated at 20 Hz and at room temperature the reaction was complete after just 15 minutes. It was also discovered that Cs^+ could be drawn into an organic phase containing the metallocrown from an aqueous solution, a property which suggests it maybe have useful properties as sequestering agent for radioactive ^{137}Cs. There is certainly scope for further research in this area.

Following success in the hosting of alkali metal ions within octametallic rings, attention in Chapter Ten turned to the sequestration of alkaline earth metals. Simple substitution as in Chapter Eight was not successful and so a different approach was used by starting from '{Cr_6} horseshoes'.[226] This method did not result in the desired {M⊂Cr6Ni2} but rather {Cr7M} where M is an alkaline earth metal (Mg, Ca or Sr); the resulting anion being charge balanced by the dialkyl ammonium used to synthesise the {Cr6} horseshoe. The mechanism of this assembly was investigated by introducing divalent metals carboxylates other than that of trimethyl acetate. From mass spectrometry and X-ray crystallography it was found that the integrity of the {Cr6} horseshoe is generally maintained (as long as the corresponding acid of the second carboxylate is not more acidic than trimethyl acetate). The number of metals ions is made up to eight by one divalent metal and one chromium, presumably from the breakdown of another sacrificial horseshoe. The carboxylates are predominantly from the introduced metal salt but can also originate from the sacrificial horseshoe. The results found here add to our understanding of the mechanism of formation for this type of ring, and to the process of self-assembly in general.

As well as small ammonium species, {Cr7M} rings can be grown around much longer ammonium threads with bulky stoppers to create rotaxanes.[159] In Chapter Eleven this concept is investigated further. Synthesis of {Cr7M} about bis(hexamethylene)triamine causes a one-pot 'stoppering-plus-macrocyclization' reaction whereby the ring forms in the normal fashion simultaneous with condensation of the terminal amines with trimethyl acetic acid, to give a bulky amide stopper. This reaction is remarkable considering the complexity evolved from a single reaction and from modest commercially available starting materials. The ^{1}H NMR of [{(tBuC(O)NHC$_6$H$_{12}$)$_2$NH$_2$}Cr$_7$MF$_8$(O$_2$CtBu$_{16}$)] (M = Co^{II}, Fe^{II}), were both studied, demonstrating the applicability of the technique to {Cr7Fe} rings for the first time. Discussed also is the dynamics of a multi-station rotaxane in solution by ^{1}H NMR. These suggested that translation of a {Cr7Co} from one ammonium group (station 1) along a 6-carbon chain to another ammonium group (station 2) took place on a time scale in the order of one second, and that rotation of the ring about a

single station took place much faster than this. The results presented in Chapter 12 demonstrate the means by which elaborate nanoscale architectures may be assembled into a structured array, as would be necessary within a QIP system. They also suggest that if external stimulus can invoke deliberate translation of rings, such rings may be controlled to interact through space in a directed fashion. Such a phenomenon could also be exploited in the creation of a future molecular machine.

Chapter Thirteen - References

[1] K. L. Taft and S. J. Lippard, *Journal of the American Chemical Society*, 1990, **112**, 9629-9630.

[2] N. V. Gerbeleu, Y. T. Struchkov, G. A. Timco, A. S. Batsanov, K. M. Indrichan and G. A. Popovich, *Docklady Akademii Nauk SSSR*, 1990, **313**, 1459-1462.

[3] G. Mezei, C. M. Zaleski and V. L. Pecoraro, *Chemical Reviews*, 2007, **107**, 4933-5003.

[4] J.-R. Li, Z.-H. Li, S.-W. Du and X.-T. Wu, *Polyhedron*, 2005, **24**, 481-485.

[5] T. Konno, T. Aridomi, M. Hattori and M. Hirotsu, *Chemistry Letters*, 2006, **35**, 316-317.

[6] T. Konno, Y. Chikamoto, K. Okamoto, T. Yamaguchi, T. Ito, and M. Hirotsu, *Angewandte Chemie-International Edition*, 2000, **39**, 4098-4101.

[7] C. von Hanisch and S. Stahl, *Angewandte Chemie-International Edition*, 2006, **45**, 2302-2305.

[8] E. C. Sañudo, C. A. Muryn, M. A. Helliwell, G .A. Timco, W. Wernsdorfer and R. E. P. Winpenny, *Chemical Communications*, 2007, 801-803.

[9] T. Konno, M .Usami, A. Toyota, M. Hirotsu and T. Kawamoto, *Chemistry Letters*, 2005, **34**, 1146-1147.

[10] L. Jäger, V. Lorenz, C. Wagner, T. Müller and H.-P. Abicht, *Zeitschrift für Kristallographie*, 2005, **220**, 183-187.

[11] V. G. Kessler, N. Y. Turova and E. P. Turevskaya, *Inorganic Chemistry Communications*, 2002, **5**, 549-551.

[12] A. Onada, Y. Yamada, T. Okamura, M. Doi, H. Yamamoto and N. Ueyama, *Journal of the American Chemical Society*, 2002, **124**, 1052-1054.

[13] J. K. Beattie, T. W. Hambley, J. A. Klepetko, A. F. Master and P. Turner, *Chemical Communications*, 1998, 45-46.

[14] P. L. Jones, K. J. Byrom, J. C. Jeffery, J. A. McCleverty and M. D. Ward, *Chemical Communications*, 1997, 1361-1362.

[15] R. H. Laye, F. K. Larsen, J. Overgaard, C. A. Muryn, E. J. L. McInnes, E. Rentschler, V. Sanchez, S. J. Teat, H. U. Güdel, O. Waldmann, G. A. Timco and R. E. P. Winpenny, *Chemical Communications*, 2005, 1125-1127.

[16] I. M. Atkinson, C. Benelli, M. Murrie, S. Parsons and R. E. P. Winpenny, *Chemical Communications*, 1999, 285-286.

[17] M. Eshel and A. Bino, *Inorganica Chimica Acta*, 2001, **320**, 127-132.

[18] M. Eshel, A. Bino, I. Felner, D. C. Johnston, M. Luban and L. L. Miller, *Inorganic Chemistry*, 2000, **39**, 1376-1380.

[19] N. V. Gerbeleu, Y. T. Struchkov, G. A. Timco, A. S. Batsanov, K. M. Indrichan and G. A. Popovich, *Docklady Akademii Nauk SSSR*, 1990, **313**, 1459-1462.

[20] R. A. Coxall, A. Parkin, S. Parsons, A. A. Smith, G. A. Timco and R. E. P. Winpenny, *Solid State Chemistry*, 2001, **159**, 321-327.

[21] J. Rinck, G. Novitchi, W. V. den Heuvel, L. Ungur, Y. Lan, W. Wernsdorfer, C. E. Anson, L. F. Chibotaru and A. K. Powell, *Angewandte Chemie-International Edition*, 2010, **49**, 7583-7587.

[22] G. A. Timco, A. S. Batsanov, F. K. Larsen, C. A. Muryn, J. Overgaard, S. J. Teat and R. E. P. Winpenny, *Chemical Communications*, 2005, 3649-3651.

[23] G. A. Timco, E. J. L. McInnes, R. G. Pritchard, F. Tuna and R. E. P. Winpenny, *Angewandte Chemie-International Edition*, 2008, **47**, 9681-9684.

[24] F. K. Larsen, J. Overgaard, S. Parsons, E. Rentschler, A. A. Smith, G. A. Timco and R. E. P. Winpenny, *Angewandte Chemie-International Edition*, 2003, **42**, 5978-5981.

[25] A. McRobbie, A. R. Sarwar, S. Yeninas, H. Nowell, M. L. Baker, D. Allan, M. Luban, C. A. Muryn, R. G. Pritchard, R. Prozorov, G. A. Timco, F. Tuna, G. F. S. Whitehead and R. E. P. Winpenny, *Chemical Communications*, 2011, **47**, 6251-6253.

[26] A. Mukherjee, I. Rudra, M. Nethaji, S. Ramasesha and A. R. Chakravarty, *Inorganic Chemistry*, 2003, **42**, 463-468.

[27] G. A. Ardizzoia, M. A. Angaroni, G. La Monica, F. Cariati, M. Moret and N. Masciocchi, *Journal of the Chemical Society, Chemical Communications*, 1990, 1021-1023.

[28] G. Mezei, P. Baran and R. G. Raptis, *Angewandte Chemie*, 2004, **116**, 584-587.

[29] I. Schroter-Schmid and J. Strahle, *Zeitschrift für Naturforschung*, 1990, **45B**, 1537-1542.

[30] K. Geetha, M. Nethaji and A. R. Chakravarty, *Inorganic Chemistry*, 1997, **36**, 6134-6137.

[31] M. S. El Fallah, A. Escuer, R. Vicente, F. Badyine, X. Solans and M. Font-Bardia, *Inorganic Chemistry*, 2004, **43**, 7218-7226.

[32] Q. Yang, K. Tang, H.Liao, Y. Han, Z. Chen and Y. Tang, *Journal of the Chemical Society, Chemical Communications*, 1987, 1076-1077.

[33] Z.-H. Li, S.-W. Du and X.-T. Wu, *Polyhedron*, 2005, **24**, 2988-2993.

[34] D. Schray, G. Abbas, Y. Lan, V. Mereacre, A. Sundt, J. Dreiser, O. Waldmann, G. E. Kostakis, C. E. Anson and A. K. Powell, *Angewandte Chemie-International Edition*, 2010, **49**, 5185-5188.

[35] M. Li, A. M. Ako, Y. Lan, W. Wernsdorfer, G. Buth, C. E. Anson, A. K. Powell, Z. Wang and S. Gao, *Dalton Transactions*, 2010, **39**, 3375-3377.

[36] C. Cañada-Vilalta, T. A. O'Brien, M. Pink, E. R. Davidson and G. Christou, *Inorganic Chemistry*, 2003, **42**, 7819-7829.

[37] H.-C. Zhou and R. H. Holm, *Inorganic Chemistry*, 2003, **42**, 11-21.

[38] J. H. Satcher Jr., M. M. Olmstead, M. W. Droege, S. R. Parkin, B. C. Noll, L. May and A. L. Balch, *Inorganic Chemistry*, 1998, **37**, 6751-6758.

[39] L. F. Jones, A. Batsanov, E. K. Brechin, D. Collison, M. Helliwell, T. Mallah, E. J. L. McInnes and S. Piligkos, *Angewandte Chemie*, 2002, **114**, 4494-4497.

[40] N. V. Gerbeleu, Y. T. Struchkov, G. A. Timco, O. S. Marole and A. S. Batsanov, *Docklady Akademii Nauk SSSR*, 1993, **331**, 184-186.

[41] O. Waldmann, R. Koch, S. Schromm, J. Schulein, P. Muller, I. Bernt, R. W. Saalfrank, F. Hampeland and E. Balthes, *Inorganic Chemistry*, 2001, **40**, 2986-2995.

[42] R. W. Saalfrank, I. Bernt, E. Uller and F. Hampel, *Angewandte Chemie-International Edition in English*, 1997, **36**, 2482-2485.

[43] S. Lin, S.-X.Liu, Z. Chen, B.-Z. Lin and S. Gao, *Inorganic Chemistry*, 2004, **43**, 2222-2224.

[44] T. C. Stamatatos, A. G. Christou, S. Mukherjee, K. M. Poole, C. Lampropoulos, K. A. Abboud, T. A. O'Brien and G. Christou, *Inorganic Chemistry*, 2008, **47**, 9021-9034.

[45] T. Kajiwara, H. Wu, T. Ito, N. Iki and S. Miyano, *Angewandte Chemie-International Edition*, 2004, **43**, 1832-1835.

[46] P. V. Rao, S. Bhaduri, J. Jiang and R. H. Holm, *Inorganic Chemistry*, 2004, **43**, 5833-5849.

[47] P. C. Andrikopoulos, D. R. Armstrong, W. Clegg, C. J. Gilfillan, E. Hevia, A. R. Kennedy, R. E. Mulvey, C. T. O'Hara, J. A. Parkinson and D. M. Tooke, *Journal of the American Chemical Society*, 2004, **126**, 11612-11620.

[48] W. Clegg, K. W. Henderson, A. R. Kennedy, R. E. Mulvey, C. T. O'Hara, R. B. Rowlings and D. M. Tooke, *Angewandte Chemie-International Edition*, 2001, **40**, 3902-3905.

[49] A. J. Tasiopoulos, W. Wernsdorfer, B. Moulton, M. J. Zaworotko and G. Christou, *Journal of the American Chemical Society*, 2003, **125**, 15274-15275.

[50] E. E. Moushi, C. Lampropoulos, W. Wernsdorfer, V. Nastopoulos, G. Christou and A. J. Tasiopoulos, *Inorganic Chemistry*, 2007, **46**, 3795-3797.

[51] H.-S. Wang, C.-B. Ma, M. Wang, C.-N. Chen and Q.-T. Liu, *Journal of Molecular Structure*, 2008, **875**, 288-294.

[52] M. Murugesu, W. Wernsdorfer, K. A. Abboud, and G. Christou, *Angewandte Chemie-International Edition*, 2005, **44**, 892-896.

[53] T. Shiga, L. Han, M. Nihei, N. Hoshino, T. Ito and H. Oshio, *Chemistry Letters*, 2006, **35**, 440-441.

[54] B. Modec, J. V. Brenčič and L. Golic, *Polyhedron*, 2000, **19**, 1219-1225.

[55] B. Modec, J. V. Brenčič, J. Koller, *European Journal of Inorganic Chemistry*, 2004, 1611-1620.

[56] B. Modec, J. V. Brenčič, R. C. Finn, R. S. Rarig and J. Zubieta, *Inorganica Chimica Acta*, 2001, **322**, 113-119.

[57] B. Modec, J. V. Brenčič, R. Rotar, L. Golic and K. Prout, *Acta Crystallographica Section C*, 1998, **C54**, 1573-1575.

[58] C. du Peloux, A. Dolbecq, P. Barboux, G. Laurent, J. Marrot and F. Secheresse, *Chemistry-A European Journal*, 2004, **10**, 3026-3032.

[59] D. J. Darensbourg, R. L. Gray and T. Delord, *Inorganica Chimica Acta*, 1985, **98**, L39-L42.

[60] N. Calin and S. C. Sevov, *Inorganic Chemistry*, 2003, **42**, 7304-7308.

[61] Q. Chen, S. Liu and J. Zubieta, *Angewandte Chemie-International Edition in English*, 1988, 27, 1724-1725.

[62] T. Zell, W. Shi, R. Langer, L. Ponikiewski and A. Rothenberger, *Dalton Transactions*, 2008, 932-937.

[63] G. Karotsis, C. Stoumpos, A. Collins, F. White, S. Parsons, A. M. Z. Slawin, G. S. Papaefstathiou and E. K. Brechin, *Dalton Transactions*, 2009, 3388-3390.

[64] I. G. Dance, M. L. Scudder and R. Secomb, *Inorganic Chemistry*, 1985, **24**, 1201-1208.

[65] R. Uson, J. Fornies, L. R. Falvello, M. A. Uson and S. Herrero, *Inorganic Chemistry*, 1993, **32**, 1066-1067.

[66] M. Ganesan, S. Gambarotta and G. P. A. Yap, *Angewandte Chemie-International Edition*, 2001, **40**, 766-769.

[67] M. S. Rau, C. M. Kretz and G. L. Geoffroy, *Organometallics*, 1994, **13**, 1624-1634.

[68] D. B. Dell'Amico, F. Calderazzo, L. Costa, E. Franchi, L. Gini, L. Labella and F. Marchetti, *Journal of Molecular Structure*, 2008, **890**, 295-297.

[69] G. Kickelbick and U. Schubert, *European Journal of Inorganic Chemistry*, 1998, 159-161.

[70] H. Burrow, D. A. Brown, N. W. Alcock, H. J. Clase and M. G. H. Wallbridge, Journal of the Chemical Society, *Chemical Communications*, 1995, 1231-1232.

[71] P. Piszczek, M. Richert, A. Grodzicki, T. Glowiak and A. Wojtczak, *Polyhedron*, 2005, **24**, 663-670.

[72] T. Frot, S. Cochet, G. Laurent, C. Sassoye, M. Popall, C. Sanchez and L. Rozes, *European Journal of Inorganic Chemistry*, 2010, 5650-5659.

[73] Y. Fu, Z. Xu and F. Zhang, *Journal of Molecular Structure*, 2008, **873**, 168-172.

[74] H. Kumagai and S. Kitagawa, *Chemistry Letters*, 1996, 471-472.

[75] Q. Chen, S. Liu and J. Zubieta, *Inorganic Chemistry*, 1989, **28**, 4433-4434.

[76] H.-X. Li, H.-Z. Wu, W.-H. Zhang, Z.-G. Ren, Y. Zhang and J.-P. Lang, *Chemical Communications,* 2007, 5052-5054.

[77] O. Cador, D. Gatteschi, R. Sessoli, F. K. Larsen, J. Overgaard, A.-L. Barra, S. J. Teat, G. A. Timco and R. E. P. Winpenny, *Angewandte Chemie-International Edition*, 2004, **43**, 5196-5200.

[78] H.-C. Yao, J.-J. Wang, Y.-S. Ma, O. Waldmann, W.-X. Du, Y. Song, Y.-Z. Li, L.-M. Zheng, S. Decurtins and X.-Q. Xin, *Chemical Communications*, 2006, 1745-1747.

[79] M. Mikuriya, S. Ikemi and S. Yao, *Chemistry Letters*, 2000, 538-539.

[80] S. A. Ivanov, M. A. Kozee, W. A. Merrill, S. Agarwal and L. F. Dahl, *Journal of the Chemical Society, Dalton Transactions*, 2002, 4105-4115.

[81] Y. Liu, H. Hou, Q. Chen and Y. Fan, *Crystal Growth & Design*, 2008, **8**, 1435-1442.

[82] H. N. Miras, I. Chakraborty and R. G. Raptis, *Chemical Communications*, 2010, **46**, 2569-2571.

[83] E. J. L. McInnes, C. Anson, A. K. Powell, A. J. Thomson, S. Poussereau and R. Sessoli, *Chemical Communications*, 2001, 89-90.

[84] M. Helliwell, A. A. Smith, S. J. Teat and R. E. P. Winpenny, *Inorganica Chimica Acta*, 2003, **354**, 49-53.

[85] S. L. Heath, R. H. Laye, C. A. Muryn, N. Lima, R. Sessoli, R. Shaw, S. J. Teat, G. A. Timco and R. E. P. Winpenny, *Angewandte Chemie-International Edition*, 2004, **43**, 6132-6135.

[86] C.-H. Chang, K. C. Hwang, C.-S. Liu, Y. Chi, A. J. Carty, L. Scoles, S.-M.Peng, G. H. Lee and J. Reedijk, *Angewandte Chemie-International Edition*, 2001, **40**, 4651-4653.

[87] L. G. Westin, M. Kritikos and A. Caneschi, *Chemical Communications*, 2003, 1012-1013.

[88] C. Benelli, S. Parsons, G. A. Solan and R. E. P. Winpenny, *Angewandte Chemie-International Edition in English*, 1996, 35, 1825-1828.

[89] G. Jiang, Y. Li, W. Hua, Y. Song, J. Bai, S. Li, M. Scheer and X. You, *CrystEngComm*, 2006, 8, 384-387.

[90] K. L. Taft, C. D. Delfs, G. C. Papaefthymiou, S. Foner, D. Gatteschi and S. J. Lippard, *Journal of the American Chemical Society*, 1994, **116**, 823-832.

[91] M. Frey, S. G. Harris, J. M. Holmes, D. A. Nation, S. Parsons, P. A. Tasker and R. E. P. Winpenny, *Chemistry-a European Journal*, 2000, **6**, 1407-1415.

[92] S.-X. Liu, S. Lin, B.-Z. Lin, C.-C. Lin and J.-Q. Huang, *Angewandte Chemie*, 2001, **113**, 1118-1121.

[93] G. S. Papaefstathiou, A. Manessi, C. P. Raptopoulou, A. Terzis and T. F. Zafiropoulos, *Inorganic Chemistry*, 2006, **45**, 8823-8825.

[94] P. King, T. C. Stamatatos, K. A. Abboud and G. Christou, *Angewante Chemie*, 2006, **118**, 7539-7543.

[95] C. Dendrinou-Samara, C. A. Muryn, F. Tuna and R. E. P. Winpenny, *European Journal of Inorganic Chemistry*, 2010, **20**, 3097-3101.

[96] K. Lei, T. Shu and H. Liang, *Solid State Sciences*, 2011, **13**, 1896-1898.

[97] E. Cadot, A. Dolbecq, B. Salignac and F. Secheresse, *Journal of Physics and Chemistry of Solids*, 2001, **62**, 1533-1543.

[98] G. Liu, S.-W. Zhang and Y.-Q. Tang, *Journal of the Chemical Society*, *Dalton Transactions*, 2002, 2036-2039.

[99] D. Fenske and A. Fischer, *Angewandte Chemie-International Edition in English*, 1995, **34**, 307-309.

[100] O. Poncelet, L. G. Hubert-Pfalzgraf, J. C. Daran and R. J. Astier, *Journal of the Chemical Society, Chemical Communications*, 1989, 1846-1848.

[101] R. Wang, M. Hong, J. Luo, R. Cao and J. Weng., *Chemical Communications*, 2003, 1018-1019.

[102] E. K. Brechin, O. Cador, A. Caneschi, C. Cadiou, S. G. Harris, S. Parsons, M. Vonci, and R. E. P. Winpenny, *Chemical Communications*, 2002, 1860-1861.

[103] O. L. Sydora, P. T. Wolczanski, E. B. Lobkovsky, *Angewandte Chemie-International Edition*, 2003, **42**, 2685-2687.

[104] N. V. Gerbeleu, S. Parsons, A. A. Smith, G. A. Timco and R. E. P. Winpenny, unpublished results.

[105] C. E. Jones, G. A. Timco and R. E. P. Winpenny, unpublished results.

[106] M. S. A. Begum, O. Seewald, U. Florke and G. Henkel, *Inorganica Chimica Acta*, 2008, **361**, 1868-1874.

[107] L.-F. Zou, L. Zhao, Y.-N. Guo, G.-M. Yu, Y. Guo, J. Tang and Y.-H. Li, *Chemical Communications*, 2011, **47**, 8659-8661.

[108] A. Caneschi, A. Cornia, A. C. Fabretti and D. Gatteschi, *Angewandte Chemie-International Edition in English*, 1999, **38**, 1295-1297.

[109] A.-A. H. Abu-Nawwas, J. Cano, P. Christian, T. Mallah, G. Rajaraman, S. J. Teat, R. E. P. Winpenny and Y. Yukawa, *Chemical Communications*, 2004, 314-315.

[110] C. P. Raptopoulou, V. Tangoulis and E. Devlin, *Angewandte Chemie-International Edition*, 2002, **41**, 2386-2389.

[111] D. Sellmann, F. Geipel and F. W. Heinemann, *Chemistry-a European Journal*, 2002, **8**, 958-966.

[112] G. L. Abbati, A. Caneschi, A. Cornia, A. C. Fabretti and D. Gatteschi, *Inorganica Chimica Acta*, 2000, **297**, 291-300.

[113] S. Konar and A. Clearfield, *Inorganic Chemistry*, 2008, **47**, 5573-5579.

[114] Y. Inagaki, T. Asano, Y. Ajiro, Y. Narumi, K. Kindo, A. Cornia and D. Gatteschi, *Journal of the Physical Society of Japan*, 2003, **72**, 1178-1183.

[115] T. Kajiwara, K. Katagiri, S. Takaishi, M. Yamashita and N. Iki, *Chemistry-an Asian Journal*, 2006, **1**, 349-351.

[116] P. C. Andrews, A. R. Kennedy, R. E. Mulvey, C. L. Raston, B. A. Roberts and R. B. Rowlings, *Angewandte Chemie-International Edition*, 2000, **39**, 1960-1962.

[117] M. M. Olmstead, W. J. Grigsby, D. R. Chacon, T. Hascall and P. P. Power, *Inorganica Chimica Acta*, 1996, 251-273.

[118] N. Thirupathi, G. P. A. Yap and D. S. Richeson, *Chemical Communications*, 1999, 2483-2484.

[119] E. M. Rumberger, S. J. Shah, C. C. Beedle, L. N. Zakharov, A. L. Rheingold and D. N. Hendrickson, *Inorganic Chemistry*, 2005, **44**, 2742-2752.

[120] Z.-H. Ni, H.-Z. Kou, L.-F. Zhang, C. Ge, A.-L. Cui, R.-J. Wang, Y. Li and O. Sato, *Angewandte Chemie*, 2005, **117**, 7920-7923.

[121] Z.-H. Ni, L.-F. Zhang, V. Tangoulis, W. Wernsdorfer, A.-L. Cui, O. Sato and H.-Z. Kou, *Inorganic Chemistry*, 2007, **46**, 6029-6037.

[122] T. Shibahara, M. Sasaki and G. Sakane, *Inorganica Chimica Acta*, 1995, **237**, 1-3.

[123] M. A. Paver, J. S. Joy and M. B. Hursthouse, *Chemical Communications*, 2002, 2150-2151.

[124] A. J. Blake, C. M. Grant, S. Parsons, J. M. Rawson and R. E. P. Winpenny, *Journal of the Chemical Society, Chemical Communications*, 1994, 2363-2364.

[125] C. Cadiou, M. Murrie, C. Paulsen, V. Villar, W. Wernsdorfer and R. E. P. Winpenny, *Chemical Communications*, 2001, 2666-2667.

[126] C. M. Grant, PhD Thesis, The University of Edinburgh, 1995.

[127] M. A. Beswick, M. K. Davies, M. A. Paver, P. R. Raithby, A. Steiner, D. S. Wright, *Angewandte Chemie-International Edition in English*, 1996, **35**, 1508-1510.

[128] Y. Zhao, G. Zhu, W. Liu, Y. Zou and W. Pang, *Chemical Communications*, 1999, 2219-2220.

[129] A. Müller, B. Neumuller and K. Dehnicke, *Angewandte Chemie-International Edition in English*, 1997, **36**, 2350-2352.

[130] I. G. Dance, L. J. Fitzpatrick, D. C. Craig and M. L. Scudder, *Inorganic Chemistry*, 1989, **28**, 1853-1861.

[131] T. C. Stamatatos, K. A. Abboud, W. Wernsdorfer and G. Christou, *Angewandte Chemie-International Edition*, 2008, **47**, 6694-6698.

[132] S.-Y. Yu, Z.-X. Zhang, E. C.-C.Cheng, Y.-Z. Li, V. W.-W. Yam, H. P. Huang and R. Zhang, *Journal of the American Chemical Society*, 2005, **127**, 17994-17995.

[133] M. Manoli, A. Prescimone, A. Mishra, S. Parsons, G. Christou and E. K. Brechin, *Dalton Transactions*, 2007, 532-534.

[134] M. Murugesu, J. Raftery, W. Wernsdorfer, G. Christou and E. K. Brechin, *Inorganic Chemistry*, 2004, **43**, 4203-4209.

[135] P. Klufers and J. Schuhmacher, *Angewandte Chemie-International Edition*, 1994, **33**, 1863-1865.

[136] J. F. You, G. C. Papaefthymiou and R. H. Holm, *Journal of the American Chemical Society*, 1992, **114**, 2697-2710.

[137] S. P. Watton, P. Fuhrmann, L. E. Pence, A. Caneschi, A. Cornia, G. L. Abbati and S. L. Lippard, *Angewandte Chemie-International Edition in English*, 1997, **36**, 2774-2776.

[138] R. T. W. Scott, C. J. Milios, A. Vinslava, D. Lifford, S. Parsons, W. Wernsdorfer, G. Christou and E. K. Brechin, *Dalton Transactions*, 2006, 3161-3163.

[139] A. Baniodeh, I. J. Hewitt, V. Mereacre, Y. Lan, G. Novitchi, C. E. Anson and A. K. Powell, *Dalton Transactions*, 2011, **40**, 4080-4086.

[140] T. C. Stamatatos, S. Mukherjee, K. A. Abboud and G. Christou, *Chemical Communications*, 2009, 62-64.

[141] M. Manoli, A. Prescimone, R. Bagai, A. Mishra, M. Murugesu, S. Parsons, W. Wernsdorfer, G. Christou and E. K. Brechin, *Inorganic Chemistry*, 2007, **46**, 6968-6979.

[142] A. L. Dearden, S. Parsons and R. E. P. Winpenny, *Angewandte Chemie-International Edition in English*, 2001, **40**, 151-154.

[143] D. Foguet-Albiol, K. A. Abboud and G. Christou, *Chemical Communications*, 2005, 4282-4284.

[144] S. Rochat, Z. Grote and K. Severin, *Organic and Biomolecular Chemistry*, 2009, **7**, 1147-1153.

[145] L. F. Jones, C. A. Kilner, M. P. De Miranda, J. Wolowska and M. A. Halcrow, *Angewandte Chemie-International Edition*, 2007, **46**, 4073-4076.

[146] L. F. Jones, S. A. Barrett, C. A. Kilner and M. A. Halcrow, *Chemistry-a European Journal*, 2008, **14**, 223-233.

[147] K. Lei, T. Shu and H. Liang, *Solid State Sciences*, 2011, **13**, 1896-1898.

[148] D. M. Low, G. Rajaraman, M. Helliwell, G. A. Timco, J. van Slageren, R. Sessoli, S. T. Ochsenbein, R. Bircher, C. Dobe, O. Waldmann, H.-U. Güdel, M. A. Adams, E. Ruiz, S. Alvarez and E. J. L. McInnes, *Chemistry-a European Journal*, 2006, **12**, 1385-1396.

[149] A. Müller, M. Koop, H. Bögge, M. Schmidtmann and C. Beugholt, *Chemical Communications*, 1998, 1501-1502.

[150] A. Müller, S. Q. N. Shah, H. Bögge and M. Schmidtmann, *Nature*, **397**, 48-50.

[151] V. Pashchenko, M. Lang, B. Wolf, L. Zherlitsyna, N. Auner, O. Shchegolikhina, Y. Pozdniakova, F. Schütz, P. Kopietz and M. Kollar, *C. R. Chimie*, 2007, **10**, 89-95.

[152] N. Hoshino, M. Nakano, H. Nojiri, W. Wernsdorfer and H. Oshio, *Journal of the American Chemical Society*, 2009, **131**, 15100-15101.

[153] O. Kahn, *Chemical Physics Letters*, 1997, **265**, 109-114.

[154] G. A. Timco, *manuscript in preparation*.

[155] O. Cador, D. Gatteschi, R. Sessoli, A.-L. Barra, G. A. Timco and R. E. P. Winpenny, *Journal of Magnetism and Magnetic Materials*, 2005, **290-291**, 55-60.

[156] G. Lorusso, F. Troiani, V. Bellini, A. Ghirri, A. Candini, S. Carretta, P. Santini, G. Amoretti, W. Wernsdorfer, G. A. Timco, R. E. P. Winpenny and M. Affronte Journal of Physics: Conference Series, 2011, **303,** 012033.

[157] M. Affronte, F. Troiani, A. Ghirri, A. Candini, M. Evangelisti, S. Carretta, P. Santini, G. Amoretti, S. Piligkos, G. A. Timco and R. E. P. Winpenny, *Polyhedron*, 2005, **24**, 2562-2567.

[158] M. Affronte, I. Casson, M. Evangelisti, A. Candini, S. Carretta, C. A. Muryn, S. J. Teat, G. A. Timco, W. Wernsdorfer, and R. E. P. Winpenny, *Angewandte Chemie-International Edition*, 2005, **44**, 6496-6500.

[159] C.-F. Lee, D. A. Leigh, R. G. Pritchard, D. Schultz, S. J. Teat, G. A. Timco and R. E. P. Winpenny, *Nature*, 2009, **458**, 314-318.

[160] G. A. Timco, S. Carretta, F. Troiani, F. Tuna, R. J. Pritchard, C. A. Muryn, E. J. L. McInnes, A. Ghirri, A. Candini, P. Santini, G. Amoretti, M. Affronte and R.E. P. Winpenny, *Nature Nanotechnology*, 2009, **4**, 173-178.

[161] G. A. Timco, E. J. L. McInnes, R. G. Pritchard, F. Tuna and R. E. P. Winpenny, *Angewandte Chemie-International Edition*, 2008, **47**, 9681-9684.

[162] A. Turing, *Proceedings of the London Mathematical Society*, 1936-37, **42**, 230-65.

[163] G. E. Moore, *Electronics*, 1965, **38**, April 19.

[164] R. Rivest, A. Shamir and L. Adleman, *Communications of the ACM*, 1978, **21**, 120-126.

[165] P. W. Shor, *Proceedings of the 35nd Annual Symposium on Foundations of Computer Science*, 1994, 124-134.

[166] L. K. Grover, *Proceedings of the Twenty-Eighth Annual ACM Symposium on the Theory of Computing*, 1996, 212-218.

[167] R. P. Feynman, *International Journal of Theoretical Physics,* 1982, **21**, 467-488.

[168] D. Deutsch, *Proceedings of the Royal Society of London A*, 1985, **400**, 97-117.

[169] H. Everett, *Reviews of Modern Physics*, 1957, **29**, 454-46.

[170] D. Deutsch, *The Fabric of Reality*, The Penguin Press, London, 1997.

[171] E. Schrödinger, *Mathematical Proceedings of the Cambridge Philosophical Society*, 1935, **31,** 555-563.

[172] D. P. DiVincenzo, *The Physical Implementation of Quantum Computation*, 2000, arXiv:quant-ph/0002077v3.

[173] D. P. DiVincenzo, *Fortschritte der Physik*, 2000, **48**, 771-783.

[174] B. E. Kane, *Nature*, 1998, **393**, 133-137.

[175] H. Haffner, W. Hansel, C. F. Roos, J. Benhelm, D. Chek-al-kar, M. Chwalla, T. Korber, U. D. Rapol, M. Riebe, P. O. Schmidt, C. Becher, O. Guhne, W. Dur and R. Blatt, *Nature*, 2005, **438**, 463-466.

[176] G. K. Brennen, C. M. Caves, P. S. Jessen and I. H. Deutsch, *Physical Review Letters,* 1999, **82**, 1060-1063.

[177] P. J. Blythe and B. T. H. Varcoe, *New Journal of Physics*, 2006, **8**, 231.

[178] R. Prevedel, P. Walther, F. Tiefenbacher, P. Bohi, R. Kaltenbaek, T. Jennewein and A. Zeilinger, *Nature*, 2006, **445**, 65-69.

[179] Y. Makhlin, G. Schon and A. Shnirman, *Applicable Algebra in Engineering, Communication and Computing*, 2000, **10**, 375-382.

[180] P. M. Platzman and M. I. Dykman**,** *Science,* 1999, **284**, 1967-1969.

[181] W. F. Koehl, B. B. Buckley, F. J. Heremans, G. Calusine and D. D. Awschalom, *Nature*, 2011, **479**, 84-88.

[182] A. P. Nizovtsev, S. Ya. Kilin, F. Jelezko, T. Gaebal, I. Popa, A. Gruber and J. Wrachtrup, *Optics and Spectroscopy*, 1999, **2**, 248-260.

[183] C. Meyer, W. Harneit, A. Weidinger and K. Lips, *physica status solidi (b)*, 2002, **233**, 462-466.

[184] F. Kuemmeth, S. Ilani, D. C. Ralph and P. L. McEuen, *Natur*e, 2008, **452**, 448-452.

[185] D. Loss and D. P. DiVincenzo, *Physical Review A*, 1998, **57**, 120-126.

[186] M. N. Leuenberger and D. Loss, *Nature*, 2001, **410**, 789-793.

[187] L. Thomas, F. Lionti, R. Ballou, D. Gatteschi, R. Sessoli and B. Barbara, *Nature*, 1996, **383**, 145-157.

[188] J. R. Friedman, M. P. Sarachik, J. Tejada and R. Ziolo, *Physical Review Letters*, 1996, **76**, 3830-3833.

[189] C. Sangregorio, T. Ohm, C. Paulsen, R. Sessoli, and D. Gatteschi, *Physical Review Letters*, 1997, **78**, 4645-4648.

[190] W. Wernsdorfer, R. Sessoli, A. Caneschi, D. Gatteschi and A. Cornia, *Europhysics Letters*, 2000, **50**, 552-552.

[191] J. S. Bashkin, H.-R. Chang, W. E. Streib, J. C. Huffman, D. N. Hendrickson and G. Christou, *Journal of the American Chemical Society*, 1987, **109**, 6502-6504.

[192] Q. Li, J. B. Vincent, E. Libby, H.-R. Chang, J. C. Huffman, P. D. W. Boyd, G. Christou, and D. N. Hendrickson, *Angewandte Chemie-International Edition in English*, 1988, **27**, 1731-1733.

[193] E. K. Brechin, J. Yoo, M. Nakano, J. C. Huffman, D. N. Hendrickson and G. Christou, *Chemical Communications*, 1999, 783-784.

[194] W. Wernsdorfer, N. Aliaga-Alcalde, D. N. Hendrickson and G. Christou, *Nature*, 2002, **416**, 406-409.

[195] R. Tiron, W. Wernsdorfer, D. Foguet-Albiol, N. Aliaga-Alcalde and G. Christou, *Physical Review Letters*, 2003, **91**, 227203.

[196] S. Hill, R. S. Edwards, N. Aliaga-Alcalde and G. Christou, *Science*, 2003, **302**, 1015-1018.

[197] E. C. Sañudo, T. Cauchy, E. Ruiz, R. H. Laye, O. Roubeau, S. J. Teat and G. Aromi, *Inorganic Chemistry*, 2007, **46**, 9045-9047.

[198] D. Aguila, L. A. Barrios, F. Luis, A. Repolle, O. Roubeau, S. J. Teat and G. Aromi, *Inorganic Chemistry*, 2010, **49**, 6784-6786.

[199] S. Lloyd, *Science*, 1993, **261**, 1569-1571.

[200] Y. Morita, Y. Yakiyama, S. Nakazawa, T. Murata, T. Ise, D. Hashizume, D. Shiomi, K. Sato, M. Kitagawa, K. Nakasuji and T. Takui, *Journal of the American Chemical Society*, 2010, **132**, 6944-6946

[201] W. Haneit, *Physical Review A*, 2002, **65**, 032322.

[202] J. J. L. Morton, A. M. Tyryshkin, A. Ardavan, S. C. Benjamin, K. Porfyrakis, S. A. Lyon and G. A. D. Briggs, *Nature Physics*, 2006, **2**, 40-43.

[203] S. C. Benjamin, A. Ardavan, G. A. D Briggs, D. A Britz, D. Gunlycke, J. Jefferson, M. A. G. Jones, D. F. Leigh, B. W. Lovett, A. N Khlobystov, S. A. Lyon, J. J. L. Morton, K. Porfyrakis, M. R. Sambrook and A. M Tyryshkin, *Journal of Physics: Condensed Matter*, 2006, **18**, S867-S883.

[204] S. Polad, PhD Thesis, The Middle East Technical University, 2010.

[205] S. Polad, Fullerene-Based Systems as Prospective Spin Cluster Qubits, VDM Publishing, Saarbrücken, 2011.

[206] C. Schlegel, J. van Slageren, G. Timco, R. E. P. Winpenny and M. Dressel, *Physical Review B*, 2011, 83, 134407.

[207] A. Ardavan, O. Rival. J. J. L. Morton and S. J. Blundell, *Physical Review Letters*, 2007, **98**, 057201.

[208] A. Schweiger and G. Jeschke, *Principles of Pulse Electron Paramagnetic Resonance,* Oxford University Press, Oxford, 2001.

[209] V. Corradini, F. Moro, R. Biagi, V. De Renzi, U. del Pennino, V. Bellini, S. Carretta, P. Santini, V. A. Milway, G. A. Timco, R. E. P. Winpenny and M. Affronte, *Physical Review B*, 2009, **79**, 144419.

[210] A. Ghirri, V. Corradini, V. Bellini, R. Biagi, U. del Pennino, V. De Renzi, J. C. Cezar, C. A. Muryn, G. A. Timco, R. E. P. Winpenny and M. Affronte, *ACS Nano*, 2011, ***5***, 7090-7099.

[211] A. Ghirri, V. Corradini, C. Cervetti, A. Candini, U. del Pennino, G. A. Timco, R. J. Pritchard, C. A. Muryn, R. E. P. Winpenny and M. Affronte, *Advanced Functional Materials*, 2010, **20**, 1-9.

[212] H. Günther, *NMR Spectroscopy*, 2nd Edition, John Wiley & Sons, Chichester, 1995.

[213] J. K. M. Saunders and B. K. Hunter, *Modern NMR Spectroscopy*, 2nd Edition, Oxford University Press, Oxford, 1993.

[214] P. J. Hore, *Nuclear Magnetic Resonance*, Oxford University Press, Oxford, 1995.

[215] J. A. Iggo, *NMR Spectroscopy in Inorganic Chemistry*, Oxford University Press, Oxford, 1999.

[216] R. V. Parish, *NMR, NQR, EPR and Mossbauer Spectroscopy in Inorganic Chemistry*, Ellis Horwood, New York, 1990.

[217] F. E. Mabbs and D. J. Machin, *Magnetism and Transition Metal Complexes*, Dover Publications, New York, 2008.

[218] J. A. Weil and J. R. Bolton, *Electron Paramagnetic Resonance*, 2nd Edition, John Wiley & Sons, Hoboken, 2007.

[219] A. Schweiger and G. Jeschke, *Principles of Pulse Electron Paramagnetic Resonance*, Oxford University Press, Oxford, 2001.

[220] A. F. Orchard, *Magnetochemistry*, Oxford University Press, Oxford, 2003.

[221] M. M. Woolfson, *An Introduction to X-ray Crystallography*, 2nd Edition, Cambridge University Press, Cambridge, 1997.

[222] W. Clegg, *Crystal Structure Determination*, Oxford University Press, Oxford, 1998.

[223] *Diamond – Key Facts*, leaflet, available from www.diamond.ac.uk, accessed 9th December 2011.

[224] B. Bleaney and K. D. Bowers, *Proceeding of the Royal Society, London A*, 1952, **214**, 451-465.

[225] A. M. W. Cargill Thompson, D. Gatteschi, J. A. McCleverty, N. A. Navas, E. Rentschler and M. D. Ward, *Inorganic Chemistry*, 1996, 35, 2701-2703.

[226] M. Rancan, G. N. Newton, C. A. Muryn, R. G. Pritchard, G. A. Timco, L. Cronin and R. E. P. Winpenny, *Chemical Communications*, 2008, 1560-1562.

Appendix - Paper 8

"Propagation of spin information at the supramolecular scale through heteroaromatic linkers"

V. Bellini, G. Lorusso, A. Candini, W. Wernsdorfer, T. B. Faust, G. A. Timco, R. E. P. Winpenny and M. Affronte, *Physical Review Letters*, 2011, **106**, 227205.

Propagation of Spin Information at the Supramolecular Scale through Heteroaromatic Linkers

V. Bellini,[1,*] G. Lorusso,[1] A. Candini,[1] W. Wernsdorfer,[2] T. B. Faust,[3] G. A. Timco,[3] R. E. P. Winpenny,[3,4] and M. Affronte[5,1]

[1]*S3-Institute Nanoscience-CNR, Via Campi 213/A, 41125 Modena, Italy*
[2]*Laboratoire Louis Néel, avenue des Martyres 24, Grenoble, France*
[3]*School of Chemistry, The University of Manchester, Oxford Road, Manchester, M13 9PL, United Kingdom*
[4]*The Photon Science Institute, The University of Manchester, Oxford Road, Manchester, M13 9PL, United Kingdom*
[5]*Dipartimento di Fisica, Universitá di Modena e Reggio Emilia, Via Campi 213/A, 41125 Modena, Italy*

(Received 28 February 2011; published 3 June 2011)

We report an in-depth study on how spin information propagates at supramolecular scale through a family of heteroaromatic linkers. By density-functional theory calculations, we rationalize the behavior of a series of Cr_7Ni dimers for which we are able to systematically change the aromatic linker thus tuning the strength of the magnetic interaction, as experimentally shown by low temperature micro-SQUID and specific heat measurements. We also predict a $\cos^2$ dependence of the magnetic coupling on the twisting angle between the aromatic cycles in bicyclic linkers, a mechanism parallel to charge transport on similar systems [L. Venkataraman *et al.*, Nature (London) **442**, 904 (2006)].

DOI: 10.1103/PhysRevLett.106.227205 PACS numbers: 75.50.Xx, 71.15.Mb, 75.30.Et

Controlling and understanding the propagation of spin information at the molecular scale is an intriguing issue involving both fundamental sciences and the possibility of designing molecular devices of interest for information technologies. In order to make two magnetic units weakly interact at supramolecular (nanometer) scale, local through-bond interactions are preferable to dipolar interactions, as the latter has essentially long-range character and is difficult to tune without large structural modification in the systems. While exchange interactions, stemming from direct overlapping of nearest neighboring metal orbitals, as well as superexchange, mediated by the orbitals of bridging, e.g., oxygen, atoms, are mechanisms which have been studied in detail both experimentally and theoretically, spin interactions between metal centers through long organic groups still remain largely unexploited. Aromatic organic linkers are suitable candidates to create local interactions and have been studied in the 1980s and 1990s within the quest for room temperature metallorganic magnets. Molecular dimers, where the magnetic parts of the single units are represented by single paramagnetic ions, have been investigated in this context. The strength of the interaction, electronic and magnetic, between the units linked by an aromatic bridge, has been found to obey some general empirical rules [1]: (1) the larger the number of bonds which compose the interaction path, the smaller the interaction is; (2) charge and spin polarization induced by bonding to a metal site proceed in an alternating fashion in aromatic cycles; (3) since a magnetic interaction can be sustained by different bond paths in the linker, the strength of the interaction should depend on whether quantum constructive or destructive interference between paths with different lengths arise [2]. These findings have been discussed so far in terms of simplified model orbital methods [3–5], and only more recently refined density-functional characterizations of dimeric complexes appeared in the literature [6–8]. The next challenge is to couple magnetically two (or more) complex molecules without perturbing the properties of the individual units. This allows the entanglement of spins of molecular units [9] and eventually the encoding of two-qubits gates or the communication of magnetic information at supramolecular (nanometer) scale [10]. Supramolecular dimers of single molecule magnets, which involve linking Mn_4 cages into dimers through C-H$\cdots$Cl hydrogen bonds, have been reported [11]. Although magnetic interaction is achieved [12], tuning this interaction is not straightforward.

Heterometallic Cr_7Ni molecular rings combine special chemical and magnetic features that allow us to define a strategy for linking molecular magnetic units. The key ingredient is the presence—within the Cr^{III}($S_{Cr} = 3/2$) wheel—of an "extra" divalent ion (Ni^{II}, $S_{Ni} = 1$) that allows us to selectively build both the chemical and the magnetic link between molecular units. A series of Cr_7Ni dimers have been recently synthesized, with the general formula $[\{Cr_7NiF_3(Etglu)(O_2C^tBu)_{16}\}_2(L)]$ with L being the heteroaromatic linker [13]. We present in the following a thorough study of five different dimers, with $L =$ pyrazine (pyr, in short), bidimethylpyrazolyl (bipz), 4,4'-bipyridyl (bipy), trans-1,2-bipyridylethene (bipyet), and bipyridyltetrazine (bipytz) (see Fig. 1 for a sketch of the molecular structures of these dimers, and EPAPS [14] for more informations). The first linker (pyr) is the only one composed of a single heterocycle, the second (bipz) is the only one built with two five-membered rings (pyrazole), the third and fourth (bipy- and bipyet-) are essentially made of two pyridine rings, while the last (bipytz) contain three aromatic rings (two pyridine and one

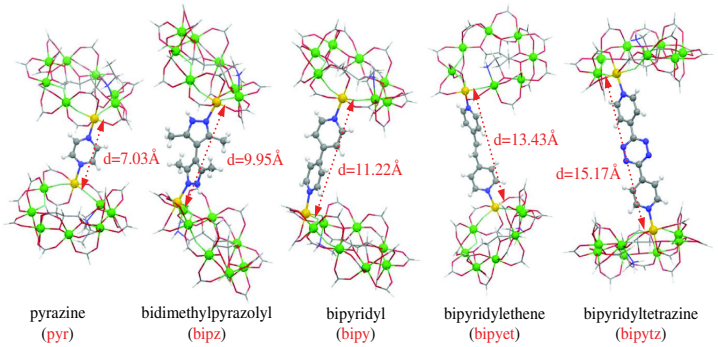

FIG. 1 (color online). The molecular structures of pyr, bipz, bipy, bipyet, and bipytz Cr_7Ni purple rings. The atoms of the linkers (N, blue; C, gray; H, white) and the metal ions in the rings (Ni, yellow; Cr, green) have been highlighted; the inter-rings through-space Ni-Ni distances (d) are also given for each dimer.

tetrazine). Ni-Ni interring distances range from 7 to more than 15 Å, as reported in Fig. 1. Dihedral angles between the cycles, as measured by x-ray diffraction, are around 41° for bipy, 56° for bipz, and 28°/32° for bipytz, while for bipyet no clear angle could be defined due to the ethene block. The dimers are found to pack into different crystal structures, with negligible interdimer magnetic interactions. The intraring magnetic coupling is of the antiferromagnetic type, leading to a molecular $S = 1/2$ Kramer ground state doublet for all the Cr_7Ni rings. The dimers depicted in Fig. 1 are only some representative derivatives of a larger family of dimers, which can be synthesized with relative ease [15].

We first address the theoretical characterization of the systems. Calculations have been performed by the density-functional theory (DFT) module of the NWCHEM quantum chemistry package [16]. The full systems (rings and bridge) have been taken into account with some pruning of the organic ligands surrounding the magnetic cores of the rings has been performed (more information on the theoretical method could be found in Sec. I in the supplemental material [14]). p electrons of the linkers are distributed over two types of orbitals, the ones that occur in localized covalent bonds (with label σ) and the ones that occupy delocalized bonds (π electrons). Conjugation due to π orbitals is a good candidate to drive magnetic interactions at nm scale. The magnetic interaction is maximum when overlap (both in space and in energy) between the spin-polarized frontier orbitals of the magnetic centers, in our case Ni, and orbitals of the linker anchoring atom N is found. Ni^{II} ions, have nominally a $3d^8$ electronic configurations; in an nearly orthorhombic environment only d orbitals with Eg-like symmetry are spin polarized. As the local axis around the Ni atoms are rotated from the plane of the heterocycles in the linkers, and some deviation from orthorhombicity is found for the coordination shell of Ni atoms, both σ and π orbital of the extended molecule can in principle favor magnetic interactions between the spin of the two rings. In Fig. 2 we plot the spin-polarized electron density isosurfaces for a very low isovalue ($= \pm 0.0005$ electrons/a.u.^{3}), and zoom onto the relevant Ni-linker-Ni coupling region. Several observations can be made. The first is that in all the linkers, an alternation of spin polarization when moving from one atom to the next, following bond paths, is present in the linkers, and this polarization involves primarily orbitals with π character. Polarization of σ orbitals in the linkers, although present on the N atoms bonded to Ni, fades away within few bonds,

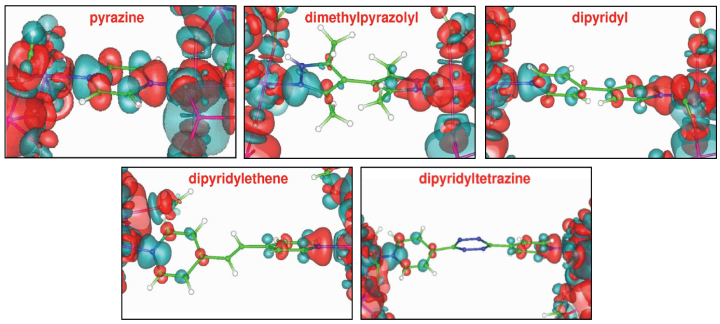

FIG. 2 (color online). Spin-polarization density in pyr, bipz, bipy, bipyet, and bipytz dimers, zoomed in the region of the linker, for isovalues of + (cyan) and − (red) 0.0005 electrons/a.u.^{3}

and vanishes altogether for inner C atoms. Because of the spin alternation rule, whether ferromagnetic or antiferromagnetic interactions between magnetic centers is seen depends on the number of C/N atoms in the bonding pathway; if an even number of C/N atoms is present the exchange is antiferromagnetic, while if an odd number of C/N atoms is present ferromagnetic coupling should be encountered. Exchange between the two Ni atoms can follow two different possible paths around the six- and five-membered rings; in bipz, there exist pathways with both odd and even numbers of C/N atoms, supporting simultaneously ferro- or antiferromagnetic exchange, respectively. Destructive interference between these two paths leads to a very low spin polarization of the orbitals in the inner region of the bipz, despite them being closer than in the other bicyclic dimers. Delocalization of the π system orbitals also becomes less efficient as the number of bonds increase; consequently the spin polarization in the inner region of the linker is larger for pyr than for bipy or bipyet; clearly if we increase the distance between the Ni atoms, spin polarization reduced still further, that being the case of bipytz.

In order to provide quantitative information, we have performed total energy calculations of broken-symmetry (BS) spin configurations, and mapped them onto the microscopic spin Hamiltonian of the type

$$H = 2J'\mathbf{S}_{\mathrm{Ni1}} \cdot \mathbf{S}_{\mathrm{Ni2}}, \tag{1}$$

where J' is the isotropic exchange between the Ni spin moments, and $\mathbf{S}_{\mathrm{Ni1}}$ and $\mathbf{S}_{\mathrm{Ni2}}$ are the spin moments of the two Ni ions ($S_{\mathrm{Ni1}} = S_{\mathrm{Ni2}} = 1$). Intraring magnetic interactions between Cr-Cr and Cr-Ni spins are of the antiferromagnetic (AFM) type, leading to a $S = 1/2$ ground state for the single Cr_7Ni rings. While retaining this AFM states for both the rings, we have characterized the two situations where the $S = 1/2 Cr_7Ni$ spins are either coupled ferromagnetic (FM) or AFM to each other. In terms of the microscopic coupling between the two $S = 1$ Ni spins, this leads to two states with energies $E_{\mathrm{FM}} = 2J'$ and $E_{\mathrm{AFM}} = -2J'$; J' is then simply given by $1/4$ of the total energy difference between the FM and AFM states of the dimer. The calculated J' values are 367, 8, 48, 56, and 22 μeV for pyr, bipz, bipy, bipyet, and bipytz, respectively (see supplemental information [14] for more details). These are tiny interactions that are near the numerical precision of the DFT method; yet if we consider the trend, the calculations show similar J' for bipy, bipyet, a value 7 times larger for pyr, and smaller values for bipz and bipytz.

This findings are fully supported by experiments. From the magnetic point of view, the family of Cr_7Ni rings behave, at low temperatures, as ideal two-level mesoscopic systems with an effective $S = 1/2$ and higher multiplets that are relevant at high temperature (T)/applied magnetic fields (H) or for effects due to the mixing of magnetic states [17,18]. Low temperature specific heat $C(T, H)$ data at 3 T (Fig. 1S in the supplemental material [14]) demonstrates that the pattern of the lowest lying states of the single Cr_7Ni rings are preserved also in the supramolecular systems. To reveal the presence of the interring interaction we have performed micro-SQUID measurements at 40 mK. The resulting magnetization curves are plotted in Fig. 3. Data are normalized to the saturation value M_S and for simplicity only the part of the hysteresis loop with increasing field is plotted. In order to enlighten the transition between the singlet and triplet states, the magnetization cycle is magnified between $H = \pm 0.1T$, whereas for all the dimers, $M(H)$ saturates above 1 T (for the complete hysteresis loops see Fig. 2S in the supplemental material [14]). If the $S_{\mathrm{tot}} = 0$ state is the ground state in zero field, we should be able to see a spin-state crossing by increasing the field, with one component of the paramagnetic $S_{\mathrm{tot}} = 1$ state falling in energy as field increases (visible as an inflection point of the magnetization curve). The crossing point in the magnetization, i.e., the gap between inflection points, can then be related to the energy gap between the $S_{\mathrm{tot}} = 0$ and $S_{\mathrm{tot}} = 1$ states [9]. We can see in Fig. 3 that the level crossings occur at $B = \pm 0.05T$ for bipy and at $B = \pm 0.04T$ for bipyet, while it appears at $B = \pm 0.30T$ for pyr. Fitting this crossing to the microscopic Hamiltonian equation (1), we obtain $J'/k_B = 1.0$ K for the pyr-linked dimers, approximately 6 times the value for the bipy dimer, where $J'/k_B = 0.16$ K [9], and $\sim 20\%$ weaker for the bipyet-linked one (positive values refer to antiferromagnetic interaction). For the other two compounds (bipytz and bipz), the magnetic coupling is too small, and no inflection points are visible in the magnetization curves. We can thus conclude that in bipytz and bipz derivatives the interaction between the two Cr_7Ni rings must be weaker than 100 mK. These data are in excellent agreement with the trend among the different dimers evidenced in the DFT analysis reported above.

It is now evident that the length of the linker is not the only attribute one has to consider when seeking a tailored spin coupling. As a matter of fact, the conformation of the

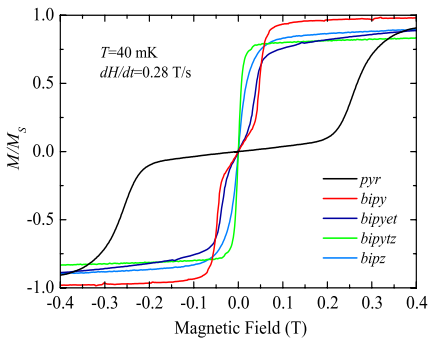

FIG. 3 (color online). Micro-SQUID magnetization $M(H)$ vs magnetic field H for the pyr, bipz, bipy, bipyet, and bipytz dimers. The experiments were performed at $T = 40$ mK, using sweeping rate $dH/dt = 0.28$ T/s. Data are normalized to the saturation value M_S.

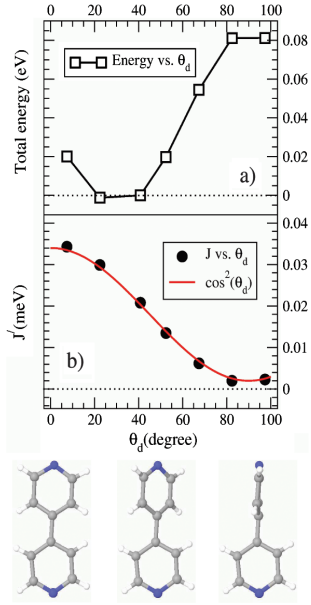

FIG. 4 (color online). (a) Total energy and b) exchange interaction parameter J' in the bipy-linked dimers, as a function of the dihedral angle θ_d between the two pyridine cycles.

linker, the angles between the two heterocycles, or the angles between the cycles and the Ni coordination axes do play an important role, modifying the conjugation level and consequently the interring spin coupling. We have thus performed computational experiments for the bipy dimer, by calculating the magnetic interaction as a function of the dihedral angle between the two pyridine cycles; to do this, we have coherently rotated the molecules in the space, keeping fixed the geometry of the Ni-linker contacts, in order to selectively study the dependence of J and total energy as a function of linker conformation only. Total energy calculations indicate a preferred twisted configuration with dihedral angle around 20–30° (see Fig. 4, upper panel). The variation of J' as a function of the dihedral angle θ_d is plotted in Fig. 4, lower panel. Maximum magnetic coupling would be achieved when the two cycles are coplanar, and overlap between π orbitals, and consequently conjugation, is at its maximum. As evidenced by the continuous line the variation of J' follows closely a $\cos^2(\theta_d)$ curve. Interestingly, the conductance through biphenyl junctions have shown similar $\cos^2(\theta_d)$ behavior [19,20], and this has been traced back to the $\cos(\theta_d)$ dependence of the overlap of the π orbitals. [21] We may qualitatively understand the similar angular dependency considering that the spin information extends through the linkers by a spin-polarization mechanism, and in first approximation, the sequential polarization of the π orbitals at the C/N sites involves hopping of electrons in the conjugated system, as much as molecular electron transfer, which is directly related to the π-π orbital overlap throughout the linker. Therefore, a very interesting parallelism between charge and spin propagation in bicyclic aromatic linker emerges from these works.

In summary, we have provided an in-depth description of the propagation of spin information between two molecular macrocycles through a family of aromatic linkers that we have considered as paradigmatic case. The numerical observation of a $\cos^2$ dependence on torsion angles is also promising, and paves the way for a whole series of possible experimental investigations, by systematically varying the organic bridges and the magnetic frontier atoms, in order to tune and choose the appropriate coupling regime, switching the interaction on and off at will, by perturbing the organic linker using a mechanical stimulus.

This work has been partially supported by FP7-ICT FET Open MolSpinQIP project, Contract No. 211284, by the EPSRC (U.K.), and from MIUR-PRIN projects (I), Contracts No. 2008PARRTS and No. 2008NX9Y7. We acknowledge the CINECA supercomputing center for the availability of high performance computing resources and support.

*valerio.bellini@unimore.it

[1] D. E. Richardson and H. Taube, J. Am. Chem. Soc. **105**, 40 (1983).
[2] V. Marvaud, J.-P. Launay, and C. Joachim, Chem. Phys. **177**, 23 (1993).
[3] J. A. McCleverty and M. D. Ward, Acc. Chem. Res. **31**, 842 (1998).
[4] H. M. McConnell, J. Chem. Phys. **39**, 1910 (1963).
[5] H. C. Longuet-Higgins, J. Chem. Phys. **18**, 265 (1950).
[6] A. Bencini *et al.*, J. Phys. Chem. A **102**, 10545 (1998).
[7] F. Nunzi *et al.*, J. Phys. Chem. C **111**, 618 (2007).
[8] J. Ferrando-Soria *et al.*, Inorg. Chim. Acta **363**, 1666 (2010).
[9] A. Candini *et al.*, Phys. Rev. Lett. **104**, 037203 (2010).
[10] F. Troiani and M. Affronte, Chem. Soc. Rev. (in press).
[11] D. N. Hendrickson *et al.*, J. Am. Chem. Soc. **114**, 2455 (1992).
[12] W. Wernsdorfer *et al.*, Nature (London) **416**, 406 (2002).
[13] G. A. Timco *et al.*, Angew. Chem., Int. Ed. **47**, 9681 (2008).
[14] See supplemental material at http://link.aps.org/supplemental/10.1103/PhysRevLett.106.227205 for supplementary information.
[15] T. B. Faust *et al.* (to be published).
[16] E. J. Bylaska *et al.*, NWChem, A Computational Chemistry Package for Parallel Computers, Version 5.1, Pacific Northwest National Laboratory, Richland, Washington, USA, 99352-0999, 2007.
[17] M. Affronte *et al.*, Phys. Rev. B **68**, 104403 (2003).
[18] S. Carretta *et al.*, Phys. Rev. B **72**, 060403(R) (2005).
[19] L. Venkataraman *et al.*, Nature (London) **442**, 904 (2006).
[20] M. S. Hybertsen *et al.*, J. Phys. Condens. Matter **20**, 374115 (2008).
[21] S. Woitellier, J.-P. Launay, and C. Joachim, Chem. Phys. **131**, 481 (1989).

Supplementary Material

Propagation of spin information at supra-molecular scale through hetero-aromatic linkers

V. Bellini,[a] G. Lorusso,[a] A. Candini,[a] W. Wernsdorfer,[b] T. B. Faust,[c] G. A. Timco,[c] R. E. P. Winpenny,[c,d] and M. Affronte [a,e]

[a] S3 - Institute Nanoscience-CNR, Via Campi 213/A, 41125 Modena, Italy.
[b] Laboratoire L. Néel, av des Martyres 24, Grenoble, France.
[c] School of Chemistry, The University of Manchester, Oxford Road, Manchester, M13 9PL, UK.
[d] The Photon Science Institute, The University of Manchester, Oxford Road, Manchester, M13 9PL, UK.
[e] Dipartimento di Fisica Università di Modena e Reggio Emila, via Campi 213/A, 41125 Modena, Italy.

Sec. I Density-functional calculations

We have used density-functional theory and Gaussian basis sets as implemented in the NWChem quantum chemistry package. Ahlrichs valence triple zeta (VTZ) contracted Gaussian basis set is used for the metal ions, while Ahlrichs valence double zeta (VDZ) is assumed for the remanent elements [1]. The hybrid B3LYP exchange and correlation potential has been used [2], which have demonstrated to give reliable results in correlated bulk oxides and molecules, although superexchange magnetic interactions are typically overestimated by a factor of 2. Low spin magnetic states of the supramolecular system, such as the singlet and triplet states, have been ensured by initially imposing

with constrained density functional theory (CDFT) [3] spin moments on the metal ions with the correct spin sign distribution, and using CDFT wave-functions as starting guesses for the standard DFT electronic minimization; convergence criterium for the total energy has been set to $5\cdot 10^{-7}$ eV.

In order to reduce the computational burden, the systems have been approximated by means of the hydrogen termination technique. The pivalate bridges $(CH_3)_3COO$-, composing the organic matrix in which the magnetic oxide core is embedded, within each Cr_7Ni ring have been approximated by HCOO-, performing two times in turn the isovalence substitution $CH_3 \rightarrow H$; a similar substitution has been done in the coordination sphere of the nitrogen atom belonging to the glucamine chain in the inner region of the rings, substituting one CH_3. No approximations have been made to the organic bridges, in order to not alter the crucial region for the intramolecular magnetic coupling.

The plot of the spin densities reported in the paper have been obtained performing calculations for the experimental atomic coordinates as obtained by X-Ray structural analysis. In order to obtain the *J*s, and to check the robustness of our numerical calculations, we allowed atoms in the linker relax towards their minimum energy positions. Indeed, the X-ray structures were measured at 100K, while micro-SQUID measurements have been performed at very low temperature. If we allow structural optimization of the dimers, we note that while *bipy* and *bipz* linkers do not modify their conformations (dihedral angles of *bipy* and *bipz* are only weakly modified with respect to the experimental values, 34° *cf.* 41° for *bipy* and 62° *cf.* 56°), due to steric hindrance of the hydrogen atoms which lock the two cycles at dihedral angles ≠ 0°, *bipyet* and *bipytz* linkers relax to a planar conformation (in *pyr*, being composed of a single heteroaromatic cycle, the minimization has only minor influence on the results. This has the important consequence of increasing noticeably the level of conjugation of the π–electron system of linkers.The calculated *J'* values, in the case of the experimental atomic positions are 476, 4, 20, 1 and 8 μeV, while the *J'* for the minimized atomic positions are 367, 8, 48, 56 and 22 μeV for *pyr*, *bipz*, *bipy*, *bipyet*, and *bipytz* respectively.

Sec. II Specific Heat Data

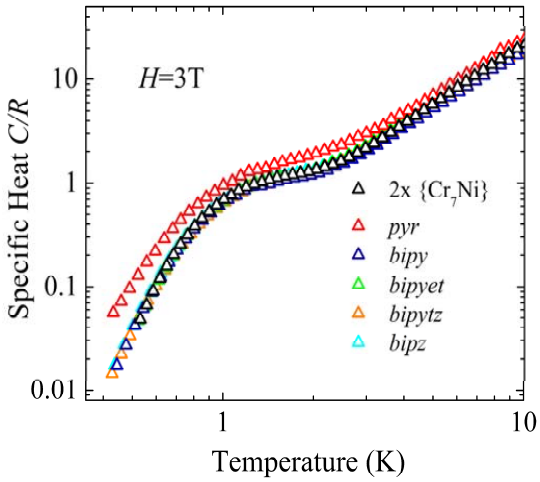

Figure S1: Specific heat for the five $\{Cr_7Ni\}_2$ dimers discussed in the text: *pyr* (red), *bipy* (dark blue), *bipyet* (green), *bipytz* (orange) and *bipz* (light blue). The curves are compared to the specific heat of the single $\{Cr_7Ni\}$ ring multiplied by two (black). Data are normalized to the gas constant *R*. Measurements were performed on thin pellets (~2 mg) of polycrystalline sample by a ^{3}He cryostat and by using the two-tau method. An external magnetic field $\mu_0 H$=3T was applied.

In Fig.S1 we report the low temperature specific heat C(T) in presence of 3T external magnetic field for the five molecular dimers of $\{Cr_7Ni\}_2$ discussed in the main body of the article. Data are compared with the specific heat multiplied by two of the single $\{Cr_7Ni\}$ ring (black markers). The curves of the dimers overlap on the specific heat of the single ring measured at the same field. For the dimer with the *pyrazine* linker the C(T) curve is slightly above the others, due to a higher phonon contribution, but still following the overall behavior of the single $\{Cr_7Ni\}$ ring. The main feature of these C(T) curves is an evident bump peaked around 1K due to the energy gaps between the lowest-lying spin levels of the molecules at 3T. The magnetic part of the specific heat for a multi-level systems indeed reads as a generalized multi-level Schottky anomaly:

$$\frac{C_m}{R} = \beta^2 \frac{\sum_i E_i^2 \exp(-\beta E_i) \sum_i \exp(-\beta E_i) - \left[\sum_i E_i \exp(-\beta E_i)\right]^2}{\left[\sum_i \exp(-\beta E_i)\right]^2}$$

where *Ei* are the eigenvalues of the Hamiltonian of the system and $\beta = 1/k_B T$.

From previous investigation[4] of the single $\{Cr_7Ni\}$ we found $S = 1/2$ ground state separated from the first excited $S = 3/2$ state by $\Delta/k_B T$ ~19K at zero field. This energy gap evolves with the field and at 3T

produces the Schottky anomaly shown in Fig.1 around 1K. The reproducibility of this magnetic feature demonstrates that the pattern of the lowest lying states of the single $\{Cr_7Ni\}$ rings are preserved also in the supramolecular systems.

Sec. III Low T Micro-SQUID measurements

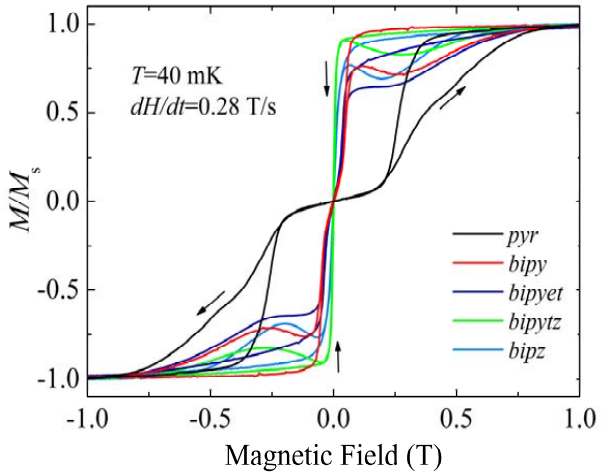

Fig.S2 Micro-SQUID magnetization hysteresis loops for the five $\{Cr_7Ni\}_2$ dimers discussed in the text. The curves are normalized to the saturation values M_S. The experiments were performed at 40 mK and with a magnetic field sweeping rate $dH/dT = 0.28\text{T/s}$.

In Fig.S2 we present the complete micro-SQUID hysteresis loops for the five $\{Cr_7Ni\}_2$ dimers as described in the main body of the article. Measurements were carried out at 40 mK and data are normalized to the saturation value M_S. All the curves show a butterfly-shaped hysteresis, typical of the phonon-bottleneck regime due to the fast sweeping rate of the magnetic field, $dH/dT = 0.28\text{T/s}$. The magnetization of the dimer linked by the *pyrazine* group distinguishes from the others for the presence of two well defined steps in correspondence of the fields $H = \pm 0.3$T. These steps, not present for the single $\{Cr_7Ni\}$, are due to transitions between the low (S=0) and high (S=1) spin states of the dimers, thus evidencing the presence of inter-molecular coupling between the rings. Analogously, in the cases of *bipy* and *biyet* dimers the interaction between the rings is revealed by the feeble knees in correspondence of the crossing fields $H = \pm 0.05$T and $H = \pm 0.04$T respectively; while for *bipytz* and *bipz* no transition (and thus no coupling) is observed. The remarkable difference between the crossing

fields relative to *pyr* dimer and those to *bipy* and *bipyet* is a direct consequence of the different strength of the inter-molecular coupling, that we can expect about five/six times greater for the dimer with the *pyridine* linker. This demonstrates our capability to establish and tuning the magnetic coupling between the {Cr_7Ni} molecular rings by means of coordination chemistry and by using different organic linkers.

Sec. IV References

[1] A. Schafer, H. Horn, and R. Ahlrichs, J. Chem. Phys. **97**, 2571 (1992).

[2] A. D. Becke, J. Chem. Phys. **98**, 5648 (1993); P. J. Stephens, F. J. Devlin, and C. F. Chabalowski and M. J. Frisch, J. Phys. Chem.**98**, 11623 (1994).

[3] P. H. Dederichs, S. Blugel, R. Zeller, and H. Akai, Phys. Rev. Letters **53**, 2512 (1984); I. Rudra and T. van Voorhis, J. Chem. Phys. **124**, 024103 (2006).

[4] A. Candini, G. Lorusso, F. Troiani, A. Ghirri, S. Carretta, P. Santini, G. Amoretti, F. Tuna, G. Timco, E. J. L. McInnes, R. E. P. Winpenny, W. Wernsdorfer, M. Affronte, Phys. Rev. Lett. **104**, 037203 (2010).